UNIVERSITY OF CALGARY

The Role of the Mrj Co-chaperone During Early Mouse Embryonic Development

by

Erica Danielle Watson

A THESIS

SUBMITTED TO THE FACULTY OF GRADUATE STUDIES

IN PARTIAL FULFILLMENT OF THE REQUIREMENTS FOR THE

DEGREE OF DOCTOR OF PHILOSOPHY

DEPARTMENT OF BIOCHEMISTRY AND MOLECULAR BIOLOGY

CALGARY, ALBERTA

SEPTEMBER, 2008

UNIVERSITY OF
CALGARY

ABSTRACT

The Mrj co-chaperone is widely expressed in adult mice, embryos and the trophoblast lineage of the placenta. Like other DnaJ proteins, Mrj targets specific substrates to the Hsp70 chaperone and activates its ATPase activity required for protein folding, degradation, trafficking and other protein-protein interactions. When the *Mrj* gene was knocked out, embryonic lethality resulted since mouse conceptuses failed to undergo chorioallantoic attachment, a major developmental milestone required for placental formation. Previous to our studies, it was unclear how Mrj functioned in vivo since only a few substrates had been identified in vitro, including keratin (K)18 intermediate proteins. We found that the keratin cytoskeleton was collapsed into large aggregates in $Mrj^{-/-}$ chorion trophoblast cells, presumably since proteasome degradation of K18 was blocked in the absence of Mrj. Interestingly, genetic removal of the keratin aggregates by generating $Mrj^{-/-}$;$K18^{-/-}$ conceptuses rescued the chorioallantoic attachment phenotype and suggested that keratin aggregates are toxic to trophoblast cell function. While assessing other cytoskeletal and extracellular matrix (ECM) proteins, we observed that actin and associated adhesion proteins as well as Laminin (Ln) α5 were misexpressed in cultured $Mrj^{-/-}$ trophoblast stem (TS) cells. Live cell imaging revealed that the cells were highly migratory and repulsive compared to wildtype, indicating that cell-cell and cell-matrix interactions were disrupted due to *Mrj* deficiency. Interestingly, by providing exogenous Lnα5 substrate to $Mrj^{-/-}$ TS cells, cell-cell interactions were normalized signifying that the adhesion phenotype is secondary to the Lnα5 defect. Remarkably, altered ECM deposition in $Mrj^{-/-}$ trophoblast cells in vivo was associated with altered chorionic patterning. Instead of forming three layers of labyrinth trophoblast precursors,

Mrj-deficient chorions remained in an unspecified, common progenitor-state. Lastly, we established that one quarter of *Mrj*$^{-/-}$ embryos had defective neural tube closure, whereas the neural tubes of the remaining mutant embryos were small with reduced proliferation. Using neurosphere cultures, we determined that Mrj is required to maintain neural stem cell self-renewal. Because the neural phenotype appears to be unrelated to a defect in keratin or other neural-specific intermediate filaments, it reinforces the notion that Mrj has a variety of substrates in vivo.

ACKNOWLEDGEMENTS

Thanks to the publishing groups Elsevier, The Company of Biologists Ltd and The American Physiology Society for copyright permission and also to my co-authors Colleen Geary-Joo, Martha Hughes and James Cross for allowing me to include excerpts from these publications. A sincere thank you to my committee Drs William Brook, Jim McGhee and Carrie Shemanko for their guidance, suggestions and for seeming outwardly interested in topics such as chaperones, cytoskeleton and mouse placenta.

During my time in the Cross lab, I have overlapped with many talented scientists including Myriam Hemberger, David Simmons and Dave Natale. These people have looked out for me, they have been my mentors, my friends and without them I would not be where I am today. For that I am forever grateful. To the den mothers Fran Snider and Martha Hughes: I appreciate your friendship, encouragement and laughter. Don't worry, I won't forget my umbrella. I am thankful for friends like Colleen Geary-Joo, Ryan Lamont, Saara Rawn and Lindsay Mickelson for providing balance, wisdom and understanding (and a falafel or two when needed).

Most importantly, I am indebted to my supervisor Jay Cross, who was confident in me as a scientist from the start, well before I was confident in myself. His encouragement to always take a step back to see the bigger picture, in both science and opportunities in life, is invaluable to me. I am fortunate to have had the experience of working with him and I hope to take the lessons learned here with me wherever I go. I would also like to thank Jay and our collaborator Roy Gravel for trusting me while I followed my 'hunch' and then permitting me to use the results to launch myself into the next phase of my career.

Finally, I want to thank my parents Ed and Jennifer, and my sisters Amanda and Katie for their love, patience and encouragement throughout my time in grad school and for thinking that having a scientist in the family is pretty cool. This thesis is dedicated with love to Dave Fyvie who has made my life infinitely better through his comedy, friendship, his encouragement and belief in me.

TABLE OF CONTENTS

CHAPTER FOUR – NEURAL TUBE CLOSURE AND STEM CELL SELF-RENEWAL REQUIRE THE MRJ CO-CHAPERONE.

APPENDIX A – GRANDMATERNAL MUTATION IN FOLATE METABOLISM CAUSES CONGENITAL MALFORMATIONS

LIST OF TABLES

LIST OF FIGURES

LIST OF ABBREVIATIONS

bFGF	Basic fibroblast growth factor
β-gal	β-galactosidase
CM	Embryonic fibroblast conditioned media
E	Embryonic day of mouse development
ECM	Extracellular matrix
EGFP	Enhanced green fluorescent protein
EM	Electron microscopy
EPC	Ectoplacental cone
ES cell	Embryonic stem cell
GlyT	Glycogen trophoblast cells
HD	Huntington's disease
IF	Intermediate filaments
IUGR	Intrauterine growth restriction
K	Keratin
Ln	Laminin
Mrj	Mammalian relative of DnaJ
MS	Methionine synthase
MTHFR	Methylene tetrahydrofolate reductase
MTRR	Methionine synthase reductase
NSC	Neural stem cell
NTD	Neural tube defect
PPH3	Phosphohistone H3
P-TGC	Parietal trophoblast giant cell
SpT	Spongiotrophoblast
S-TGC	Sinusoidal trophoblast giant cell
SynT-I	Syncytiotrophoblast layer I
SynT-II	Syncytiotrophoblast layer II
TS cell	Trophoblast stem cell
TGC	Trophoblast giant cell

CHAPTER ONE

INTRODUCTION

The content of section 1.4.4 “The role of simple epithelial keratins during mammalian development” and section 1.5 “Development of the chorioallantoic placenta” were in part originally published as (Watson, 2007) and (Watson and Cross, 2005), respectively, and were used with permission.

1.1 General introduction

The gene encoding Mrj (*M*ammalian *r*elative of Dna*J*, also known as Dnaj6b or Hsj2 – Mouse Genome Informatics) was initially identified in the Cross lab during a gene trap screen in mouse embryonic stem (ES) cells (Hunter et al, 1999). Mrj belongs to the large family of DnaJ/Hsp40 co-chaperone proteins related to the DnaJ co-chaperone in *E. coli*. Almost 10 years ago it was shown that *Mrj* is required for placental development in mice (Hunter et al, 1999), but the precise molecular and cellular function of the Mrj protein had remained a mystery until specific substrates were identified. Mrj is broadly expressed in a variety of cell types in the adult and in the placenta and embryo during development, but embryonic lethality associated with placental defects in *Mrj* mutants has previously precluded a full understanding of its function.

1.2 The Mrj co-chaperone

1.2.1 The cellular function of Mrj

Members of DnaJ/Hsp40 co-chaperone protein family have three distinct domains including a conserved J domain (~70 amino acids) found at the N-terminus, a Gly/Phe-rich flexible linker region and a highly variable substrate binding domain at the C-terminus (Ohtsuka and Hata, 1999). Through the J domain, DnaJ family members interact with the chaperone Hsp70 to regulate its ATPase activity and to facilitate substrate binding (Hartl and Hayer-Hartl, 2002). In contrast, divergence of the amino acid sequence within the C-terminus of DnaJ proteins transmits substrate specificity to Hsp70 (Fan et al, 2003). Together this chaperone complex has many functions including protein folding, degradation, trafficking and other protein-protein interactions required for

normal cell function (Esser et al, 2004), depending on the type of DnaJ co-chaperone, its subcellular localization and the substrate bound to it.

Mrj can bind and activate Hsp70 through its J domain (Izawa et al, 2000; Chuang et al, 2002). Several substrates of Mrj have recently been identified (Table 1.1) and suggest that Mrj may play a role in the prevention of protein aggregate formation (Chuang et al, 2002; Fayazi et al, 2006), regulation of the keratin intermediate filament cytoskeleton (Izawa et al, 2000), cell cycle control (Zhang et al, 2008; Li et al, 2008; Mitra et al, 2008), gene regulation (Dai et al, 2005; Hurst et al, 2006; Pan et al, 2008) and protein trafficking (Zhang et al, 2008; Cheng et al, 2008). However, despite the diversity of these substrates, the exact function of the Hsp70/Mrj complex in vivo remains elusive.

Two alternatively spliced Mrj isoforms have been identified (Hanai and Mashima, 2003; Tateossian et al, 2004; Mitra et al, 2008; Cheng et al, 2008). The long (L) isoform (365 amino acids compared to 242 amino acids in the short (S) isoform) includes two extra C-terminal exons that extend its substrate binding domain. The additional exons include a functional nuclear localization signal (Mitra et al, 2008) and, as a result, Mrj (L) is preferentially located in the nucleus whereas Mrj (S) appears to be restricted to the cytoplasm (Tateossian et al, 2004; Mitra et al, 2008). Furthermore, FGF1 signalling can differentially regulate Mrj isoform expression: the absence of FGF1 results in higher expression of Mrj (S) in ES cells compared to Mrj (L) whereas the addition of FGF1 up-regulates Mrj (L) and suppresses the expression of Mrj (S) (Tateossian et al, 2004). The functional difference between these two isoforms with respect to differential substrate binding or tissue specificity has not been determined.

Table 1.1 – Known substrates that bind to the co-chaperone Mrj.

Table 1.1 – Known substrates that bind to Mrj (continued)

1.2.2 Mrj is required for normal mouse development

The importance of Mrj during development is exemplified by its broad temporal and spatial expression pattern throughout the developing embryo and the placenta (Hunter et al, 1999; Chuang et al, 2002). Mrj expression within the mouse placenta is particularly high in the trophoblast giant cells, although Mrj is also present in the chorion cells at embryonic (E) day 8.5 and later in the labyrinth (Hunter et al, 1999). Previously, the Cross lab in collaboration with G.E. Lyons (University of Wisconsin) generated mice deficient for *Mrj* as a result of random insertion of the βgeo gene trap cassette into intron 2 of the *Mrj* gene (Hunter et al, 1999). As a result, no *Mrj* mRNA was detected by northern blotting in $Mrj^{-/-}$ tissue (Hunter et al, 1999) indicating that both Mrj splice isoforms are ablated in these mice. $Mrj^{-/-}$ embryos fail in a key developmental milestone called chorioallantoic attachment (Hunter et al, 1999), a process that is required for normal placenta formation (see Section 1.5). Without a placenta, the exchange of nutrients and gases between the mother and fetus does not occur and, therefore, $Mrj^{-/-}$ embryos die at midgestation (E10.5).

An abnormality in the trophoblast layer of $Mrj^{-/-}$ chorions was hypothesized to be the main cause of the chorioallantoic attachment defect for several reasons. First, Mrj expression appeared to be restricted to the chorionic trophoblast cells and was unappreciable within the underlying chorionic mesothelium or allantois (Hunter et al, 1999). However, it was still necessary to clarify the exact location of Mrj function to understand how chorioallantoic attachment and subsequent placental development is affected. Secondly, the allantois appeared to be morphologically and molecularly normal in *Mrj* mutants at E8.5 (Hunter et al, 1999). Lastly, chorionic trophoblast-specific genes,

Err2 and *Gcm1*, were down-regulated at E8.5 due to *Mrj* deficiency suggesting that this layer is abnormal in mutant chorions (Hunter et al, 1999). Further investigation into how Mrj functions at a cellular level within the chorion trophoblast layer and which protein substrates it binds to in order to regulate chorioallantoic attachment is crucial to understanding normal placenta morphogenesis.

No obvious developmental defects were initially observed in the embryo proper due to *Mrj* deficiency prior to E9.25 (Hunter et al, 1999). However, *Mrj* is widely expressed within the embryo itself, particularly in the brain (Hunter et al, 1999; Chuang et al, 2002), suggesting that Mrj also plays a role in the development of the embryo proper. This is difficult to assess since $Mrj^{-/-}$ embryos die prior to the development of most organ systems. Insight into how Mrj acts in different developmental contexts will shed light onto the cellular function of Mrj.

1.3 The effects of protein aggregates on normal cell function

1.3.1 The role of chaperones in preventing protein aggregate formation

Numerous human disorders, including neurodegenerative diseases and cirrhosis of the liver, are caused by the presence of protein aggregates or inclusion bodies within the affected cells. Aggregate formation is traditionally thought to result due to genetic mutations within the protein in question preventing normal protein folding, such as with the expanded polyglutamine repeat mutations in the Huntington's disease (HD) protein (DiFiglia et al, 1997). However, failure of the protein folding/degradation machinery itself can also result in protein aggregation (Carrell, 2005; McClellan et al, 2005). For example, when proteasome function is chemically inhibited or a ubiquitin mutation is

present in hepatocytes, both result in the formation of large aggregates of keratin intermediate filament proteins (Mallory bodies) (Bardag-Gorce et al, 2004; Bardag-Gorce et al, 2003). Molecular chaperones, such as Hsp70, are key players in this sophisticated protein quality-control system by ensuring that proteins are properly folded and/or are targeted to the proteasome for degradation (McClellan et al, 2005). The co-chaperone or adaptor protein bound to Hsp70 largely dictates whether it will undergo substrate folding or degradation (Esser et al, 2004). When a misfolded protein is recognized, a chaperone complex will try to refold it. If unsuccessful, the misfolded protein is either sequestered within the cell or it is targeted for degradation. Interestingly, the Hsp70-Mrj chaperone complex has been shown to eliminate aggregates containing polyglutamine-expanded huntingtin protein from cells in vitro (Chuang et al, 2002) although the mechanism by which this happens is unknown. Regardless, the protein quality control machinery is necessary to prevent the formation of protein aggregates that are potentially harmful to the cell.

1.3.2 Protein aggregates alter normal cell function

There is debate within the literature concerning whether the disease-state of 'aggregation' diseases is caused by the loss of function of the aggregated protein or rather the gain of function due to toxicity of the misfolded species (McClellan et al, 2005). In fact, the effect of inclusion bodies on cell function is not well understood and is likely dependent upon the cell type and characteristics of the affected protein. Cystic fibrosis is a disease that results from the loss-of-function mutation within the *CFTR* gene causing protein misfolding, which prevents CFTR transport to the plasma membrane thus thwarting

normal function (Amaral, 2005). Alternatively, gain-of-function mutations in proteins causing aggregation are toxic to the cell, affecting viability. For example, many neurodegenerative disorders, including amyotrophic lateral sclerosis (ALS), Alzheimer's disease, Parkinson's disease and Huntington's disease, contain mutations in proteins with no sequence similarity and yet they form similar amyloid deposits (McClellan et al, 2005). Whether these deposits themselves are toxic to the cell or whether the cell forms an aggregate to protect itself from the toxicity of the mutant protein is uncertain (Ross and Poirier, 2005). Many researchers suggest, at least in the case of neurodegenerative diseases, that early soluble intermediates in the aggregation pathway seem to be the toxic species and the later larger inclusion bodies themselves are not pathogenic (Carrell, 2005; McClellan et al, 2005; Ross and Poirier, 2005). It is only recently, however, that researchers have focused on cellular events independent of how the aggregate forms (Stefani, 2007), such as how the presence of the aggregate affects normal cell function prior to the onset of cell death by apoptosis or necrosis. Prior to cell death, Huntington's disease-affected cells have changes in intracellular free Ca^{2+} levels and altered redox status (Butterfield et al, 2001; Kourie, 2001). These inclusion bodies can interfere with gene transcription by creating abnormal interactions with various transcriptional co-activator and co-repressor proteins (e.g. Sp1 and CBP) (Ross, 2002; Dunah et al, 2002; Nucifora et al, 2001). Furthermore in Alzheimer's disease, the formation of aggregates often alters the effectiveness of proteasome function by overloading it and preventing the cell from clearing the aggregated protein (Upadhya and Hegde, 2007). Although these studies have begun to shed light on abnormal cellular events caused by inclusion body

formation, much more research is needed to fully understand what occurs in the cell prior to degeneration and pathogenesis.

1.4 Regulation of the keratin cytoskeleton

1.4.1 The biology of intermediate filaments

The identification of intermediate filament (IF) proteins as cytoskeletal scaffolds in muscle occurred 40 years ago (Ishikawa et al, 1968). Since then, approximately 70 conserved genes encoding intermediate filament proteins in human, mouse and other mammals have been described (Kim and Coulombe, 2007) including keratin, neurofilaments, nestin, lamins and vimentin. Other organisms, such as *C. elegans*, *Drosophila* and zebrafish, also contain several IF proteins (Karabinos et al, 2001; Melcer et al, 2007; Zimek and Weber, 2005). It is clear, however, that IFs are unnecessary for life at a single cell level since yeast and some mammalian cell lines do not contain IF proteins (Erber et al, 1998). IF proteins are largely cytoplasmic, with the exception of lamins which are found exclusively within the nucleus. All IFs can be broken down into monomer proteins that are tripartite in structure: the α-helical central rod domain that mediates dimer formation is flanked by two non-helical head and tail domains that differ in length, sequence and substructure between each type of IF to transmit diversity (reviewed by Fuchs and Weber, 1994). To form a filament, monomers must interact in an in-register, parallel orientation to form dimers, which then assemble into an anti-parallel arrangement to produce apolar tetramers. A filament is composed of several subfibrils of tetramers and ranges from 10 to 12 nm in diameter, depending on the type of IF (reviewed by Fuchs and Weber, 1994). The end domains of the filament are thought to

mediate interactions with other filaments and cellular proteins to regulate structure, organization and function (Kim and Coulombe, 2007).

Keratin (K) filaments form a large family of IF proteins that are expressed primarily within epithelial cells. Keratins account for most of the IF genes in the human genome, encompassing 54 functional genes (Schweizer et al, 2006). There are two groups of keratins, type I (acidic, including K9-K23) and type II (basic-to-neutral; including K1-K8) (Schweizer et al, 2006). Each keratin filament is composed of heterodimers of type I and type II proteins, and each gene pair exhibits epithelial tissue type- and differentiation-specific regulation (Coulombe and Omary, 2002). Owing to the fact that few keratin-associated proteins have been identified, the regulation and function of the keratin cytoskeleton is largely unknown.

1.4.2 Keratin cytoskeleton organization, dynamics and regulation

The keratin cytoskeleton forms a filamentous network throughout the cytoplasm, incorporating with the actin and microtubule cytoskeletons (Kim and Coulombe, 2007). A keratin filament usually spans from the cell membrane where it associates with cell membrane protein complexes (e.g. desmosomes and integrin-associated complexes) (Fuchs and Cleveland, 1998) all the way to the nucleus to which it adheres via plectin (Wilhelmson et al, 2005). However, the organization of the keratin cytoskeleton depends upon the cell type in which it is expressed. For example, keratinocytes have a dense, pan-cytoplasmic network (Coulombe and Omary, 2002). Alternatively, polarized simple epithelial cells have a sparser network that is localized at the apical pole (Coulombe and

Omary, 2002). The location of keratin within a cell may translate to different functions in different contexts.

Depending on the cell type, the keratin cytoskeleton can be quite dynamic (Helfand et al, 2004). However, the co-factors regulating keratin dynamics are largely unknown. Unlike actin and microtubules, keratin can self-assemble with no defined "nucleator" (Kim and Coulombe, 2007). Self-assembly of keratin appears to occur at the periphery of the cell near focal contacts of the actin cytoskeleton (Windhoffer et al, 2006). Whether it requires these focal contacts for assembly is uncertain. Once synthesized, keratin filaments are extremely stable, boasting a long half-life (Kim and Coulombe, 2007). Despite this stability, keratin can be rapidly degraded by the proteasome in a ubiquitin- and phosphorylation-dependent manner (Ku and Omary, 2000). Mrj is one co-chaperone known to bind K8/K18 filaments and it is hypothesized to regulate keratin organization and/or turnover (Izawa et al, 2000). However, the mechanism by which this occurs remains elusive.

1.4.3 Keratin filaments are required for more than mechanical strength

The existence of more than forty diseases associated with IF proteins (Fuchs and Cleveland, 1998) emphasize the functional importance of the keratin cytoskeleton. Epithelial cells undergo extensive mechanical stress during growth, healing and development. In the past, the only identified function of the IF network was structural in nature. Evidence that keratins are required to maintain structural support of the cell comes from dominantly inherited epithelial fragility disorders, such as epidermolysis bullosa simplex and epidermolytic hyperkeratosis, diseases that causes skin blistering and

cell fragility due to loss-of-function mutations within keratin genes, such as K14 and K10 (Coulombe et al, 1991; Vassar et al, 1991; Porter and Lane, 2003). For the keratin network to provide sufficient structural support, it must amalgamate with the other cytoskeletons within the cell and with proteins at the nucleus and the cell membrane (Kim and Coulombe, 2007). A vast number of other cellular proteins that interact with keratin such as kinases, phosphatases and chaperone proteins have been identified (reviewed by Coulombe and Omary, 2002) and suggest that keratin filaments may play an additional, non-mechanical role in the cell.

Recent studies indicate that keratin is involved in the regulation of tissue growth (Kim et al, 2006) and cell cycle progression (Ku et al, 2002). Keratin proteins are widely expressed both temporally and spatially during embryonic development (Lu et al, 2005), a time when extensive tissue growth is occurring. K17, in particular, has been shown to interact with the adaptor protein 14-3-3σ, causing its partial retention in the cytoplasm (Kim et al, 2006). 14-3-3 proteins have been implicated in the regulation of protein synthesis via the indirect activation of mTOR kinase (Bertram et al, 1998; Cai et al, 2006). K17 deficiency in keratinocytes prevents 14-3-3σ localization in the cytoplasm and, as a result, these cells are small and have reduced Akt and mTOR activity (Kim et al, 2006). K18 and 14-3-3σ also associate (Liao et al, 1996) and preventing this interaction by mutating the 14-3-3σ binding site in K18 causes cell cycle arrest in adult hepatocytes (Ku et al, 2002). It would be interesting to examine whether K18-expressing trophoblast giant cells are smaller and have an altered endoreduplication cycle in the absence of K18 filaments. Together these data provide a role for the keratin cytoskeleton in normal tissue growth and development.

Similar to the actin and microtubule cytoskeleton, the keratin cytoskeleton is dynamic (Windhoffer et al, 2004). However, keratin does not bind and metabolize nucleotides and is not a track for motor molecules (Kim and Coulombe, 2007). Despite this, there are multiple examples of keratin involvement in protein targeting in polarized epithelial cells (Ameen et al, 2001; Salas et al, 1997; Gilbert et al, 2001; Styers et al, 2004; Oriolo et al, 2006). Polarized epithelia are divided into two cellular regions: apical or basal-lateral cell membrane to which certain proteins are segregated. Normal targeting of various apical proteins (e.g. CFTR ion channel, alkaline phosphatase and syntaxin 3) is disrupted in K8-deficient gut epithelium (Ameen et al, 2001). Furthermore, down-regulation of K19 in polarized CACO-2 epithelial cells in vitro also causes protein mistargeting to the apical membrane of the cell (Salas et al, 1997). One explanation for this mispolarization is that K8 interacts with GCP6, a protein that normally localizes microtubule organizing centers (MTOCs) to the subapical region of gut cells (Oriolo et al, 2006). In K8-null cells, MTOCs are mislocalized, which causes microtubule disorganization and therefore aberrant polarity within the cell. As more keratin interacting factors are identified, further understanding of the function of keratin will come to light.

1.4.4 The role of simple epithelial keratins during mammalian development

Simple epithelial keratins (K8, K18, K19) are historically absent from a growing list of human disease-causing keratin mutations suggesting that they may be necessary for embryonic development (Porter and Lane, 2003). Accordingly, K8, K18 and K19 are the earliest expressed keratins during mouse embryonic development (8-16 cell stage pre-

implantation embryos) (Lu et al, 2005). Despite this early expression, mice with loss-of-function mutations in K8, K18 and K19 indicate that these keratins are not necessary for development until midgestation (Hesse et al, 2000; Tamai et al, 2000; Jaquemar et al, 2003). Normally, K8 (a type II keratin) heterodimerizes with either K18 or K19 (both type I keratins) and the resulting K8/K18 or K8/K19 heterodimers then polymerize to form keratin filaments (see above, Lu et al, 2005). When the K18 or K19 genes were individually knocked out, the mice were viable and fertile (Tamai et al, 2000; Magin et al, 1998) suggesting redundant functions for these keratins. $K8^{-/-}$ (Jaquemar et al, 2003), $K8^{-/-}$;$K19^{-/-}$ (Tamai et al, 2000) or $K18^{-/-}$;$K19^{-/-}$ (Hesse et al, 2000) knockout conceptuses lack keratin filaments in simple epithelial cells and result in lethality by E10.5 due to what was described as extensive placental site hemorrhaging. Trophoblast giant cells surrounding the implantation site are particularly at risk, even though all trophoblast cells express these keratins (Lu et al, 2005). It is unclear, however, whether the cells themselves are fragile and break apart or whether the cells remain intact but the cell-cell adhesion complexes are weakened without their filamentous component, preventing proper adhesion to the neighboring cells. Regardless, when the barrier between the conceptus and the maternal tissue breaks, maternal blood inundates the space abutting the embryo resulting in lethality. A trophoblast defect was undoubtedly the cause of death in $K18^{-/-}$;$K19^{-/-}$ mutants given that when tetraploid aggregation was used to rescue the trophoblast lineage, conceptuses were able to survive until at least E14.5 (Hesse et al, 2005). Further research needs to be done to explore the role of K8, K18 and K19 in other trophoblast cell types, for example during the development of the labyrinth, in addition to

the investigation of other functions that may be disrupted independent of structural stability in the absence of these keratins.

1.5 Development of the chorioallantoic placenta

Survival and growth of the fetus are critically dependent on the placenta. It forms the interface between the maternal and fetal circulation, facilitating metabolic and gas exchange as well as fetal waste disposal. In addition, the placenta produces hormones that alter maternal physiology during pregnancy and forms a barrier against the maternal immune system (Cross et al, 2003). In humans and rodents, the fully developed placenta is composed of three major layers: the outer maternal layer, which includes decidual cells of the uterus as well as the maternal vasculature that brings blood to/from the implantation site; a middle "junctional" region, which attaches the fetal placenta to the uterus and contains fetoplacental (trophoblast) cells that invade the uterine wall and maternal vessels; and an inner layer, composed of highly branched villi that are designed for efficient nutrient exchange (Rossant and Cross, 2001). The villi are bathed by maternal blood and are composed of outer epithelial layers that are derived from the trophoblast cell lineage and an inner core of stromal cells and blood vessels.

Many targeted mutations in mice exemplify how single gene mutations can affect placental development or function (Tables 1.2, 1.3, and 1.4). A common feature among these placental mutants is the reduced ability to transport nutrients, which results in fetal growth restriction or, under more serious circumstances, embryonic death. The vast majority of the placental phenotypes that have been described to date result in defects in the establishment or maturation of the placental villi, the so-called labyrinth layer in

mice. Most of the defects are structural in nature, although some of the mutants offer insights into the regulation of nutrient transport.

1.5.1 General placental development and structure

Although the gross architecture of the human and mouse placentas differ somewhat in their details, their overall structures and the molecular mechanisms underlying placental development are thought to be quite similar (Rossant and Cross, 2001). As a result, the mouse is increasingly used as a model for studying the essential elements of placental development. In mice, placental development begins in the blastocyst at embryonic day (E) 3.5 when the trophectoderm layer is set aside from the inner cell mass (Fig. 1.1) (Cross et al, 2003). At the time of implantation (E4.5), the mural trophectoderm cells, which are those not in contact with the inner cell mass, become trophoblast giant cells (Rossant and Cross, 2001). These cells stop dividing, yet they continue to replicate DNA (endoreduplication) to become polyploid. In contrast, two diploid cell types emerge from the polar trophectoderm, which are those cells immediately adjacent to the inner cell mass: the extraembryonic ectoderm and the ectoplacental cone (Rossant and Cross, 2001). Subsequently, the extraembryonic ectoderm will develop into the trophoblast cells of the chorion layer and, later, the labyrinth. While developing, the labyrinth is supported structurally by an ectoplacental cone-derived layer called the spongiotrophoblast. It forms a compact layer of cells sandwiched between the labyrinth and the outer giant cell layer (Rossant and Cross, 2001). During later gestation, glycogen trophoblast cells begin to differentiate within the spongiotrophoblast layer, and subsequently they diffusely invade into the uterine wall (Adamson et al, 2000).

FIGURE 1.1 – Placental development of the mouse.

The origins of the mouse extraembryonic lineages begin at E3.5 with the formation of the blastocyst. At E8.0, chorioallantoic attachment occurs, followed by branching morphogenesis of the labyrinth to form dense villi, within nutrients are exchanged (E8.5-E10.5). The mature placenta (E14.5) consists of three layers: the labyrinth (Lab), the junctional zone including the spongiotrophoblast (SpT) and parietal trophoblast giant cells (P-TGC) and maternal decidua (De). Inset of E14.5 labyrinth layer: trilaminar trophoblast layer consists of a bilayer of syncytiotrophoblast (SynT-I and SynT-II) that surround the fetal blood vessel endothelium and the sinusoidal trophoblast giant cell (S-TGC) layer surrounds the maternal blood spaces. EPC, ectoplacental cone; TGC, trophoblast giant cell; GlyT, glycogen trophoblast cell; RBC, red blood cell. Adapted from (Watson and Cross, 2005).

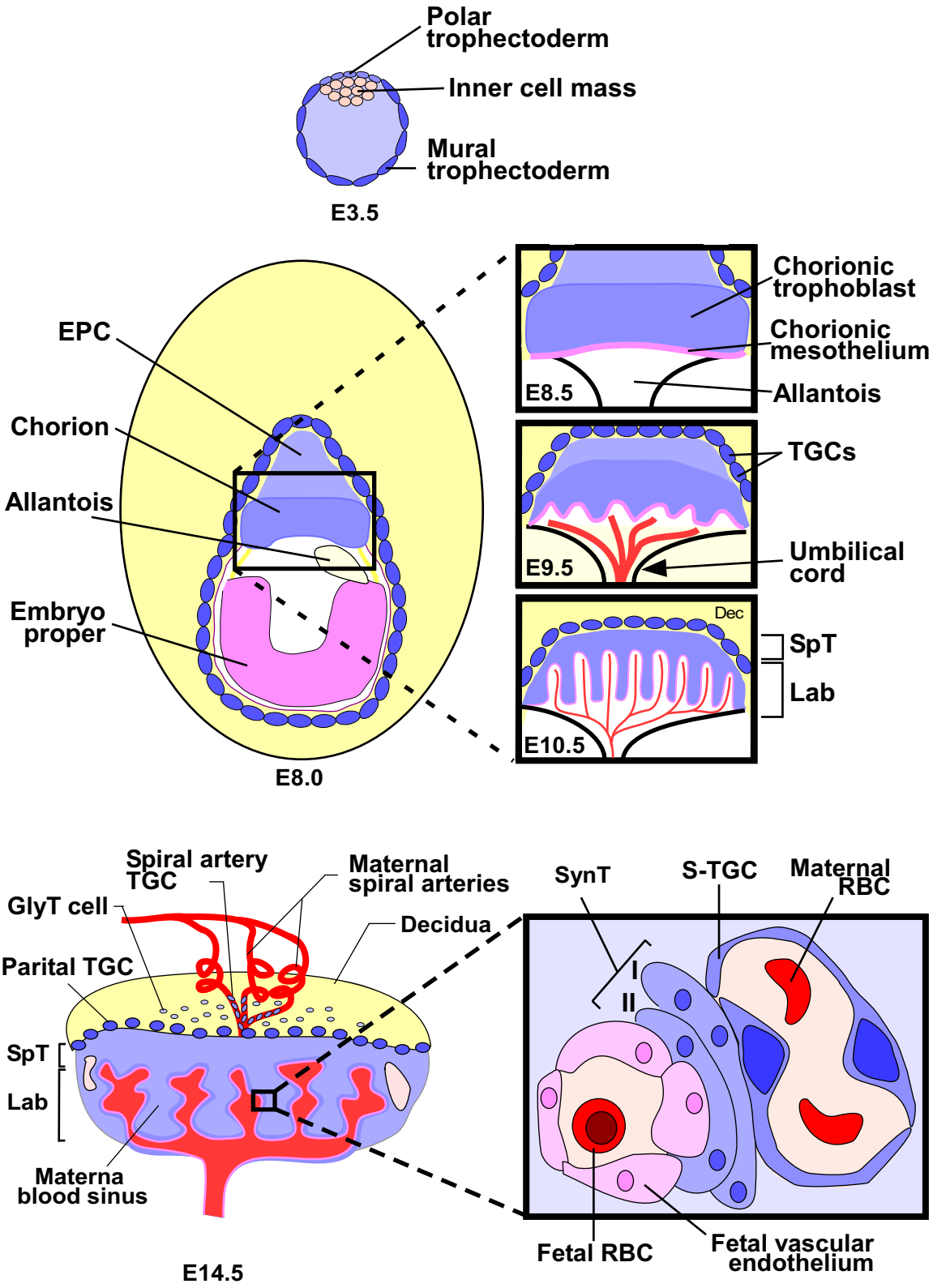
Polar trophectoderm
Inner cell mass
Mural trophectoderm
E3.5
EPC
Chorion
Allantois
Embryo proper
E8.0
Chorionic trophoblast
Chorionic mesothelium
Allantois
E8.5
TGCs
Umbilical cord
E9.5
Dec
SpT
Lab
E10.5
Spiral artery TGC
Maternal spiral arteries
GlyT cell
Decidua
Parital TGC
SpT
Lab
Materna blood sinus
E14.5
SynT
S-TGC
Maternal RBC
I
II
Fetal RBC
Fetal vascular endothelium

The vascular portion of the placenta is derived from extraembryonic mesoderm (allantois) that extends from the posterior end of the embryo at E8.0 (Cross et al, 2003). At E8.5, the allantois and the chorion join together in a process called chorioallantoic attachment. Soon thereafter, the chorion begins to fold to form the villi, creating a space into which the fetal blood vessels grow from the allantois (Cross et al, 2003). At this time, the chorionic trophoblast cells begin to differentiate into two labyrinth cell types. Multinucleated syncytiotrophoblast cells, formed by the fusion of trophoblast cells, surround the fetal endothelium of the capillaries (Fig. 1.1). Sinusoidal trophoblast giant cells line the maternal blood sinuses. Together the trophoblast and fetal vasculature generate branched villi of the labyrinth, which become larger and more extensively branched until birth (E18.5–19.5) (Adamson et al, 2002). Maternal and fetal blood flows in a countercurrent manner within the labyrinth to maximize nutrient transport (Adamson et al, 2002). If the labyrinth is not appropriately vascularized with suitable patterning, branching, and dilation, placental perfusion is impaired resulting in poor oxygen and nutrient diffusion (Pardi et al, 2002).

1.5.2 Chorioallantoic attachment

The first step in labyrinth development is chorioallantoic attachment. Defects in this process are among the most common causes of midgestation embryonic lethality (Rossant and Cross, 2001). The allantois and chorion trophoblast cells are derived in parallel from distinct cell populations. Originating from the epiblast, the allantois is composed of extraembryonic mesoderm (Downs et al, 2001). Many genes are necessary for proper development of the allantois (Table 1.2). However, the bone morphogenetic

TABLE 1.2 – Mouse mutants that affect chorioallantoic attachment

Gene	Gene Product	Expression in Placenta	Placental Phenotype of Mutant Mouse	Reference
Allantoic Development				
Bmp2	Bone morphogenetic protein	Mesodermal derivatives	Allantoic failure*	(Ying and Zhao, 2001)
Bmp4 **chimera**	Bone morphogenetic protein	Allantoic mesoderm, trophoblast	Allantoic failure	(Fujiwara et al, 2002)
Bmp5/Bmp7	Bone morphogenetic proteins	Allantoic mesoderm	Unknown defect of chorioallantoic attachment*	(Solloway and Robertson, 1999)
Brachyury (T)	T-box transcription factor	Allantoic mesoderm	Allantoic failure	(Rashbass et al, 1991)
Cdx2 **chimera**	Homeobox transcription factor	Mesodermal derivatives; trophoblast	Allantoic failure	(Chawengsaksophak et al, 2004)
Cdx2 $^{+/-}$***; Cdx4*** $^{-/-}$	Homebox transcription factor	Mesodermal derivatives; trophoblast	Allantoic failure*	(van Nes et al, 2006)
Edd	E3 ubiquitin ligase	Not known	Allantoic failure*	(Saunders et al, 2004)
Foxf1	Forkhead transcription factor	Allantoic mesoderm	Allantoic failure; loss of *Bmp4* expression	(Mahlapuu et al, 2001)
Lim1(Lhx1)	Lim domain transcription factor	Mesodermal derivatives	Allantoic failure	(Shawlot et al, 1995)
Smad1	BMP signaling intermediate	Mesodermal derivatives	Allantoic failure*; downreg of *Vcam1*	(Lechleider et al, 2001)
Chorionic Development				
Elf5 (Ese5)	Ets family transcription factor	Extra-embryonic ectoderm and chorionic trophoblast	Extra-embryonic ectoderm not maintained and therefore chorion not formed	(Donnison et al, 2005)
Err β***(Esrrb)***	Nuclear hormone receptor	Chorionic trophoblast	Failure of chorioallantoic attachment; trophoblast self-renewal defect	(Luo et al, 1997)
Fgfr2 **null**	Fibroblast growth factor receptor	Trophoblast derivatives	Failure of chorioallantoic attachment; trophoblast self-renewal defect*	(Xu et al, 1998)
Chorioallantoic Attachment				
α4 integrin (Itga4)	Adhesion molecule; VCAM1 receptor	Chorionic mesothelium	Failure of chorioallantoic attachment*	(Yang et al, 1995)

* Incomplete penetrance of chorioallantoic attachment defect

TABLE 1.2 – Mouse mutants that affect chorioallantoic attachment (continued)

Gene	Gene Product	Expression in Placenta	Placental Phenotype of Mutant Mouse	Reference
Chorioallantoic Attachment (continued)				
CtBP1/CtBP2	C-terminal binding proteins (downstream of WNT and BMP signaling)	Chorionic trophoblast	Unknown defect of chorioallantoic attachment*	(Hildebrand and Soriano, 2002)
CyclinF	Cell cycle regulator; SCF E3-ubiquitin ligase complex	Trophoblast	Unknown defect of chorioallantoic attachment*	(Tetzlaff et al, 2004)
Cyr61 (Cnn1)	ECM protein (integrin ligand)	Trophoblast; Allantoic mesoderm	Unknown defect of chorioallantoic attachment*	(Mo et al, 2002)
Dhd11 (ChlR1)	DNA helicase	Not known	Unknown defect of chorioallantoic attachment	(Inoue et al, 2007)
Dnmt1	DNA methyltransferase	Not known	Unknown defect of chorioallantoic attachment	(Li et al, 1992)
Erf	Ets2 repressor factor	Extraembyonic ectoderm; chorion; cuboidal cells of labyrinth	Failure of chorioallantoic attachment; chorionic trophoblast defect; failure of ectoplacental cavity closure	(Papadaki et al, 2007)
Grb2 **hypomorph**	Adaptor protein (MAPK pathway)	Trophoblast derivatives	Unknown defect of chorioallantoic attachment*	(Saxton et al, 2001)
Lpp3	Lipid phosphate phosphatase (inhibitor of Wnt signaling)	Chorionic trophoblast; Allantoic mesoderm/endoderm	Failure of chorioallantoic attachment; chorionic trophoblast defect	(Escalante-Alcalde et al, 2003)
Mpi	Mannose phosphotase isomerase	Not known	Unknown defect in chorioallantoic attachment	(DeRossi et al, 2006)
Mrj	Co-chaperone	Chorionic trophoblast	Failure of chorioallantoic attachment	(Hunter et al, 1999)
Rbp-Jκ	Transcription factor (Notch signaling pathway)	Mesodermal derivatives	Unknown defect of chorioallantoic attachment	(Oka et al, 1995)
Tcf1/Lef-1	Transcription factors (downstream of Wnt signaling)	Not known	Unknown defect of chorioallantoic attachment	(Galceran et al, 2001)
Vcam1	Adhesion molecule (α4 integrin ligand)	Allantoic mesoderm	Failure of chorioallantoic attachment*	(Gurtner et al, 1995; Kwee et al, 1995)
Wnt7b	Secreted signaling molecule	Chorionic trophoblast	Failure of chorioallantoic attachment; downreg. of α4 integrin	(Parr et al, 2001)

* Incomplete penetrance of chorioallantoic attachment defect

TABLE 1.2 – Mouse mutants that affect chorioallantoic attachment (continued)

Gene	Gene Product	Expression in Placenta	Placental Phenotype of Mutant Mouse	Reference
Chorioallantoic Attachment (continued)				
Yap1 (Yap65)	Yes-associated protein 1	Trophoblast derivatives, tip of allantoic mesoderm	Unknown defect of chorioallantoic attachment	(Morin-Kensicki et al, 2006)
Zfp36L1	Zinc finger protein (RNA transcript destabilizer)	Allantoic mesoderm; Chorionic trophoblast	Unknown defect of chorioallantoic attachment*	(Stumpo et al, 2004)

* Incomplete penetrance of chorioallantoic attachment defect

protein (BMP) signaling pathway appears to be particularly important. Critical molecules have been knocked out in mice, including Bmp2, -4, -5, and -7 (Fujiwara et al, 2002, Solloway and Robertson, 1999, Ying and Zhao, 2001) as well as Smad1, a downstream effector of BMP signaling (Lechleider et al, 2001). These mutants display mesodermal differentiation defects contributing to abnormal allantoic development. Fetal blood vessels arise de novo within the allantois due to vasculogenesis, and this is not dependent on attachment of the allantois to the chorion (Downs et al, 2001).

The majority of chorionic cells are derived from the extraembryonic ectoderm, although they overlie a thin layer of chorionic mesothelium (Rossant and Cross, 2001). Both Err2 (Errβ), a nuclear hormone receptor (Luo et al, 1997), and fibroblast growth factor receptor 2 (Fgfr2) (Xu et al, 1998) are expressed within chorion trophoblast cells and are required for maintenance of these cells. Proper formation of the chorion and allantois are necessary for attachment to occur. However, many mutants exist in which the allantois and the chorion appear to have formed normally, yet chorioallantoic attachment fails to occur (Table 1.2). It is known that attachment is dependent on the cell adhesion molecule VCAM1 (Gurtner et al, 1995, Kwee et al, 1995), which is expressed on the allantois, and its ligand α4-integrin (Yang et al, 1995), which is expressed by the chorionic mesothelium. However, not all *Vcam1*- or *α4-integrin*-deficient mice fail in chorioallantoic attachment, suggesting that other redundant adhesion mechanisms are involved. Indeed, other mutants with defects in chorioallantoic attachment also display incomplete penetrance (Table 1.2). It will be necessary to look more closely at these mutant placentas to determine if this seemingly random collection of genes shares a common molecular pathway, allowing for a better understanding of the attachment

process. Importantly, in the event that chorioallantoic attachment does occur in these incompletely penetrant mutants, they will often exhibit later defects in morphogenesis of the labyrinth.

1.5.3 Early chorionic patterning

The extraembryonic ectoderm is thought to be a homogeneous population of trophoblast stem cells at E7.5 (Tanaka et al, 1998, Uy et al, 2002). By E8.5, the ectoplacental cavity between the extraembryonic ectoderm and the ectoplacental cone close, resulting in the formation of the chorion which is hypothesized to contain at least three distinct layers of trophoblast precursor populations based on distinct cell morphologies (Hernandez-Verdun, 1974) and distinct gene expression patterns (Simmons et al, 2008). Each precursor population corresponds to one of the three trophoblast cell types of the mature labyrinth (Fig. 1.2). Specifically, the cells on the apical side of the chorion closest to the maternal blood sinuses express *Hand1*, a gene that is later expressed in sinusoidal trophoblast giant cells lining the maternal sinuses in the labyrinth (Simmons et al, 2007, Simmons et al, 2008). *Syna* gene expression is restricted to the chorionic cell layer just below *Hand1*-positive cells (Simmons et al, 2008). Within the mature labyrinth, *Syna* is expressed in syncytiotrophoblast cell layer I but not layer II (Simmons et al, 2008). Lastly, clusters of cells in the basal layer of the chorion closest to the allantoic interface express *Gcm1*, *Synb* and *Cebpα*, genes that are later exclusively expressed within syncytiotrophoblast cell layer II, which abuts the fetal endothelial cells in the mature placenta (Simmons et al, 2008).

FIGURE 1.2 – Early chorionic patterning determines labyrinth cell fate.

(Top) At the time of chorioallantoic attachment, the chorion is patterned into at least three layers based on gene expression patterns, each of which corresponds to (bottom) cells within the mature labyrinth layer of the placenta. Yellow, allantois and fetal vascular endothelium; purple, basal layer of chorion and syncytiotrophoblast layer II (express *Gcm1*, *Synb* and *Cebpa* genes); pink, apical layer of chorion and syncytiotrophoblast layer I (expresses *Syna*); green, base of the ectoplacental cone (EPC) and sinusoidal trophoblast giant cells (expresses *Hand1* [not exclusive]); red (top panel), fetal blood vessel. The top panel is adapted from (Simmons et al, 2008) and the bottom panel is adapted from (Watson and Cross, 2005).

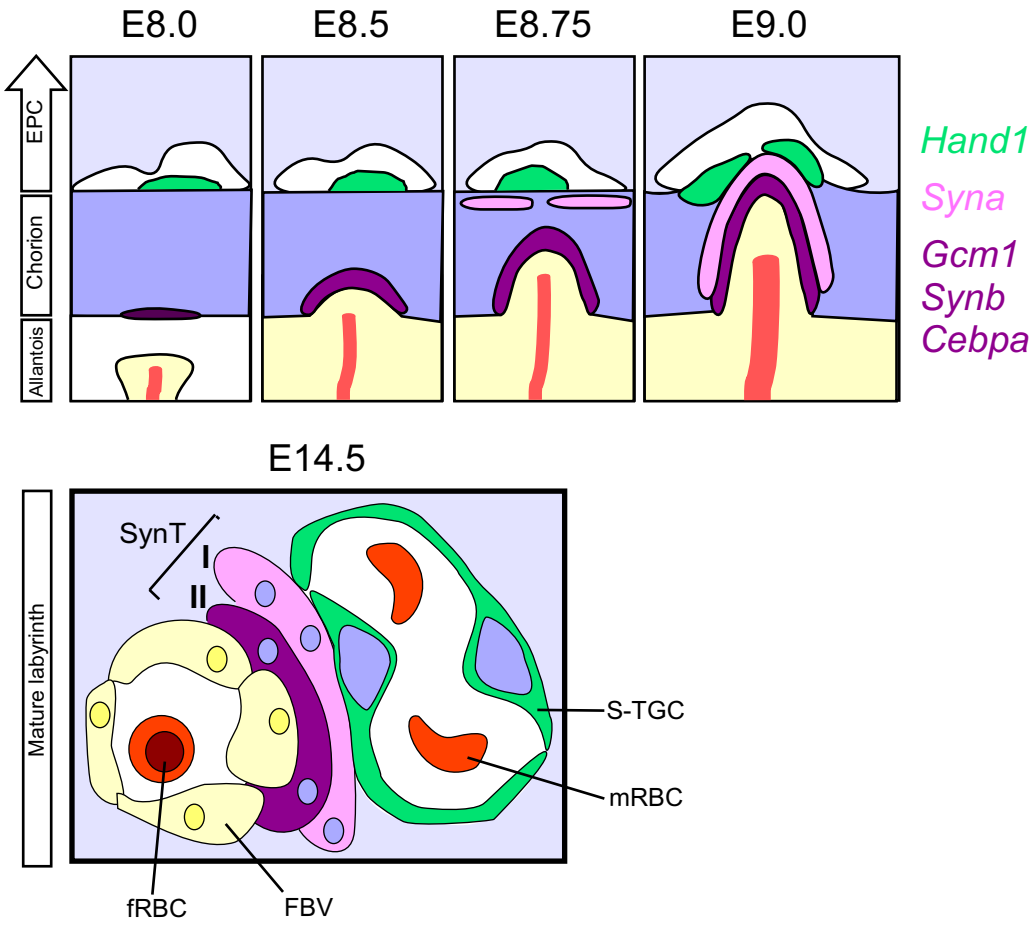
E8.0
E8.5
E8.75
E9.0
EPC
Chorion
Allantois
Hand1
Syna
Gcm1
Synb
Cebpa
E14.5
Mature labyrinth
SynT
I
II
S-TGC
mRBC
fRBC
FBV

To date, it is not well understood how these cell layers are specified or whether interaction between cell layers is necessary for proper development. However, neither the induction nor the maintenance of *Syna* or *Hand1* requires the presence of *Gcm1*/*Synb*/*Cepbα* expressing cells since *Syna* and *Hand1* patterns are properly specified in both *Gcm1* mutant and *Cebpα*;*Cebpb* compound mutant placentas (Simmons et al, 2008). The role that the allantois plays in the specification and/or maintenance of the chorionic layers is unknown. *Gcm1* expression is turned on prior to allantoic attachment (Anson-Cartwright et al, 2000). However, allantoic attachment is required for maintenance of its expression (Hunter et al, 1999; Stecca et al, 2002). Further examination of chorions from mutants that lack chorioallantoic attachment such as *Mrj* (Hunter et al, 1999) and *Grb2* (Saxton et al, 2001) should be assessed for proper chorionic patterning.

1.5.4 Initiation of branching morphogenesis

At E9.0, immediately after chorioallantoic attachment, evenly spaced primary villi begin to develop across the chorionic surface (Cross et al, 2003), and blood vessels from the allantois soon fill in the villous folds (Rossant and Cross, 2001). The process is often described as “vascular invasion” of the chorion, but this is misleading because the process requires active participation of chorion trophoblast and allantoic mesoderm. The branchpoints are actively selected by clusters of chorion trophoblast cells that express the *Gcm1* gene (Anson-Cartwright et al, 2000). As each branch elongates, *Gcm1* expression remains at the distal tip and continues to be expressed as long as villi are branching. *Gcm1* expression also initiates the differentiation of chorionic trophoblast into syncytiotrophoblast (Anson-Cartwright et al, 2000). Embryos deficient for *Gcm1* do not

initiate chorioallantoic branching; their chorion layer remains flat, trophoblast cells do not differentiate, and the fetal vasculature remains restricted to the allantois.

Gcm1 mRNA expression is first detected in the chorion before chorioallantoic attachment, and therefore branchpoint selection appears to be independent of allantoic attachment (Anson-Cartwright et al, 2000). However, the phenotypes of several mouse mutants have suggested that the initiation of morphogenesis after selection has occurred may require the interaction of chorion trophoblast and allantois. For example, the expression of *Gcm1* mRNA is down-regulated in *Mrj* mutant mice in which chorioallantoic attachment fails to occur (Hunter et al, 1999) and, in the absence of allantoic mesoderm, chorion trophoblast cells remain undifferentiated (Hernandez-Verdun and Legrand, 1975). Additionally, *Gcm1* expression is not maintained in *Hsp90β* mutant embryos that undergo chorioallantoic attachment but branching morphogenesis is stalled shortly thereafter due to defective allantoic development (Stecca et al, 2002). In addition, mutations in various genes within the Notch signaling pathway, including *Notch1/Notch4* (Krebs et al, 2000), the Notch receptor *Delta-like 4* (Duarte et al, 2004), and transcription factors *Hey1*/*Hey2* (Fischer et al, 2004) and *Rbpsuh* (Krebs et al, 2004), all appear to result in early blocks to chorioallantoic branching. Expression of these genes has only been reported within the allantoic mesoderm/blood vessels, suggesting that the fetal vasculature may be important for initiation of branching of the chorioallantoic interface. There are several caveats with this hypothesis, however. First, it is possible that these mutant mice are simply developmentally delayed or slowed and not arrested at the flat chorion stage, as with *Gcm1* mutants. To address this possibility, later-stage placentas should be examined. Second, *Hey1* mRNA has also been detected within the trophoblast

cells of the ectoplacental cone at least at E8.5 (K. Dawson and J. C. Cross, unpublished data), and therefore expression of the Notch signaling components is not restricted to allantois. Third, human chorionic villi develop before becoming vascularized (Castellucci et al, 2000), implying that vascular interactions are not important for villous development, at least in humans. Given these findings, it is clear that more work needs to be done to address the signaling interactions between chorion trophoblast and allantois during early stages of villous development.

1.5.5 Signalling and morphogenesis of the labyrinth

A large number of genes have been identified that are required for labyrinth development after chorioallantoic attachment (Table 1.3). However, for most of the genes, the specific cellular phenotype is not clear based on the published studies. Indeed, the most accurate description is that the labyrinth is simply underdeveloped or "small," meaning that the chorioallantoic interface remains under-branched and as a result there is a relative reduction in the density of fetal blood vessels (Fig. 1.3). Some mutants exhibit defects early in labyrinth development such that their chorionic plates remain compact with little branching and little fetal blood vessel growth (Barak et al, 1999, Begay et al, 2004, Giroux et al, 1999, Hildebrand and Soriano, 2002, Parekh et al, 2004, Yang et al, 2000). Embryos in this case will die between E10.5 and E12.5. Many other labyrinth phenotypes manifest slightly later, with some evidence of chorioallantoic branching but with thick trilaminar trophoblast layers and/or reduced vascularization (Arai et al, 2003, Constancia et al, 2002, Itoh et al, 2000, Rodriguez et al, 2004, Sachs et al, 2000, Ware et al, 1995).

TABLE 1.3 – Mouse mutants that affect branching morphogenesis of the labyrinth

Gene	Gene Product	Expression in Placenta	Placental Phenotype of Mutant Mouse	Reference
Branching Initiation				
Gcm1	Transcription factor	Chorionic plate; distal tip of branches in labyrinth	No labyrinth; block in branching morphogenesis	(Anson-Cartwright et al, 2000)
Hai-1 (Spint1)	Hepatocyte growth factor activator inhibitor type 1	Chorionic plate; Syncytiotrophoblast layer II	No labyrinth, no branching	(Kirchhofer et al, 2007; Szabo et al, 2007)
Branching Morphogenesis				
α-adreno-receptors 2a/2b/2c	Adrenaline receptors (MAPK pathway)	Trophoblast giant cells, spongiotrophoblast	Small labyrinth; low Erk1 and Erk2 expression	(Philipp et al, 2002)
α4 integrin (Itga4)	Adhesion molecule; VCAM1 receptor	Chorionic trophoblast	Small labyrinth	(Yang et al, 1995)
αv integrin (Itgav)	Transmembrane adhesion molecule	Trophoblast, allantoic mesoderm	Small labyrinth	(Bader et al, 1998)
Arnt (Hif-1β)	bHLH/PAS transcription factor	Labyrinth trophoblast	Small labyrinth; labyrinth trophoblast defect; decreased VEGF expression	(Adelman et al, 2000; Kozak et al, 1997)
β8 integrin	Transmembrane receptor (adhesion molecule)	Trophoblast giant cells	Small labyrinth	(Zhu et al, 2002)
B-Raf2	B-Raf transforming gene (Erk activation)	Not known	Small labyrinth	(Galabova-Kovacs et al, 2006)
Bmp2	Bone morphogenetic protein	Mesodermal derivatives	Not known	(Yang and Zhao, 2001)
Bmp5/Bmp7	Bone morphogenetic proteins	Allantoic mesoderm	Not known	(Solloway and Robertson, 1999)
Bruce	E2/E3 ubiquitin ligase	Chorionic and labyrinth trophoblast, endothelial cells	Labyrinth normal size, decreased branching	(Lotz et al, 2004)
Cacnb3	Beta subunit of voltage-dependent calcium channel	Chorion and labyrinth trophoblast	Isolated patches of disorganized labyrinth with fewer S-TGCs	(Singh et al, 2007)
C-EBPα/C-EBPβ	Transcription factors	Chorionic plate	Small labyrinth; limited branching potential	(Begay et al, 2004)
Cited1 (Msg1)	Transcriptional co-factor	Labyrinth trophoblast and Spongiotrophoblast	Small labyrinth, enlarged spongiotrophoblast	(Rodriguez et al, 2004)
Chm	Choroideremia, (MAPK pathway)	Ubiquitous	Small labyrinth	(Shi et al, 2004)

Table 1.3 – Mouse mutants that affect branching morphogenesis of the labyrinth (continued)

Gene	Gene Product	Expression in Placenta	Placental Phenotype of Mutant Mouse	Reference
Branching Morphogenesis (continued)				
c-Met	Met tyrosine kinase (HGF receptor)	Not known	Small labyrinth	(Maina et al, 1996)
CtBP2	C-terminal binding protein (downstream of WNT and BMP signaling pathways)	Labyrinth trophoblast and fetal blood vessels	Small labyrinth	(hildebrand and Soriano, 2001)
Cx26 (Gjb2)	Connexin, Gap junction protein	Labyrinth trophoblast	Small labyrinth, defect in glucose transport	(Gabriel et al, 1998)
Cx31 (Gjb3)	Connexin, Gap junction protein	Trophoblast derivatives	Small labyrinth; trophoblast proliferation defect	(Plum et al, 2001)
Cx45	Connexin, Gap junction protein	Allantoic mesoderm	Small labyrinth	(Kruger et al, 2000)
CyclinF	Cell cycle regulator; SCF E3-ubiquitin ligase complex	Trophoblast	Small labyrinth	(Tetzlaff et al, 2004)
Dlx3	Homeodomain transcription factor	Trophoblast derivatives	Small labyrinth	(Morasso et al, 1999)
Edd	E3 ubiquitin ligase	Not known	Not known	(Saunders et al, 2004)
Erk2	Extracellular signal related kinase 2 (MAPK signaling pathway)	Labyrinth trophoblast	Small labyrinth	(Hatano et al, 2003)
Erk5	Extracellular signal related kinase 5 (MAPK signaling pathway)	Not known	Small labyrinth	(Yan et al, 2003)
Fzd5	Wnt receptor	Labyrinth trophoblast	Small labyrinth	(Ishikawa et al, 1995)
***Fgfr2* null**	Fibroblast growth factor receptor	Trophoblast derivatives	Small labyrinth; trophoblast self-renewal defect	(Xu et al, 1998)
Fra1	AP transcription factor	Trophoblast giant cells, yolk sac	Small labyrinth	(Schreiber et al, 2000)
Gab1	Gab/Dos adaptor protein family (MAPK signaling pathway)	Labyrinth trophoblast	Small labyrinth	(Itoh et al, 2000; Sachs et al, 2000)
***Grb2* hypomorph**	Adaptor protein (MAPK pathway)	Trophoblast derivatives	Small labyrinth	(Saxton et al, 2001)
Hgf (Sf)	Hepatocyte growth factor/Scatter factor (through c-Met receptor)	Not known	Small labyrinth, fewer trophoblast cells	(Schmidt et al, 1995; Sibley et al, 1998)
Hsp90β (Hsp84)	Heat shock protein	Labyrinth trophoblast and allantoic mesoderm	Small labyrinth; trophoblast differentiation defect	(Voss et al, 2000)
Igf2 (P0)	Insulin-like growth factor 2	Labyrinth trophoblast	Small labyrinth, diffusional surface area decreased	(Constancia et al, 2002)

Table 1.3 – Mouse mutants that affect branching morphogenesis of the labyrinth (continued)

Gene	Gene Product	Expression in Placenta	Placental Phenotype of Mutant Mouse	Reference
Branching Morphogenesis (continued)				
Junb	AP-1 transcription factor	Trophoblast derivatives	Small labyrinth	(Schorpp-Kistner et al, 1999)
Keratin8/ Keratin19	Intermediate filaments (cytoskeleton)	Trophoblast derivatives	Small labyrinth; vascular lesions	(Tamai et al, 2000)
Laminin α5	Non-collagenous glycoprotein	Vascular endothelial cells	Small labyrinth, adhesion between vascular endothelial cells and trophoblast lost	(Miner et al, 1998)
Lbp-1a	Grainyhead transcription factor	Ubiquitous	Small labyrinth	(Parekh et al, 2004)
Lifr	Leukemia inhibitory factor receptor	Trophoblast and mesodermal derivatives	Small labyrinth, vascular lesions	(Ware et al, 1995)
Lkb-1	Ser/Thr kinase	Labyrinth	Small labyrinth	(Ylikorkala et al, 2001)
Lpp3 chimera	Lipid phosphate phosphatase (inhibitor of Wnt signaling)	Trophoblast; Allantoic endoderm and mesoderm	Small labyrinth	(Escalante-Alcalde, 2001)
Mek1 (Map2k1)	ERK/MAP kinase	Labyrinth trophoblast	Small labyrinth	(Giroux et al, 1999)
Mekk3 (Map3k3)	MAP kinase cascade	Not known	Small labyrinth	(Yang et al, 2000)
Muc1	Downstream effector of PPARγ pathway	Trophoblast cells surrounding maternal blood spaces	Small labyrinth, vascular lesions	(Shalom-Barak et al, 2004)
Ncx1	Na^{+}/Ca^{2+} exchanger	Trophoblast derivatives	Small labyrinth	(Wakimoto et al, 2000)
Nodal hypomorph	TGFβ family secreted signaling molecule	Spongiotrophoblast	Small labyrinth, large spongiotrophoblast and giant cell layers	(Ma et al, 2001)
Nte	Neuropathy target esterase	Chorion trophoblast, EPC	Small labyrinth	(Moser et al, 2004)
p38α MAPK (Map2k2)	Mitogen activated protein kinase	Labyrinth trophoblast	Small labyrinth	(Adams et al, 2000; Mudgett et al, 2000)
Pbp	PPARγ coactivator	Not known	Small labyrinth	(Zhu et al, 2000)
Pdgfb	Platelet derived growth factor chain B	Trophoblast, mesodermal derivatives	Small labyrinth	(Ohlsson et al, 1999)
Pkbα (Akt1)	Protein kinase Bα (PPARγ pathway)	Labyrinth	Small labyrinth	(Yang et al, 2003)

Table 1.3 – Mouse mutants that affect branching morphogenesis of the labyrinth (continued)

Gene	Gene Product	Expression in Placenta	Placental Phenotype of Mutant Mouse	Reference
Branching Morphogenesis (continued)				
Plcd1;Plcd2	Phospholipase C delta 1 and 3 isoforms	Trophoblast derivatives	Small labyrinth	(Nakamura et al, 2005)
Plk2 (Snk)	Polo-like kinase (cell cycle regulator)	Not known	Small labyrinth	(Ma et al, 2003)
Pparγ	Perioxisome proliferator-activating receptor γ transcription factor	Labyrinth trophoblast, EPC derivatives	Small labyrinth, defect in trophoblast differentiation	(Barak et al, 1999)
Prip (Rap250/Aib3)	PPARγ-interacting protein	Not known	Small labyrinth	(Antonson et al, 2003; Kuang et al, 2002; Zhu et al, 2003)
Raf1	Kinase in MAPK pathway	Not known	Small labyrinth	(Huser et al, 2001)
Rb	Retinoblastoma tumor suppressor	Throughout placenta, strongest in labyrinth	Excessive trophoblast proliferation, decreased vascularization, defect in essential fatty acid transport	(Wu et al, 2003)
Rxrα/Rxrβ	Retinoid nuclear receptors (dimerize with PPARγ)	EPC and derivatives	Small labyrinth, defect in trophoblast proliferation	(Wendling et al, 1999)
Smad1	BMP signaling intermediate	Mesodermal derivatives	Not known	(Lechleider et al, 2001)
Snx13	Sorting nexin protein family (endocytic pathway)	Not known	Small labyrinth	(Zheng et al, 2006)
Sos1	Ras-specific exchange factor (MAPK pathway)	Labyrinth and spongiotrophoblast	Small labyrinth, low ERK activity	(Qian et al, 2000)
Tfeb	bHLH –Zip transcription factor	Labyrinth trophoblast	Small labyrinth, decreased vascularization	(Steingrimmson et al, 1998)
UbcM4	Ubiquitin-conjugating enzyme	Ubiquitous	Small labyrinth	(Harbers et al, 1996)
Vcam1	Adhesion molecule (α4 integrin ligand)	Allantoic mesoderm	Small labyrinth	(Gurtner et al, 1996; Li et al, 1997)
Vhlh	Tumor suppressor	Trophoblast	Small labyrinth, decreased vascularization	(Gnarra et al, 1997)
Wnt2	Secreted glycoprotein	Allantoic mesoderm, chorionic plate, fetal blood vessels	Small labyrinth, vascular lesions	(Monkley et al, 1996)
Zfp36L1	Zinc finger protein (RNA transcript destabilizer)	Allantoic mesoderm; Chorionic trophoblast	Small labyrinth	(Stumpo et al, 2004)

The associated fetuses die either late in gestation or perinatally. The lethality in all cases is a result of insufficient metabolic exchange.

Despite the uncertainty about the specific underlying cellular defects, an important general conclusion to emerge from the study of small-labyrinth mutants is that labyrinth development depends on a number of intercellular signaling pathways. Specific pathways that are critical include Fgf (Xu et al, 1998), Egf (Threadgill et al, 1995), Notch (Krebs et al, 2000), Lif (Ware et al, 1995), Pdgfb (Ohlsson et al, 1999), and Wnt (Monkley et al, 1996). Likewise, a number of signaling adaptor proteins downstream of these signaling events are implicated given the similarity of their mutant phenotypes, including Chm (Shawlot and Behringer, 1995), CtBP2 (Hildebrand and Soriano, 2002), Erk2 (Hatano et al, 2003), Erk5 (Sohn et al, 2002, Yan et al, 2003), Gab1 (Itoh et al, 2000, Sachs et al, 2000), Grb2 (Saxton et al, 2000), Mek1 (Giroux et al, 1999), Mekk3 (Yang et al, 2000), p38α MAPK (Adams et al, 2000, Mudgett et al, 2000), and Sos1 (Qian et al, 2000). Based on restricted patterns of expression or chimera experiments, it is apparent that these signaling pathways are largely required in the trophoblast cell compartment of the labyrinth (Hatano et al, 2003, Philipp et al, 2002, Shi et al, 2004, Sohn et al, 2002, Thumkeo et al, 2003, Yan et al, 2003; reviewed in Rossant and Cross, 2001).

1.5.6 Direct and indirect controls on vascularization of the labyrinth

When morphogenesis of the labyrinth is diminished, one of the most obvious differences is that the layer remains cell dense and there are fewer maternal and fetal blood spaces. However, in the vast majority of labyrinth mutants the differences are likely to be

secondary effects, and there are only a few examples of mutants with primary vascular defects.

The maternal blood spaces in the labyrinth (termed sinusoids) often appear to be larger than normal in mutants (Mo et al, 2002, Rodriguez et al, 2004), but this can be an indirect effect. The maternal sinusoids within the labyrinth are lined and shaped by trophoblast cells and normally diminish in size as gestation proceeds as a simple consequence of the increasing density of trophoblast villous branching (Adamson et al, 2002). Therefore, whenever chorioallantoic branching is reduced, the maternal blood spaces in the presumptive labyrinth layer will remain larger. The more critical question would be whether the overall maternal blood volume in the presumptive labyrinth is altered in a mutant. This can be difficult to assess accurately in histological sections, however, because the blood will readily leak out during tissue dissection unless the uterine blood vessels are ligated before dissection and tissue fixation (Adamson et al, 2002; Natale et al, 2006).

Focusing only on fetal blood spaces within the labyrinth can give investigators a false impression about the nature of the primary defect in the labyrinth. Many of the genes whose mutant phenotypes were originally described as “vascular” in nature, are expressed exclusively within the trophoblast and not the vasculature itself (Table 1.3). More importantly, since fetal vessels can only grow into the core of villi within the labyrinth, all small labyrinth phenotypes with fewer villi would also be described as having fewer overall fetal blood spaces. The more accurate way to assess these mutants is to compare vascular density with the density of differentiated villi to determine if the

reduction in fetal blood vessel space is simply proportional to reduction in villi (Wu et al, 2003).

There are perhaps only a few examples of mouse mutants that show a reduction in the vasculature of the labyrinth that is not proportional to the extent of villous development (Table 1.4). The extracellular matrix protein Cyr61 (Mo et al, 2002) and the Notch-signaling components Dll4 (Duarte et al, 2004), Notch1/4 (Krebs et al, 2000), Hey1/2 (Fischer et al, 2004), and Rbpsuh (Krebs et al, 2004) are expressed in the vasculature itself, and mutations in their genes result in a poorly vascularized allantois. The *Esx1* gene, by contrast, encodes a homeobox transcription factor that is expressed solely in trophoblast cells of the labyrinth (Li and Behringer, 1998, Li et al, 1997). Placentas from *Esx1* mutants appear to undergo normal chorioallantoic branching morphogenesis but have obvious deficiencies in fetal blood vessel growth into the labyrinth villi (Fig. 1.3) (Li and Behringer, 1998). This indicates that trophoblast cells are actively involved in the vascularization of the labyrinth and suggests that a possible transcriptional target of Esx1 is a signal from the trophoblast cells that induces or directs vascular morphogenesis. The trophoblast-derived factor(s) that directly influence the development of fetal blood vessels in the labyrinth remain elusive.

The overall size and extent of vascularization of the placenta can change in an apparent attempt to compensate for primary defects. *Esx1* mutant placentas are actually larger than their wild-type counterparts, perhaps suggesting an attempt to compensate for the reduced vascularization and nutrient transport (Li and Behringer, 1998). Placentas from mothers who smoke throughout their pregnancy are disproportionately large (Pfarrer et al, 2002). Impaired oxygen transport caused by an increase in carbon

TABLE 1.4 – Mouse mutants that affect vascularization of the labyrinth

Gene	Gene Product	Expression in Placenta	Placental Phenotype of Mutant Mouse	Reference
Vascularization of labyrinth				
Alk1 (Acvrl1)	Activin receptor-like kinase 1	Allantois and fetal vascular endothelial cells	Small labyrinth, reduced vasculature	(Hong et al, 2007)
Cdx2$^{+/-}$;Cdx4$^{-/-}$	Homebox transcription factors	Allantois and fetal vasculature	Vascularization of allantois defective, reduced villous branching	(van Nes et al, 2006)
Cyr61 (Cnn1)	ECM protein (integrin ligand)	Trophoblast; Allantoic mesoderm/endothelium	Small labyrinth, downreg of VEGF	(Mo et al, 2002)
Dll4	Delta-like 4 (Notch ligand)	Umbilical and vitelline arteries	Small labyrinth, reduced fetal vasculature	(Duarte et al, 2004)
Esx1	Homeobox transcription factor	Chorion, labyrinth trophoblast	Vascularization defects; labyrinth trophoblast differentiation defects	(Li and Behringer, 1998; Li et al, 1997)
Hey1/Hey2	bHLH transcription factors (Notch signaling pathway)	Mesodermal derivatives	Small labyrinth; reduced fetal blood vasculature	(Fischer et al, 2004)
Notch1/Notch4	Transmembrane receptors	Vascular endothelial cells	No labyrinth; no fetal blood vessels	(Krebs et al, 2000)
Prdm1 (Blimp1)	Zinc finger transcriptional repressor	Vascular endothelial cells	Small labyrinth	(Vincent et al, 2005)
Rbpsuh	Transcription factor (Notch signaling pathway)	Not known	Small labyrinth, reduced fetal vasculature	(Krebs et al, 2004)

FIGURE 1.3 – Fetoplacental vascularization defects in various mutant placentas.

Within a wildtype placenta, the labyrinth trophoblast forms extensively branched villi, creating a path for the fetal vasculature to grow. *Esx1* mutants appear to undergo normal branching morphogenesis, yet the fetal vasculature does not develop normally. In contrast, *Rb*-deficient labyrinths exhibit defects in trophoblast proliferation and differentiation and thus have reduced branching and extension of the trophoblast villi. Accordingly, these placentas attempt to compensate for reduced nutrient transport by increasing their fetal capillary density. Most other mutants with a “small labyrinth” phenotype have reduced branching morphogenesis and villi formation and an apparent reduction in vascularization, yet detailed analysis have not been done to determine the nature of the labyrinth defect and/or if compensation occurs. P-TGC, parietal trophoblast giant cell; SpT, spongiotrophoblast; Lab, labyrinth; Dec, maternal decidua; UC, umbilical cord/allantois.

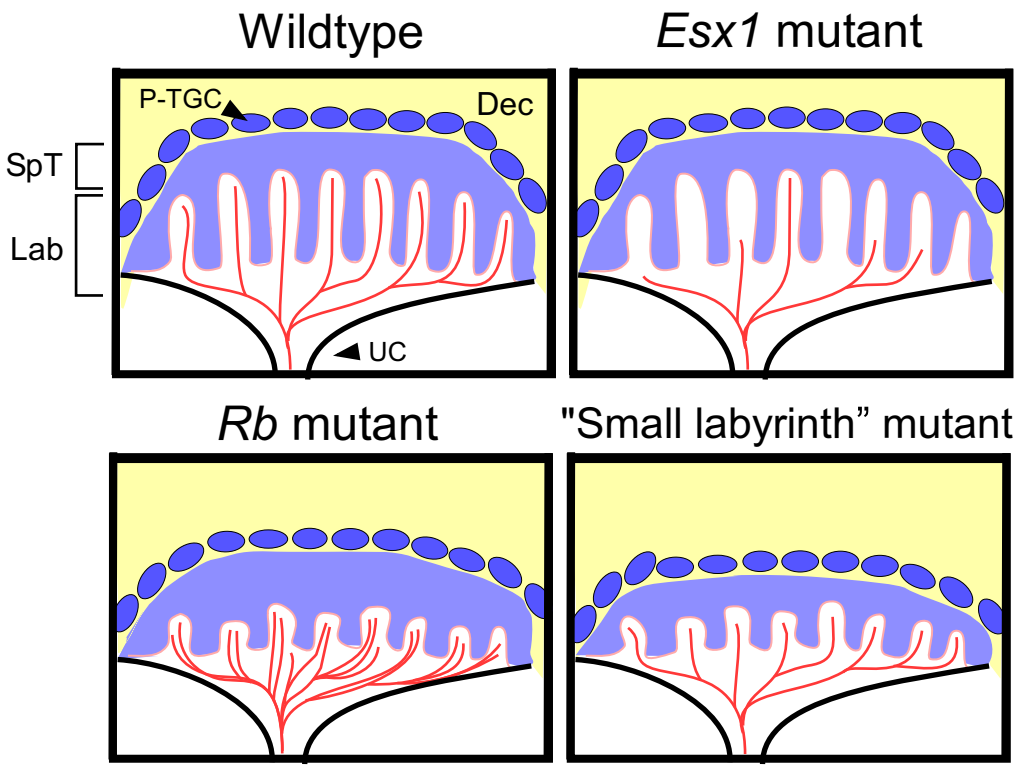
Wildtype
Esx1 mutant
P-TGC
Dec
SpT
Lab
UC
Rb mutant
"Small labyrinth" mutant

monoxide concentration induces additional angiogenesis of the fetoplacental vasculature (Pfarrer et al, 2002). Accordingly, one would expect that the majority of mutant placentas with defective labyrinth morphogenesis might also compensate for reduced nutrient and gas exchange. The *Rb* mutant placenta is a well-documented example of this phenomenon. *Rb*-deficient labyrinths have abnormal architecture associated with fewer villi due to an inappropriate proliferation of trophoblast cells and block to differentiation (Wu et al, 2003). The villous surface area of *Rb* mutant labyrinth trophoblast is reduced to 62% of wildtype. However, fetal capillary density is only reduced to 88% and essential fatty acid transport, as a measure of nutrient uptake capacity, is 86% of wild type (Wu et al, 2002). Therefore, the villi that are able to form in *Rb* mutants are relatively hypervascularized, and this is apparently able to partially compensate at least for fatty acid transport (Fig. 1.3). Proper detailed analyses of other small-labyrinth mutants may reveal similar compensatory measures.

1.5.7 Trophoblast defects as a cause of intrauterine growth restriction

Placental flux of nutrients throughout gestation is proportional to the size of the fetus, and therefore intrauterine growth restriction (IUGR) in humans may be linked to defects in either placental development or nutrient transport capacity (Kingdom et al, 2000, Sibley et al, 1998). The mouse models based on mutation of *Esx1* (Li and Behringer, 1998) and the placental-specific isoform of *Igf2* (Constancia et al, 2002) have surfaced as the only models that result in IUGR but not fetal death. Both mutations affect nutrient exchange by directly reducing uptake capacity of the villi, although they have distinctive defects in labyrinth trophoblast cells. Loss of *Esx1* prevents the normal development of the fetal

vasculature into the placenta, and thus nutrients from the mother cannot be passed adequately to the fetal bloodstream. The *Igf2* mutants, on the other hand, have reduced diffusional capacity, thereby reducing the amount of nutrient exchange that can occur. Based on this evidence in mice that not all IUGR placentas have the exact same phenotype, it is plausible that IUGR in humans may actually have distinct underlying changes. As a result, it may be important to categorize human IUGR into distinct conditions based on which developmental stage is affected, which cell type is affected, and whether nutrient transporters are properly expressed.

1.6 Early neural development

An embryo can survive until birth despite the occurrence of severe defects within the developing brain (Copp et al, 2003a). The formation of the neural tube is one of the most studied of all organ systems. However, little is understood about the mechanisms involved in its development from the neurectoderm of the neural plate to the neuroepithelium of the neural tube. Defects in neural tube closure including exencephaly and spina bifida are very serious and their consequences can range from perinatal death or still-birth to severe disability in humans. Therefore, fully understanding the morphogenesis of the neural tube and the molecular mechanisms behind it will help to prevent the occurrence of neural tube defects (NTDs).

1.6.1 Neurulation

Neurulation is the fundamental process that leads to neural tube development, the precursor of the brain and spinal cord. In the mouse, there are two phases of neurulation that occur in early embryonic development. Primary neurulation takes place when the

anterior region of the neural plate undergoes shaping, folding and fusion to form the neural tube that is destined to become the brain and most of the spinal cord (Copp et al, 2003a). Secondary neurulation, on the other hand, forms the neural tube in caudal-most regions of the spinal cord and is different from primary neurulation as neural folding does not occur. Instead, mesenchymal cells in the tail bud undergo condensation and epithelialisation to form a tube (Copp et al, 2003a). Many cellular events must occur during neurulation including cell shape changes, migration, proliferation and convergent extension, and therefore it is a highly complex and tightly regulated process (Kibar et al, 2007). If any of these processes go awry, serious NTDs result (Harris and Juriloff, 2007).

Primary neurulation (Fig. 1.4A), in simple terms, is initiated during early embryogenesis when the neural plate forms from the neurectoderm with the help of BMP antagonists from the underlying mesoderm, in addition to Wnt and FGF signalling (Stern, 2006). After its formation, the elliptical neural plate becomes a key-hole shaped structure (broad cranially and narrow in the spinal cord region) by undergoing a process called convergent extension whereby the neuroepithelial cells intercalate in the midline leading to a narrowing and lengthening of the neural plate (Copp et al, 2003a). Next, the neural plate bends at the midline to create bilateral neural folds (Fig. 1.5A). The dorsal regions of the neural folds elevate, contact each other at the midline and fuse to form the neural tube which is then covered by future epidermal ectoderm (Fig. 1.5B). Regional diversity is established very early in neural tube development such that the rostral neural tube is divided into the regions of the brain: forebrain, midbrain and hindbrain (rhombomeres). The caudal neural tube becomes the spinal cord.

FIGURE 1.4 – Shaping of the mouse neural plate prior to neural tube closure.

(A) Views from the left side and from the top of an E7.5-E8.0 embryo (left) and an E8.5 embryo (right). Each embryo has been stripped of its extra-embryonic membranes. At E7.5-E8.0, the embryo appears cup-shaped with an allantois protruding from the posterior end. The retreating node, which is the site of origin for most midline tissues including the notochord and neural tube floor plate, is prominent at the anterior end of the primitive streak. Anterior to the node, cells move medially and intercalate in the midline, a process called convergent extension, thereby increasing embryonic length relative to its width. By E8.5, the primitive streak is at the caudal part of the embryo, with a well defined anterior neural plate that is flanked by five pairs of somites. Closure site one occurs at the third somite pair. (B) A schematic drawing of the position of the neural tube closure sites in an E9.5 mouse embryo. The sites of closure are depicted by asterisks and numbers. The direction the neural tube closes from these sites is depicted by blue arrows. A neuropore is a region in which two sites of closure meet. This figure is adapted from (Copp et al, 2003a).

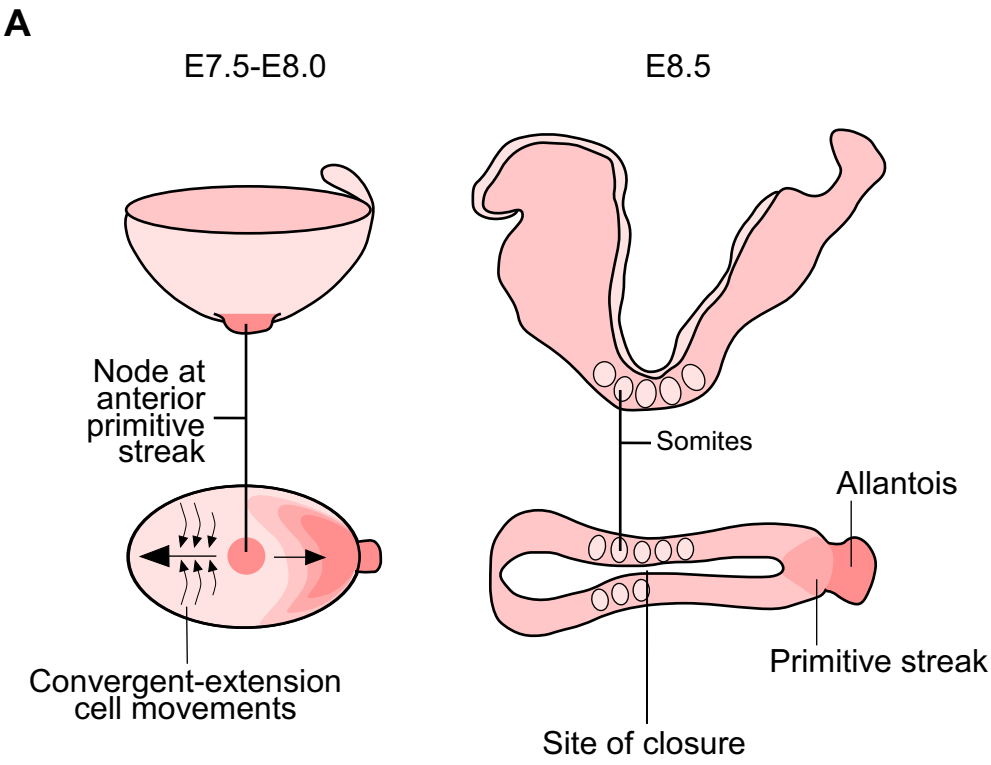
A
E7.5-E8.0
E8.5
Node at anterior primitive streak
Somites
Allantois
Primitive streak
Convergent-extension cell movements
Site of closure

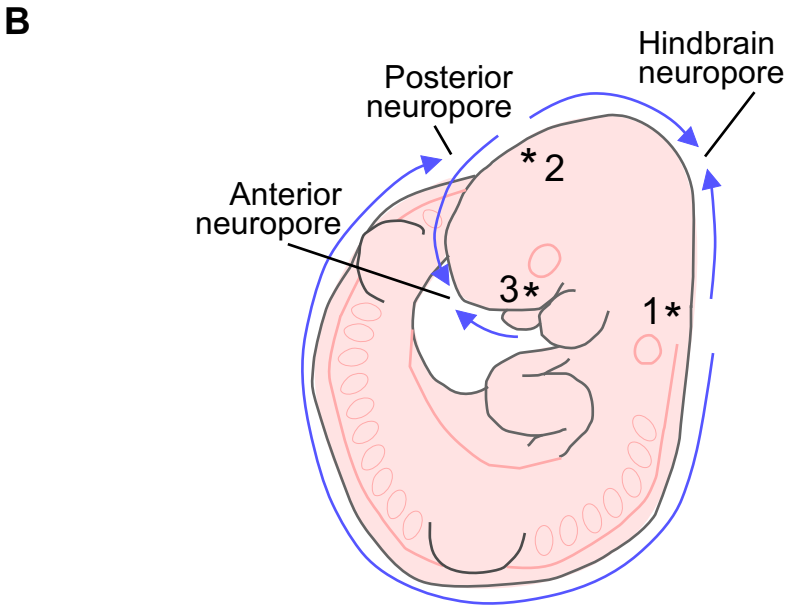
B
Hindbrain neuropore
Posterior neuropore
*2
Anterior neuropore
3*
1*

FIGURE 1.5 – Neural tube closure in the mouse spinal cord and cranial regions.

(A) After neural plate formation and the initial neural fold bending in the spinal cord region, the points at which the neural fold bends along the body axis varies in morphology, with bending solely at the medial hinge point at upper levels, at both medial and dorsolateral hinge points at the intermediate spinal levels and only at the dorsolateral hinge in the lower spine. (B) At the time of neural tube closure, the neural folds come together, adhere and fuse. This process results in the formation of two separate tissue layers: the epidermal ectoderm that contributes to the skin on the back of embryo and the neuroepithelium of the neural tube proper. Remodelling of the epithelia occurs and involves apoptosis at the dorsal midline, which separates these two cell layers. (C) Specific events that occur within the cranial region for closure to occur. The elevation of the neural folds is assisted by the expansion of the cranial mesoderm. Subsequently, dorsolateral bending begins at the apices of the neural folds in close proximity at the dorsal midline. Contraction of sub-apical actin, emigration of the neural crest, balanced proliferation and apoptosis in neuroepithelium all play a role in dorsolateral bending. This figure was adapted from (Copp et al, 2003a).

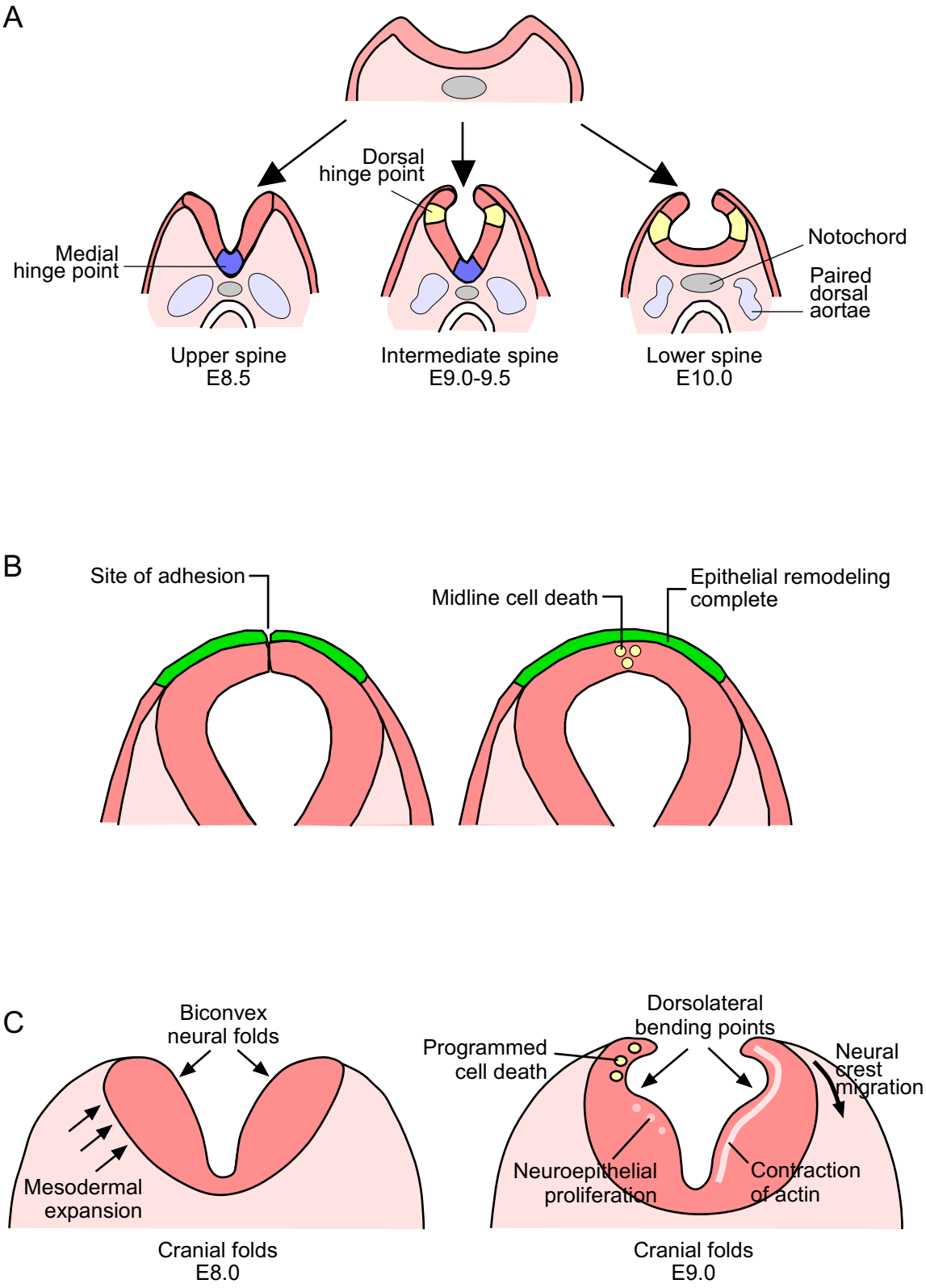
A
Dorsal
hinge point
Medial
hinge point
Notochord
Paired
dorsal
aortae
Upper spine
E8.5
Intermediate spine
E9.0-9.5
Lower spine
E10.0
B
Site of adhesion
Midline cell death
Epithelial remodeling
complete
C
Biconvex
neural folds
Mesodermal
expansion
Cranial folds
E8.0
Dorsolateral
bending points
Programmed
cell death
Neural
crest
migration
Neuroepithelial
proliferation
Contraction
of actin
Cranial folds
E9.0

Although neural tube closure is not necessary for the differentiation of neural cells or for the establishment of nerve connections, it is essential for brain development as a whole (Copp, 2005). Closure is initiated at three distinct locations and time points (Fig. 1.4B). The initial site of closure occurs between the cervical-hindbrain boundary at E8.0-8.5 (site 1). Subsequently, fusion proceeds both rostrally and caudally in a zipper-like fashion from the initial site of fusion (Nagy et al, 2003a) (Fig. 1.4B). Two additional de novo closure sites occur between the forebrain-midbrain boundary (site 2) and at the extreme rostral end of the forebrain (site 3) (Fig. 1.4B). Closure between these initiation sites leads to the completion of cranial neurulation at the anterior and hindbrain neuropores by E9.0 (Copp et al, 2003; Nagy et al, 2003a). Closure along the spinal cord is unidirectional and terminates at the posterior neuropore at the caudal end of the neural tube by E10.5 (Nagy et al, 2003a). When closure site 1 fails, almost the entire neural tube from the midbrain to the lower spine remain open (craniorachischisis). Failure of closure at sites 2 and 3 lead to exencephaly whereas spina bifida results from closure defects within the posterior neuropore (Kibar et al, 2007).

1.6.2 Mechanisms of neural tube closure

Despite the large number (~200) of diverse mouse models with disrupted neurulation available (Harris and Juriloff, 2007), we are only just beginning to grasp the intricacies of the molecular mechanisms required to regulate neural tube closure. Each of the key developmental milestones of neural tube closure above (convergent-extension, bending, elevation and fusion) is represented by NTDs in these mutants and emphasizes the vital molecular pathways and cell-cell interactions necessary.

Planar cell polarity genes are responsible for the convergent extension and elongation of the neural plate in many organisms. The proof lies in the disruption of the genes *dishevelled* and *strabismus* in *Xenopus* embryos, which are from the non-canonical Wnt/frizzled signalling pathway, which results in neural plates that do not undergo convergent extension (Park and Moon, 2001; Darken et al, 2002; Wallingford and Harland, 2001; Wallingford and Harland, 2002;). Instead, the neural plate is abnormally short and broad, and fails to undergo neural tube closure throughout its entire length due to widely spaced neural folds that are unable to meet at the midline. This NTD phenotype is recapitulated by mutations in mouse Wnt/frizzled pathway orthologs in the form of failure to close at site 1 resulting in craniorachischisis (exencephaly + spina bifida) (Curtain et al, 2003; Hamblet et al, 2002; Wang et al, 2006; Lu et al, 2004; Murdoch et al, 2001a; Kibar et al, 2001; Murdoch et al, 2001b; Copp et al, 2003b; Murdoch et al, 2003). Interestingly, all of the known mutants with craniorachischisis are caused by mutations in planar cell polarity-related genes. The exact mechanism by which the planar cell polarity pathway regulates convergent extension is poorly understood. However, it is hypothesized that the mitotic spindle orientation becomes randomized when polarity is disrupted (Gong et al, 2004; Ciruna et al, 2006). This threatens the organization of the neural plate and prevents proper intercalation of cells into the neuroepithelium.

Bending of the neural plate is required to form neural folds and occurs at two sites: the medial hinge point that lies along the midline of the neural plate overlying the notochord and the paired dorsolateral hinges (cranial and lower spinal cord regions only; Fig. 1.5) (Shum and Copp, 1996; Copp et al, 2003a). Little is known about the signals involved in initiating bending and elevation of the neural folds. However, sonic hedgehog

(Shh) is secreted by the notochord and is known to act as a negative regulator of dorsolateral bending. Evidence to support this includes mice with a null mutation in the gene encoding the Shh receptor *Patched1* (*Ptch1*). This mutation results in constitutively active Shh signalling, no dorsolateral bending and, therefore, severe NTDs (Goodrich et al, 1997). During the elevation of the neural folds after bending is initiated, the cells must undergo a dramatic shape change that requires the subapical actin microfilaments (Copp, 2005). Interestingly, the application of the drug cytochalasin D to the neural tube, which causes the disassembly of actin filaments, prevents cranial-only neural tube closure (Morriss-Kay and Tuckett, 1985; Smedley and Stanisstreet, 1986). In fact, the targeted mutation of many actin regulatory genes in mice including *shroom* (Hildebrand and Soriano, 1999), *vinculin* (Xu et al, 1998), *Marks* (Stumpo et al, 1995), *Abi1* (Rakeman and Anderson, 2006) and *RhoGAP p190* (Brouns et al, 2000) also resulted only in exencephaly and did not affect closure in the spinal cord region. This suggests that different molecules may be necessary for the regulation of actin during cranial versus spinal neural tube closure. Alternatively, the rearrangement of the actin cytoskeleton during spinal neurulation may induce different molecular signals and cellular events in this region compared to the cranial region. The mechanism that induces the actin filament contraction in either context is, to date, largely unknown.

Eventually to complete the formation of the neural tube, the neural folds come together at the dorsal midline and adhere. Disruption of this process inadvertently prevents neural tube closure. However, it has been difficult to distinguish experimentally between the failure of neural fold elevation and neural tube fusion in mutant embryos because defects in either process result in neural folds that are splayed open (Copp et al,

2003a). There are only a few genetic NTD models that are known specifically to affect neural fold adhesion and as a result, the process is poorly understood at a molecular level. Ephrin-A5 ligand and EphA7 receptor are required for neural fold fusion based on null mutations in these genes that result in exencephaly (Holmberg et al, 2000). This Ephrin-Eph interaction suggests a non-traditional adhesive role for proteins usually involved in axon repulsion. Other known adhesion molecules that are expressed by the neuroepithelium (N-CAM and N-cadherin) are not essential for closure since null mutations in these genes have normal neural tubes (Cremer et al, 1994; Radice et al, 1997). Further insight into the adhesion mechanism is required to fully understand neural tube closure.

The high frequency of mouse knockouts with exencephaly compared to spina bifida (Harris and Juriloff, 2007) indicates that cranial closure is far more susceptible to instability than spinal closure. Mechanistic themes only relevant to successful closure of the cranial region have come forward (Fig. 1.5C) including the hypothesis that a delicate balance within the neuroepithelium between the regulation of apoptosis (Kuida et al, 1998; Haken et al, 1998; Sah et al, 1996), proliferation (Wilson, 1980; Lardelli et al, 1996) and differentiation (Oka et al, 1995; Ishibashi et al, 1995; Zhong et al, 2000) is required for normal closure. Furthermore, cells outside of the neuroepithelium have an impact on cranial closure. Elevation of the cranial neural folds is highly dependent on proliferation and expansion of the cranial mesenchyme as evidenced by *Twist* and *Cart1* knockout mice, both of which display exencephaly due to proliferation defects in the mesenchyme (Chen and Behringer, 1995; Zhao et al, 1996). Mice that over-express the gap junction protein connexin 43 have defects in neural crest cell emigration and also

develop exencephaly (Morriss-Kay and Tan, 1987) suggesting that the two processes are interdependent.

1.6.3 Neural tube defects and folate

The prevalence of NTDs in the human population is quite high, with spina bifida as the most common defect (Blom et al, 2006). It has been well known for about 20 years that women can reduce their risk of having an NTD-affected pregnancy by supplementing their diet with the vitamin folate. In fact, studies in Canada have shown that folate fortification of cereal products has reduced the incidence of NTDs from 1.58 per 1000 births to 0.86 per 1000 births (46% reduction) (De Wals et al, 2007). Despite all of the efforts to understand the mechanism by which folate acts to prevent NTDs, it still remains unclear. Further complications lie in the fact that folate supplementation given to some NTD mouse models with mutations in molecular pathways thought to be independent of folate metabolism show a decrease in NTD frequency (Zhao et al, 1996; Barbera et al, 2002; Carter et al, 1999; Fleming and Copp, 1998; Wlodarczyk et al, 2006). However, this is not true of all NTD models (Essien, 1992; Greene and Copp, 1997; Ting et al, 2003; Juriloff et al, 2001; Holmberg et al, 2000; Chi et al, 2005; Stottmann et al, 2006). Additionally, the knockout mouse *folate binding protein 1* (*Folb1*) (Piedrahita et al, 1999) is the only one of the five known null-mutants for genes (*Cbs*, *Folr2*, *Mthfr*, *Mtr*) involved in the folate pathway that have NTDs (Watanabe et al, 1995; Piedrahita et al, 1999, Chen et al, 2001; Swanson et al, 2001). Yet, certain polymorphisms in human homologs of folate metabolic enzymes are associated with the appearance of NTDs in humans.

Recent studies have focused on the role of folate as a regulator of methylation reactions (see Fig. A1.1 in Appendix I for a schematic of the folate cycle) (Friso et al, 2002; Castro et al, 2004; Blom et al, 2006). The disruption of folate metabolism results in the trapping of methyl groups in the form of 5-methyltetrahyrofolate. This sequesters methyl groups, which blocks downstream methylation of targets such as DNA. DNA methylation is necessary to regulate transcription by manipulating chromatin structure. Interestingly, a genetic mutation in the *MTHFR* gene in humans (Friso et al, 2002; Castro et al, 2004) and folate deficiency in pregnant sheep results in a global reduction in the methylation of DNA (Sinclair et al, 2007). In addition to this, there are NTDs in null mutants of several genes that contribute to genome methylation or chromatin structure including *Dnmt3b* (Okano et al, 1999), *Dnmt3l* (Hata et al, 2002), *Gtf2i* (Enkhmandakh et al, 2006), *Hdac4* (Ishibashi et al, 1995) and *Smarca4* (Bultman et al, 2000). Together this suggests that the methylation status of DNA and chromatin structure is very important during development, especially with respect to proper transcription of genes required for neurulation.

1.7 Neural stem cells

A stem cell has the unique capacity to generate daughter cells with properties that are identical to the mother cell (self-renewal) in addition to cells with more restricted potential (differentiation). Stem cells are generally defined as multipotent cells meaning that they can generate multiple types of differentiated cells. If a cell is capable of only producing one type of differentiated cell, it is unipotent and considered a progenitor cell. Progenitors are usually the descendents of stem cells, and are different only in that they

are limited in their differentiating potential and capacity for self-renewal. Therefore, a stem cell must avoid cell-cycle exit and differentiation and yet ward off uncontrolled proliferation and tumour formation.

1.7.1 The properties of neural stem cells

Neural stem cells (NSCs) are a subtype of cell in the nervous system that can self-renew and generate both neurons and glia (Temple, 2001). The first NSCs were isolated from many regions of the embryonic mammalian central nervous system (CNS) (Temple, 1993; Cattaneo and McKay, 1990; Reynolds et al, 1992; Kilpatrick and Bartlett, 1993) and then later in the neurogenic regions of the adult brain (the hippocampus and subventricular zone) (Reynolds and Weiss, 1992; Lois and Alvarez-Buylla, 1993). During embryonic development of the CNS, the neuroepithelial cells of the neural plate are neural progenitor cells, can self-renew and will eventually differentiate into neurons or glia (Rao, 2004). The default model of neurogenesis suggests that neural tissue is induced by avoiding a series of signals that would otherwise promote their differentiation into non-neural lineages (Wnt, FGF and TGFβ superfamily signalling) (Tropepe et al, 2001). By the time of neural tube closure, these progenitor cells are already spatially restricted as determined by the highly spatially- and temporally-regulated expression of proneural genes such as basic helix-loop-helix (bHLH) transcriptional activators (Jessel, 2000). Proneural gene expression is the molecular switch between progenitor maintenance and neuronal differentiation. It is not known whether the neural plate consists solely of NSCs or both stem cells and restricted progenitor cells (Temple, 2001). However, by E10.0 in the mouse telencephalon, 5-20% of cells are estimated to be stem

cells (Kilpatrick and Bartlett, 1993; Qian et al, 2000; He et al, 2001) and this number decreases during development (Kalyani et al, 1998).

Studying NSCs can be difficult in vivo and therefore a method was established to analyze their properties in culture. Neurospheres are floating multicellular structures that can be obtained by exposing dissociated embryonic or adult CNS tissue to growth factors in culture (Reynolds et al, 1992; Reynolds and Weiss, 1992; Reynolds and Weiss, 1996) Neurospheres are heterogeneous groups of cells in that they contain only a small percentage (<5%) of stem cells amongst differentiated neurons, astrocytes and oligodendrocytes (Campos et al, 2004) and therefore provide a method to evaluate both NSC self renewal and multipotentiality. The capacity for self-renewal can be measured by the dissociating neurospheres and assessing their ability to form secondary spheres assuming that each stem cell has the ability to form a new neurosphere. The three dimensional structure and extracellular matrix deposition within a sphere is thought to provide conditions that create a niche required for NSC maintenance (Campos, 2004).

1.7.2 Factors regulating neural stem cell self-renewal

The ability of a stem cell to balance between self-renewal and differentiation is crucial to the maintenance of its population and for proper development of the tissue in question. When the self-renewal regulation goes awry, the result is tumour formation in the case of over-proliferation or developmental diseases due to the pre-mature loss of a stem cell population (Doe, 2008). NSCs like many other types of stem cells require a complex combination of signalling molecules, cell-matrix interactions and transcription factors for self-renewal.

Many studies have implicated both Notch and canonical Wnt signalling in the prevention of differentiation and the maintenance of stem cell identity. When Notch, its ligand Dll, and many of its downstream targets (RBPJκ, Hes1, Hes3) are mutated, the result is precocious differentiation and depletion of NSCs in mouse embryos (de la Pompa et al, 1997; Hatakeyama et al, 2004; Mizutani et al, 2007). Interestingly, temporal β-catenin stabilization during Wnt signalling plays a dual role: at E10, β-catenin promotes self-renewal (Chenn and Walsh, 2002) yet later in development it promotes differentiation (Hirabayashi and Gotoh, 2005). Further studies are necessary to understand which factors are involved in this switch in regulation (Doe, 2008).

As mentioned previously, neurosphere cultures have shown the importance of cell-ECM interaction in stem cell maintenance (Campos et al, 2004). In vivo, the basal processes of neuroepithelial cells are in contact with ECM (Doe, 2008). Integrin β1 (*Itgb1*), a receptor for ECM proteins such as laminin, is expressed in regions that contain embryonic and adult NSCs in vivo and in the periphery of cultured neurospheres where NSCs reside (Campos et al, 2004). When *Itgb1* was conditionally knocked out in the forebrain of mouse pups from postnatal day (P) 1 to P10, mutant forebrain tissue had reduced neurosphere-forming ability (Leone et al, 2005) indicating that both ECM components and integrin signalling is important to promote NSC self-renewal.

Proneural genes (e.g. *Mash1* (*Ascl1*), Ngn1) encode transcription factors that are spatially regulated and convey restricted differentiation of various neuronal cell types throughout the developing neural tube (Doe, 2008). Interestingly, both NSCs and newly differentiated neurons express proneural genes (Guillemot, 2007) suggesting that a mechanism must exist to prevent NSCs from differentiating even in the presence of

proneural gene expression. The SoxB1 family of proteins are also expressed in NSCs and differentiated neurons (Graham et al, 2003). Reduced *SoxB1* expression leads to the depletion of progenitor pools due to increased differentiation (Byland et al, 2003; Ferri et al, 2004; Graham et al, 2003). Alternatively, over-expression of *SoxB1* results in the maintenance of progenitor populations although without maintaining proliferation (Byland et al, 2003). Therefore, the balance of neurogenesis and NSC maintenance is regulated by the mutual antagonism of SoxB1 and Mash1/Ngn proteins (Bertrand et al, 2002; Byland et al, 2003, Ge et al, 2006). The Bmi1 Polycomb group transcription factor is another well known regulator of stem cell self-renewal not only in NSCs but also hematopoietic stem cells (Molofsky et al, 2003; Molofsky et al, 2005). *Bmi1*-deficient mice have a reduced neurosphere-forming ability postnatally since Bmi1 normally blocks the cell cycle inhibitor p16Ink4a to promote proliferation conditions (Molofsky et al, 2003). Therefore, not only is Bmi1 important for proliferation but also NSC self-renewal. However, it is unknown whether Bmi1 regulates self-renewal in embryonic NSCs.

1.8 Summary

Prior to the studies in this thesis, little was known about how Mrj functions in vivo during development of the trophoblast lineage or the embryo proper since only a few substrates had been identified in vitro. Our studies here reveal that Mrj regulates the keratin cytoskeleton in vivo by interacting specifically with K18-containing filaments and large keratin aggregates result in the trophoblast cells of *Mrj*-deficient chorions (Chapter 2). Genetic removal of these aggregates by generating *Mrj*;*K18* double knockout conceptuses rescued chorioallantoic attachment indicating that keratin aggregates are toxic to normal

trophoblast cell function. Further analysis of *Mrj*$^{-/-}$ chorionic trophoblast cells in vitro uncovered defects in actin cytoskeleton organization, adhesion molecule expression and in laminin (Ln) α5 extracellular matrix protein deposition resulting in erratic adhesion and migratory behaviour (Chapter 3). Interestingly, the adhesion phenotype was normalized by the provision of Ln α5 matrix to *Mrj*$^{-/-}$ TS cells. These cytoarchitectural defects were associated with disrupted chorionic polarity and patterning within *Mrj*$^{-/-}$ chorions in vivo required for the specification of labyrinth trophoblast cell precursor populations. Together this suggests that Mrj regulates normal cell-cell and cell-matrix interactions crucial for placenta formation and trophoblast differentiation. During our investigation of the placental phenotype, we observed that some *Mrj*-deficient embryos lacked neural tube closure or had small neural tubes due to reduced proliferation (Chapter 4). Furthermore, we showed that *Mrj*$^{-/-}$ neural stem cells had a reduced capacity to self-renew, a defect that was not dependent on associations with keratin or other intermediate filaments and emphasizes that Mrj interacts with more than one substrate in vivo.

Completely independent of the Mrj project, we began analyzing the function of another gene (Methionine synthase reductase, *Mtrr* or *Msr*) implicated in neural tube development (Appendix A). Mtrr is a key enzyme in the folate cycle required for the transfer of methyl groups to downstream targets such as DNA. We found that a grandmaternal mutation in the *Mtrr* gene resulted in severe congenital defects including developmental delay, placental and heart abnormalities, neural tube defects and embryonic lethality even when both the mother and the fetus were wildtype for *Mtrr*. This implies that the full impact of folate fortification may take more than one generation to overcome.

CHAPTER TWO

THE MRJ CO-CHAPERONE MEDIATES KERATIN TURN-OVER AND PREVENTS THE FORMATION OF TOXIC INCLUSION BODIES IN TROPHOBLAST CELLS OF THE PLACENTA

The contents of this chapter were originally published as (Watson et al, 2007). The tetraploid aggregation experiment was performed by C. Geary-Joo and the derivation of *Mrj*$^{-/-}$ trophoblast stem cells was performed by M. Hughes. The remaining experiments, as well as the writing of the majority of the manuscript, represent the work of E. Watson.

2.1 Abstract

Defects in protein-folding and -degradation machinery have been identified as a major cause of intracellular protein aggregation and of aggregation-associated diseases. In general, it remains unclear how these aggregates are harmful to normal cellular function. We demonstrate here that, in the developing placenta of the mouse, the absence of the Mrj (Dnajb6) co-chaperone prevents proteasome degradation of keratin 18 (K18; Krt18) intermediate filaments, resulting in the formation of keratin inclusion bodies. These inclusions in chorionic trophoblast cells prevent chorioallantoic attachment during placental development. We show further that keratin-deficient embryos undergo chorioallantoic attachment and that, by genetically reducing keratin expression in *Mrj*$^{-/-}$ conceptuses, chorioallantoic attachment was rescued. Therefore, the chorioallantoic attachment phenotype in *Mrj* mutants is not due to a deficiency of the normal keratin cytoskeleton, but rather is cytotoxicity caused by keratin aggregates that disrupt chorion trophoblast cell organization and function.

2.2 Introduction

Protein aggregation and the formation of intracellular protein inclusion bodies are associated with many degenerative disorders, including Parkinson's and Huntington's diseases, and with cirrhosis of the liver (Carrell, 2005). In many cases, the role of protein aggregates in disease pathogenesis is unclear. Efforts to understand aggregation disorders have focused mainly on mutations within the disease-associated protein. However, mounting evidence suggests that a major cause of protein inclusion body formation is failure of the protein quality-control system (McClellan et al, 2005). This surveillance

mechanism recruits both molecular chaperones and proteases to safeguard against protein aggregation by maintaining the equilibrium between protein folding and degradation (Hohfeld et al, 2001).

A malfunction in the ubiquitin-proteasome degradation pathway is hypothesized to be one cause of Mallory body formation in the hepatocytes of patients with chronic liver disorders (Bardag-Gorce et al, 2003; Bardag-Gorce et al, 2004; Denk et al, 2000). Mallory bodies are inclusions composed of the keratin intermediate filaments keratin 8 (K8; also known as Krt8) and keratin 18 (K18; also known as Krt18), as well as ubiquitin, the proteasome complex and molecular chaperones, including heat shock protein 70 (HSP70; HSPA1B) and heat shock protein 90 (HSP90) (Coulombe and Omary, 2002). Cells that have been treated with a chemical inhibitor of proteasome function (Bardag-Gorce et al, 2004) or that contain the UBB^{+1} ubiquitin mutation (Bardag-Gorce et al, 2003) form Mallory bodies due to an accumulation of non-degraded keratin.

Misfolded proteins also tend to aggregate. Proper protein folding within a cell often does not occur spontaneously and, thus, molecular chaperones are required for some proteins to reach its native state efficiently (Hartl and Hayer-Hartl, 2002). Hsp70 is a ubiquitous chaperone that, together with diverse co-chaperone binding partners, facilitates protein folding and the presentation of proteins to the proteasome for degradation (Esser et al, 2004). Co-chaperones of the DnaJ (Hsp40) protein family are characterized by a conserved J domain that regulates substrate binding and release by activating the ATPase activity of Hsp70 (Fan et al, 2003). These co-chaperones differ in their tissue and subcellular patterns of expression, and convey substrate specificity to

Hsp70 (Fan et al, 2003). However, little is known about the precise substrates that are regulated in this manner.

The *Mrj* (*M*ammalian *r*elative of Dna*J*; also known as *Dnajb6* – Mouse Genome Informatics) gene encodes a co-chaperone that is widely expressed throughout the adult mouse and during development of the embryo and placenta (Chuang et al, 2002; Dai et al, 2005; Hunter et al, 1999; Izawa et al, 2000; Seki et al, 1999). *Mrj*$^{-/-}$ embryos die at mid-gestation due to a failure of chorioallantoic attachment during placental development (Hunter et al, 1999). Recently, a few diverse Mrj-interacting proteins have been identified, including Huntington disease (HD) protein (Chuang et al, 2002) and K18 (Izawa et al, 2000). Here, we show that *Mrj* deficiency prevents normal keratin turnover, resulting in the formation of large keratin aggregates that are toxic to trophoblast cells, inhibiting their normal function.

2.3 Results

2.3.1 Mrj is required within the chorionic trophoblast and not the mesothelium

The chorion layer of the mouse placenta is composed of two cell types at embryonic day (E) 7.5: chorionic trophoblast cells and a thin inner layer of extra-embryonic mesothelium. Normally, chorioallantoic attachment begins at approximately E8.0 when the allantois, composed of extra-embryonic mesoderm, grows from the posterior end of the embryo across the exocoelomic cavity to first contact and then firmly attach to the chorionic mesothelium (Downs, 2002). Stable attachment is required for allantoic spreading along the surface of the chorion and for the formation of trophoblastic villi (reviewed by Watson and Cross, 2005). *Mrj* mutant conceptuses fail to undergo

chorioallantoic attachment and as a result do not form a mature placenta, dying by E10.5 (Hunter et al, 1999). *Mrj* mutant allantoises appear to both expand and elongate normally compared to wild type at E8.0 (Hunter et al, 1999), and grow across the exocoelomic cavity to contact the chorion. However, despite the close proximity of the allantois to the chorion, subsequent firm attachment to the chorion is not observed. Our initial observations have been confirmed in careful dissections of conceptuses after E8.5, showing the inability of the allantois to stay attached to the chorion in all mutants (n=81). Presumably as a consequence of failing to attach to the chorion, the allantois rapidly collapsed and shrunk back to form a bud of tissue at the posterior end of the embryo by E9.5 (Fig. 2.1). This phenomenon has been observed in other mutants with defects in chorioallantoic attachment (Hildebrand and Soriano, 2002; Tetzlaff et al, 2004; Yang et al, 1995).

Failure of chorioallantoic attachment in the *Mrj* mutants was presumably due to a chorionic cell defect, because *Mrj* expression has been detected within the chorion and not the allantois (Hunter et al, 1999). Using β-galactosidase activity driven from the *Mrj* genetrap allele (Fig. 2.2A) and Mrj antibody staining (Fig. 2.2B) on E8.25 histological sections, we detected Mrj expression throughout the chorionic trophoblast. However, expression within the chorionic mesothelium could not be determined because of the thinness of this cell layer.

To address better whether Mrj is required within the chorionic trophoblast and/or the mesothelium for chorioallantoic attachment, we used tetraploid aggregation, a technique that has previously been shown to produce chimeric conceptuses with genetically distinct chorionic cell compartments (Fig. 2.2C) (Tarkowski et al, 1977).

FIGURE 2.1 – The allantois in *Mrj*$^{-/-}$ conceptuses is initially expanded but gradually contracts back to become a compact 'bud' after E9.0. (A) The allantoises of three representative *Mrj*$^{-/-}$ embryos at E9.0, E9.25 and E9.5 (left to right). Each box includes an allantois and indicates the regions of higher magnification below (B-D). (B-D) Higher-magnifications of E9.0 (B), E9.25 (C) and E9.5 (D) allantoises (broken lines). Scale bars: 0.5 mm.

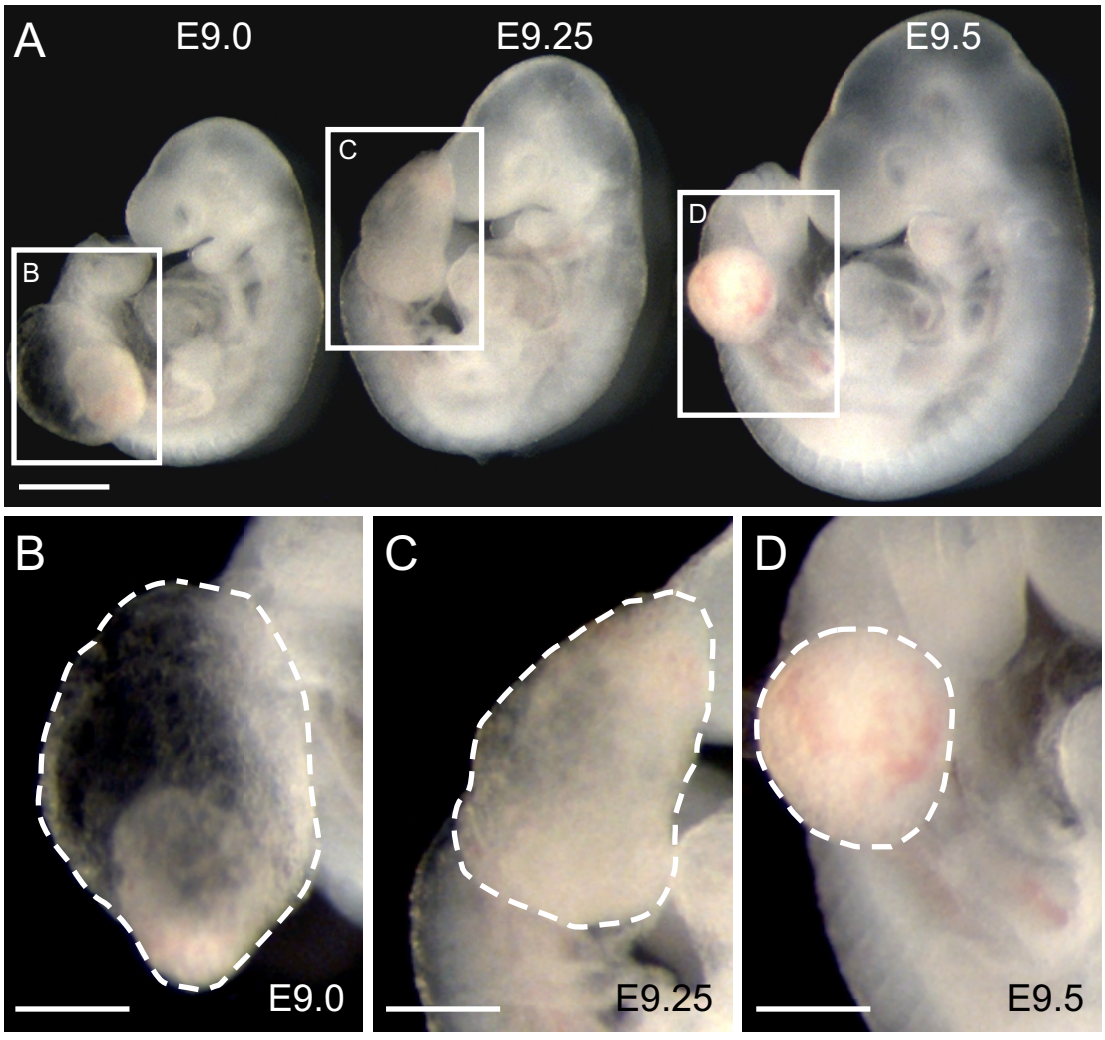
A
E9.0
E9.25
E9.5
B
C
D
B
E9.0
C
E9.25
D
E9.5

Wildtype tetraploid embryos were aggregated with diploid embryos derived from *Mrj* heterozygous matings. The resulting conceptuses developed so that the chorionic mesothelium, embryo proper and allantois were almost exclusively composed of diploid cells (Tarkowski et al, 1977). By contrast, wildtype tetraploid cells contributed to the trophoblast lineage, resulting in a chorionic trophoblast layer that contains wildtype cells (Tarkowski et al, 1977). Therefore, we expected that, if Mrj is required only within chorionic trophoblast cells, and not in the mesothelium or allantois, then chorioallantoic attachment would be rescued in *Egfp*↔*Mrj*$^{-/-}$ (tetraploid↔diploid) chimeric conceptuses.

Chimeric blastocysts (*n*=24) were transferred into the uteri of pseudopregnant female mice. At E9.5, 1 day after chorioallantoic attachment is normally complete, all 15 surviving chimeric embryos had undergone chorioallantoic attachment. Genotyping revealed that two of these embryos were *Mrj* mutants (Fig. 2.2D, E), indicating that Mrj is not required within the mesothelium or allantois for chorioallantoic attachment to occur. Furthermore, development proceeded normally up to E9.5 in *Egfp*↔*Mrj*$^{-/-}$ chimeric placentas, as indicated by the initiation of branching morphogenesis (Fig. 2.2H), similar to *Egfp*↔*Mrj*$^{+/+}$ and *Egfp*↔*Mrj*$^{+/-}$ littermates (Fig. 2.2F and data not shown). This is in contrast to *Mrj*-deficient chorions, which remained flat (Fig. 2.2G). These data imply that Mrj function was required exclusively within the trophoblast compartment at the chorioallantoic interface.

2.3.2 Keratin cytoskeleton is collapsed in primary cultures of Mrj mutant trophoblast cells

Previous studies have demonstrated that Mrj binds to both soluble and filamentous K18 (Izawa et al, 2000). Because, in our study, Mrj function in the placenta was restricted to

FIGURE 2.2 – *Mrj*$^{-/-}$ embryos fail to undergo chorioallantoic attachment because of defects within the chorionic trophoblast layer. (A, B) Expression of the β-galactosidase (β-gal; A; blue) and Mrj (B; red) proteins in E8.25 chorions. (C) Aggregation of a diploid *Mrj*$^{-/-}$ embryo (blue) with a wildtype tetraploid embryo expressing the *Egfp* transgene (green) results in a genetically mosaic chorionic trophoblast, ectoplacental cone and trophoblast giant cell layer (Rossant and Cross, 2001). The chorionic mesothelium, allantois and embryo proper are almost exclusively composed of *Mrj*-deficient diploid cells. (D, E) Rescued chorioallantoic attachment in an *Egfp*↔*Mrj*$^{-/-}$ chimeric conceptus at E9.5. (E) Higher-magnification of boxed region in D. (F-H) Initiation of branching morphogenesis in the placental labyrinth layer (arrowheads) at E9.5 in *Egfp*↔*Mrj*$^{+/+}$ (F) and *Egfp*↔ *Mrj*$^{-/-}$ (H) chimeric placentas, but not in a *Mrj*$^{-/-}$ chorion (G), which remains flat. al, allantois; ch, chorion; em, embryo; me, chorionic mesothelial layer; tr, chorionic trophoblast layer. Scale bars: 10 μm in A, B, F-H; 1 mm in D; 0.5 mm in E.

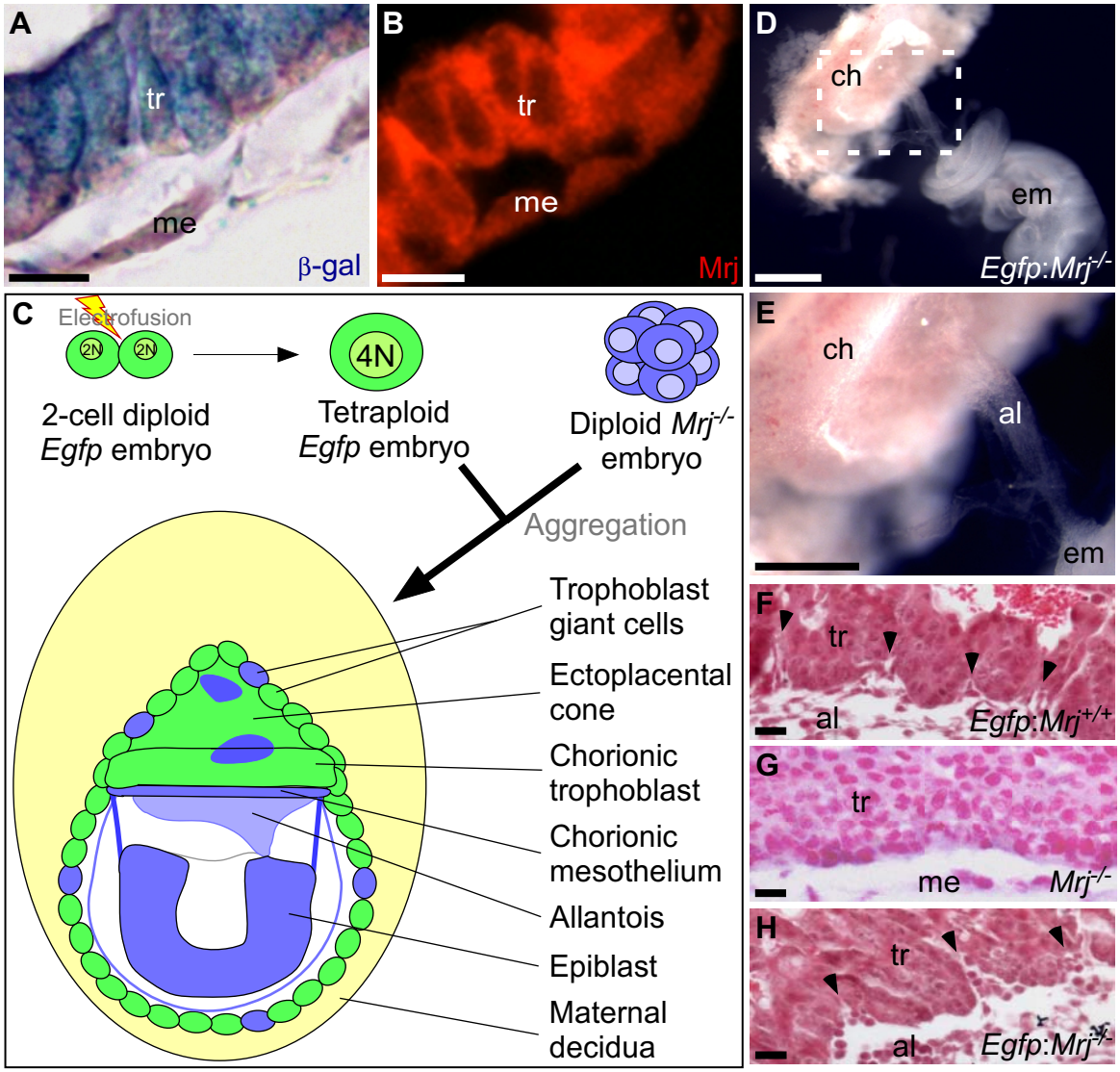
A
tr
me
β-gal
B
tr
me
Mrj
D
ch
em
Egfp:Mrj-/-
C
Electrofusion
2N
2N
4N
2-cell diploid
Egfp embryo
Tetraploid
Egfp embryo
Diploid Mrj-/-
embryo
Aggregation
Trophoblast
giant cells
Ectoplacental
cone
Chorionic
trophoblast
Chorionic
mesothelium
Allantois
Epiblast
Maternal
decidua
E
ch
al
em
F
tr
al
Egfp:Mrj+/+
G
tr
me
Mrj-/-
H
tr
al
Egfp:Mrj-/-

the trophoblast lineage, where keratin is also expressed, we explored whether *Mrj* mutant cells had a defective keratin cytoskeleton. Using immunofluorescence, we examined K18-containing filament organization within $Mrj^{-/-}$ trophoblast cells derived from primary cultures of explanted chorion-ectoplacental cone tissues. The chorionic trophoblast and ectoplacental cones are thought to be composed of multiple progenitor populations (Simmons and Cross, 2005), yet in culture they spontaneously differentiate primarily into trophoblast giant cells. Compared with 89.7% of wildtype trophoblast giant cells (*n*=659), only 36.9% of *Mrj*-deficient cells (*n*=634) had a normal, dense keratin filamentous network (Fig. 2.3A, B). Strikingly, the majority of $Mrj^{-/-}$ cells exhibited a collapsed keratin network, in which large perinuclear inclusions of keratin were present (53.9% compared with only 5.0% of wildtype cells). The remaining $Mrj^{-/-}$ cells contained either sparse keratin filaments (5.8%), or K18 levels were undetectable (3.4%).

All trophectoderm-derived cells express simple epithelial type I (K18 and K19) and type II (K7 and K8) keratins (Lu et al, 2005). Each keratin filament is composed of type I and type II heterodimers. K8 can dimerize with both K18 and K19 (Owens and Lane, 2003). Therefore, we also immunostained cells using K8, K19 and pan-cytokeratin antibodies. Interestingly, the results were similar to the collapsed K18 cytoskeleton or sparse K18 filaments observed (Fig. 2.3A, B). Ultrastructural analysis of keratin aggregates using electron microscopy in vivo revealed that they consisted of closely packed, parallel filaments (Fig. 2.3C). From this, we concluded that Mrj was required for the maintenance and/or turnover of the keratin cytoskeleton, but not for the assembly of filaments per se.

FIGURE 2.3 – The keratin cytoskeleton is collapsed in primary cultures of *Mrj*$^{-/-}$ trophoblast cells. (A) Keratin filament (red) organization in trophoblast giant cells derived from wildtype and *Mrj*$^{-/-}$ chorion/ectoplacental cone explants. (B) Quantification of the types of keratin-filament organization observed in trophoblast giant cells derived from wildtype and *Mrj*$^{-/-}$ chorion/ectoplacental cone explants. (C) Ultrastructure of a keratin aggregate (surrounded by broken line) in a *Mrj*$^{-/-}$ trophoblast giant cell at E8.25. (D) Mrj expression (red) in trophoblast giant cells of a wildtype conceptus at E8.25. Right, higher-magnification of boxed region in the left panel. (E) Nuclear (left), cytoplasmic (center), and both nuclear and cytoplasmic (right) Mrj expression in wildtype trophoblast giant cells in vitro. Arrowheads indicate trophoblast giant cells with undetectable Mrj expression. Broken line indicates the periphery of a trophoblast giant cell. (A, D, E) DNA is blue. ch, chorion; em, embryo; pan-CK, pan-cytokeratin; TGC, trophoblast giant cells. Scale bars: 10 μm in A, E; 0.5 μm in C; 20 μm (left) and 10 μm (right) in D.

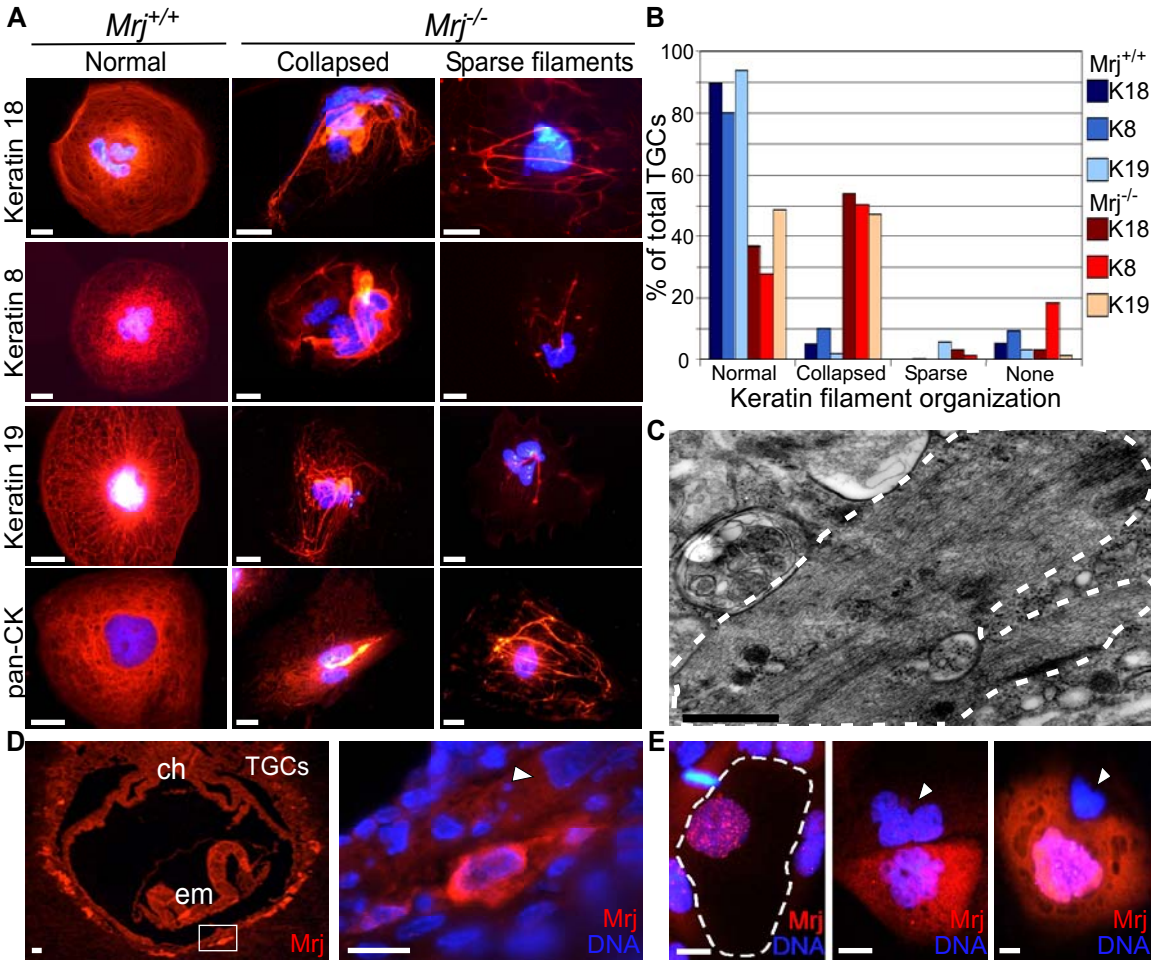
A
Mrj+/+
Mrj-/-
Normal
Collapsed
Sparse filaments
Keratin 18
Keratin 8
Keratin 19
pan-CK
B
% of total TGCs
100
80
60
40
20
0
Normal
Collapsed
Sparse
None
Keratin filament organization
Mrj+/+
K18
K8
K19
Mrj-/-
K18
K8
K19
C
D
ch
TGCs
em
Mrj
Mrj
DNA
E
Mrj
DNA
Mrj
DNA
Mrj
DNA

The keratin cytoskeleton appeared normal in approximately a third of *Mrj*-deficient trophoblast giant cells derived from explants (Fig. 2.3B). However, we noted that 37.4% of wildtype trophoblast giant cells (*n*=1478) had undetectable levels of Mrj at E8.25 (Fig. 2.3D), indicating that not all trophoblast giant cells would be expected to show a phenotype. This suggests an alternative method of keratin regulation in *Mrj*-negative cells. Mrj was heterogeneously expressed in cultured trophoblast giant cells, either within the nucleus, the cytoplasm or both (Fig. 2.3E). This may be attributed to the presence of several trophoblast giant cell subtypes that appear both in vitro and in vivo (Simmons et al, 2007) that may differentially express different Mrj splice isoforms (Hanai and Mashima, 2003; Tateossian et al, 2004; Mitra et al, 2008; Cheng et al, 2008).

2.3.3 Keratin inclusion bodies disrupt the organization of Mrj mutant chorionic trophoblast

To investigate whether Mrj regulates the keratin cytoskeleton within the chorion, we analyzed K18 expression both in vitro and in vivo. In contrast to trophoblast giant cells, which showed heterogeneous expression, Mrj was uniformly expressed throughout the chorionic trophoblast layer (Fig. 2.4A). Trophoblast stem (TS) cell cultures are an established model for studying chorionic trophoblast cells in vitro (Tanaka et al, 1998; Uy et al, 2002). Therefore, we derived both wildtype and *Mrj*-deficient TS cell lines from littermate blastocysts generated from *Mrj* heterozygote crosses. Approximately 80% of wildtype TS cells (*n*=494) had normal K18 expression (Fig. 2.4B), whereas the remaining 20% had undetectable levels. By contrast, 78% of $Mrj^{-/-}$ TS cells (*n*=469) lacked a normal keratin network and contained keratin inclusions similar to, albeit smaller than, those

seen within primary cultures of *Mrj*$^{-/-}$ trophoblast giant cells (Fig. 2.4C). K18 expression was less-apparent in histological sections of *Mrj*$^{-/-}$ chorionic trophoblast cells in vivo compared with wild type (Fig. 2.4E-H). However, electron microscopy confirmed the presence of filamentous aggregates (Fig. 2.4D). These data indicate that *Mrj* mutant chorionic trophoblast cells show the same type of keratin defects as trophoblast giant cells – both the lack of normal keratin cytoskeleton and the presence of large keratin aggregates – albeit at a higher frequency owing to the fact that a subset of giant cells do not express Mrj protein.

Next, we examined the ultrastructure of *Mrj*-deficient chorions to determine the effects of keratin aggregate formation on tissue integrity. In comparison to wildtype chorionic trophoblast cells (Fig. 2.4I, K), *Mrj*$^{-/-}$ cells were disorganized and rounded (Fig. 2.4J, L). This suggested that the adhesive properties of *Mrj*-null cells may have been altered. Therefore, we analyzed the expression of desmoplakin, a protein that links keratin filaments to desmosomes at the cell membrane. Remarkably, both *Mrj*$^{-/-}$ chorionic trophoblast cells and TS cells showed a significant reduction in desmoplakin immunofluorescence (Fig. 2.4O, P, R) compared with wildtype (Fig. 2.4 M, N, Q). Ultrastructurally, desmosomes appeared to be dense and disorganized in *Mrj*$^{-/-}$ chorionic trophoblast cells compared to wildtype (Fig. 2.4S, T). Together, these data imply that keratin inclusion bodies disrupt the organization of chorionic trophoblast cells, which in turn may affect the ability of the allantois to attach to the chorion. Notably, although they were disorganized, the *Mrj*$^{-/-}$ chorionic trophoblast cells showed no signs of cell death.

FIGURE 2.4 – Keratin inclusion bodies disrupt cell-cell adhesion and disrupt the organization of *Mrj*-deficient chorionic trophoblast cells. (A) Mrj expression (red) in a wildtype chorion at E8.25. (B, C) K18 expression (red) in wildtype (B; +/+) and *Mrj*-deficient (C; –/–) trophoblast stem (TS) cells. DNA is blue. (D) Ultrastructure of a keratin inclusion body (arrowheads) within a $Mrj^{-/-}$ chorionic trophoblast cell at E8.25. (E-H) K18 expression (red) in wildtype (E, F) and $Mrj^{-/-}$ (G, H) chorionic trophoblast cells at E8.25. (F, H) Higher-magnifications of boxed regions in E and G, respectively. (I-L) Morphology of *Mrj* mutant chorionic trophoblast cells in vivo (J) and in vitro (L) in contrast to wildtype cells (I, K). (M-P) Desmoplakin (Dp) expression (red) in wildtype (M, N) and $Mrj^{-/-}$ (O, P) chorionic trophoblast cells at E8.25. (N, P) Higher-magnifications of boxed regions in M and O, respectively. (Q, R) Desmoplakin expression (green) in wildtype (Q) and $Mrj^{-/-}$ (R) TS cells. (S, T) Electron micrographs of desmosomes (arrowheads) in wildtype (S) and $Mrj^{-/-}$ (T) chorionic trophoblast cells at E8.25. ch, chorion; DP, desmoplakin; EPC, ectoplacental cone; me, chorionic mesothelium; TGCs, trophoblast giant cells; tr, chorionic trophoblast. Scale bars: 10 μm in A-C, E-R; 0.5 μm in D, S, T.

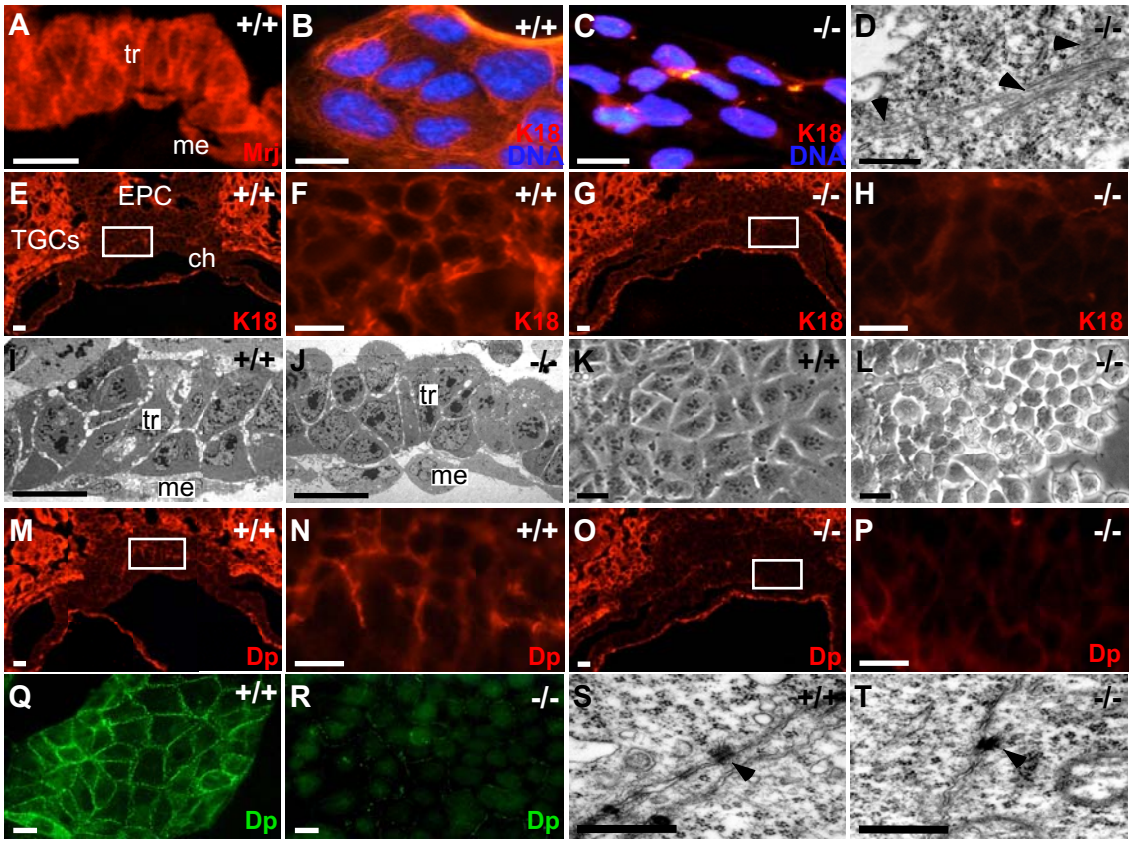
A
+/+
tr
me
Mrj
B
+/+
K18
DNA
C
-/-
K18
DNA
D
-/-
E
EPC
+/+
TGCs
ch
K18
F
+/+
K18
G
-/-
K18
H
-/-
K18
I
+/+
tr
me
J
-/-
tr
me
K
+/+
L
-/-
M
+/+
Dp
N
+/+
Dp
O
-/-
Dp
P
-/-
Dp
Q
+/+
Dp
R
-/-
Dp
S
+/+
T
-/-

2.3.4 Proteasome degradation of keratin filaments requires Mrj

Keratin filaments can oligomerize without catalysts or co-factors (Owens and Lane, 2003; Quinlan et al, 1986). Accordingly, keratin inclusions both in *Mrj*-deficient chorionic trophoblast and in trophoblast giant cells contained filaments (Fig. 2.3C, 2.4D), indicating that Mrj was not necessary for filament assembly. Therefore, we reasoned that Mrj may have played a structural role or have been required for keratin turnover. We found that Mrj protein did not co-localize with K18-containing filaments in trophoblast giant cells (Fig. 2.5), implying that Mrj was not playing a direct role in the organization of the keratin filamentous network.

It was previously shown that Mrj can interact with the soluble forms of K8/K18 (Izawa et al, 2000). Therefore, we next questioned whether Mrj regulated keratin by modulating the activity of the proteasome. Immunofluorescence of Mrj and 20S proteasome core subunits revealed that these two proteins co-localized (Fig. 2.6A). We then inhibited the proteasome complex in wildtype trophoblast giant cells by adding lactacystin (10 μM) and found that proteasome-inhibited cells contained large, perinuclear keratin inclusions (Fig. 2.6B) similar to *Mrj*$^{-/-}$ cells (Fig. 2.3A, 2.4C). Interestingly, Mrj co-localized with keratin inclusions within proteasome-inhibited cells (Fig. 2.6C). These data suggest that, without Mrj, keratin filaments are not properly degraded by the proteasome, leading to filament accumulation.

2.3.5 A minority of Mrj$^{-/-}$ *conceptuses have hemorrhages reminiscent of keratin null embryos*

FIGURE 2.5 – Mrj protein expression does not co-localize to K18-containing filaments. (A, B) Deconvolved images of a trophoblast giant cell immunostained for Mrj (red), K18 (green) and DNA (blue). (B) Higher-magnification of the boxed region in A. A cross-section (broken line) appears on the far right side of B. Scale bar: 10 μm in A.

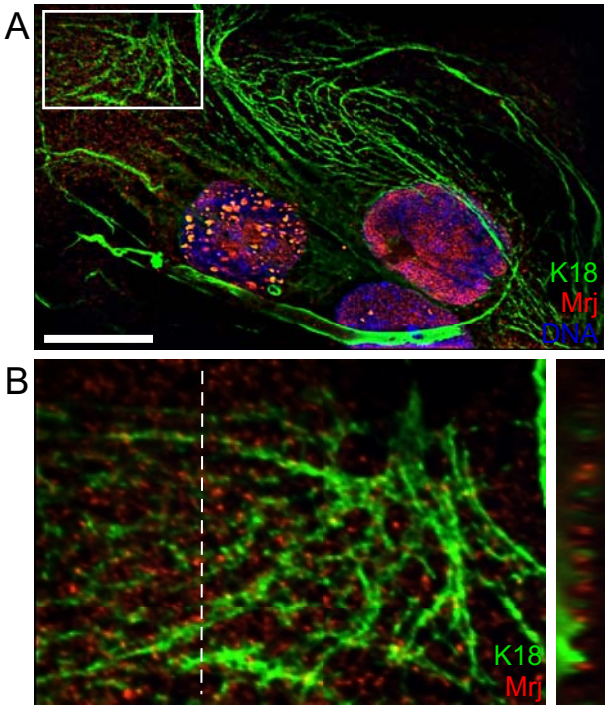
A
K18
Mrj
DNA
B
K18
Mrj

FIGURE 2.6 – Mrj is required for proteasome degradation of keratin filaments.

(A) Expression of Mrj (red) and 20S proteasome core subunits (green) in wildtype trophoblast giant cells in vitro. (B) K18 expression (green) in trophoblast giant cells cultured with (right) or without (left) the proteasome inhibitor clasto-lactacystin β-lactone. (**C**) Mrj expression (red) in trophoblast giant cells treated with clasto-lactacystin β-lactone. K18 is green. (B, C) DNA is blue. Scale bars: 10 μm.

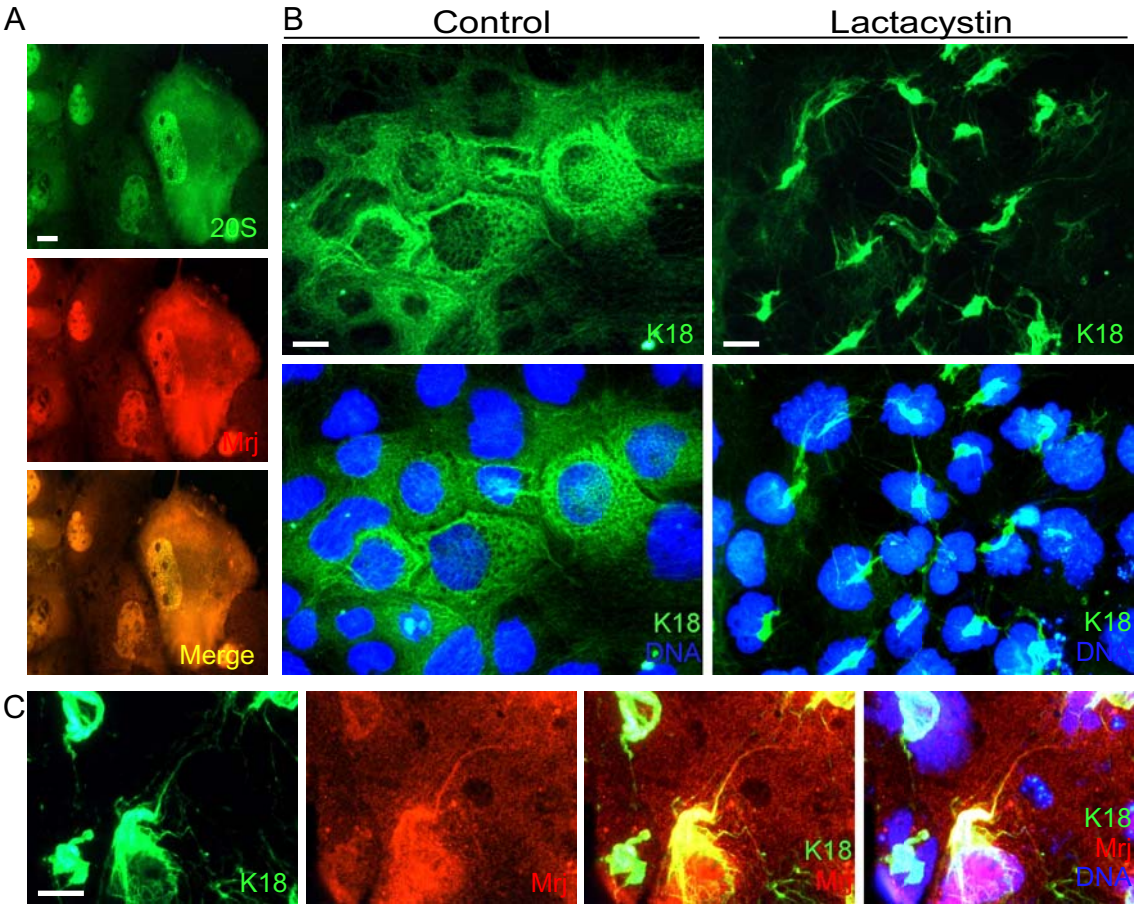
A
B
Control
Lactacystin
20S
Mrj
Merge
K18
K18
DNA
K18
K18
DN
C
K18
Mrj
K18
Mrj
K18
Mrj
DNA

Along with the formation of keratin aggregates, *Mrj*$^{-/-}$ trophoblast cells also lacked a properly organized keratin cytoskeleton. Previous studies have shown that an absence of the epithelial keratin cytoskeleton results in hemorrhaging within the trophoblast giant cell layer due to a loss of trophoblast cell integrity (Hesse et al, 2000; Jaquemar et al, 2003; Tamai et al, 2000). Interestingly, only 6.8% of *Mrj*-deficient embryos (4/59) developed placental site hemorrhages (Fig. 2.7). No hemorrhages were observed in wildtype or heterozygous conceptuses (0/147). The rarity of placental hemorrhage in *Mrj* mutants indicated that the consequences of *Mrj* deficiency differ from those of keratin deficiency.

2.3.6 Keratin inclusion bodies are toxic to chorionic trophoblast cell function

To investigate further whether keratin deficiency was responsible for the placental phenotype in *Mrj*$^{-/-}$ embryos, we assessed the occurrence of chorioallantoic attachment in keratin mutant mice. Chorioallantoic attachment was normal in both *K18*$^{-/-}$ and *K19*$^{-/-}$ knockout embryos (Fig. 2.8B, C and data not shown), resulting in mice that are viable and fertile (Hesse et al, 2000; Magin et al, 1998; Tamai et al, 2000). Although *K18*$^{-/-}$; *K19*$^{-/-}$ embryos have placental hemorrhages (Hesse et al, 2000), they all exhibited chorioallantoic attachment (*n*=8 double mutants from five litters) (Fig. 2.8D), indicating that this process can occur in the absence of a keratin cytoskeleton. This raised the possibility that keratin aggregation causes the *Mrj* phenotype. To address this, *Mrj*$^{+/-}$;*K18*$^{+/-}$ mice were mated and the resulting progeny (*n*=9 litters) were assessed for the presence of placental hemorrhages and chorioallantoic attachment. The incidence of placental hemorrhage in *Mrj* mutants was unaltered in *Mrj*$^{-/-}$;*K18*$^{+/-}$ (1/13) or *Mrj*$^{-/-}$;*K18*$^{-/-}$

FIGURE 2.7 – Placental hemorrhages reminiscent of *K18*/*K19* double-knockout embryos form in a minority of *Mrj*-null conceptuses. *Mrj*-deficient conceptuses at E9.5 with placental hemorrhages (white arrowhead) in the trophoblast giant cell layer (A) or chorion (B). Boxed region in left panels represents higher-magnification in right panels. Black arrowhead indicates an allantois that has not attached to the chorion (broken line in A). Scale bars: 1.0 mm. ch, chorion; ys, yolk sac.

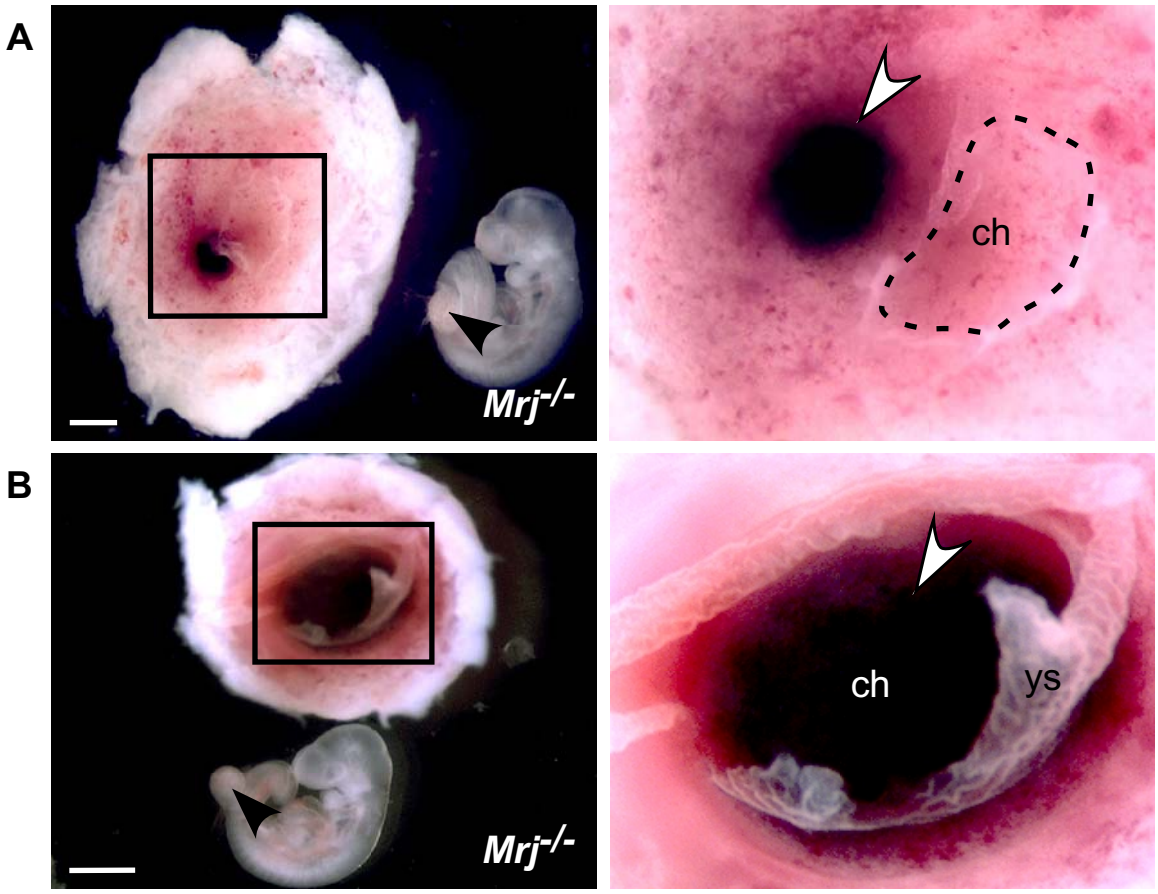
A
Mrj-/-
ch
B
Mrj-/-
ch
ys

FIGURE 2.8 – Chorioallantoic attachment is rescued in *Mrj*$^{-/-}$;*K18*$^{+/-}$ and *Mrj*$^{-/-}$;*K18*$^{-/-}$ conceptuses. (A) An unattached allantois (arrow) of an E9.5 *Mrj*$^{-/-}$ embryo appears as a bud at the posterior end of the embryo. Broken line outlines the chorion (Ch). (B-D) Chorioallantoic attachment of *K18*$^{-/-}$ (B, C) and *K18*$^{-/-}$;*K19*$^{-/-}$ (D) conceptuses at E9.5. (C) Higher-magnification of the boxed region in B. (E, F) Rescued chorioallantoic attachment in *Mrj*$^{-/-}$;*K18*$^{+/-}$ (E) and *Mrj*$^{-/-}$;*K18*$^{-/-}$ (F) conceptuses at E9.5. (G-I) Branching morphogenesis in *Mrj*$^{-/-}$;*K18*$^{+/-}$ (H) and *Mrj*$^{-/-}$;*K18*$^{-/-}$ (I) placentas with rescued chorioallantoic attachment at E9.5 compared to a *Mrj*$^{+/-}$;*K18*$^{+/+}$ littermate placenta (G). White arrowheads, fetal blood space/branchpoint; asterisks, maternal blood space; Ch, chorion; Al, allantois; black arrowhead, allantois. Scale bars: 1 mm in A, B; 0.5 mm in C, D; 0.5 mm in E, F; 20 μm in G-I.

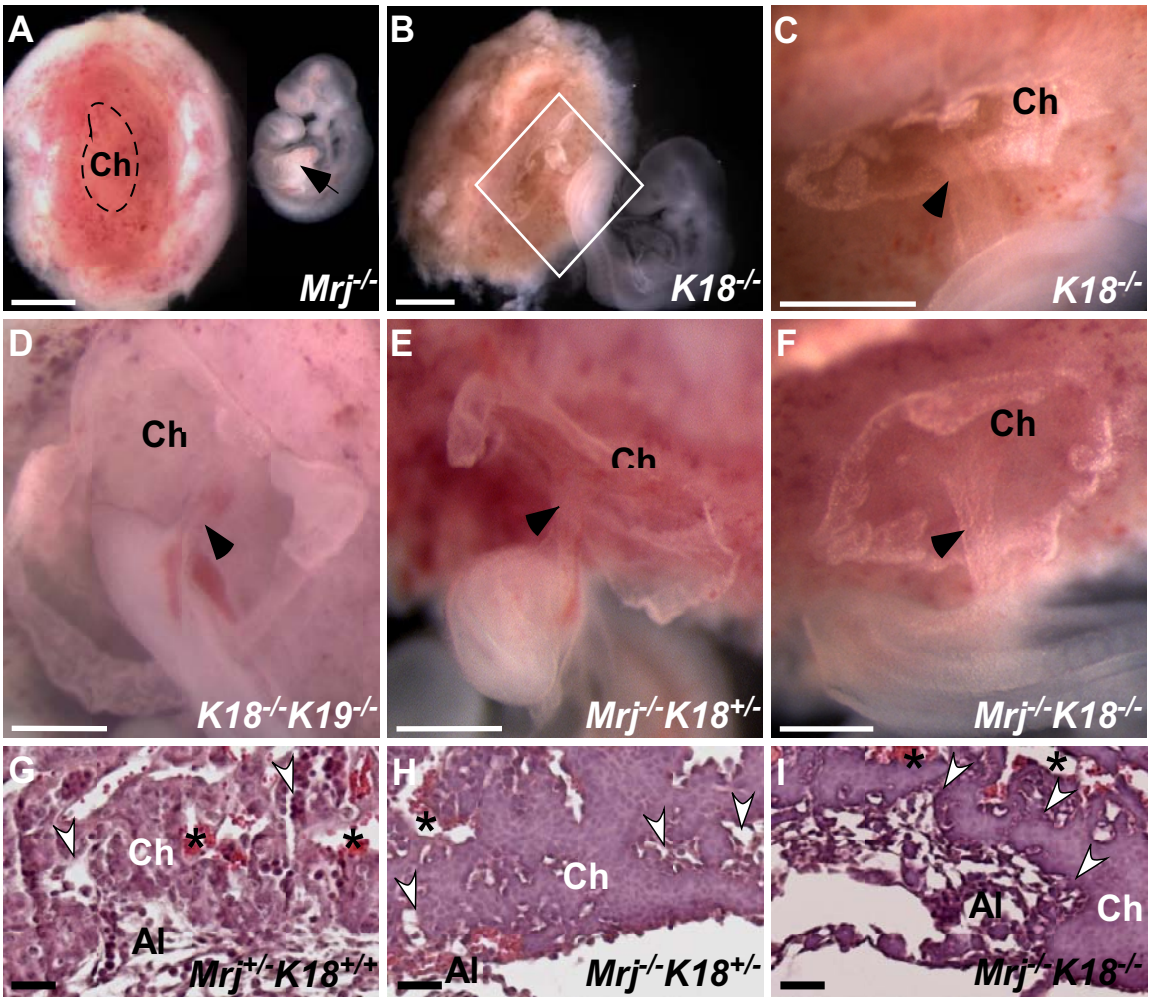
A
Ch
Mrj-/-
B
K18-/-
C
Ch
K18-/-
D
Ch
K18-/-K19-/-
E
Ch
Mrj-/-K18+/-
F
Ch
Mrj-/-K18-/-
G
Ch
Al
Mrj+/-K18+/+
H
Ch
Al
Mrj-/-K18+/-
I
Al
Ch
Mrj-/-K18-/-

(1/9) conceptuses. By contrast, 77% of *Mrj*$^{-/-}$;*K18*$^{+/-}$ embryos (10/13) and 100% of *Mrj*$^{-/-}$;*K18*$^{-/-}$ embryos (9/9) exhibited rescue of chorioallantoic attachment (Fig. 2.8E, F; Table 2.1). Histological analysis of rescued *Mrj*$^{-/-}$;*K18*$^{+/-}$ and *Mrj*$^{-/-}$;*K18*$^{-/-}$ placentas at E9.5 confirmed that chorioallantoic attachment had occurred and that subsequent villous formation was initiated. However, the chorionic plates remained compact with little branching or fetal blood vessel growth (Fig. 2.8H, I). Furthermore, fewer branchpoints were seen in *Mrj*$^{-/-}$;*K18*$^{+/-}$ chorionic plates (Fig. 2.8H) compared with those of *Mrj*$^{-/-}$;*K18*$^{-/-}$ (Fig. 2.8I). This contrasted with wildtype and *Mrj*$^{+/-}$;*K18*$^{+/+}$ littermate placentas (data not shown and Fig. 2.8G, respectively), which had extensive branching and vascularization within the labyrinth layers of their placentas.

Notably, *Mrj* and *K18* mutant mouse strains were maintained on different genetic backgrounds (CD1 and 129Sv, respectively). However, *Mrj*$^{-/-}$ conceptuses in both CD1 and 129Sv backgrounds fail to undergo chorioallantoic attachment (Hunter et al, 1999), indicating that the 129Sv genetic background, itself, is not sufficient to rescue chorioallantoic attachment in *Mrj*$^{-/-}$;*K18*$^{+/-}$ or *Mrj*$^{-/-}$;*K18*$^{-/-}$ embryos. Together, these results suggest that, by reducing the amount of keratin expressed, and thus aggregated, chorionic trophoblast cell function was restored and chorioallantoic attachment was rescued.

2.4 Discussion

It is well-known that protein aggregation is associated with several degenerative diseases. We have shown here that both *Mrj*-deficient trophoblast giant cells and chorionic trophoblast cells lack a normal keratin cytoskeleton and contain large keratin inclusion

TABLE 2.1 – Incidence of chorioallantoic attachment in E9.5 embryos from intercrosses of *Mrj*$^{+/-}$;*K18*$^{+/-}$ mice

Genotype	Observed embryos with chorioallantoic attachment (%)*	Observed genotypic proportions (%)†	Expected genotypic proportions (%)†
Mrj$^{+/+}$;*K18*$^{+/+}$	100 (5/5)	6.2	6.25
Mrj$^{+/+}$;*K18*$^{+/-}$	100 (8/8)	9.9	12.5
Mrj$^{+/+}$;*K18*$^{-/-}$	100 (6/6)	7.4	6.25
Mrj$^{+/-}$;*K18*$^{+/+}$	100 (14/14)	17.3	12.5
Mrj$^{+/-}$;*K18*$^{+/-}$	100 (18/18)	22.2	25.0
Mrj$^{+/-}$;*K18*$^{-/-}$	100 (6/6)	7.4	12.5
Mrj$^{-/-}$;*K18*$^{+/+}$	0 (0/2)	2.5	6.25
Mrj$^{-/-}$;*K18*$^{+/-}$	77 (10/13)	16.0	12.5
Mrj$^{-/-}$;*K18*$^{-/-}$	100 (9/9)	11.1	6.25

*Total number of embryos=81. †Total=100%

bodies. Furthermore, we have implicated Mrj in the regulation of keratin filament degradation. The inclusions resulting from *Mrj* deficiency are cytotoxic and prevent chorioallantoic attachment during placental development by affecting cell function but not viability.

2.4.1 The effect of **Mrj** *deficiency is distinct from keratin deficiency*

Cells containing keratin inclusions, such as Mallory bodies, also have a diminished keratin cytoskeleton (Denk et al, 2000). To date, this has complicated our understanding of the consequences of protein aggregation. In this study, we have shown directly that keratin deficiency and keratin inclusion bodies have different effects. In the developing placenta, complete deficiency of the keratin cytoskeleton (e.g. *K8* mutants or *K18/19* double mutants) is associated with normal chorioallantoic attachment, whereas keratin inclusions (e.g. *Mrj* mutants) are associated with a failure in chorioallantoic attachment.

An essential function of keratin is to protect the cell against mechanical stresses (Owens and Lane, 2003). Mice that lack *K8* (Jaquemar et al, 2003), both *K8* and *K19* (Tamai et al, 2000) or both *K18* and *K19* (Hesse et al, 2000) fail to form keratin filaments in simple epithelial cells, such as trophoblast cells. As a result, mutant embryos die at approximately E10.5 because of compromised trophoblast cell integrity, which leads to placental site hemorrhages that are particularly associated with trophoblast giant cells. Despite a compromised keratin cytoskeleton in *Mrj* mutants, placental hemorrhage was rare, indicating that *Mrj* deficiency is distinct from keratin deficiency. One explanation for this is that Mrj is not expressed in all trophoblast giant cells and, therefore, not all *Mrj*-deficient trophoblast giant cells lack a normal cytoskeleton or contain aggregates.

This implies the involvement of another co-chaperone in the regulation of keratin degradation within these cells. As a result, trophoblast giant cells with a normal keratin cytoskeleton are probably interspersed with affected cells. This arrangement may be sufficient to maintain the integrity of the trophoblast giant cell layer surrounding the implantation site, preventing hemorrhage.

2.4.2 Disorganization of the chorionic trophoblast layer may disrupt intercellular signaling

Intermediate filaments support a cell by attaching to desmosomes, cell-cell adhesion junctions at the cell membrane. Desmoplakin is not only required to attach filaments to the desmosome but it also maintains desmosomal stability (Gallicano et al, 1998). Desmoplakin mutants die at E6.5 because unstable desmosomes lead to a loss of integrity within extra-embryonic tissues (Gallicano et al, 1998; Gallicano et al, 2001). Normal localization of desmoplakin at the desmosome within $K18^{-/-}$;$K19^{-/-}$ trophoblast cells (Hesse et al, 2000) suggests that, in the absence of keratin filaments, desmosomes remain relatively stable. By contrast, *Mrj*-deficient chorionic trophoblast cells showed a significant reduction of desmoplakin expression. As a result, desmosomes in $Mrj^{-/-}$ trophoblast cells may be unstable, resulting in disrupted chorionic organization. This implies further that keratin inclusion bodies disrupt cell function independently of keratin deficiency. Presumably, the reduction of *K18* expression in $Mrj^{-/-}$;$K18^{+/-}$ and $Mrj^{-/-}$;$K18^{-/-}$ conceptuses decreased the amount of keratin aggregated, which in turn salvaged chorionic organization and rescued chorioallantoic attachment.

During chorioallantoic attachment, the allantois attaches directly to the chorionic mesothelium (Downs, 2002). However, there are a handful of genes, including *Mrj*, that are expressed only in the chorionic trophoblast and which, when knocked-out, result in chorioallantoic attachment defects (Hildebrand and Soriano, 2002; Parr et al, 2001; Saxton et al, 2001; Tetzlaff et al, 2004). This reveals that the mesothelium must interact with the trophoblast compartment for it to become receptive to the allantois. Conceptuses deficient for *Wnt7b*, a gene encoding a signaling protein secreted by chorionic trophoblast cells, fail to express α4-integrin (encoded for by *Itga4*), a mesothelially expressed adhesion molecule required for allantoic attachment (Parr et al, 2001; Yang et al, 1995). Interestingly, *Wnt7b*$^{-/-}$ chorions are disorganized (Parr et al, 2001), a phenotype reminiscent of *Mrj* deficiency. Although it was previously shown that α4-integrin is expressed in *Mrj*$^{-/-}$ chorionic mesothelium (Hunter et al, 1999), it is unknown whether it is properly presented and active at the cell surface. Regardless, there are probably other unidentified adhesion mechanisms that are required because the chorioallantoic attachment phenotype in α4-integrin-deficient embryos is incompletely penetrant (Yang et al, 1995). This suggests that the disorganization of the *Mrj*$^{-/-}$ chorionic trophoblast layer may disrupt signaling between the trophoblast and mesothelium. Without this interaction, the mesothelium may not be prepared to receive the allantois, resulting in a failure of chorioallantoic attachment.

2.4.3 Mrj may be required for keratin degradation by the proteasome

Molecular chaperones are components of the protein-folding machinery and can also be transformed into protein-degradation factors when bound to the correct regulatory

proteins (Esser et al, 2004). The DnaJ co-chaperones not only regulate the ATPase activity and substrate-binding specificity of Hsp70, but also play a significant role in determining which chaperone pathway Hsp70 should pursue (Esser et al, 2004). For example, binding of Ydj1, a yeast homolog of DnaJ, to Hsp70 promotes the proper folding of its substrate (Meacham et al, 1999). By contrast, a human DnaJ homolog, HSJ1 (also known as DNAJB2 – Human Gene Nomenclature Database), and HSP70 stimulate substrate-ubiquitination and -sorting to the proteasome for degradation (Westhoff et al, 2005). MRJ can bind and activate HSP70 (Chuang et al, 2002; Izawa et al, 2000) yet, until now, determining whether this complex is involved in protein-folding or –degradation had never been pursued.

A limited number of chaperones interact with intermediate filaments, giving us few clues about how chaperone complexes regulate the keratin cytoskeleton (Izawa et al, 2000; Liao et al, 1995; Liao et al, 1997; Perng et al, 1999). The keratin network is highly dynamic, but surprisingly little is known about its regulation (Coulombe and Omary, 2002). A simple keratin filament, composed of heterodimers of type I (K18 or K19) and type II (K7 or K8) keratins, can form spontaneously without catalysts (Owens and Lane, 2003; Quinlan et al, 1986). Hsp70 (Izawa et al, 2000; Liao et al, 1995) and Mrj (Izawa et al, 2000) can associate with both soluble and filamentous forms of K8/K18. However, our finding that keratin filaments do form, albeit ending up in aggregates, within *Mrj*$^{-/-}$ trophoblast cells indicates that Mrj is not required for either keratin folding or keratin-filament assembly.

With the help of various proteins, keratin filaments bundle together and attach to desmosomes at the cell membrane to become organized into a dense network (Coulombe

and Omary, 2002; Owens and Lane, 2003). We have shown here that Mrj is diffusely expressed throughout the cytoplasm, but does not localize onto K18-containing filaments in trophoblast cells. This suggests that Mrj is not involved in playing a structural role, which contradicts previous findings that described Mrj expression as filamentous (Izawa et al, 2000). This difference may be explained by the use of different cell types, the detection of different Mrj splice-isoforms (Hanai and Mashima, 2003; Tateossian et al, 2004; Mitra et al, 2008; Cheng et al, 2008) or by the resolution of imaging.

Keratin filaments can be remodeled or degraded by varying the levels of phosphorylation and ubiquitination (Coulombe and Omary, 2002; Ku and Omary, 2002). Our study demonstrates the involvement of Mrj in keratin degradation. As indicated above, Mrj does not colocalize to K18-containing filaments. However, it was previously demonstrated that Mrj can interact with the soluble fraction of K8/K18 proteins (Izawa et al, 2000). Furthermore, keratin inclusions in *Mrj*$^{-/-}$ cells are ultrastructurally similar to Mallory bodies that appear in the hepatocytes of patients with chronic liver disorders (Denk et al, 2000). A defect in the degradation mechanism of the proteasome is one cause of Mallory body formation because cells treated with inhibitors of proteasome function (Bardag-Gorce et al, 2004) or cells that contain the UBB^{+1} ubiquitin mutation (Bardag-Gorce et al, 2003) accumulate K18 and K8. We have shown here that Mrj protein co-localizes to the proteasome in trophoblast giant cells. When we chemically inhibited proteasome function in these cells, keratin aggregates formed that were similar to those in *Mrj*-deficient cells, suggesting that, in the absence of Mrj, K18 is not targeted to and/or degraded by the proteasome.

Mrj deficiency was associated with effects on the entire keratin cytoskeleton, such that K8-, K18- and K19-containing filaments aggregated. Previously, Mrj was shown to specifically interact with K18 but not with K8 (Izawa et al, 2000); however, whether Mrj associates with K19 is unknown. Because K18 and K19 are both type I keratins, it is plausible that Mrj also directly regulates K19-filament degradation. Alternatively, what may start as a primary effect on K18 protein aggregation may indirectly impair the activity of the ubiquitin-proteasome system, causing a vicious circle of protein aggregation (Bence et al, 2001; Esser et al, 2004). Another hypothesis suggests that there is interdependence between K8/K18 and K8/K19 filaments such that, if one type of filament aggregates, the other collapses into the inclusion body as well.

Our study clearly supports the hypothesis that the formation of keratin inclusion bodies in *Mrj*-deficient trophoblast cells is detrimental to cellular function rather than protective. If non-degraded keratin is sequestered to protect the cell, we would expect that the chorioallantoic attachment defect observed in $Mrj^{-/-}$ conceptuses is due to a non-functioning keratin cytoskeleton. However, $K18^{-/-}$;$K19^{-/-}$ embryos underwent chorioallantoic attachment. Instead, by genetically reducing or eliminating *K18* expression in *Mrj*-deficient embryos ($Mrj^{-/-}$;$K18^{+/-}$ or $Mrj^{-/-}$;$K18^{-/-}$), and thus reducing the amount of keratin aggregated, we observed that chorionic trophoblast cell function was restored and chorioallantoic attachment was rescued. This suggests that the keratin inclusions themselves are toxic to cells. Although we have not documented when keratin aggregates first appear in the trophoblast giant cells of *Mrj* mutants, it is remarkable that implantation occurs and that post-implantation development progresses as far as it does.

2.4.4 Keratin inclusion bodies are toxic to cellular function

There are many mutants within the literature with defects in chorioallantoic attachment, yet several of these display incomplete penetrance (reviewed by Watson and Cross, 2005). Interestingly, mutant conceptuses that achieve chorioallantoic attachment will often exhibit later defects in morphogenesis of the labyrinth layer of the placenta (reviewed by Watson and Cross, 2005). Although chorioallantoic attachment was rescued in the majority of *Mrj*$^{-/-}$;*K18*$^{+/-}$ and *Mrj*$^{-/-}$;*K18*$^{-/-}$ placentas, the labyrinth layer remained under-developed such that little villous branching occurred within the chorionic plate and only a small amount of fetal vascularization was apparent. Furthermore, *Mrj*$^{-/-}$;*K18*$^{+/-}$ labyrinths were more-severely affected compared to those of *Mrj*$^{-/-}$;*K18*$^{-/-}$, suggesting that the continued presence of keratin aggregates, even at a reduced level, affects branchpoint morphogenesis and the subsequent development of the labyrinth. Reduced villous formation in *Mrj*$^{-/-}$;*K18*$^{-/-}$ placentas compared to wild type suggests that Mrj function may be required for labyrinth development independent of its role in keratin turnover. This implies that Mrj probably interacts with another substrate during this stage in placental development.

Mrj deficiency may affect a variety of tissues that express keratins, apart from the placenta, because *Mrj* is widely expressed both during later embryonic development and in the adult (Chuang et al, 2002; Hunter et al, 1999; Seki et al, 1999). In addition, Mrj has been shown to interact with other substrates (Pei et al, 1999; Chuang et al, 2002; Dai et al, 2005; Hurst et al, 2006; Pan et al, 2008; Li et al, 2008; Zhang et al, 2008; Cheng et al, 2008), notably the HD protein (Chuang et al, 2002). In Huntington's disease, mutant HD proteins with expanded N-terminal repeats aggregate within neurons (DiFiglia et al,

1997). In vitro, the Mrj-Hsp70 complex can reduce the accumulation of mutant HD aggregates (Chuang et al, 2002). These data are consistent with a general role for Mrj in preventing intracellular inclusion bodies, probably by promoting protein degradation through the proteasome.

2.5 Materials and Methods

Mice. *Mrj*$^{+/-}$ mice were originally generated by *6AD1 β-geo* gene-trap insertion as previously described (Hunter et al, 1999). *Mrj*$^{-/-}$ embryos were produced by mating *Mrj*$^{+/-}$ mice. *K18*/*K19* double-null embryos were generated by mating *K18*$^{-/-}$ mice (Magin et al, 1998) with *K19*$^{-/-}$ mice (Hesse et al, 2000) (provided by T. Magin, University of Bonn, Bonn, Germany) and then mating the resulting double heterozygous progeny. *Mrj*$^{-/-}$;*K18*$^{-/-}$ and *Mrj*$^{-/-}$;*K18*$^{+/-}$ embryos were generated by mating *Mrj*$^{+/-}$ mice with *K18*$^{-/-}$ mice and then mating their resulting *Mrj*$^{+/-}$;*K18*$^{+/-}$ progeny together. Enhanced green fluorescent protein (*Egfp*) transgenic mice (Hadjantonakis et al, 1998) were maintained at heterozygosity in a CD1 background. Experiments were performed in accordance with the Canadian Council on Animal Care and the University of Calgary Committee on Animal Care (Protocol no. M01025).

Genotyping. *Mrj* genotypes were determined by PCR using primers 5'-CCAAT-AGCAGCCAGTCCCTTCCC-3' and 5'-TTCGGCTATGACTGGGCACAACA-3' to detect the neomycin-resistance gene of the β-*geo* cassette (226 bp, mutant allele); and 5'-ACAGGGTCTTGCTACAAGTAGTGC-3' and 5'-TTTCTCTGTCCATGAAGGACTG-GG-3' to detect the β-*geo* gene-trap insertion site in *Mrj* intron 2 (463bp, wildtype allele). The PCR parameters were 30 seconds at 94°C, 30 seconds at 63°C and 30 seconds at

72°C for 30 cycles. Genotyping for *K18* and *K19* (*Krt19*) mice was performed as previously described (Hesse et al, 2000; Magin et al, 1998).

Generation of tetraploid aggregation chimeras. Tetraploid aggregation chimeras were generated as described previously (Nagy et al, 2003b). Briefly, tetraploid embryos were formed by electrofusing two-cell *Egfp* embryos, which were then aggregated with eight-cell diploid embryos from *Mrj* heterozygous matings. Aggregated chimeric embryos were allowed to develop to the blastocyst stage and were then transferred into the uteri of pseudopregnant CD1 females [noon of the day that the vaginal plug is detected was defined as embryonic day (E)0.5]. Embryos were dissected at E9.5. The existence of wildtype tetraploid cells within the placenta was determined by the presence or absence of EGFP expression using a GFP filter (41017 EN GFP, Leica). The yolk sac and embryo tissue was removed for *Mrj* genotyping. Placentas were fixed in 4% paraformaldehyde (PFA; VWR) in 1X phosphate buffered saline (PBS) and embedded in paraffin. Tissue sections were stained with hematoxylin (Sigma) and Eosin (Sigma).

Cell culture. Wildtype (line EDW6-3) and *Mrj* homozygous mutant (lines EDW1-4 and EDW4-1) trophoblast stem (TS) cell lines were derived from littermate blastocysts generated from *Mrj* heterozygote matings. Blastocysts were allowed to outgrow on embryonic feeder cells in TS cell medium (Tanaka et al, 1998). These TS cell lines and the *Rs26* TS cell line (provided by J. Rossant, Hospital for Sick Children, Toronto, Canada) (Tanaka et al, 1998) were maintained in 25 ng/ml basic fibroblast growth factor (bFGF), 1 µg/ml heparin in TS cell medium, 70% of which was pre-conditioned by embryonic fibroblasts, at 37°C under 95% humidity and 5% CO2. Cells

were differentiated by withdrawing bFGF, heparin and fibroblast-conditioned medium (Tanaka et al, 1998).

Chorion-ectoplacental cones were dissected at E7.5 from *Mrj* heterozygous crosses in 1X PBS. Explants were placed in 0.125% trypsin/EDTA (Gibco) in PBS for 10 minutes at 37°C. Dispersed cells were then cultured on coverslips in fibroblast-conditioned TS cell medium with bFGF and heparin for 5 days at 37°C in 95% humidity, 5% CO2, with daily medium change. Yolk sacs were removed during dissection for genotyping.

X-gal and immunofluorescence antibody staining. Mouse conceptuses were dissected at E8.25 and E9.5. For X-gal staining, tissue was fixed, stained as whole mount and was then paraffin embedded as previously described (Hunter et al, 1999). For antibody staining, tissue was fixed in 4% PFA and embedded in paraffin. Paraffin sections (7 µm) were rehydrated in ethanol, treated with trypsin tablets (Sigma) in PBS for 10 minutes and blocked in 1% bovine albumin serum (BSA; Sigma), 5% host serum for 1 hour. Cell cultures were fixed in 4% PFA for 10 minutes, treated with 0.1% Triton X-100 (Fisher Biotech) for 10 minutes and blocked in 1% BSA for 30 minutes. Primary antibodies and dilutions used include: anti-cytokeratin 18 (Ks18.04, 1:100; RDI), anti-keratin 8 (Ks8.7, 1:100; Progen), anti-keratin 19 (Troma.3, 1:100; a gift from T. Magin), anti-pan-cytokeratin (1:100; DAKO), anti-desmoplakin (DP1&2, neat; RDI), anti-20S proteasome core subunits (1:100; Calbiochem) and anti-Mrj (020417, 1:100; a gift from M. Inagaki, Aichi Cancer Centre Research Institute, Aichi, Japan) (Izawa et al, 2000). Secondary antibodies were used at a dilution of 1:300 and included: goat anti-rabbit Cy3, goat anti-rat Cy3, goat anti-mouse Cy3 and goat anti-rabbit FITC (Jackson

ImmunoResearch Laboratories), and goat anti-mouse Alexa Fluor 488 (Molecular Probes). Antibody dilutions were made in 1% BSA, 5% host serum. DNA was counterstained with 1:10,000 bisbenzimide (Sigma).

Electron Microscopy. E8.25 implantation sites from *Mrj* heterozygous matings were fixed in 2% EM-grade glutaraldehyde (Sigma), 2% PFA in 0.2 M sodium cacodylate (pH 7.4; Sigma) overnight at 4°C, and were post-fixed in 1% osmium tetroxide (EM Sciences) in 0.2 M sodium cacodylate (pH 7.4) for 2 hours at 4°C. Tissue was dehydrated in increasing concentrations of ethanol up to 70%, treated in 2% uranyl acetate (ProSciTech) in 70% ethanol, and further dehydrated in increasing ethanol concentrations (70-100%). Tissue was treated with propylene oxide (EM Sciences) and was resin embedded (EMBED 812 kit, EM Sciences). Yolk sacs were removed for genotyping prior to fixation.

Proteasome inhibition. Rs26 TS cells were differentiated by withdrawal of bFGF, heparin and fibroblast-conditioned media for 4 days on coverslips. Cells were exposed to 10 μM clasto-lactacystin β-lactone (Invitrogen) in differentiating TS medium overnight at 37°C under 95% humidity and 5% CO2. Cells were washed with 1X PBS, fixed in 4% PFA and immunostained as described above.

Equipment and software. A Leica DMR light microscope (for fluorescent and light images), Leica DMIL inverted light microscope (for cell culture images) and Leica MZ95 dissection microscope (for dissected embryo/placenta images) with Photometrics Coolsnap cf camera and Open Lab 2.2.2 imaging software program were used to obtain micrographs. Filters used were from Chroma: DAPI (31000), TRITC (31002) and FITC (31001). De-convolved images were captured using an Axioplan 2 Imaging (Zeiss)

microscope and Axiovision 4.1 acquisition software. Electron micrographs were taken on a Hitachi 7000 transmission electron microscope. Minimal image processing was performed using Adobe Photoshop 7.0 and figures were constructed using Canvas X.

CHAPTER THREE

DISRUPTED POLARITY IN *MRJ*-DEFICIENT TROPHOBLAST CELLS IS ASSOCIATED WITH REDUCED LAMININ DEPOSITION AND FAILURE TO PATTERN THE CHORION

The majority of the experiments represent the work of E. Watson. A portion of the in situ hybridizations in Fig. 3.1 were performed by D. Natale and D. Simmons. The northern blots (Fig. 3.2) and western blot (Fig. 3.5) were carried out by M. Hughes and D. Natale.

3.1 Abstract

Changes in cell-cell and cell-extracellular matrix (ECM) interactions can dictate gene expression patterns required for progenitor maintenance and differentiation during tissue morphogenesis. Conceptuses deficient for the gene encoding the Mrj co-chaperone fail to undergo chorioallantoic attachment during placental development. We show here the ECM protein Laminin (Ln) α5 is improperly expressed on the basal surface of *Mrj*$^{-/-}$ trophoblast cells. This is associated with collapse of the actin cytoskeleton, misexpression of cell adhesion molecules (e.g. β-catenin and E-cadherin) and altered cell adhesion, and providing exogenous Ln α5 substrate rescues the cell adhesion phenotype. These cell-cell and cell-matrix interactions are particularly important for the regulation of trophoblast progenitor cells within the labyrinth since early chorionic patterning necessary for the trilaminar trophoblast structure in the labyrinth did not occur in *Mrj*$^{-/-}$ chorions. Instead, chorion trophoblast cells are maintained as common labyrinth progenitor cells and the induction of more restricted syncytiotrophoblast cell precursors was inhibited. Therefore, changes in cell-cell and cell-matrix communications are part of a complex network of interactions required for normal patterning of the chorion, allantoic receptivity and progenitor cell differentiation.

3.2 Introduction

The maintenance and differentiation of precursor cell populations are dependent upon environmental cues that regulate differentiation programs including both cell-cell and cell-extracellular matrix (ECM) interactions. Multipotent trophoblast stem (TS) cells of the placenta are present in the extraembryonic ectoderm of the chorion layer (Uy et al,

2002). The potential of these cells becomes more restricted after embryonic day (E) 7.5 as indicated by the down regulation of TS cell-specific genes *Cdx2*, *Esrrb* (*Err2*) and *Eomes* (Beck et al, 1995; Hancock et al, 1999; Pettersson et al, 1996). This coincides with the closure of the ectoplacental cavity which brings the top of the chorion and the bottom of the ectoplacental cone (EPC) in juxtaposition (Uy et al, 2002). Shortly thereafter, the allantois attaches to the chorion to initiate the branching of villi and formation of the mature labyrinth (reviewed by Watson and Cross, 2005). Little is known about the labyrinth trophoblast cell precursor populations. However, it was recently shown that the chorion is patterned and divided into at least three layers as determined by genetic markers (Simmons et al, 2008). Each layer is hypothesized to contain distinct and autonomous progenitor cells that correspond to specific differentiated cell types within the labyrinth: the layer that first comes in contact with the allantois, the basal cell layer, contributes to syncytiotrophoblast (SynT-II) cells that line the fetal vasculature; the apical layer differentiates into syncytiotrophoblast (SynT-I) cells nearest to the maternal blood sinuses; and cells at the very top of the chorion/base of the EPC produce sinusoidal trophoblast giant cells (S-TGCs) that line the maternal blood sinuses (Simmons et al, 2008). The cell-cell and cell-matrix interactions required to specify these precursor populations and to maintain them in a progenitor-state or to promote a differentiation program remains to be determined.

Mrj mutant embryos die at midgestation due to a failure in chorioallantoic attachment during placental development (Hunter et al, 1999). We previously determined that *Mrj* deficiency prevents normal keratin turnover, resulting in the formation of large keratin aggregates that are toxic to trophoblast cells (Chapter 2). Additionally, we found

that the chorion cells are highly disorganized in *Mrj* mutants (Chapter 2). The goal of this study was to further characterize how *Mrj* deficiency and the presence of keratin aggregates affect chorionic cell function and prevent chorioallantoic attachment. We show that *Mrj*$^{-/-}$ chorionic trophoblast cells have disorganized actin cytoskeletons, lack proper cell adhesions and display defective laminin expression, all of which alter cell behaviour and prevent both chorionic patterning and labyrinth progenitor cell differentiation.

3.3 Results

3.3.1 Cytoskeletal and cell-cell adhesion defects in Mrj mutants

We previously found that trophoblast cells within the chorion of *Mrj*$^{-/-}$ mutants were disorganized in vivo (Chapter 2). Consistent with this, *Mrj*$^{-/-}$ cultured TS cells appeared rounded and lacked normal association with their neighbouring cells in vitro (Fig. 3.1A, B). We hypothesized that there would be associated changes in the actin cytoskeleton and cell adhesion molecules. We observed that wildtype TS cells were tightly adherent, with the majority of actin filaments located at the cell periphery (Fig. 3.1C, E). In contrast, *Mrj*$^{-/-}$ TS cell colonies were dispersed with limited regions of cell-cell contact and lacked the stereotypical rectangular shape (Fig. 3.3D). Actin filaments were not localized at the cell perimeter of mutant TS or differentiated cells (Fig. 3.3D, H). Instead, perinuclear actin aggregates formed (Fig. 3.1D, H) which, at least in differentiated cells, co-localized with K18-containing aggregates (Fig. 3.1H, I).

Actin filaments attach to the cell membrane at adherens junctions, protein complexes that contain β-catenin and E-cadherin and are involved in cell adhesion

FIGURE 3.1 – *Mrj* deficiency alters the actin cytoskeleton and cell-cell interactions. (A, B) Phase contrast of $Mrj^{+/+}$ (A) and $Mrj^{-/-}$ (B) TS cells. (C-D) Immunofluorescence staining of actin cytoskeleton (red) expression in $Mrj^{+/+}$ (C) and $Mrj^{-/-}$ (D) proliferating TS cell cultures. DNA, blue. (E-J) Triple immunofluorescence labelling of actin (red), keratin 18 (green) and DNA (blue) in $Mrj^{+/+}$ (E-G) and $Mrj^{-/-}$ (H-J) differentiated TS cell cultures. (K-N) β-catenin expression in undifferentiated (red) (K, L) and differentiated (green) (M, N) TS cell cultures. (O-R) E-cadherin (red) expression in undifferentiated (O, P) and differentiated (Q,R) TS cell cultures. +/+ = wildtype; -/- = $Mrj^{-/-}$. DNA, blue. Arrowheads, cells without cell-cell contacts. Arrow, trail of cytoplasm as revealed by β-catenin staining. Scale bars = 50 μm.

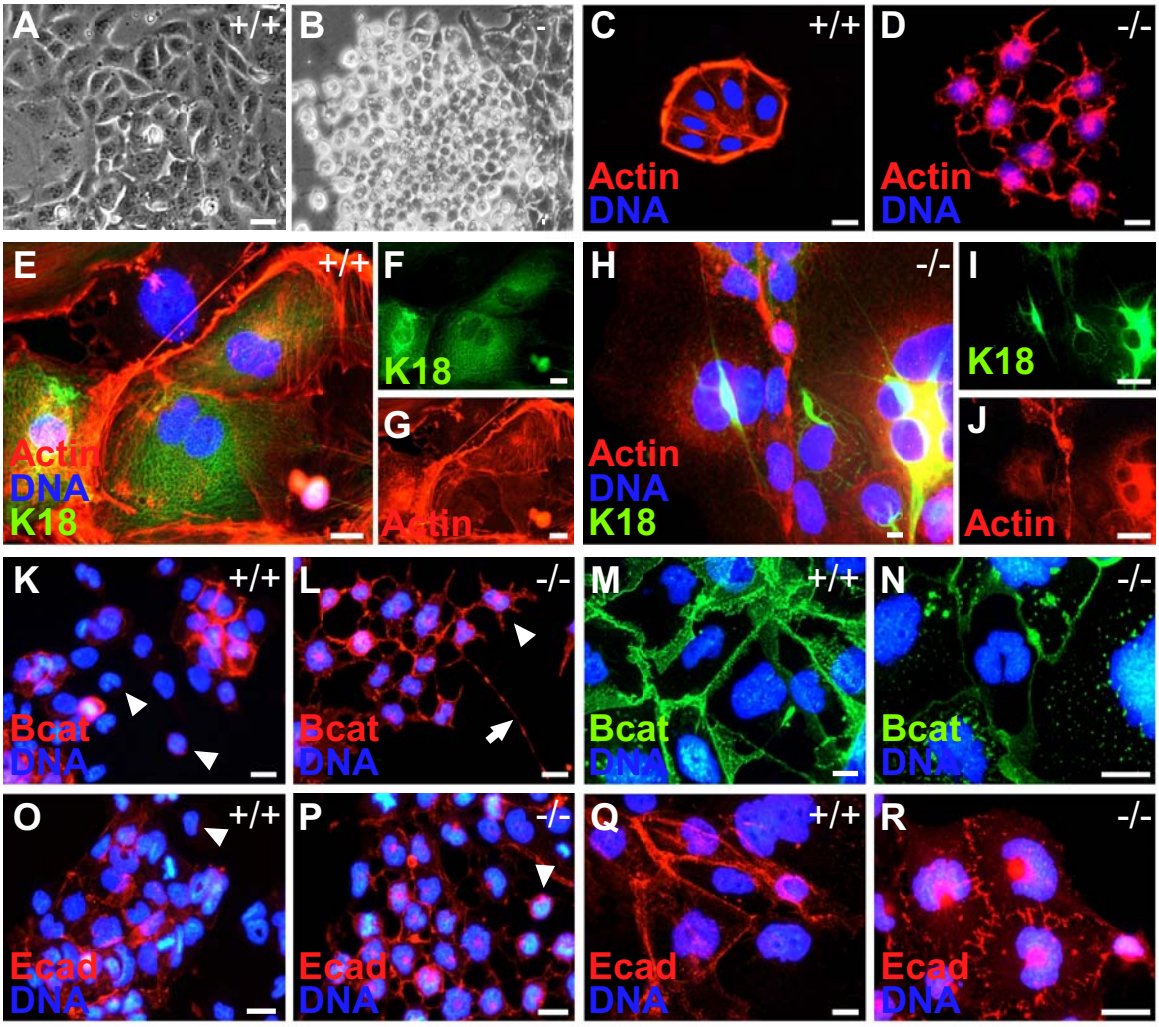
A
+/+
B
-
C
+/+
Actin
DNA
D
-/-
Actin
DNA
E
+/+
Actin
DNA
K18
F
K18
G
Actin
H
-/-
Actin
DNA
K18
I
K18
J
Actin
K
+/+
Bcat
DNA
L
-/-
Bcat
DNA
M
+/+
Bcat
DNA
N
-/-
Bcat
DNA
O
+/+
Ecad
DNA
P
-/-
Ecad
DNA
Q
+/+
Ecad
DNA
R
-/-
Ecad
DNA

(Pokutta and Weis, 2002). In most wildtype TS cells, β-catenin and E-cadherin expression were located at the cell membrane (Fig 3.1K, M, O, Q). Independent cells not in contact with other cells had low to undetectable expression of both proteins (Fig 3.1K, O). By contrast, both β-catenin and E-cadherin were up-regulated in *Mrj*$^{-/-}$ TS cells including unusually robust expression in cells without cell contacts (Fig 3.1L, P). Additionally, expression was not restricted to the membrane and appeared in large cytoplasmic aggregates (Fig 3.1L, P). Under differentiation conditions, *Mrj*$^{-/-}$ cells expressed less β-catenin at cell-cell boundaries compared to wildtype and contained multiple punctate aggregates throughout the cytoplasm (Fig 3.1N versus M). E-cadherin was also abnormal in differentiated *Mrj*$^{-/-}$ cells. Instead of running parallel to the membrane as in wildtype cells (Fig 3.1Q), expression was ragged and discontinuous at the membrane (Fig 3.1R). Furthermore, the bulk of E-cadherin was detected within large perinuclear aggregates (Fig 3.1R). Despite the expression of adhesion proteins, it appeared that mutant cells were unable to maintain stable cell adhesions. This suggested that either the cytoskeleton was not sufficient to stabilize adhesion complexes or a trafficking defect may prevent adhesion proteins from reaching the cell membrane for proper function.

3.3.2 Mrj-deficient TS cells are highly migratory and repulsive

Changes in the expression of actin cytoskeleton and adhesion molecules are associated with altered migratory behaviour of cells (Miyoshi and Takai, 2008). Therefore, we used time-lapse video microscopy to capture the behaviour of undifferentiated wildtype and *Mrj*$^{-/-}$ TS cells over a span of 120 minutes (Fig 3.2). Upon attaching to the culture plate,

FIGURE 3.2 – *Mrj*$^{-/-}$ TS cells are highly migratory and repulsive.

Time lapse microscopy of *Mrj*$^{+/+}$ (A) and *Mrj*$^{-/-}$ (B) TS cells plated on plastic cell culture (without substrate) in TS cell media with bFGF, heparin and CM. Each image represents 10 minute increments. Scale bars = 50 μm.

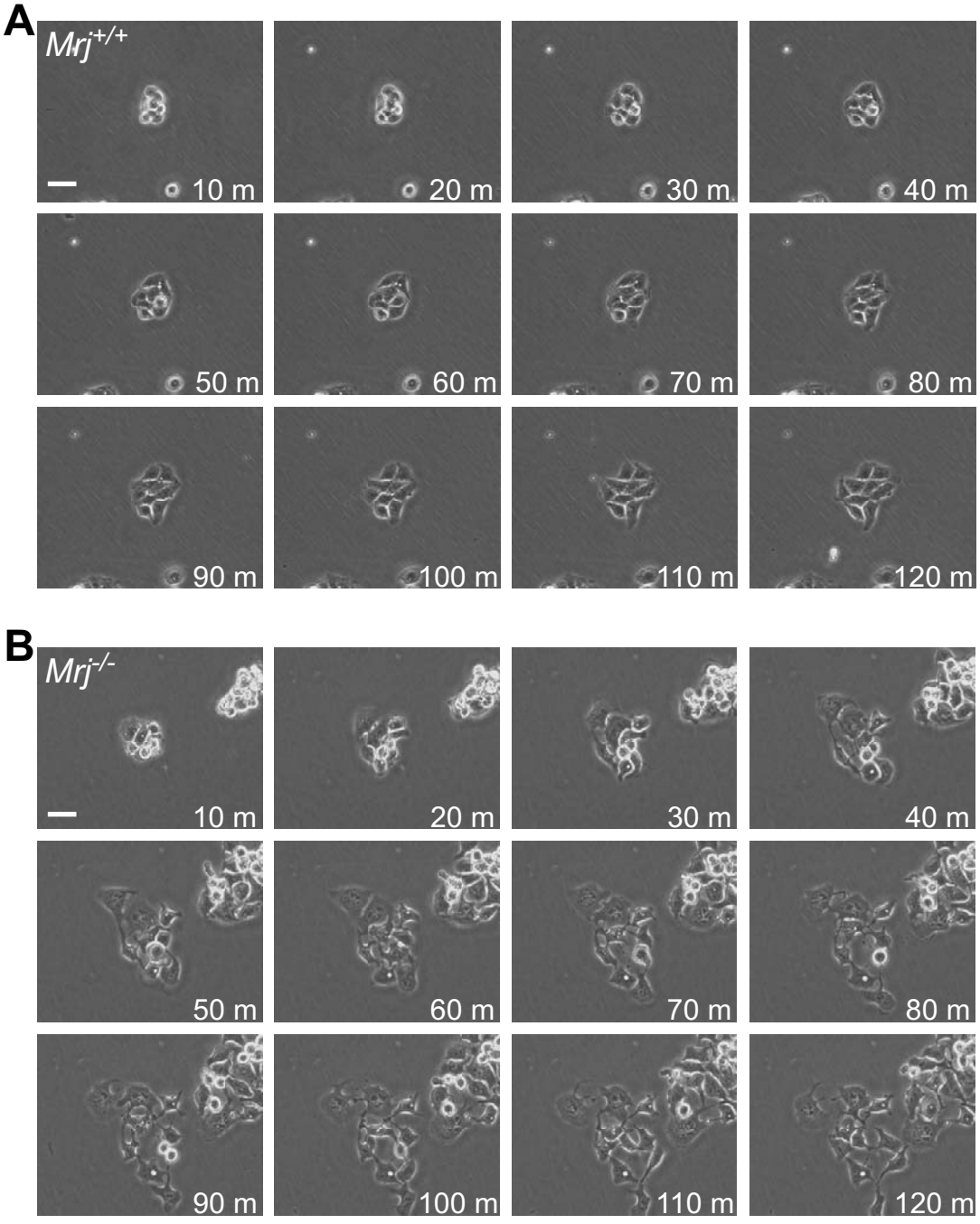
A
Mrj+/+
10 m
20 m
30 m
40 m
50 m
60 m
70 m
80 m
90 m
100 m
110 m
120 m
B
Mrj-/-
10 m
20 m
30 m
40 m
50 m
60 m
70 m
80 m
90 m
100 m
110 m
120 m

wildtype cells remained tightly clustered together over the entire time period (Fig 3.2A). After approximately 80 minutes, some cells began to send out lamellopodia-like projections but remained adherent to the rest of the cell colony, with little to no migration. The behaviour of *Mrj*$^{-/-}$ TS cells was drastically different. Immediately after *Mrj*$^{-/-}$ cells contacted the culture plate, they formed lamellopodia and migrated away from each other, though keeping in contact with neighbouring cells via thin projections (Fig 3.2B). The paths of these highly migratory cells often converged but instead of adhering upon contact, they moved in a repulsive manner in opposite directions. Interestingly, cytoplasmic "trails" were frequently observed in the wake of *Mrj*-deficient cells, a phenomenon never observed in wildtype cultures. Although most of these "trails" were able to retract back into the cells (Fig 3.2B), long ropes of cytoplasm were left trailing behind some cells as revealed by β-catenin staining (Fig 3.1L). From this, we concluded that a disruption in the actin cytoskeleton and associated adhesion molecules resulting from *Mrj* deficiency affects normal cell behaviour, perhaps due to perturbed cell-cell interactions.

3.3.3 Laminin α5 expression is altered in Mrj$^{-/-}$ *trophoblast cells*

The ECM environment is directly linked to the actin cytoskeleton via focal adhesions. Therefore, the observed changes in cell behaviour could have been due to direct effects of *Mrj* deficiency or secondary to changes in the ECM since we previously observed less ECM between the trophoblast and mesothelial cell layers of *Mrj*$^{-/-}$ chorions at E8.25 compared to wildtype (Chapter 2, Fig 2.5J versus I). Laminin is a key component of trophoblast basement membrane (Klaffky et al, 2001). In particular, the laminin isoform

α5 (Ln α5; contributes to both laminins 10 and 11) is expressed between the chorionic trophoblast and mesothelium from E6.5 to E8.5 (Klaffky et al, 2001; Alpy et al, 2005; Miner et al, 1998) and later between the syncytiotrophoblast cells and fetal vasculature in the mature labyrinth (Miner et al, 1998). To determine whether the reduction in ECM deposition in *Mrj*$^{-/-}$ chorions was the result of decreased Ln α5 expression, histological sections of E8.5 chorions were immunostained using an antibody against Ln α5. Wildtype and *Mrj*$^{-/-}$ chorions both expressed Ln α5 protein between the trophoblast and mesothelial cell layers (Fig. 3.3A, B) as previously described (Miner et al, 1998; Klaffky et al, 2001). However, Ln α5 expression was more robust at the periphery of *Mrj*$^{-/-}$ chorions (Fig. 3.3B) compared to wildtype (Fig. 3.3A). Additionally, it appeared that some of this expression was within the cytoplasm of the *Mrj*$^{-/-}$ trophoblast cells (Fig. 3.3B). To further analyze Ln α5 localization, we immunostained undifferentiated TS cell cultures for Ln α5. Wildtype TS cells displayed diffuse Ln α5 expression, the majority of which presumably formed part of the basement membrane between the cell and tissue culture plate (Fig. 3.3C). In contrast, both *Mrj* mutant TS cell lines (EDW1.4 and EDW4.1) exhibited Ln α5 staining throughout the cytoplasm (Fig. 3.3D; data not shown). Even though the intensity of Ln α5 expression seemed higher in *Mrj* mutant cells, western blot analysis on undifferentiated TS cell lysates revealed similar concentrations of Ln α5 protein in wildtype and *Mrj*$^{-/-}$ cultures (Fig. 3.3F). Interestingly, when growth factors were removed and TS cells were allowed to differentiate for 5 days, Ln α5 protein expression decreased in wildtype cells but remained unchanged in *Mrj*$^{-/-}$ cultures (Fig.

FIGURE 3.3 – Laminin α5 protein deposition is affected in *Mrj*$^{-/-}$ chorions and trophoblast cells. (A, B) Laminin (Ln) α5 protein expression (brown) in histological paraffin sections of wildtype (A) and *Mrj*$^{-/-}$ (B) placentas at E8.5. White arrowheads depict chorionic trophoblast cells that express Lnα5. Small boxes in left-hand panels represent regions of higher magnification in center and right-hand panels. Right-hand panels are regions of the chorion where the mesothelial layer has pulled away due to the fixation process. Scale bars = 500 μm (left panel A, B) and 50 μm (center and right panels A, B). RM, Reichert's membrane; Ch, chorion; EPC, ectoplacental cone; P-TGC, parietal trophoblast giant cells; Al, allantois; Tr, trophoblast layer of the chorion; Me, mesothelial layer of the chorion. (C-D) Ln α5 (red) expression in *Mrj*$^{+/+}$ (C) and *Mrj*$^{-/-}$ (D) in TS cells in proliferating conditions. Blue, DNA. Scale bars = 100 μm. (E) Western blot detecting Lnα5 protein (top) from cell lysates of *Mrj*$^{-/-}$ and *Mrj*$^{+/+}$ TS cells cultured in proliferating conditions (cultured with bFGF and CM for 2 days; indicated by "+") and differentiating conditions (cultured without bFGF and CM; indicated by "-"). Actin (bottom) was used as a loading control.

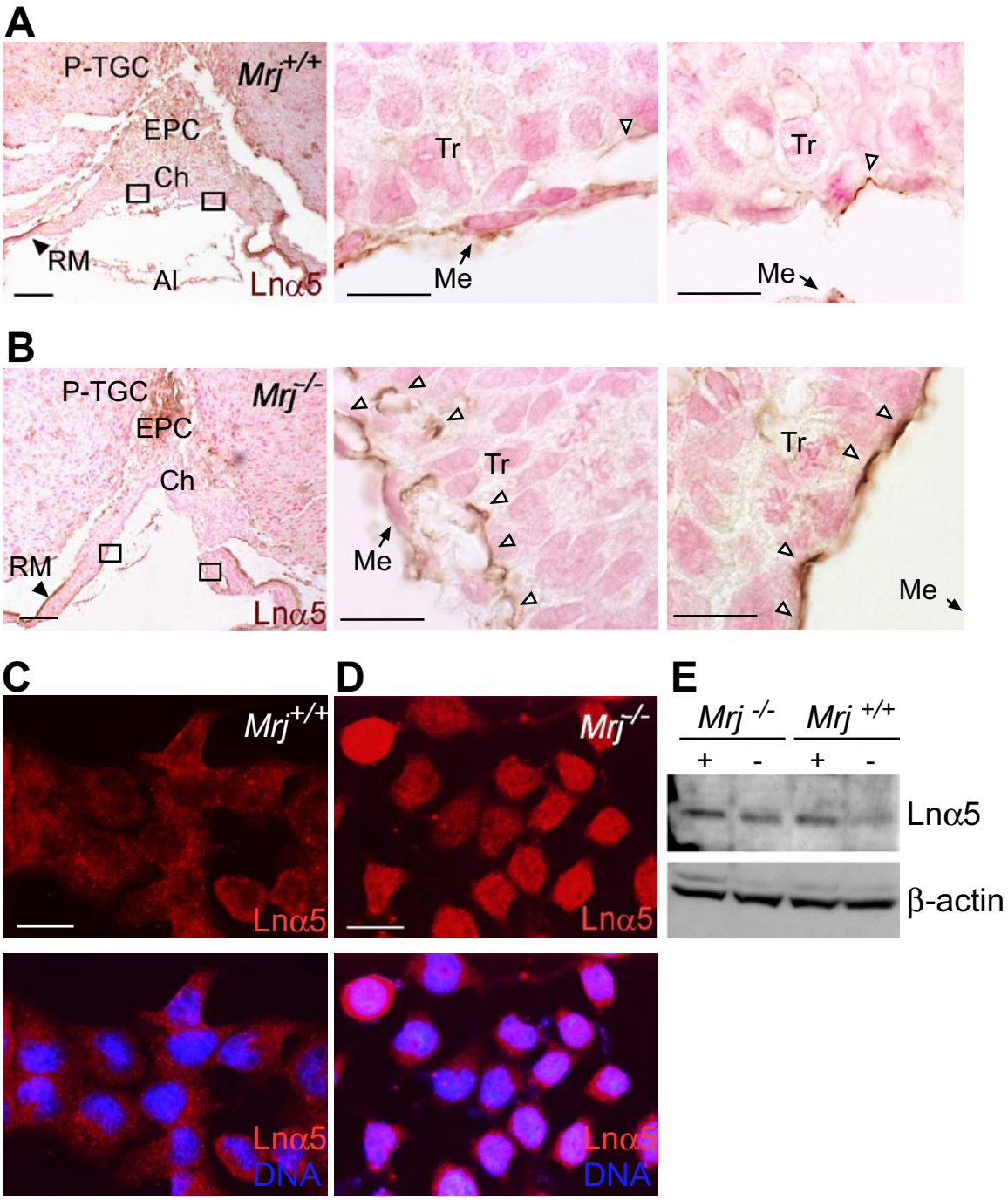
A
P-TGC
Mrj+/+
EPC
Ch
RM
Al
Lnα5
Tr
Me
Tr
Me
B
P-TGC
Mrj-/-
EPC
Ch
RM
Lnα5
Tr
Me
Tr
Me
C
Mrj+/+
Lnα5
Lnα5
DNA
D
Mrj-/-
Lnα5
Lnα5
DNA
E
Mrj -/-
Mrj +/+
+
-
+
-
Lnα5
β-actin

3.3F). Together these data implied that Ln α5 is expressed at normal levels in *Mrj*$^{-/-}$ chorionic trophoblast cells but it is not likely targeted to the cell membrane for extra-cellular deposition. This in turn may prevent a normal interaction between the chorionic mesothelium and trophoblast cells in vivo.

3.3.4 Exogenous Laminin α5 normalizes Mrj$^{-/-}$ *TS cell behaviour in culture*

Laminin α1 (Ln α1; a component of laminins 1 and 3) and Ln α5 isoforms have distinct effects on trophoblast cell behaviour (Klaffky et al, 2006), data we confirmed here in our study (Fig 3.4). Wildtype TS cells plated on Ln α1 were somewhat dispersed and appeared spindle-like with many thin, filopodia-like projections (Fig 3.4C) compared to cells plated on plastic (Fig 3.4A). Time lapse imaging revealed that these cells were not particularly migratory but actively extended and retracted their projections in all directions. On the other hand, plating wildtype TS cells on Ln α5 caused a general increase in cell circumference and the formation of large lamellopodia-like projections at their leading edges (Fig 3.4E). Moreover, time lapse imaging revealed that these cells were more motile compared to cells plated either on Ln α1 or without a substrate (data not shown).

Next, we determined whether the behaviour of *Mrj*-deficient TS cells could be normalized by providing a laminin substrate. On Ln α1, *Mrj*$^{-/-}$ cells were more comparable to wildtype cells with respect to an increased frequency of filopodial-like projections and rounding of cells (Figs 3.4C, D), but they retained an inability to adhere to other cells (Figs 3.4B, C, D). Furthermore, time lapse microscopy revealed that *Mrj*$^{-/-}$ cells had a reduced ability to migrate on Ln α1 compared to plating on plastic (data not

FIGURE 3.4 – Exogenous Laminin α5 normalizes *Mrj*-deficient cell behaviour. *Mrj*$^{+/+}$ and *Mrj*$^{-/-}$ TS cells in the presence of bFGF, heparin and CM plated on no substrate (A, B), laminin α1 (Ln α1) (C, D) and laminin α5 (Ln α5) (E, F). (G,H) Time lapse microscopy for wildtype and *Mrj*$^{-/-}$ TS cells plated on Ln α5. Each image represents 10 minute increments one hour after initial plating. Scale bars = 50 μm.

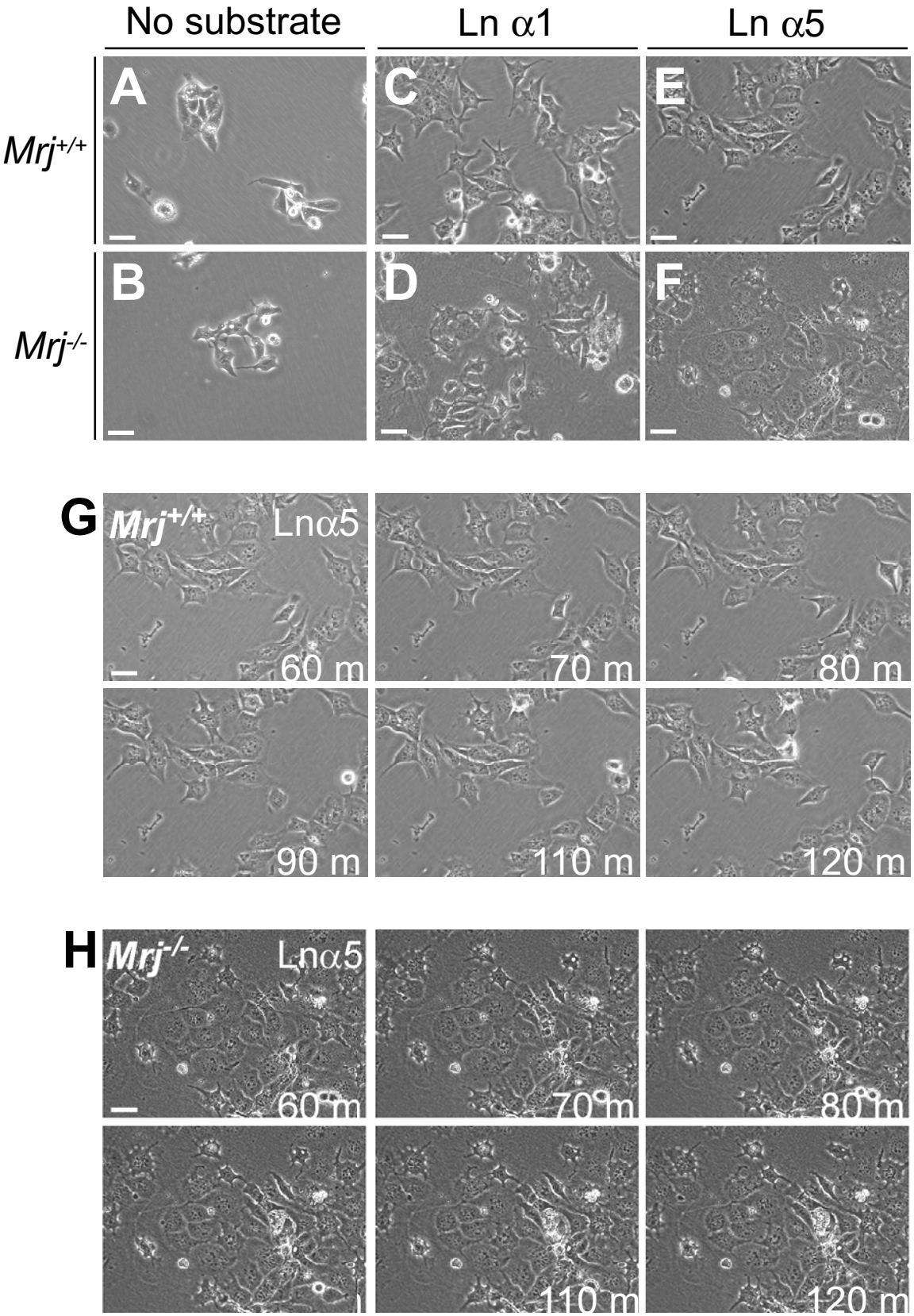
No substrate
Ln α1
Ln α5
Mrj+/+
Mrj-/-
A
B
C
D
E
F
G
Mrj+/+
Lnα5
60 m
70 m
80 m
90 m
110 m
120 m
H
Mrj-/-
Lnα5
60 m
70 m
80 m
110 m
120 m

shown) but they were still more migratory than wildtype cells on Ln α1 (data not shown). In contrast to the impact of exogenous Ln α1, *Mrj*$^{-/-}$ TS cells on plated Ln α5 were more likely to form attachments to neighbouring cells (Fig 3.4F) suggesting that adhesion complexes were more stable in the presence of Ln α5. Although some mutant cells still had many processes extended, they were considerably more like lamellopodia and were comparable to wildtype cells on Ln α5 (Figs 3.4E, F). Time lapse imaging revealed that *Mrj*$^{-/-}$ cells were significantly less migratory than *Mrj*$^{-/-}$ cells plated on plastic (Figs 3.2B, 3.4H) and were more similar to wildtype cells plated on Ln α5 (Fig 3.4G).

3.3.5 Mrj deficiency prevents chorion patterning and trophoblast differentiation

To address whether or not disruption of cell-cell interactions in the chorion affected its developmental organization, we analyzed the expression of several chorion layer-specific genes at E8.5. These genes are markers of precursor populations destined to form the three differentiated trophoblast cell types in the mature labyrinth (Simmons et al, 2008). It is important to note that Mrj is normally expressed throughout all three chorionic layers at E8.5 (Fig 3.5G). In wildtype conceptuses at this time, the basal layer of the chorion contains clusters of proliferating *Rhox4b* (*Ehox*)-expressing cells (A. Davies, E. Mariusdottir, D.G. Simmons, D.R. Natale and J.C. Cross, unpublished observations) (Figs 3.5A, B). These clusters are interspersed with branchpoint initiation sites containing non-proliferating *Rhox4b*-negative cells that express *Gcm1*, *Synb*, *Cebpα* (Simmons et al, 2008) and *Vegf* (Fig 3.5D). Interestingly, *Rhox4b* expression was not restricted in *Mrj*$^{-/-}$ chorions but was detected throughout the entire basal layer with apical expansion (Fig 3.5C). Furthermore, expression of the *Gcm1*, *Synb*, *Cebpα* and *Vegf* genes were down-

regulated or undetectable in mutant chorions (Fig 3.5D) suggesting that sites of branchpoint initiation were either not established or not maintained in *Mrj* mutant chorions. Genes that are normally expressed throughout the apical layer of the chorion such as *Syna* and *Snail* were also undetectable in $Mrj^{-/-}$ chorions compared to wildtype (Fig 3.5E). Together, these data suggest that *Mrj* deficiency impedes the formation of both SynT lineages and results in cells that are maintained in a proliferative and undifferentiated state.

Interestingly, the uppermost layer of the chorion, which is hypothesized to give rise to S-TGCs (Simmons et al, 2008), was normal in $Mrj^{-/-}$ chorions. *Hand1*, a marker for these cells, was similarly expressed in wildtype and $Mrj^{-/-}$ chorions at E8.5 (Fig 3.5F). We also observed that *Hand1* is expressed throughout the basal layer of wildtype chorions, an expression pattern recapitulated in $Mrj^{-/-}$ chorions (Fig 3.5F). This suggests that *Mrj* deficiency does not perturb all patterning and gene expression within the chorion and that specification of S-TGC precursors may be cell-autonomous.

To assess the ability of $Mrj^{-/-}$ trophoblast cells to differentiate, we compared two independent $Mrj^{-/-}$ TS cell lines with a simultaneously-derived $Mrj^{+/+}$ TS cell line (Chapter 2) in differentiating conditions for 5 days (after withdrawal of fibroblast growth factor, heparin and fibroblast-conditioned medium). We observed that even in the absence of growth factors, $Mrj^{-/-}$ cells continued to proliferate and revealed a 4-8 fold increase in the number of cells after 5 days of differentiation compared to $Mrj^{+/+}$ cultures (Fig 3.6A). Furthermore, we observed that 96.9% of $Mrj^{+/+}$ TS cells preferentially differentiated into TGCs over 5 days (Fig 3.6B) as determined by the presence of cells with expansive cytoplasm and large nuclei. By comparison, only 31.5% and 29.7% of

FIGURE 3.5 – *Mrj*$^{-/-}$ chorions lack early patterning at E8.5.

In situ hybridizations for various genes that denote progenitor populations and future layers of the labyrinth on E8.5 cryosections of *Mrj*$^{+/+}$ and *Mrj*$^{-/-}$ littermate chorions. (A-C) Expression of the labyrinth progenitor cell marker, *Rhox4b*, in *Mrj*$^{+/+}$ (A, B) and *Mrj*$^{-/-}$ chorions (C). Box in A represents higher magnification in panel B. Dotted lines in A outline ectoplacental cone. Regions boxed in panels B and C are shown to the right in higher magnification. Ch, chorion (arrow); EPC, ectoplacental cone; TGC, trophoblast giant cells (arrowheads); De, decidua. (D) Expression of basal chorion-specific genes *Gcm1*, *Cepbα*, *Synb* and *Vegf* in *Mrj*$^{+/+}$ and *Mrj*$^{-/-}$ chorions. (E) Expression of apical chorion-specific genes *Syna* and *Snail* in *Mrj*$^{+/+}$ and *Mrj*$^{-/-}$ chorions. (F) *Hand1* expression in *Mrj*$^{+/+}$ and *Mrj*$^{-/-}$ chorions. (G) β-galactosidase (*β-gal*) activity driven from the *Mrj* gene-trapped allele depicts Mrj expression pattern in *Mrj*$^{+/-}$ chorion at E8.5. Scale bars = 50 μm.

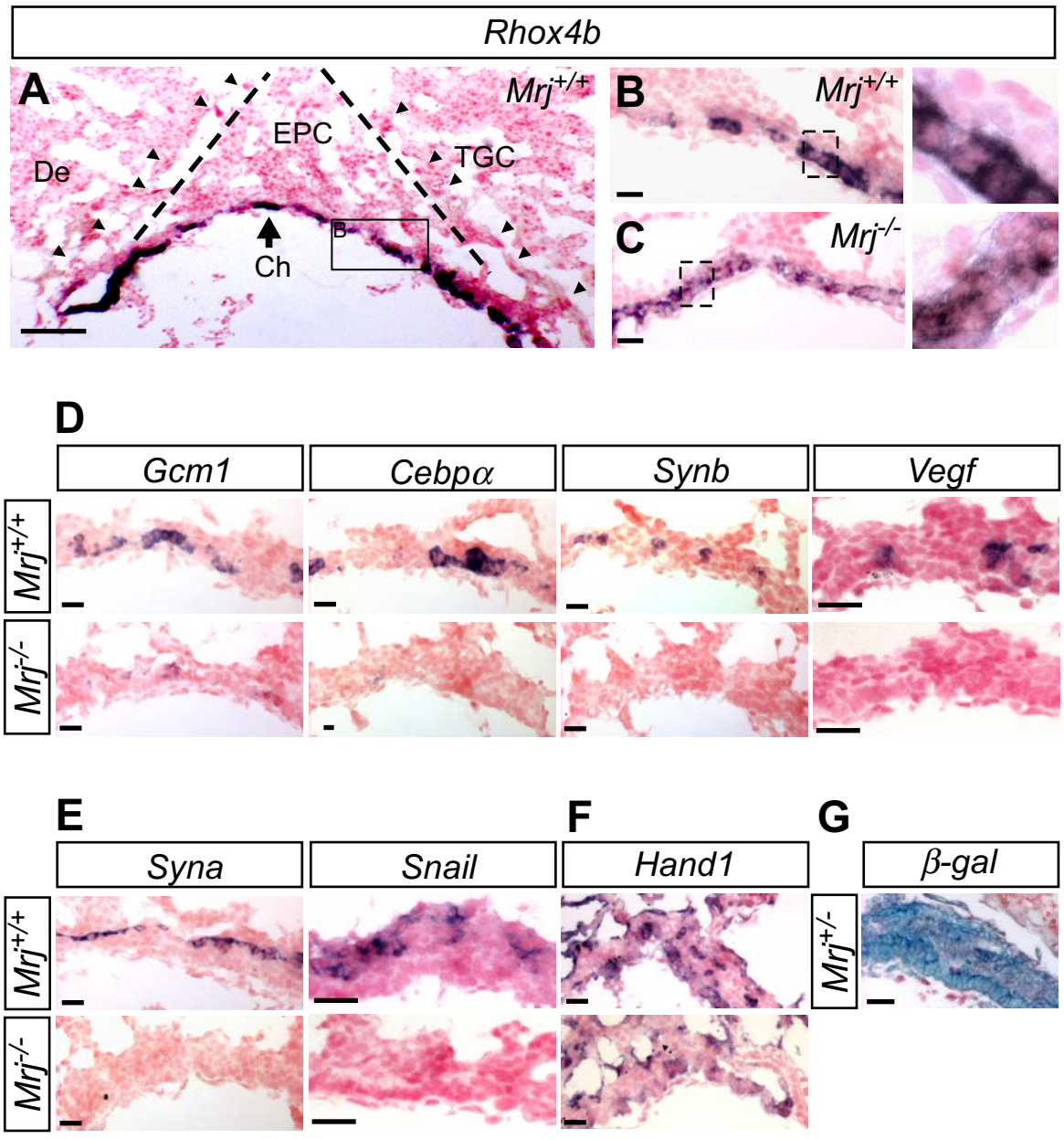
Rhox4b
A
Mrj+/+
EPC
TGC
De
Ch
B
B
Mrj+/+
C
Mrj-/-
D
Gcm1
Cebpα
Synb
Vegf
Mrj+/+
Mrj-/-
E
Syna
Snail
F
Hand1
G
β-gal
Mrj+/-
Mrj+/+
Mrj-/-

FIGURE 3.6 – *Mrj*$^{-/-}$ TS cells remain in a labyrinth progenitor-like state and do not differentiate. (A) Average number of trophoblast cells per cell island over 5 days of differentiation. (B) Percentage of trophoblast giant cells (TGCs), as characterized by expansive cytoplasm and large nucleus, over 5 days of differentiation. Pink = *Mrj*$^{+/+}$ (EDW6.3), blue = *Mrj*$^{-/-}$ (EDW1.4), green = *Mrj*$^{-/-}$ (EDW4.1). (C) Northern blot analysis of *Err2*, *Cdx2*, *Rhox4b*, *Gcm1*, *Synb*, *Syna*, *Hand1*, *Tpbpα* and *Mash2* expression in TS cell cultures on days 0, 2, 4 and 6 of differentiation (after withdrawal of growth factors). 18S ribosomal RNA was used as a loading control. Cell line EDW6.3 = *Mrj*$^{+/+}$; cell lines EDW1.4 and EDW4.1 = *Mrj*$^{-/-}$.

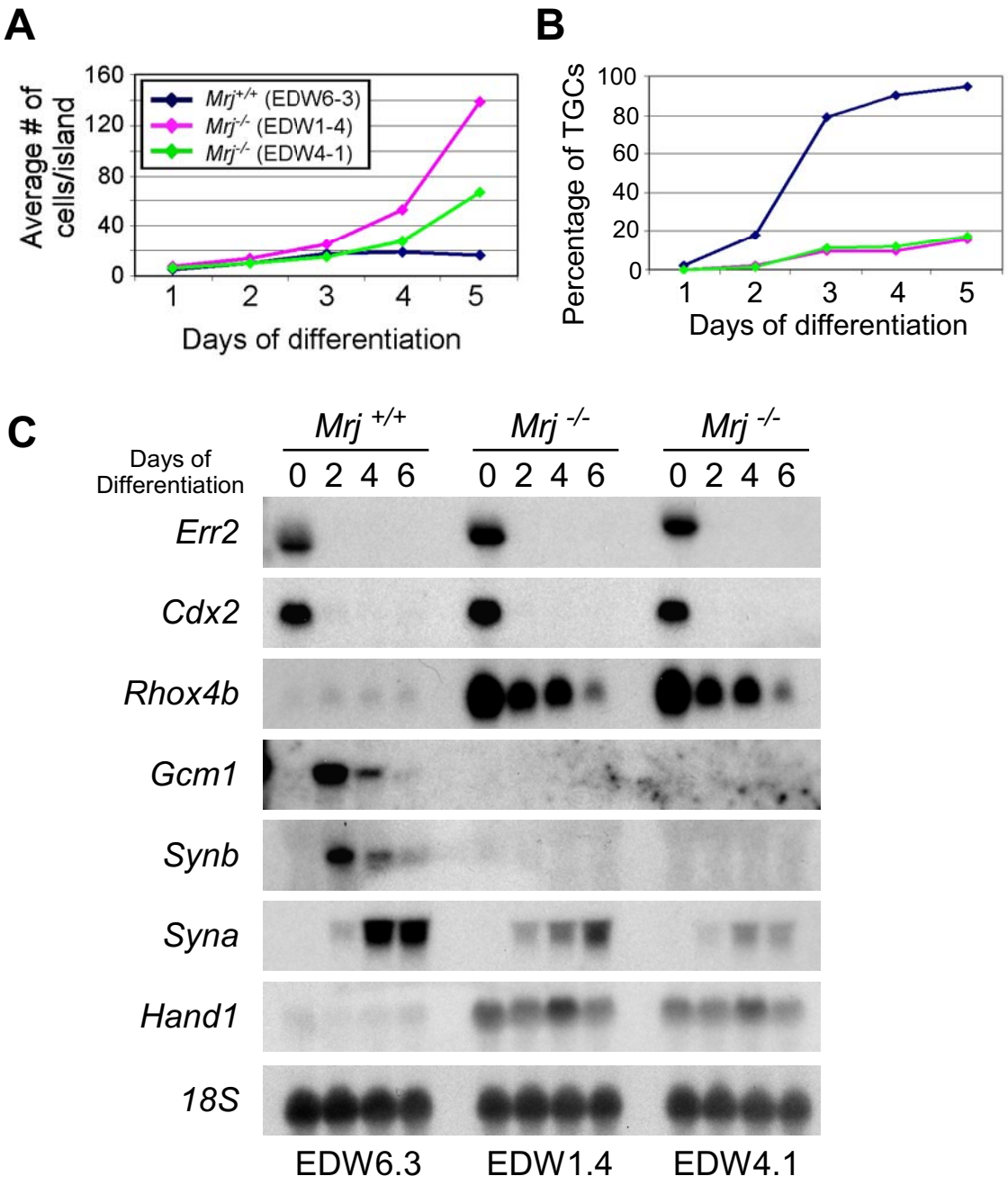
A
Average # of cells/island
160
120
80
40
0
Mrj+/+ (EDW6-3)
Mrj-/- (EDW1-4)
Mrj-/- (EDW4-1)
1 2 3 4 5
Days of differentiation
B
Percentage of TGCs
100
80
60
40
20
0
1 2 3 4 5
Days of differentiation
C
Mrj +/+
Mrj -/-
Mrj -/-
Days of Differentiation
0 2 4 6
0 2 4 6
0 2 4 6
Err2
Cdx2
Rhox4b
Gcm1
Synb
Syna
Hand1
18S
EDW6.3
EDW1.4
EDW4.1

cells from the two *Mrj*$^{-/-}$ TS cell lines were characterized as TGCs (Fig 3.6B) demonstrating that *Mrj*$^{-/-}$ cells have a reduced ability to differentiate.

To further examine if *Mrj*$^{-/-}$ chorionic cells were capable of differentiating into SynT cells, we performed northern blot experiments on RNA from TS cell cultures. No differences were apparent in the expression patterns of trophoblast stem cell markers *Err2* (*Esrrb*, *Errβ*) and *Cdx2* between *Mrj*$^{+/+}$ and *Mrj*$^{-/-}$ cells (Fig 3.6C). This suggested that multipotent stem cells were present in *Mrj*$^{-/-}$ TS cultures and that these cells were able to differentiate when growth factors were removed. Conversely, *Rhox4b* expression, a marker of labyrinth progenitors, was significantly up-regulated in both mutant cell lines compared to wildtype cells (Fig 3.6C). The expression of genes specific to differentiated SynT cells such as *Gcm1*, *Synb* and *Syna* were undetectable or markedly reduced in *Mrj*$^{-/-}$ cells (Fig 3.6C). The expression of *Hand1* which denotes ectoplacental cone, spongiotrophoblast and TGCs, however, was up-regulated throughout all days of differentiation in *Mrj*$^{-/-}$ cells (Fig 3.6C). Together, these data suggested that in the absence of *Mrj*, labyrinth progenitors have a reduced ability to differentiate into SynT cells. Instead, these cells remain as progenitors or, alternatively, may differentiate into *Hand1*-positive cells, though by morphology they do not differentiate into TGCs as frequently.

3.4 Discussion

Our data suggest that *Mrj* is required for patterning and differentiation of the multiple layers of trophoblast cells in the chorion. Interestingly, *Mrj*$^{-/-}$ TS cells are able to initiate differentiation since they can shut off the expression of genes associated with multipotent

TS cells (*Err2*, *Cdx2*). However, they are inhibited in their ability to progress beyond the *Rhox4b*-positive (common labyrinth progenitor) stage to form more differentiated syncytiotrophoblast precursors. This is likely associated with the altered Ln α5 expression in the basement membrane leading to a dramatic change in cell-cell adhesion, since the cell adhesion phenotype can be reversed by providing exogenous Ln α5 extracellular matrix. Therefore, changes in cell-cell and cell-matrix communications are part of a complex network of interactions required for normal patterning of the chorion, allantoic receptivity and progenitor cell differentiation.

3.4.1 Laminin α5 substrate stabilizes **Mrj** *mutant cell behaviour*

Laminin is a critical component of the basement membrane and is required for normal development and function of many tissues. Changes in laminin deposition are detected by membrane-bound integrin receptors at focal adhesion complexes that cause the reorganization of the actin cytoskeleton and the transduction of signals to the nucleus which alter cell proliferation, migration and differentiation programs (Boudreau et al, 1995). Ln α5 and Ln α1 in particular are differentially expressed within the developing conceptus and have distinct effects on trophoblast cell behaviour (Klaffky et al, 2001; Klaffky et al, 2006). Ln α1 discourages migration and spreading of the cell onto the substrate whereas Ln α5 promotes spreading, enhances cadherin-mediated cell-cell adhesion and persistent migration (Klaffky et al, 2006; this study). Thus altering laminin deposition and/or organization can drastically change the behaviour of a cell.

The importance of Ln α5 and its receptor α7 integrin in placental development is emphasized by *Ln α5* (*Lama5*) and *α7 integrin* (*Itga7*) mutant conceptuses which both

undergo chorioallantoic attachment but die shortly thereafter due to improper interaction between the SynT cells and the fetal blood vessels leading to reduced branching within the developing labyrinth (Miner et al, 1998; Welser et al, 2007). The differentiation capability of trophoblast cells in these mutants was not determined. We have shown that Ln α5 is typically expressed between the trophoblast and mesothelial layers of the chorion. Therefore, interactions between these cell layers necessary for allantoic receptivity and chorionic patterning may be mediated by Ln α5 expression. *Mrj*$^{-/-}$ chorions and TS cells both revealed that Ln α5 protein may not be presented on the basal extracellular surface. Disruption of the keratin cytoskeleton (Ameen et al, 2001; Salas et al, 1997; Gilbert et al, 2001; Styers et al, 2004; Oriolo et al, 2006) and the actin cytoskeleton (Quinlan and Hyatt, 1999) or misexpression of cell adhesion complexes (Peifer, 1993; Martin-Belmonte and Mostov, 2008) can alter the polarity of a cell which affects the trafficking of apically- or basally-destined proteins to their appropriate location. Analysis of Ln α5 expression in *Mrj*$^{-/-}$ chorion trophoblast cells revealed that it is not appropriately localized at the basal region of the cell suggesting that protein aggregation may disrupt cell polarity which in turn may prevent the extracellular secretion of Ln α5. Alternatively, Ln α5 protein may be deposited outside of the cell but it may be inappropriately organized for receptor recognition. Further analysis to detect the exact localization and organization of Ln α5 using deconvolution or electron microscopy is required. Regardless, improper secretion or organization of Ln α5 would result in a situation similar to *Ln α5* deficiency.

Remarkably, providing *Mrj*$^{-/-}$ TS cells with a normal Ln α5 substrate can rescue their erratic migratory and repulsive behaviour. Typically, a normal ECM can cluster

specific integrin receptors at focal adhesion sites on the cell surface which in turn can reorganize the actin cytoskeleton and alter gene expression (Chan et al, 2007). Because *Mrj*-deficient TS cells behave similar to wildtype cells when plated on Ln α5, it implies that the actin cytoskeleton, though aggregated in *Mrj* mutants, is still responsive to the extracellular environment and specifically to Ln α5. Therefore, Ln α5 functional deficiency in *Mrj* mutant chorions likely impedes proper signalling required for allantoic attachment and labyrinth progenitor induction. *Mrj* deficiency is more severe than *Ln α5* deficiency possibly due to abnormal presentation of other ECM proteins [e.g. Cyr61 (Mo et al, 2002) and HAI-1 (Szabo et al, 2002; Fan et al, 2007)] in $Mrj^{-/-}$ chorions or effects associated with other Mrj-substrate interactions (Dai et al, 2005; Hurst et al, 2006; Pan et al, 2008; Li et al, 2008; Zhang et al, 2008).

The cell-cell adhesion and actin cytoskeleton phenotype in *Mrj* mutant chorions could theoretically be the consequence of keratin aggregation. We are in the process of formally testing this hypothesis by examining the state of cell-cell adhesion and actin localization in *Mrj/K18* double mutant chorions. However, given that providing exogenous Ln α5 protein in vitro reverts the cell-cell adhesion phenotype in *Mrj*-deficient TS cells, we strongly favour the hypothesis that the adhesion and actin defects are secondary to the ECM defect. We are in the process of determining if the actin cytoskeleton and trophoblast gene expression are normalized in *Mrj* mutant cells plated on Ln α5 substrate.

3.4.2 Patterning of the chorion is impeded in Mrj *mutants*

The three differentiated trophoblast cell types in the labyrinth (SynT-I, SynT-II and S-TGC) are thought to be derived from distinct precursors in the chorion that are determined as early as E8.5 (Simmons et al, 2008) (see Fig. 1.2). Although lineage tracing experiments have not been completed to clarify the origins of these cells, they have been defined by cell-layer-restricted gene expression (Simmons et al, 2008). The basal layer of the chorion contains clusters of proliferative *Rhox4b*$^{+}$ cells hypothesized to be labyrinth progenitors based on the fact that *Rhox4b* expression co-localizes with *Err2* and *Cdx2* at early post-implantation stages and persists in cells with similar morphology even after *Err2* and *Cdx2* expression decline (D. Simmons, D. Natale and J. Cross, unpublished observations). *Rhox4b*$^{+}$ cells are flanked by *Gcm1*/*Synb*/*Cebpa*-expressing cell clusters that mark branchpoint initiation sites and give rise to SynT-II cells. The apical layer of the chorion, which later becomes SynT-I cells, expresses *Syna*. Lastly, the cells at the base of the ectoplacental cone/top of the chorion express *Hand1* and are the precursors to S-TGCs. Abnormal chorionic patterning likely affects the differentiation of labyrinth cell types, the function of the placenta and survival of the fetus.

We show here that the two basal-most layers of *Mrj*$^{-/-}$ chorions are mispatterned. Genes normally expressed within these layers (*Gcm1*/*Synb*/*Cebpa* and *Syna*) are down-regulated or undetectable suggesting that the induction of both SynT cell precursors is prevented by *Mrj*-deficient conditions. Instead, *Mrj*$^{-/-}$ chorionic trophoblast cells continue to express *Rhox4b* and thus are maintained in a progenitor-state. The lack of SynT precursor specification is likely attributed to the fact that *Mrj* mutant cells have abnormal cytoskeletons and cell-cell/cell-matrix contacts which in turn alters cell polarity and thus

signalling between cells. However, it is important to note neither the induction nor the maintenance of *Syna* and *Hand1* expression patterns is dependent upon the presence of *Gcm1*/*Synb*/*Cebpa*-expressing cells since both are properly specified in *Gcm1*$^{-/-}$ and *Cebpa*$^{-/-}$;*Cebpb*$^{-/-}$ mutant placentas (Simmons et al, 2008). Furthermore, the *Hand1*-expressing S-TGC precursor cells are appropriately positioned at the top layer of *Mrj*$^{-/-}$ chorions, suggesting that S-TGCs are able to form independently of the SynT precursors and that these cells cannot induce *Syna*$^{+}$ or *Gcm1/Synb/Cebpa*$^{+}$ precursor cells. As a result, signalling between cell layers is not necessary for induction yet non-autonomous signalling within each cell layer may be required. To fully understand these interactions, it will be important to assess other mutants with trophoblast defects in their chorion or labyrinth for the establishment of chorionic patterning between E7.5 and E9.5 [e.g. *CtBP1*$^{-/-}$;*CtBP2*$^{-/-}$ (Hildebrand and Soriano, 1999); *CyclinF*$^{-/-}$ (Tetzlaff et al, 2004); *Grb2* hypomorph (Saxton et al, 2001); *Wnt7b*$^{-/-}$ (Parr et al, 2001)].

3.4.3 **Mrj** *mutant chorionic trophoblast cells are maintained in a progenitor state*

Little is known regarding the trophoblast stem cell populations in the chorion and labyrinth. The ability to derive multipotent TS cell lines from the chorion declines after the occlusion of the ectoplacental cavity at E8.5 (Uy et al, 2002) suggesting that a common labyrinth cell precursor may not exist past the chorion stage. However, the number of trophoblast cells in the mature labyrinth outnumbers that of the chorion indicating that trophoblast cell proliferation continues and therefore implies the presence of a progenitor population (Simmons et al, 2008). In the chorion at E8.5, clusters of proliferative *Rhox4b*-positive cells are located at its base close to the chorioallantoic

interface and may represent this progenitor pool (Cross et al, 2006; A. Davies, E. Mariusdottir, D.R. Natale, D.G. Simmons and J.C. Cross, unpublished observations). How these *Rhox4b*$^{+}$ progenitor cells are regulated and how they contribute to the developing labyrinth is uncertain.

Mrj mutant chorion trophoblast cells are preserved in a labyrinth progenitor-state as evidenced by their continued expression of *Rhox4b* and failure to increase expression of genes specific to SynT-I and SynT-II cells. Furthermore, *Mrj*$^{-/-}$ TS cells continue to proliferate even in differentiating conditions. Based on our data, there are several explanations for why this may occur. First, altered expression of laminin may alter the niche of the progenitor cells. ECM proteins are essential to the establishment of stem cell niches (Morrison and Kimble, 2006). For example, the absence of ECM proteins in the haematopoietic stem cell niche results in continued proliferation and an increased number of haematopoietic stem cells (Nilsson et al, 2005). Second, altered cell polarity could affect asymmetric stem cell division, a mechanism required by some stem cell populations for the asymmetric partitioning of components that determine cell fate or the asymmetric placement of daughter cells to extrinsic cues (Morrison and Kimble, 2006). Symmetric (produces two stem cells) versus asymmetric division (produces one stem cell and one differentiated cell) is dependent upon the positioning of the microtubule organizing centre (MTOC) within the cell (Morrison and Kimble, 2006). Interestingly, the location of the MTOC prior to cell division relies on its interaction with the keratin cytoskeleton (Oriolo et al, 2006). Third, *Mrj* may be directly involved in cell cycle regulation (Pei et al, 1999; Hurst et al, 2006; Li et al, 2008; Zhang et al, 2008). We have observed that Mrj is expressed in the nuclei of TS cells (Chapter 2). Others have shown

that Mrj can stabilize the cell cycle regulator Schlafen-1 (Slfn1), an interaction that prevents cell cycle progression via cyclin D1 down-regulation (Zhang et al, 2008). Therefore, it is possible that Mrj acts in concert with this or other cell cycle regulators to control whether a labyrinth progenitor continues to proliferate or whether these cells undergo cell cycle arrest and start down the path of SynT differentiation.

In addition to remaining in a proliferative and undifferentiated state, *Mrj* mutant TS cells are highly migratory as indicated by live cell imaging and are unable to adhere to neighbouring cells, a phenotype reminiscent of tumour cells (Bilder, 2004). Interestingly, breast cancer tumour cells stably transfected with the long isoform of Mrj have reduced motility, migration and invasion capabilities both in vitro and in vivo (Mitra et al, 2008).

3.5 Materials and Methods

Mice and tissue preparation. *Mrj*$^{-/-}$ conceptuses were generated by crossing *Mrj*$^{+/-}$ females to *Mrj*$^{+/-}$ male mice (Hunter et al, 1999). The pregnant females were dissected at E8.5 (noon of the day that the vaginal plug was detected was considered E0.5). Genotyping was done as previously described (Chapter 2). Experiments were performed in accordance with the Canadian Council on Animal Care and the University of Calgary Committee on Animal Care (Protocol no. M06045).

Histology. For in situ hybridization, E8.5 implantation sites were removed from the uterus, fixed overnight at 4ºC in 4% paraformaldehyde (PFA)/1xPBS overnight at 4ºC, processed through a sucrose gradient and embedded in OCT compound (Sakura Finetek USA Inc.) for preparation of frozen sections. Eight to 10 µm frozen sections were adhered to Super Frost Plus slides (VWR International, Inc.) and stored at -80ºC until

used. For immunohistochemical staining, E8.5 implantation sites still maintained in the uterus were fixed in 4%PFA/1xPBS overnight at 4ºC, embedded in paraffin and cut sagitally into 7 μm paraffin sections.

Probes. The following cDNA probes were previously described: *Gcm1* (Basyuk et al, 1999), *Cebpα*, *Synb*, *Syna* (Simmons et al, 2008), *Err2* (also known as *Errβ*; Luo et al, 1997), *Vegf* (Breier et al, 1992), *Snail* (Smith et al, 1992), *Rhox4b* (also known as *Ehox*, Jackson et al, 2003; D. Natale and J. Cross, unpublished data), *Tpbpα* (previously known as 4311; Lescisin et al, 1988), *Hand1* (Cross et al, 1995) and *Mash2* (Guillemot et al, 1994). The *Cdx2* probe was a generous gift from J. Rossant (Hospital for Sick Children, Toronto) (Tanaka et al, 1998).

In situ hybridization. In situ hybridization was carried out as previously described (Simmons et al, 2007).

Northern Blots. Total RNA from TS cell cultures was collected at days 0, 2, 4 and 6 of differentiation (cultured without FGF4, Heparin and embryonic fibroblast conditioned media) and was isolated using QIAshredder and RNeasy columns (Qiagen, Inc.) following the manufacturers instructions. Ten 10 μg of total RNA was separated on a 1.1% formaldehyde agarose gel, blotted onto GeneScreen nylon membrane (Perkins Elmer) and UV cross-linked. Random-primed DNA labelling of cDNA probes was carried out with 25 μCi ^{32}P-dCTP and probes were isolated on Sephadex G-50 columns (Amershan Biosciences Inc). Hybridizations were done at 60ºC overnight in hybridization buffer as previously described (Church and Gilbert, 1984). Following post-hybridization washers, signals were detected by exposure to BioMaz MR film (Kodak) at -80ºC.

Cell culture. Wildtype (line EDW6-3) and *Mrj* homozygous mutant (lines EDW1-4 and EDW4-1) trophoblast stem (TS) cell lines (Chapter 2) and the *Rs26* TS cell line (kindly provided by J. Rossant, Hospital for Sick Children, Toronto, Canada) (Tanaka et al., 1998) were maintained in 25 ng/ml basic fibroblast growth factor (bFGF), 1 µg/ml heparin in TS cell medium, 70% of which was pre-conditioned by embryonic fibroblasts, at 37°C under 95% humidity and 5% CO2. Cells were differentiated by withdrawing bFGF, heparin and fibroblast-conditioned medium (Tanaka et al., 1998).

X-gal and immunofluorescence antibody staining. For X-gal staining, tissue was fixed, stained as whole mount and paraffin embedded as previously described (Hunter et al., 1999). Cell cultures were fixed in 4% PFA for 10 minutes, treated with 0.1% Triton X-100 (Fisher Biotech) for 10 minutes and blocked in 1% BSA/1xPBS for 30 minutes. Primary antibodies and dilutions used include: anti-cytokeratin 18 (Ks18.04, 1:100; RDI), rhodamine conjugated anti-phalloidin (1:1000; Sigma Aldrich), anti-β-catenin (1:100; BD Biosciences), anti-E-cadherin (1:100; Zymed Laboratories Inc). Immunofluorescence staining for laminin α5 required that the cells be fixed with 4% PFA/1xPBS for 30 minutes and subsequently with -20ºC methanol for 10 minutes on ice. Cells were blocked with 0.8% BSA/1xPBS and exposed to anti-laminin α5 (1:30; G-20 Santa Cruz). Secondary antibodies were used at a dilution of 1:300 and included: goat anti-mouse Cy3 (Jackson ImmunoResearch Laboratories), donkey anti-goat Cy3 (Jackson ImmunoResearch Laboratories) and goat anti-mouse Alexa Fluor 488 (Molecular Probes). Antibody dilutions were made in 1% BSA, 5% host serum. DNA was counterstained with 1:10,000 bisbenzimide (Sigma). For immunohistochemical staining, rehydrated paraffin sections of E8.5 conceptuses were treated with 3% H_2O_2/1xPBS for

30 minutes to block endogenous peroxidase activity and then with 1mg/mL Trypsin (Sigma) for 10 minutes for antigen retrieval. Sections were blocked with 1% BSA/1xPBS for 30 minutes and then exposed to Laminin α5 primary antibody (G-20 Santa Cruz) was diluted 1:30 in 1% BSA/1xPBS for 1 hour followed by donkey anti-goat HRP-conjugated secondary antibody (1:300; Santa Cruz) in 1%BSA/1xPBS for 1 hour. Sections were counterstained in nuclear fast red for 2 minutes, dehydrated in ethanol, treated with xylene and mounted in Cytoseal® (Richard-Allen Scientific).

Western Blots. Whole cell protein lysates were collected from wildtype (Rosa26) and *Mrj*$^{-/-}$ (EDW1-4) TS cells cultured in proliferating conditions (2 days of culture in the presence of bFGF and CM) or in differentiation conditions (5 days of culture in the absence of bFGF and CM). Using standard procedures, 60 μg of protein/well was electrophoresed on a 10% polyacrylamide gel and transferred onto an Immobilon-PSQ® membrane (Millipore, cat no. ISEQ15150). The membrane was blocked in 3% donkey serum in TBST (Tris-buffered saline plus 0.1% tween-20) for 1 hour at room temperature and then incubated in 1:500 goat polyclonal anti-laminin α5 (G-20, Santa Cruz) diluted in 0.1% donkey serum/TBST overnight at 4ºC. After the membrane was washed three times in TBST for 10 minutes each wash, it was incubated in 1:5,000 HRP-conjugated donkey anti-goat IgG secondary antibody (Santa Cruz) diluted in 0.1% donkey serum/TBST for 1 hour at room temperature. Protein bands were detected with the ECL kit (Amersham Biosciences).

Time lapse video microscopy. Time lapse microscopy was carried out as previously described (Klaffky et al, 2006). Briefly, Rs26 or *Mrj*$^{-/-}$ (EDW1-4) TS cells were plated on 35 mm Greiner tissue culture dishes with or without laminin substrate coating (1.25 mL

of a 10 μg/mL solution in PBS without calcium and magnesium-CMF-PBS) and blocked with 1% BSA (Sigma). Laminin α1 (EHS sarcoma laminin) was obtained from BD Biosciences. Laminin α5 (human placental laminin) was obtained from EMD Biosciences. Cells were cultured in TS cell medium with FGF and CM, overlaid with mineral oil and incubated in a PMDI-2 stage incubator (Harvard Apparatus) on an Olympus IX70 microscope equipped with phase optics. Digital images were collected every 2 minutes over a period of 18 hours. Images were captured using a Hamamatsu Orca camera driven by Openlab 2.0 software on a Macintosh G3 computer.

Equipment and software. A Leica DMR light microscope (for fluorescent and light images) and Leica DMIL inverted light microscope (for cell culture images) with Photometrics Coolsnap cf camera and Openlab 2.2.2 imaging software program were used to obtain micrographs. Cell area was measured using Openlab 2.2.2. Filters used were from Chroma: DAPI (31000), TRITC (31002) and FITC (31001). Minimal image processing was performed using Adobe Photoshop 7.0 and figures were constructed using Canvas X.

CHAPTER FOUR

NEURAL TUBE CLOSURE AND STEM CELL SELF-RENEWAL REQUIRE THE MRJ CO-CHAPERONE

E. Watson performed all experimental aspects of this chapter.

4.1 Abstract

The Mrj co-chaperone is required for placental development by preventing the formation of toxic keratin aggregates in trophoblast cells. Mrj is widely expressed throughout the mouse conceptus but a role for Mrj in the development of the embryo proper has never been determined. Here we show that *Mrj*$^{-/-}$ embryos exhibit neural phenotypes at embryonic day (E) 9.5 including small neural tubes or, in more serious cases, exencephaly, independently of their placenta defect. The small size of *Mrj*$^{-/-}$ neural tubes was due to fewer proliferating cells whereas levels of apoptosis were normal. This indicated that Mrj may influence neural stem cell proliferation. Neurospheres cultured from *Mrj*$^{-/-}$ telencephalons at E9.5 had fewer cells and a reduced ability to form secondary neurospheres upon subcloning compared to wildtype. Therefore, Mrj was required for stem cell self-renewal. The Bmi-1 transcription factor is one of the few proteins known to be involved in self-renewal of neural stem cells and *Bmi-1*$^{-/-}$ neurospheres have a similar self-renewal phenotype to *Mrj*$^{-/-}$ neurospheres. However, we found that Mrj and Bmi-1 proteins had different subcellular expression patterns in vivo and Bmi-1 expression was normal in *Mrj*$^{-/-}$ neural tubes compared to wildtype. Nestin, an intermediate filament protein that is expressed in neural stem cells, does co-localize with Mrj in the cytoplasm. However, no obvious aggregates of Nestin were observed in *Mrj*$^{-/-}$ neural tubes by immunohistochemistry suggesting that we have yet to identify a substrate for Mrj in neural tube development. Whether the exencephaly phenotype is related to the self-renewal phenotype in *Mrj*$^{-/-}$ neural tubes remains to be determined.

4.2 Introduction

The Mrj co-chaperone is required for normal mouse embryo development since *Mrj*$^{-/-}$ conceptuses fail to undergo the first step of placenta development called chorioallantoic attachment. The absence of placenta development causes embryonic lethality at E10.5 due to a lack of nutrient transfer from the mother to the fetus (Hunter et al, 1999). As previously discussed in Chapter 2, this chorioallantoic attachment phenotype is caused by the formation of large toxic aggregates of keratin intermediate filaments in the chorionic trophoblast cells due to improper targeting of Keratin 8/18 filaments to the proteasome for degradation. These aggregates disrupt chorion polarity by preventing normal cell-cell interactions. Mrj is widely expressed in many tissues of both the embryo and adult mouse (Hunter et al, 1999) suggesting that Mrj may also play an important role in the development of the embryo proper and later in adult life. Interestingly, we observed that *Mrj*$^{-/-}$ embryos also exhibit neural tube defects including exencephaly and small neural tubes, independently of their placenta defect.

There are 190 known mouse models for neural tube defects (NTDs) that result in failure of neural tube closure (exencephaly and/or spina bifida) (reviewed by Harris and Juriloff, 2007). Despite this large list of mutants, there are only a few molecular pathways that have emerged; therefore, the mechanisms of neural tube closure are not well understood. Since keratin is not expressed within the neural lineage, Mrj must act on another substrate during this process. Therefore, how Mrj fits into the molecular scheme requires further exploration.

During tube closure, the neural plate must undergo substantial changes including convergence and extension to establish planar cell polarity, neural crest migration,

apoptosis, proliferation and differentiation (Copp, 2005). The latter two processes indicate a role for stem cells in neural tube closure. To sustain a stem cell population, a delicate balance between self-renewal and differentiation must be maintained either by intrinsic factors or via the interaction of stem cells with their niche. Here we implicate Mrj in neural stem cell self-renewal, adding it to a short list of proteins that are known to be involved in this process.

4.3 Results

4.3.1 Mrj$^{-/-}$ *embryos exhibit exencephaly at E9.5 independently of the extra-embryonic defect*

To determine whether Mrj is required for the development of the embryo proper, we analyzed embryos from *Mrj*$^{+/-}$ intercrosses at embryonic (E) day 9.5. We observed that 26.9% of *Mrj*$^{-/-}$ embryos (n=41 embryos) displayed open neural tubes exclusively within the cranial region (exencephaly) (Fig. 4.1B). By contrast, the neural tubes of the remaining 73.1% of *Mrj*$^{-/-}$ embryos were closed (Fig. 4.1A) similar to wildtype and *Mrj*$^{+/-}$ embryos (n=171). Using β-galactosidase activity driven from the *Mrj* gene-trap allele in whole mount embryos (Fig, 4.1C-E), Mrj expression was detected throughout the neural tube during the period of neural tube closure (E7.5-E9.5). Together these data indicate that the Mrj co-chaperone plays an important role in neural tube development.

It has previously been shown that irregular placenta development can secondarily cause embryonic defects including brain abnormalities (Wu et al, 2003). To determine whether the neural tubes of *Mrj*$^{-/-}$ embryos remained open as a result of the chorioallantoic attachment defect, we re-analyzed our results from the tetraploid

FIGURE 4.1 – *Mrj*$^{-/-}$ embryos exhibit exencephaly with incomplete penetrance at E9.5. (A) A *Mrj*$^{-/-}$ embryo at E9.5 including a neural tube (nt) with normal closure. The center panel (higher magnification of the boxed region in the left panel) shows the cranial neural tube region. A dorsal view of the embryo (right panel) with normal closure in the future spinal cord region. Scale bars = 250 μm. (B) A *Mrj*$^{-/-}$ embryo at E9.5 with an open neural tube in the cranial region (left and center panels; center panel represents a higher magnification of the boxed region in the left panel). Dorsal view (right panel) of embryo shows closure of the future spinal cord region. Scale bars = 250 μm. (C-E) Mrj expression (blue) was determined in E7.5 (C), E8.5 (D) and E9.5 (E) embryos using β-galactosidase activity driven from the Mrj gene-trap allele in *Mrj*$^{+/-}$ embryos. (C) Left panel shows a *Mrj*$^{+/+}$ embryo (white) without β-galactosidase expression.

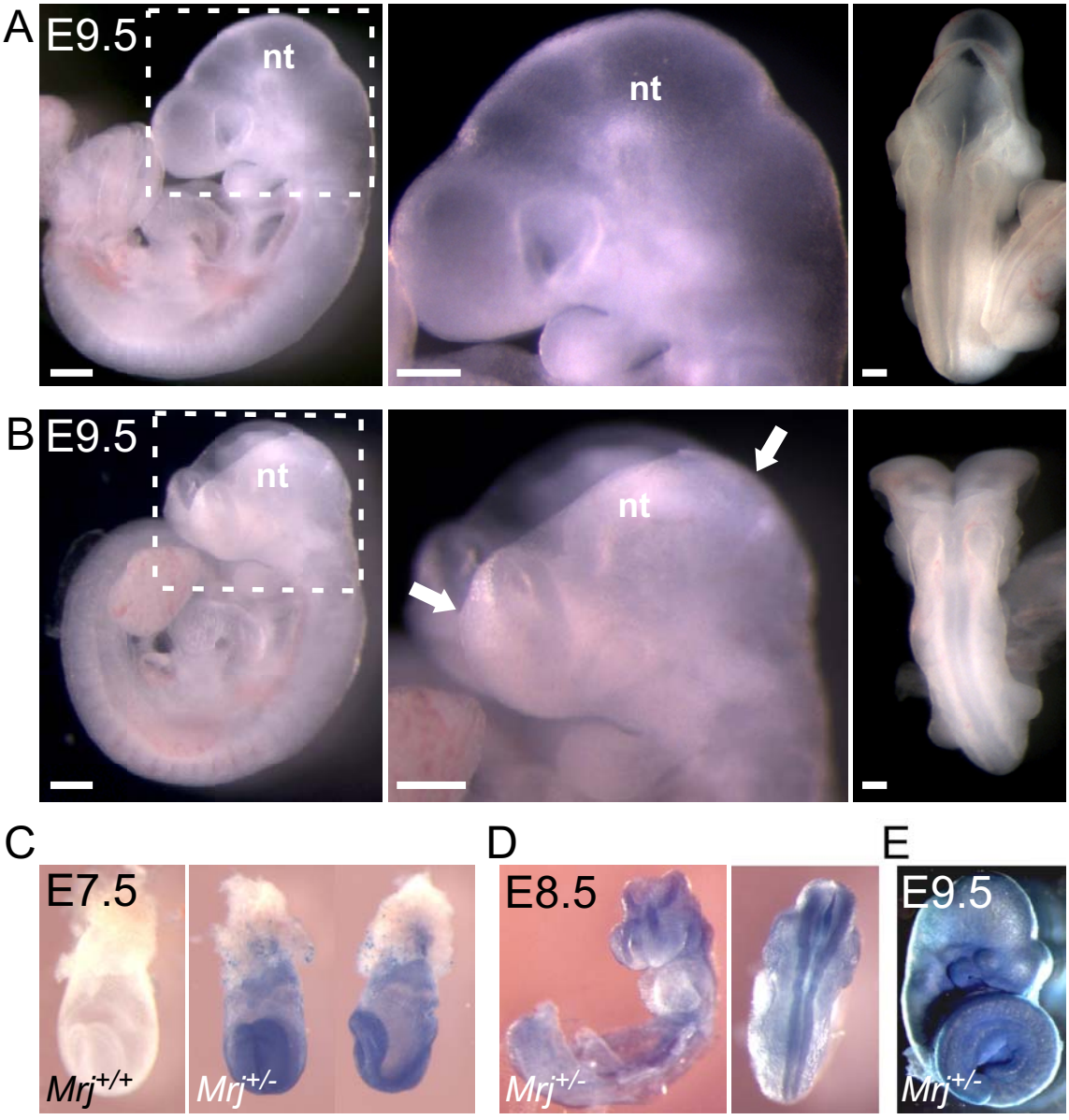
A
E9.5
nt
nt
B
E9.5
nt
nt
C
E7.5
Mrj+/+
Mrj+/-
D
E8.5
Mrj+/-
E
E9.5
Mrj+/-

aggregation experiments in Chapter 2. One of two *Mrj*$^{-/-}$ embryos in which chorioallantoic attachment was rescued displayed exencephaly at E9.5 (data not shown) similar to *Mrj*$^{-/-}$ embryos lacking chorioallantoic attachment. This implied that the neural tube closure defect seen in *Mrj*$^{-/-}$ embryos was independent of the placental defect.

4.3.2 Mrj mutant neural tubes are small and thin at E9.5 due to reduced proliferation

Since the neural tube closure phenotype in *Mrj*$^{-/-}$ embryos displayed incomplete penetrance, we assessed *Mrj*$^{-/-}$ embryos with closed neural tubes for other defects. Using histological sections of E9.5 embryos from *Mrj*$^{+/-}$ intercrosses, we measured the average neural tube diameter and wall thickness within the cranial and the future spinal cord regions (Fig. 4.2A-C). *Mrj*$^{-/-}$ neural tubes had similar average neural tube diameters in the cranial region (103.2 ± 3.2 µm [± s.e.m.], n=5 embryos) compared to *Mrj*$^{+/+}$ (103.1 ± 5.0 µm, n=4) and *Mrj*$^{+/-}$ (123.5 ± 4.8 µm, n=5) embryos (Fig. 4.2A, C). However, the average diameter of *Mrj*$^{-/-}$ neural tubes within the future spinal cord region was significantly smaller (59.8 ± 4.4 µm, n=5 embryos; $P<0.05$) compared to control neural tubes (*Mrj*$^{+/+}$ = 74.1 ± 4.3 µm [n=4]; *Mrj*$^{+/-}$ = 72.0 ± 4.0 µm [n=5]) (Fig. 4.2A, C). Additionally, we found that the walls of *Mrj*$^{-/-}$ neural tubes were considerably thinner in the spinal cord region (30.6 ± 1.1µm, n=5 embryos; $P<0.01$) compared to the neural tubes of wildtype (37.7 ± 1.6 µm; n=4) and *Mrj*$^{+/-}$ (37.4 ± 1.7 µM; n=5) embryos (Fig. 4.2B, C). Together, these data implied that even *Mrj*$^{-/-}$ neural tubes that managed to close were abnormal.

We hypothesized that *Mrj*-deficient neural tubes were smaller and thinner due to an increase in apoptotic cells and/or a decrease in cell proliferation. Therefore, we first performed TUNEL labelling on histological sections at E9.5 and calculated the percentage of TUNEL positive (apoptotic) cells within the neural tube. $Mrj^{-/-}$ embryos contained an average of 4.3 ± 0.38% of cells (n=5 embryos) that were TUNEL positive (Fig. 4.2E), a percentage comparable to neural tubes from both wildtype (4.1 ± 0.67%, n=4) and $Mrj^{+/-}$ (4.3 ± 0.38%, n=5) embryos (Fig. 4.2E). This suggested that *Mrj* deficiency does not affect apoptosis within the neural tube. Alternatively, an antibody against phosphohistone H3 (PHH3) was used to detect cells undergoing mitosis. Normally, mitotic cells are found adjacent to the lumen of the neural tube. Within $Mrj^{+/+}$ and $Mrj^{+/-}$ embryos, 24.1 ± 1.58% (n=4 embryos) and 21.6 ± 0.68% (n=5) of these cells, respectively, were PHH3 positive (Fig. 4.2D). By contrast, $Mrj^{-/-}$ neural tubes contained only 11.4 ± 0.96% (n=5; $P<0.0001$) (Fig. 4.2D). From this, we concluded that *Mrj* deficiency reduces the ability of neural stem cells/progenitors to proliferate.

4.3.3 Mrj$^{-/-}$ *neural stem cells display a reduced ability to self-renew*

Due to a failure of placental formation, $Mrj^{-/-}$ embryos die at E10.5 (Hunter et al, 1999) prior to the development of most brain structures. As a result, it is difficult to assess the role of Mrj during brain development. To circumvent this, we derived neurosphere cultures from $Mrj^{-/-}$ telencephalons at E9.5 which allowed us to study the characteristics of $Mrj^{-/-}$ neural stem cells in vitro. Neurospheres are floating spheroid structures that derive from neural stem cells and contain heterogeneous clones of cells including neurons and glia in

FIGURE 4.2 – *Mrj*$^{-/-}$ neural tubes at E9.5 are smaller due to reduced proliferation. (A-B) Graphs depicting the diameter of neural tubes in cranial and future spinal cord regions (A) and thickness of neural tubes in the future spinal cord region (B) from *Mrj*$^{+/+}$, *Mrj*$^{+/-}$ and *Mrj*$^{-/-}$ embryos at E9.5. Data are presented as means ± s.e. from at least four independent experiments. Student's *t* test: *P<0.05, **P<0.01. (C-E) Histological sections of neural tubes from *Mrj*$^{+/+}$ (left column), *Mrj*$^{+/-}$ (center column) and *Mrj*$^{-/-}$ embryos (right column) at E9.5. Bottom panels are higher magnifications of the boxed in regions depicted in the panels directly above in C and D. (C) Hematoxylin (blue; nuclei) and eosin (pink; cytoplasm) staining. Black bars in bottom panels portray region measured for neural tube thickness. (D) Phosphohistone H3 (PPH3) antibody staining (brown) with nuclear fast red counterstaining (pink; nuclei). (E) TUNEL staining (brown) with hematoxylin counterstaining (blue; nuclei).

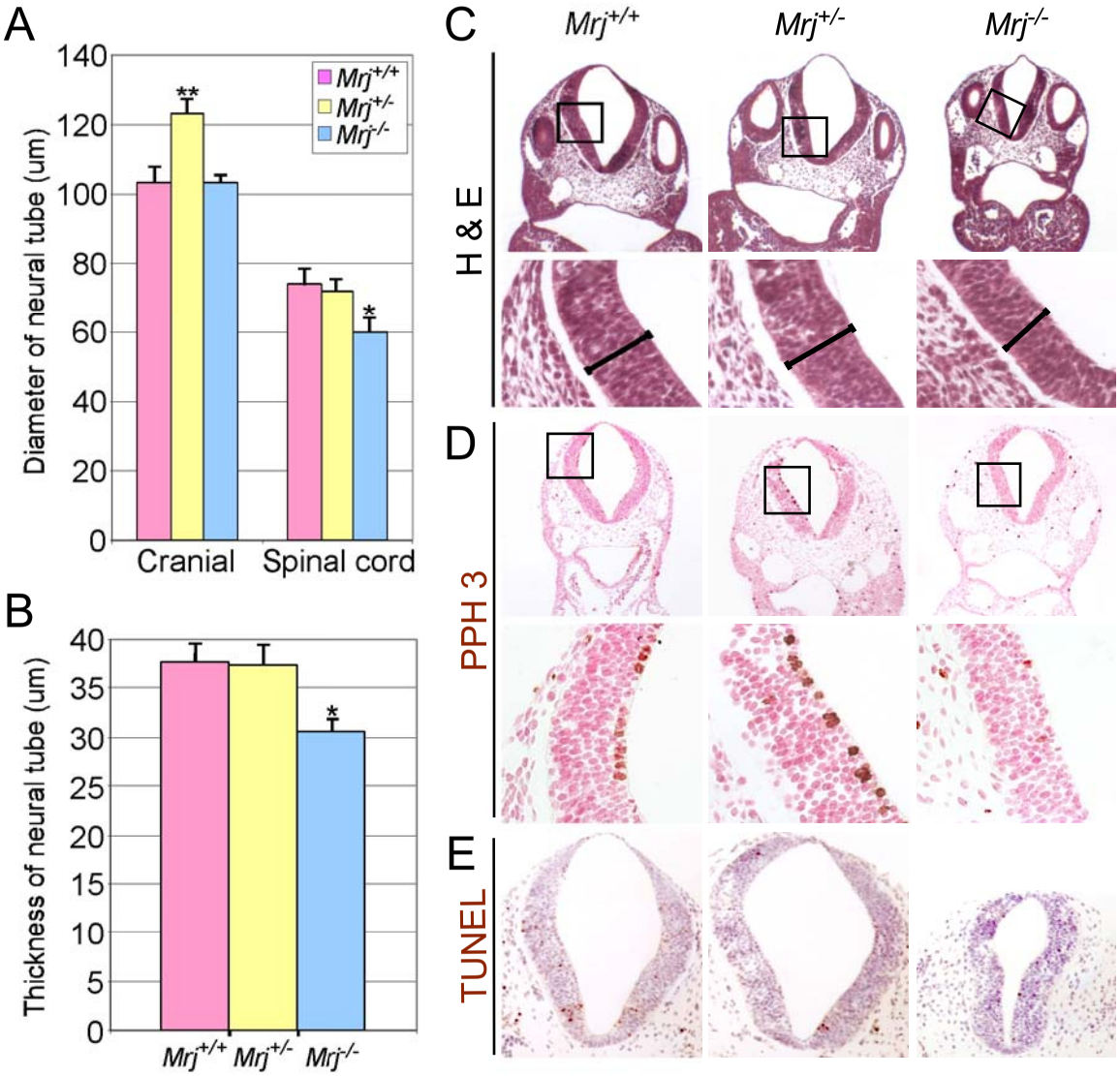
A
Diameter of neural tube (um)
140
120
100
80
60
40
20
0
Mrj+/+
Mrj+/-
Mrj-/-
**
*
Cranial
Spinal cord
B
Thickness of neural tube (um)
40
35
30
25
20
15
10
5
0
*
Mrj+/+
Mrj+/-
Mrj-/-
C
Mrj+/+
Mrj+/-
Mrj-/-
H & E
D
PPH 3
E
TUNEL

addition to more neural stem cells (Campos, 2004). Since all E9.5 embryos are relatively small and it is estimated that only 5-20% of cells within the telencephalon are stem cells (Temple, 2001), telencephalons were pooled together into two groups as determined by their chorioallantoic attachment phenotype: the first group (control) contained $Mrj^{+/+}$ embryos together with $Mrj^{+/-}$ embryos, and the second group contained only $Mrj^{-/-}$ embryos. The heads were mechanically dissociated and plated in neurosphere media in fibroblast growth factor (FGF) for 5 days (Fig. 4.3A). $Mrj^{-/-}$ telencephalon cells were able to form neurospheres, although at a lower frequency (6.65 ± 1.41 neurospheres/10^5 cells plated, n=9 pools, $P<0.05$) than $Mrj^{+/+}$/$Mrj^{+/-}$ pooled telencephalon cells (14.92 ± 2.52 neurospheres/10^5 cells plated, n=14) (Fig. 4.3B, D) suggesting that there are significantly fewer stem cells in $Mrj^{-/-}$ telencephalons. Furthermore, $Mrj^{-/-}$ neurospheres were also approximately 5-fold smaller in area (29 ± 13 μm^2, n=171 neurospheres, $P<0.0001$) compared to $Mrj^{+/+}$/$Mrj^{+/-}$ neurospheres (142 ± 1 μm^2, n=418) (Fig. 4.3C) and gave rise to 6-fold fewer (2.18 ± 0.54 neurospheres, n=9 pools, $P<0.001$) secondary neurospheres upon subcloning compared to $Mrj^{+/+}$/$Mrj^{+/-}$ neurospheres (13.27 ± 2.00 neurospheres, n=14) (Fig. 4.3D, E). Together, these data indicated that Mrj is required to maintain self-renewal of neural stem cells.

4.3.4 Bmi-1 expression pattern is normal in $Mrj^{-/-}$ neural tubes at E9.5

Few factors are known to be involved in stem cell self-renewal. One protein, the Bmi-1 transcriptional repressor, is required for self-renewal but not survival or differentiation of neural stem cells (Molofsky et al, 2003). Mrj, itself, has been implicated in transcriptional regulation (Dai et al, 2005; Hurst et al, 2006; Pan et al, 2008) and, at least in trophoblast

FIGURE 4.3 – *Mrj*$^{-/-}$ neural stem cells exhibit a reduced ability to self-renew.

(A) Schematic diagram depicting the neurosphere culture method. (B) Primary neurospheres from *Mrj*$^{+/+}$ and *Mrj*$^{+/-}$ pooled embryos (top) and *Mrj*$^{-/-}$ embryos (bottom). Scale bars = 50 μm. (C) Average areas of primary and secondary neurospheres from *Mrj*$^{+/+}$ and *Mrj*$^{+/-}$ pooled embryos and *Mrj*$^{-/-}$ embryos. (D) Average number of primary and secondary neurospheres from *Mrj*$^{+/+}$ and *Mrj*$^{+/-}$ pooled embryos and *Mrj*$^{-/-}$ embryos per 10^5 cells plated. (E) Ratio of number of secondary neurospheres to primary neurospheres from data in D. Data in C-E are presented as means ± s.e., Student's *t* test: *P<0.05, ***P<0.001.

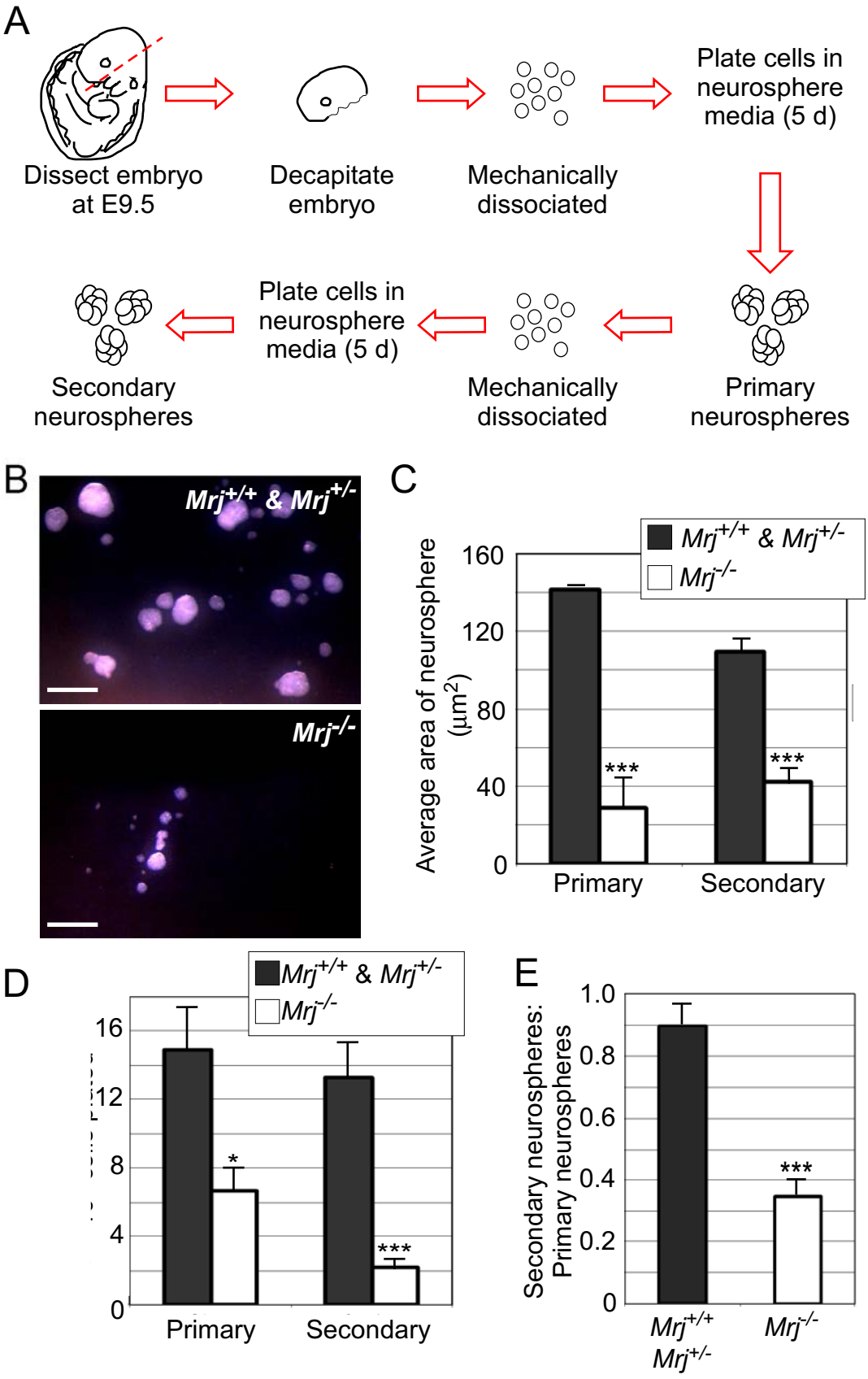
A
Dissect embryo at E9.5
Decapitate embryo
Mechanically dissociated
Plate cells in neurosphere media (5 d)
Primary neurospheres
Mechanically dissociated
Plate cells in neurosphere media (5 d)
Secondary neurospheres
B
Mrj+/+ & Mrj+/-
Mrj-/-
C
Mrj+/+ & Mrj+/-
Mrj-/-
Average area of neurosphere (µm2)
160
120
80
40
0
***
***
Primary
Secondary
D
Mrj+/+ & Mrj+/-
Mrj-/-
16
12
8
4
0
*
***
Primary
Secondary
E
Secondary neurospheres: Primary neurospheres
1.0
0.8
0.6
0.4
0.2
0
***
Mrj+/+ Mrj+/-
Mrj-/-

cells, has a “speckled” nuclear expression pattern (Chapter 2) reminiscent of Bmi-1 (Stauffer et al, 2001). Furthermore, *Bmi-1*-deficient neurospheres display a self-renewal phenotype (Molofsky et al, 2003), similar to $Mrj^{-/-}$ neurospheres. As a result, we hypothesized that Mrj and Bmi-1 may interact. Using Mrj and Bmi-1 antibodies to stain E9.5 histological sections, we detected the expression of both proteins throughout the neural tube although they did not co-localize at the subcellular level (Fig. 4.4A, B). Bmi-1 expression was restricted to the nucleus except in some cells adjacent to the lumen where Bmi-1 was undetectable (Fig. 4.4B). Mrj expression, on the other hand, was also expressed in all cells of the neural tube but was cytoplasmic (Fig. 4.4A). However, higher resolution microscopy is required to rule out Mrj nuclear expression. Regardless, it is unlikely that Mrj and Bmi-1 co-localize.

To better address whether Mrj directly or indirectly affects Bmi-1, Bmi-1 expression was assessed in $Mrj^{-/-}$ neural tubes. The nuclei of $Mrj^{-/-}$ neural tube cells showed Bmi-1 immunolocalization in a similar pattern and at a comparable intensity to $Mrj^{+/+}$ nuclei (Fig. 4.4B, E). There were, however, fewer *Mrj*-deficient cells adjacent to the lumen that lacked Bmi-1 expression (Fig. 4.4E) most likely due to the presence of fewer mitotic cells (Fig. 4.2D). Together, these data suggest that Mrj does not interact, directly or indirectly, with Bmi-1 and that another substrate acts together with Mrj during self-renewal.

4.3.5 Mrj and the intermediate filament Nestin are co-expressed in E9.5 neural tubes

FIGURE 4.4 – Nestin but not Bmi-1 is co-expressed with Mrj in the neural tube at E9.5. (A-D) Histological sections of *Mrj*$^{+/+}$ neural tubes at E9.5 stained with antibodies (brown) against (A) Bmi-1, (B) Nestin, (C) Mrj and (D) Neurofilaments (NF). (E-F) *Mrj*$^{-/-}$ neural tubes at E9.5 stained with antibodies (brown) against (E) Bmi-1 and (F) Nestin. Boxes represent higher magnified region in image directly below. Counterstain: (A, C-D, F) Nuclear fast red (pink), (B and E) Hematoxylin (blue). Arrows in B and E indicate nuclei with undetectable Bmi-1 antibody staining. Scale bars = 50 μm in top two rows of each panel, 10 μm in bottom row of each panel.

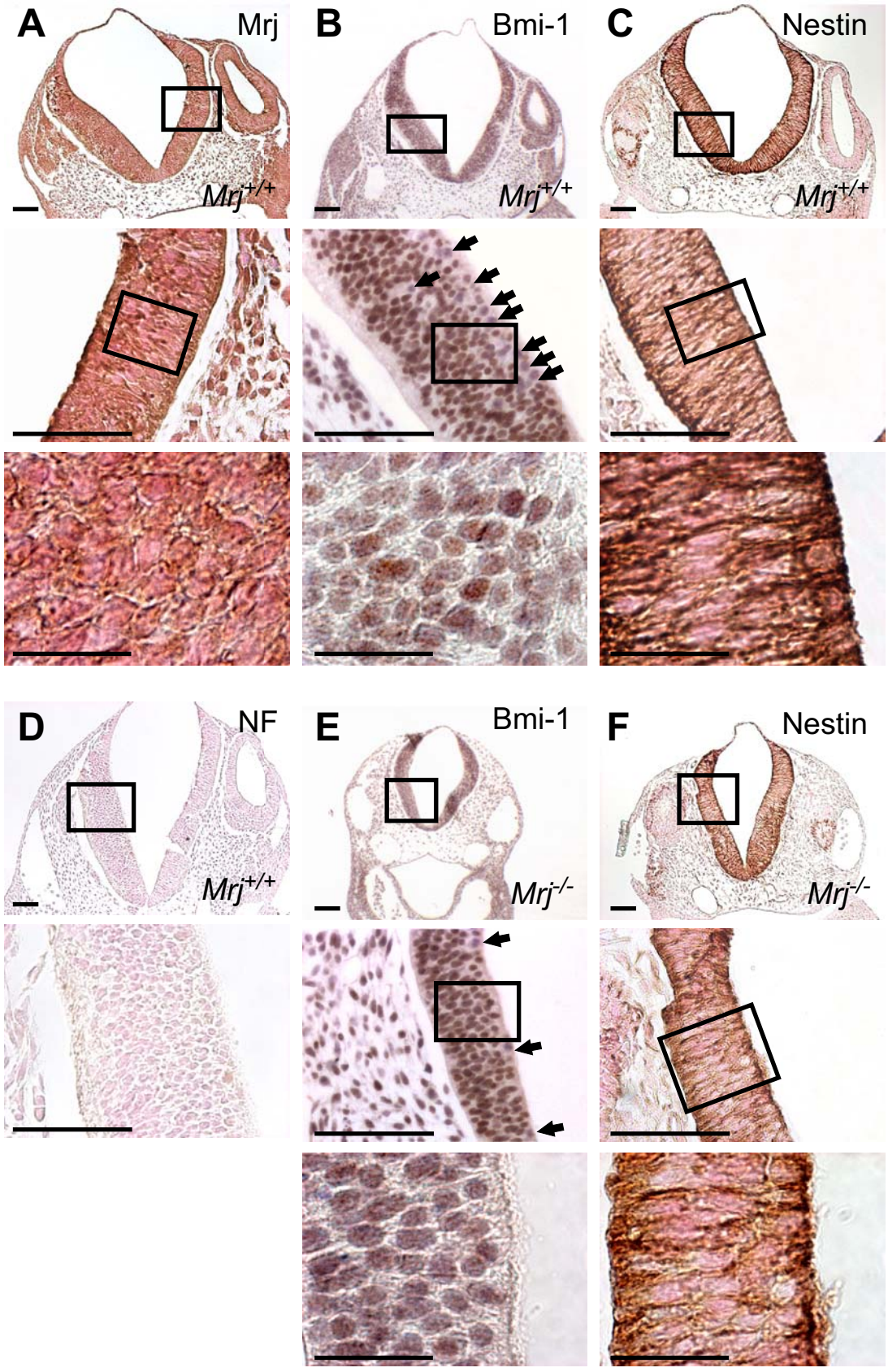
A
Mrj
Mrj+/+
B
Bmi-1
Mrj+/+
C
Nestin
Mrj+/+
D
NF
Mrj+/+
E
Bmi-1
Mrj-/-
F
Nestin
Mrj-/-

It was previously shown that Mrj interacts with the intermediate filament protein keratin (K) 18 (Izawa et al, 2000) and that *Mrj* deficiency leads to the formation of toxic aggregates of K8/18 filaments in trophoblast cells preventing normal cell-cell interactions (Chapter 2). Keratin is not expressed within the neural lineage (Thorey et al, 1993), but other intermediate filaments, such as nestin (a neural stem cell marker) and neurofilament (a neuronal marker), are expressed (Dahlstrand et al, 1995; Lardelli et al, 1996). To determine if Mrj interacts with either of these cytoskeletal proteins during neural development, we assessed Mrj expression in comparison to that of nestin and neurofilament in the neural tube at E9.5. Neurofilament was not detectable via antibody staining at E9.5 (Fig. 4.4F). On the other hand, nestin expression was detectable and was cytoplasmic and uniform throughout the neural tube similar to Mrj expression (Fig. 4.4A, C) suggesting that Mrj and nestin may co-localize. Other experiments such as high-resolution microscopy and/or co-immunoprecipitation assays are required to answer this definitively. Despite this, nestin expression was normal in $Mrj^{-/-}$ neural tubes without any obvious aggregation of Nestin filaments (Fig 4.4F) suggesting that Mrj and nestin may not interact.

4.4 Discussion

It is well known that improper neural tube development can lead to serious congenital malformations including exencephaly and spina bifida. We have shown here that a proportion of *Mrj*-deficient embryos have exencephaly independently of their placenta defect. Furthermore, we have implicated Mrj in neural stem cell self-renewal. Without self-renewal, progenitor populations in the remaining $Mrj^{-/-}$ embryos become depleted

and the neural tubes are significantly smaller. Since *Mrj*-deficient embryos die at E10.5 because they do not form a placenta, it is difficult to determine the consequences of this self-renewal phenotype in later embryonic development. Whether the exencephaly and self-renewal defect are directly connected is unclear. Neither Bmi-1 nor nestin appear to interact with Mrj and therefore a substrate for Mrj during these developmental processes remains unknown. Regardless, Mrj is involved in one or more mechanisms for normal neural development to occur.

4.4.1 Potential roles for Mrj in neural tube closure

The genetic cause for NTDs is complex and multifactorial. This is exemplified by the fact that ~200 different mouse mutants and strains with NTDs have been identified thus far (reviewed by Harris and Juriloff, 2007). A large proportion (~70%) of these has exencephaly only, with no apparent consistency in the molecular pathway that they belong to. As a result, it is uncertain how Mrj fits into this scheme. Mrj has been shown to have diverse functions from transcriptional repression due to association with histone deacetylase complexes (Dai et al, 2005; Hurst et al, 2006; Pan et al, 2007) to prevention of protein aggregation through the proteasome pathway (Chapter 2; Chuang et al, 2002). In general, DnaJ co-chaperone proteins can have numerous substrates and, as a result, there may be other substrates that complex with Mrj during neural tube closure yet to be identified.

We demonstrated here that improper neural tube closure is not caused by a lack of chorioallantoic attachment in *Mrj*$^{-/-}$ embryos. Several other mutants are afflicted with both exencephaly and placental defects (reviewed by Harris and Juriloff, 2007). Three of

these do not undergo chorioallantoic attachment similar to *Mrj*$^{-/-}$ embryos including Autotoxin (Atx) involved in DNA hydrolysis (van Meeteren et al, 2006), Rbp-Jκ transcription factor downstream of Notch signalling (Oka et al, 1995), and *Zfp36L1* RNA transcript destabilizer (Stumpo et al, 2004). All of these proteins, including Mrj, have what seem to be unrelated functions making it difficult to determine whether they act together in the processes of neural tube closure and/or chorioallantoic attachment. It would be interesting to determine whether they act similarly in both the neuroepithelium and the trophoblast lineage.

Ciliogenesis is necessary for normal neural tube closure since many mutants with abnormal ciliary formation exhibit exencephaly (reviewed by Kibar et al, 2007). Cilia interact with components of the Hedgehog pathway, which is necessary for the formation of ventral neural cell types (Huangfu et al, 2003). Additionally, cilia are required for proper planar cell polarity signalling in *Xenopus* (Simons et al, 2005), an indispensable mechanism for neural tube formation. Interestingly, Mrj was found to interact with the intraflagellar transport protein IFT88 (a ciliary protein and homologue to the mouse gene *Polaris*) in a yeast two-hybrid analysis (personal communication, J.C. Besharse, Medical College Wisconsin). Additionally, we have observed that a few *Mrj*$^{-/-}$ embryos have demonstrated reversed heart looping (E. Watson and J. Cross, unpublished observations), a phenotype similar to the hypomorphic *Polaris* mutant embryos (Murcia et al, 2000). Therefore, Mrj may be required for normal ciliary function, without which neural tube closure cannot properly occur.

The multifactoral nature of NTDs may be explained by the involvement of proteins necessary for regulation of the chromatin structure such as histone deacetylases

(HDAC; Vega et al., 2004) and DNA methyltransferases (Hata et al., 2002; Okano et al., 1999) and thus large scale transcription of genes required for neural tube closure. Mrj associates with HDACs (Dai et al., 2005; Pan et al, 2008) and is expressed, at least in trophoblast cells, in a punctuate manner throughout the nucleus (Chapter 2) suggesting that the Mrj-HDAC complex may be involved in transcriptional regulation by chromatin remodelling. Although we did not detect Mrj expression in the nuclei of neurepithelium, additional studies with higher resolution are necessary before nuclear localization can be excluded. Exencephaly has been detected in mice with mutations in genes encoding DNA methyltransferases (*Dnmt3b* and *Dnmt3l*) (Hata et al., 2002; Okano et al., 1999). Additionally, folate metabolism plays a role in the transfer of methyl groups destined for DNA methylation and mutations within the folate cycle and folate deficiency are associated with NTDs (Castro et al., 2004; Sinclair et al., 2007; Appendix A). Maternal folate supplementation can rescue NTDs in multiple seemingly unrelated mutants (reviewed by Harris and Juriloff, 2007), even if their relationship to the folate pathway has never been determined. Whether Mrj is involved in establishing DNA methylation patterns is unknown. Rescuing exencephaly by treating pregnant $Mrj^{+/-}$ females with folate or determining global DNA methylation levels may provide some answers.

4.4.2 Mrj is required for neural stem cell self-renewal

The delicate balance between stem cell self-renewal and differentiation is necessary for organ development. When self-renewal is not properly controlled, stem cells can produce either a large number of cells much like a tumour that disrupt tissue architecture or too few cells causing malformation or degeneration of a tissue. Our data here demonstrate

that Mrj is involved in the regulation of neural stem cell self-renewal since *Mrj*-deficient neurospheres were small and had a severely reduced ability to form secondary neurospheres. Whether Mrj functions by actively preventing differentiation of self-renewing cells or by initiating a proliferative stimulus to maintain a cell's capacity to self-renew is uncertain.

There are only a few factors known to be involved in the regulation of stem cell self-renewal (reviewed by Shi et al, 2008). One of them, the Bmi-1 polycomb group transcription factor, regulates self-renewal in both haematopoietic and neural lineages by actively suppressing genes that drive differentiation (Molofsky et al, 2003; Park et al, 2003). Both *Mrj*- and *Bmi-1*-deficient neurospheres have a reduced capacity to self-renew (this study; Molofsky et al, 2003), and the punctate nuclear pattern of Mrj in trophoblast cells (Chapter 2) is reminiscent of Bmi-1 expression in HEK293 cells (Stauffer et al, 2001). However, Mrj is undetectable within the nuclei of the neuroepithelium at E9.5 and, as a result, did not co-localize with Bmi-1. Therefore it is unlikely that Bmi-1 and Mrj interact in neural stem cells and function together in the self-renewal process.

Cell-cell interactions, both signalling and adhesion, are essential for maintaining a stem cell-state as suggested by the importance of stem cell niches. We previously determined that *Mrj* deficiency in trophoblast cells caused the formation of toxic aggregates of the keratin filaments. These aggregates prevent normal cell-cell interactions and disrupt cell polarity (Chapters 2 and 3). Although keratin is not expressed within the neural lineage (Thorey et al, 1993), it is possible that Mrj may interact with Nestin, another intermediate filament protein that is expressed within neural stem cells. Mrj and Nestin were expressed within the cytoplasm of neuroepithelial cells of an E9.5 neural

tube, yet it was difficult to determine whether they directly interact only using light microscopy. However, no obvious Nestin aggregates were apparent in the *Mrj*$^{-/-}$ neural tubes, although further analysis would be required to completely rule it out. The state of cell-cell adhesions between neural stem cells themselves and with other cells within the neuroepithelium should be assessed to determine whether it is a lack of proper cell contacts that prevent self-renewal in *Mrj*$^{-/-}$ stem cells.

Mrj is expressed in many tissue types throughout the developing embryo suggesting that it may be involved in self-renewal of other stem cells. Contrary to *Mrj*$^{-/-}$ neurosphere cultures, which had reduced proliferation and fewer stem cells, *Mrj*$^{-/-}$ trophoblast stem cell cultures continue to proliferate even under differentiating conditions when growth factors are removed (Chapter 3). This suggests that Mrj may affect self-renewal in various stem cell types in diverse ways, most likely as a result of alternative substrate binding.

4.4.3 The relationship between neural tube closure and stem cell self-renewal

To date, there are no clear connections in the literature between NTDs and abnormal self-renewal. Recently, however, a few mechanistic themes for normal neural tube closure have surfaced, some of which are also required for normal stem cell maintenance, including a balance between cell proliferation and differentiation and the establishment of cell polarity (Campos, 2004; Copp, 2005). It is well acknowledged that the Notch pathway plays an important role in maintaining the self-renewal state of neural stem cells (Yoon and Gaiano, 2005). Interestingly, both Notch over-expression, which causes

excessive proliferation (Lardelli et al, 1996), and loss-of-function mutations within the Notch pathway, which leads to premature differentiation in the neural plate (Ishibashi et al, 1995; Oka et al, 1995; Zhong et al, 2000), results in exencephaly. This indicates that de-regulation of self-renewal may lead to NTDs. Alternatively the establishment of cell polarity is paramount for shaping of the neural plate and later, normal neural tube closure. Several mouse mutants with planar cell polarity defects display abnormal neural tube closure (reviewed by Harris and Juriloff, 2007). Cell polarity within a stem cell niche is also very important as expression of extracellular matrix and signalling proteins on niche cells are required for maintaining stem cell character (Shi et al, 2008). Defective niche polarity prevents normal cell-cell interactions between stem and niche cells which can, in turn, prevent asymmetric stem cell divisions necessary for replenishing the stem cell population (Shi et al, 2008). This suggests that neural plate organization may affect stem cell maintenance and/or differentiation. Whether defective neural stem cell self-renewal in *Mrj*$^{-/-}$ embryos causes exencephaly or abnormal polarity/cell-cell interactions within the neural plate prevents self-renewal remains to be determined.

4.5 Materials and Methods

Mice. *Mrj*$^{+/-}$ mice were originally generated by *6AD1 β-geo* gene-trap insertion as previously described (Hunter et al, 1999). *Mrj*$^{-/-}$ embryos were produced by mating *Mrj*$^{+/-}$ mice. PCR genotyping was performed as previously described (Chapter 2) using DNA from yolk sac tissue. Experiments were performed in accordance with the Canadian Council on Animal Care and the University of Calgary Committee on Animal Care (Protocol no. M06045).

X-gal staining. Mouse conceptuses were dissected at embryonic (E) day 7.5, E8.5 and E9.5 (noon of the day that the vaginal plug was detected was defined as E0.5) in 1X phosphate buffered saline (PBS). Embryos were fixed and stained as whole mount as previously described (Hunter et al, 1999).

Tetraploid aggregation. Tetraploid aggregation chimeras were generated as described previously (Chapter 2; Nagy et al, 2003b).

Histology and immunostaining. Prior to paraffin embedding and sectioning, E9.5 embryos were fixed in 4% paraformaldehyde/1X PBS and embedded in 0.5% agarose/1X PBS to ensure optimal orientation for sectioning. Tissue sections were stained with hematoxylin (Sigma) and eosin (Sigma) or TUNEL labelled using the ApopTag® Peroxidase In Situ Apoptosis Detection Kit (S7100, Chemicon International) according to the manufacturer's instructions. For immunostaining, embryo sections were deparaffinised and treated as described in Chapter 2. Primary antibodies and dilutions used include: anti-phosphohistone H3 (PPH3, Ser10; 1:300, Upstate), anti-Bmi-1 (clone 229F6; 1:50, Upstate), anti-Mrj (020419, 1:50; a gift from M. Inagaki, Aichi Cancer Centre Research Institute, Aichi, Japan) (Izawa et al, 2000), anti-Neurofilament (200kDa + 160kDa, SMI-310; 1:1000, Abcam), and anti-Nestin (2Q178; 1:100, Abcam). Secondary antibodies were used at a dilution of 1:300 and included: horseradish peroxidase (HRP)-conjugated donkey anti-rabbit IgG and HRP-conjugated sheep anti-mouse Ig (both Amersham Biosciences). Antigen retrieval methods included trypsin tablets (Sigma) in 1X PBS (10 min) for anti-PPH3 or 0.01 M sodium citrate pH6.0 plus heat treatment for anti-Bmi-1, anti-Mrj, anti-Neurofilament and anti-Nestin. Sections were counterstained with nuclear fast red.

Neurosphere culture assay. The culture media used (media hormone mix [MHM]) was composed of DMEM:F12 (1:1) (both Gibco) including 5mM HEPES buffer (Fisher Scientific), 3mM sodium bicarbonate (Fisher Scientific), 25 µg/ml insulin (Sigma), 100 µg/ml transferrin (Sigma), 20 nM progesterone (Sigma), 10 µM putrescine (Sigma) and 30 nM sodium selenite (Sigma). Embryos from *Mrj*$^{+/-}$ intercrosses were dissected at E9.5 in sterile 1X PBS and pooled into two categories based on their chorioallantoic attachment phenotype: *Mrj*$^{+/+}$ and *Mrj*$^{+/-}$ embryos versus *Mrj*$^{-/-}$ embryos that had failed to undergo chorioallantoic attachment. Yolk sacs were collected for genotyping and in all cases the genotypes were consistent with the chorioallantoic placenta phenotype that was used to categorize embryos. Embryos were decapitated above the first branchial arches and telencephalons were mechanically dissociated in MHM using a fire-polished Pasteur pipette into a single cell suspension. To derive primary neurospheres, cells were plated at 10^5 cells/mL in MHM with 20ng/mL basic fibroblast growth factor (bFGF) and incubated for 5 d at 37ºC under 95% humidity and 5% CO_2. After counting and measuring the area of the resulting neurospheres, they were mechanically dissociated in MHM using a fire-polished Pasteur pipette into a single cell suspension. To derive secondary neurospheres, these cells were re-plated at 10^5 cells/mL in MHM with 20ng/mL bFGF and incubated under the same conditions for 5 d. Neurospheres were counted and their area was measured.

Equipment and software. A Leica DMR light microscope (for light images), Leica DMIL inverted light microscope (for cell culture images) and Leica MZ95 dissection microscope (for dissected embryo images) with Photometrics Coolsnap cf camera and Open Lab 2.2.2 imaging software program were used to obtain micrographs. Neural tube

measurements were taken using Canvas X line dimensioning tool and neurosphere area was measured using Open Lab 2.2.2. Minimal image processing was performed using Adobe Photoshop 7.0 and figures were constructed using Canvas X.

CHAPTER FIVE

DISCUSSION AND FUTURE DIRECTIONS

5.1 Discussion and Future Directions

Prior to initiating these studies, little was known about how the Mrj co-chaperone functioned within a cell, particularly the identity of its substrates in vivo and how these interactions influence chorioallantoic attachment and neural tube closure. Over the course of our analyses, we revealed that Mrj is required for proteasome degradation of keratin (K) 18 filaments in the trophoblast layer of the chorion. In the absence of *Mrj*, non-degraded keratin builds up in chorionic trophoblast cells causing the formation of keratin aggregates that prevent chorioallantoic attachment. Further exploration into how *Mrj* deficiency alters cell function determined that Laminin (Ln) α5 was not properly expressed on the basal surface of $Mrj^{-/-}$ trophoblast cells causing the disruption of cell-cell interactions since the adhesion phenotype could be rescued when $Mrj^{-/-}$ TS cells were provided with exogenous Ln α5 substrate in vitro. Consequently, changes in cell-matrix and cytoarchitecture in $Mrj^{-/-}$ chorions prevents cell-cell signalling required for allantoic receptivity, chorionic patterning and the differentiation of labyrinth progenitor cells into more developmentally restricted syncytiotrophoblast (SynT) precursor cells. In addition to its role in placental development, Mrj also plays an important role in neural tube closure, a phenotype independent of the placental defect. Neural tubes that do close are small and thin due to the reduced ability of $Mrj^{-/-}$ neural stem cells to self-renew. Because the neural tube phenotype appears to be unrelated to a defect in keratin or other intermediate filaments that are expressed in the developing nervous system, it reinforces the notion that Mrj has a variety of substrates in vivo.

5.1.1 The cellular function of Mrj

Independent of our studies, Mrj has been implicated in a wide variety of cellular processes including the prevention of protein aggregate formation (Chuang et al, 2002; Fayazi et al, 2006), regulation of the keratin cytoskeleton (Izawa et al, 2000), cell cycle control (Zhang et al, 2008; Li et al, 2008; Mitra et al, 2008), gene regulation (Dai et al, 2005; Hurst et al, 2006; Pan et al, 2008) and protein trafficking (Zhang et al, 2008; Cheng et al, 2008). Furthermore, distinctive subcellular localization of Mrj isoforms (Tateossian et al, 2004) dictates which Mrj-substrate interactions occur. Despite the wide spectrum of substrate function and localization (Table 1.1), a common mechanism for Mrj may exist involving the regulation of protein degradation. Our results implicate the cytoplasmic form of Mrj in K18 degradation. Others have shown that Mrj can reduce the accumulation of polyglutamine-expanded Huntington's disease protein aggregates in the cytoplasm (Chuang et al, 2002) presumably by promoting proteasome degradation. Other documented Mrj-substrate interactions predominantly occur within the nucleus [Alkbh1 (Pan et al, 2008); Brms1 (Hurst et al, 2002); HDAC (Dai et al, 2005); NFATc3 (Dai et al, 2005); Slfn1 (Zhang et al, 2008); MLF1 (Li et al, 2008); Pttg (Pei, 1999)], implicating the nuclear isoform of Mrj in transcriptional regulation and cell cycle control. This may be achieved through nuclear degradation of these substrates since the proteasome complex is detected (Chapter 2) and functional (Petrs-Silva et al, 2008) within the nucleus. Whether Mrj simply targets its substrates to the proteasome or aids in the degradation process is still unclear and thus further characterization of the Mrj-proteasome relationship is necessary.

An alternative hypothesis implicates Mrj in multiple mechanisms depending on the isoform in question. As indicated above, the cytoplasmic short isoform may be particularly involved in protein degradation, such as K18. The longer of the two isoforms includes two additional exons containing a nuclear localization signal (Mitra et al, 2008) and possibly other important sequence to convey an alternative function within the nucleus. The Mrj/Hsp70 complex is implicated in nuclear shuttling of Schlafen1 (Slfn1) and Vpx (Zhang et al, 2008; Cheng et al, 2008). In some cultured trophoblast cells, Mrj appears in a speckled patterning within the nucleus (Chapter 2) suggesting that Mrj is directly involved in gene regulation perhaps through interactions with the transcriptional repressor HDAC (Dai et al, 2005). More work is required to assess differential functions and specific substrate binding of each Mrj isoform. Transfecting either the long or short Mrj isoform into *Mrj*$^{-/-}$ TS cells and then characterizing changes in phenotype, gene expression and specific substrate interactions will determine how each isoform functions independently. Additionally, both isoforms are knocked out in *Mrj*$^{-/-}$ embryos suggesting that the chorioallantoic attachment phenotype may be a compounded effect. Generating mice in which only one isoform is expressed will prove whether one or both are conducive to life and for further study of individual cellular functions.

With respect to Mrj-substrate interactions in the developing neural tube, we were unable to pinpoint a particular substrate (Chapter 4). Of the known substrates for Mrj, a few are expressed within the brain [e.g. Brms1 (Hurst et al, 2006); HDAC (Dai et al, 2005); NFATc3 (Dai et al, 2005); MLF1 (Li et al, 2008)] and may interact with Mrj in the context of neural tube or neural stem cell self-renewal. Apart from doing a yeast 2-hybrid analysis using Mrj as the bait to identify more substrates, bioinformatics analysis

could be used to determine a common “Mrj binding domain” among the known substrates to recognize additional substrates for testing.

5.1.2 The effects of protein aggregation

Protein aggregates often lead to tissue degeneration, as in the case of keratin inclusion bodies in cirrhosis of the liver (Carrell, 2005). Recent focus has shifted from the effects of cell death and tissue degeneration caused by protein inclusions to the cellular events of aggregates that lead up to cell death (Stefani, 2007). We observed that *Mrj* deficiency causes keratin aggregation in trophoblast cells, which prevents chorioallantoic attachment (Chapter 2). Keratin aggregation prevents normal chorionic cell function since genetic removal of these aggregates in $Mrj^{-/-}$;$K18^{-/-}$ conceptuses rescues attachment (Chapter 2). Interestingly, however, the majority of $Mrj^{-/-}$ trophoblast cells are not apoptotic by E9.5 (Hunter et al, 1999). Rather, they remain in a progenitor state and continue to proliferate even in differentiating conditions (Chapter 3). Therefore, $Mrj^{-/-}$ TS cells are a good model for studying how protein aggregation affects normal cell function. It is unclear whether defective Ln α5 expression in $Mrj^{-/-}$ chorions is caused by the presence of keratin aggregates. This question can be addressed by examining laminin expression and deposition in *Mrj*;*K18* double mutant chorions. Likewise, it is unclear at this point whether the changes in actin, β-catenin and E-cadherin localization in *Mrj* mutant cells are a primary phenotype or simply secondary to the altered laminin expression.

Plating *Mrj* mutant TS cells on exogenous Ln α5 rescues the erratic behaviour and cell-adhesion phenotype suggesting that the actin, β-catenin and E-cadherin localization defect/aggregation may be secondary to Ln α5 misexpression. However, it is possible that we may observe that actin and adherens junctions protein expression is not normalized in

cells plated on exogenous Ln α5 matrix. If this is the case, aggregation may result from the following possibilities: 1) Independently of keratin aggregation, Mrj may assist in proteasome degradation by directly interacting with any one of these proteins, similar to keratin filaments (Chapter 2; Izawa et al, 2000). Therefore, in *Mrj*-deficient conditions, un-degraded actin/E-cadherin/β-catenin would accumulate in the cell and aggregates would result. Disruption of actin organization can affect the stability of adherens junctions and vice versa (Quinlan and Hyatt, 1999; Peifer, 1993). Therefore, Mrj may only need to interact with one of these proteins for all three to be affected. 2) Un-degraded keratin may overload the proteasome and for that reason it would be unable to degrade other proteins, thus resulting in their aggregation. This is similar to amyloid-containing aggregates in Alzheimer's disease that overload the proteasome and affect its normal function (Upadhya and Hegde, 2007). 3) Keratin aggregates caused by *Mrj* deficiency are quite large and may act as a sink for other proteins. In cirrhosis of the liver, proteins such as β-catenin, zonula occludens-1 and 14-3-3ζ have been shown to "stick to" keratin inclusions in diseased hepatocytes (Hanada et al, 2007). We observed that E-cadherin- and β-catenin-containing aggregates are peri-nuclear in $Mrj^{-/-}$ trophoblast cells (Chapter 3), similar to keratin aggregates (Chapter 2). Furthermore, actin and keratin aggregates co-localize at least in differentiated $Mrj^{-/-}$ trophoblast cell cultures. To fully understand whether the toxicity of keratin aggregation is related to subsequent aggregation and disruption of proteins associated with the actin cytoskeleton, analysis of actin, E-cadherin and β-catenin expression in $Mrj^{-/-}$;$K18^{-/-}$ chorions is required.

Disorganization of the actin cytoskeleton can affect cell morphology, motility, adhesion and signal transduction (Miyoshi and Takai, 2008). Therefore the presence of

actin, E-cadherin and β-catenin aggregates caused by *Mrj* deficiency ultimately changes the character of the cell. We observed that *Mrj*$^{-/-}$ chorionic trophoblast cells were rounded and disorganized and *Mrj*$^{-/-}$ TS cells were highly migratory and did not form normal cell-cell connections suggesting that these changes in the cytoarchitecture may influence cell signalling. Reorganization of the actin cytoskeleton in trophoblast cells has been shown to alter signalling through the Rho GTPase protein family (eg RhoA, Rac1, Cdc42) in vitro (Mana et al, 2001), which likely influences the expression of genes required for trophoblast cell differentiation. However, little is known about how actin and its associated molecules are involved in chorionic trophoblast development as there are currently no mutants for actin-associated proteins available that display chorionic defects (Tables 1.2, 1.3, 1.4). β-actin (*Actb*) knockout embryos develop normally up to E8.5 but become severely growth retarded and die shortly thereafter (Shawlot et al, 1998). The trophoblast lineage, however, was not assessed for defects. On the other hand, E-cadherin (*Cdh1*) and β-catenin (*Ctnnb1*) knockout mice die well before the development of the extraembryonic ectoderm and establishment of the chorion (Riethmacher et al, 1995; Haegel et al, 1995). As a result, further studies are required to identify how these aggregates alter actin- or adherens junctions-initiated signalling and affect chorionic trophoblast cell function and differentiation, and whether these effects are similar to actin, E-cadherin or β-catenin deficiency.

5.1.3 Mrj is required for chorioallantoic attachment, chorionic patterning and syncytiotrophoblast formation

The labyrinth region of the placenta is necessary for nutrient and gas exchange between the mother and fetus. We are only beginning to understand the developmental origins, genetic regulation and cell-cell interactions necessary for proper labyrinth formation. The first developmental milestone necessary for labyrinth development is chorioallantoic attachment, a process that fails in *Mrj* mutant conceptuses (Hunter et al, 1999; Chapter 2). Although many other mouse mutants exist with the same phenotype (Watson and Cross, 2005; Table 1.2), they are generally not well characterized and therefore the mechanism behind chorioallantoic attachment is not well understood. Our studies reveal that the chorionic trophoblast and mesothelial cells must interact with each other for allantoic attachment to occur since *Mrj* is expressed only within the trophoblast cells but the mesothelium is the first cell layer to come into contact with the allantois. It is likely that the improper expression of Ln α5 by $Mrj^{-/-}$ chorionic trophoblast and altered cell polarity prevents a suitable interaction.

Recently published work by the Cross lab has shown that the origins of the three differentiated trophoblast cell types of the labyrinth can be traced back to specific layers within the chorion as early as E8.5 based on gene expression patterns (Simmons et al, 2008) (Fig. 5.1). Normally, the cells on the apical side of the chorion closest to the maternal blood sinuses express *Hand1* and are destined to become sinusoidal-TGCs (Simmons et al, 2008). *Syna* gene expression is restricted to the chorionic cell layer just below *Hand1*-positive cells, and these cells are the precursors to SynT-I cells (Simmons et al, 2008). Lastly, clusters of cells in the basal layer of the chorion closest to the allantoic interface that express *Gcm1*, *Synb* and *Cebpα* genes are SynT-II cell precursors (Simmons et al, 2008). Other cells in the basal layer express *Rhox4b* and are believed to

Figure 5.1 – Trophoblast cell lineage of the labyrinth.

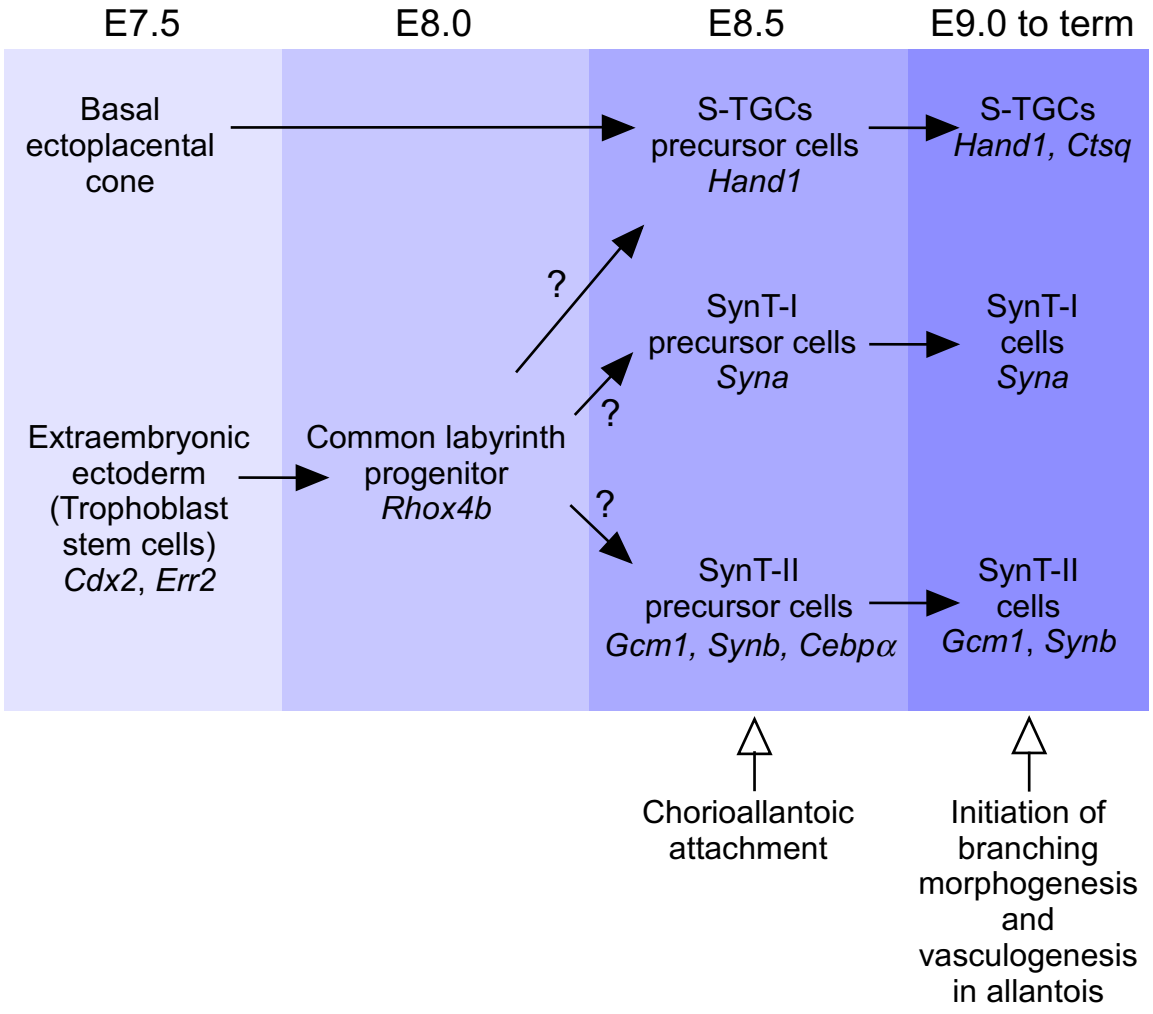
E7.5
E8.0
E8.5
E9.0 to term
Basal ectoplacental cone
S-TGCs precursor cells Hand1
S-TGCs Hand1, Ctsq
?
SynT-I precursor cells Syna
SynT-I cells Syna
?
Extraembryonic ectoderm (Trophoblast stem cells) Cdx2, Err2
Common labyrinth progenitor Rhox4b
?
SynT-II precursor cells Gcm1, Synb, Cebpα
SynT-II cells Gcm1, Synb
Chorioallantoic attachment
Initiation of branching morphogenesis and vasculogenesis in allantois

be labyrinth precursor cells based on their co-expression of trophoblast stem cell markers at early post-implantation stages and continued proliferation (A. Davies, D. Natale, D. Simmons, E. Mariusdottir, and J. Cross, in preparation) (Fig. 5.2). Lineage tracing experiments are necessary to determine the true developmental origins of these cells similar to experiments using *Z/AP* mice to determine the EPC lineage (Simmons et al, 2007).

Many patterned tissues require cell autonomous and non-autonomous signalling for the induction of distinctive differentiation pathways (Rossant and Spence, 1998). Evidence provided by *Gcm1* and *Mrj* mutant chorions suggests that various cell-matrix and cell-cell interactions are required for the specification of labyrinth precursor populations. *Mrj* mutant chorions are disorganized due to inappropriate cell-cell and cell-matrix associations. As a result, the majority of $Mrj^{-/-}$ chorionic trophoblast cells remain in a $Rhox4b^{+}$ labyrinth progenitor-state, preventing the specification of more restricted SynT progenitor cells (Fig. 5.2). *Hand1*-positive S-TGC precursor cells are present suggesting that neither *Gcm1*/*Synb*/*Cebpa*-positive nor *Syna*-positive cell layers are required to induce this cell population. In contrast to the broad impact that *Mrj* deficiency has on patterning of the chorion, *Gcm1* is necessary only for the induction of the SynT-II precursor cells in the basal layer of the chorion (Simmons et al, 2008) since the entire cell layer in *Gcm1* mutants consists of *Rhox4*-positive labyrinth progenitor cells (D. Natale, D. Simmons and J. Cross, unpublished observations) and subsequently fail to initiate branching morphogenesis (Anson-Cartwright et al, 2001). Interestingly, the *Syna*- and

Figure 5.2 – *Gcm1*$^{-/-}$ and *Mrj*$^{-/-}$ chorions display restricted developmental potential. A section through an E8.5 conceptus (top). The box indicates the region of the chorion depicted in the panels below. The differences in patterning between wildtype (bottom left), *Gcm1* mutant (bottom center) and *Mrj* mutant (bottom right) chorions at E8.5. EPC, ectoplacental cone; MBS, maternal blood sinus; S-TGC, sinusoidal trophoblast giant cell; SynT-I, syncytiotrophoblast layer I; SynT-II, syncytiotrophoblast layer II; Lab, labyrinth; FBV, fetal blood vessel.

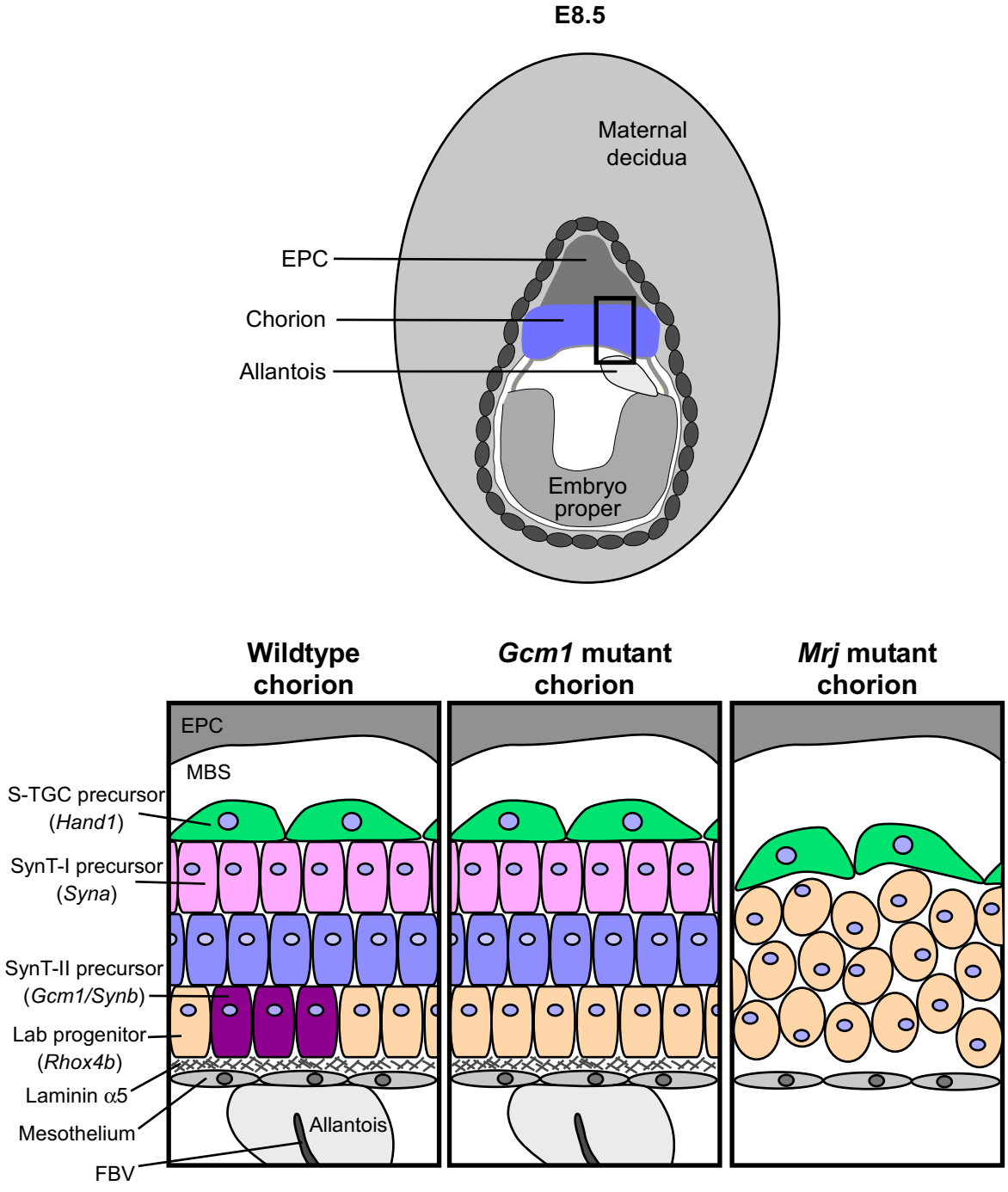
E8.5
Maternal decidua
EPC
Chorion
Allantois
Embryo proper
Wildtype chorion
Gcm1 mutant chorion
Mrj mutant chorion
EPC
MBS
S-TGC precursor (Hand1)
SynT-I precursor (Syna)
SynT-II precursor (Gcm1/Synb)
Lab progenitor (Rhox4b)
Laminin α5
Mesothelium
FBV
Allantois

Hand1-positive cell populations are still present in *Gcm1* mutants demonstrating that neither is dependent on the basal layer for induction (Simmons et al, 2008) (Fig. 5.2). Based on these data, we hypothesize that the chorion is patterned first through interaction of *Rhox4b* expressing cells with the underlying Ln α5-containing ECM which allows the*Rhox4b*-positive cells to polarize. Once polarity is established, cells within their individual layers signal between themselves to induce precursors of the individual layers.

Even though the effect of *Mrj* deficiency is restricted to the chorion trophoblast cells (Chapter 2), it is likely that signals from the chorionic mesothelium and/or the allantois are necessary for patterning of the chorion. Defective signalling between the mesothelium and trophoblast cells due to abnormal laminin expression in *Mrj* mutant chorions might ultimately affect how the chorion is patterned. Patterning is initiated when *Gcm1* expression appears within the extra-embryonic ectoderm one full day (~E7.5) before allantoic attachment (Anson-Cartwright et al, 2001; Simmons et al, 2008). However, *Gcm1* expression is down-regulated in *Mrj* mutant chorions in the absence of allantoic attachment (this study; Hunter et al, 1999) and is not maintained in *Hsp90β* mutants that undergo allantoic attachment but branching morphogenesis is stalled due to improper allantoic development (Stecca et al, 2002). This suggests that allantoic interaction is not necessary for initial specification of the three precursor layers of the chorion, but is required to maintain proper gene expression for continued differentiation into SynT cells. The specific molecules that mediate the signalling interactions are unknown.

5.1.4 Mrj regulates stem cell biology

Two distinct stem cell populations require *Mrj* during development, though it appears to be involved in opposing functions. Within the trophoblast lineage, Mrj is necessary to promote cell cycle exit and the differentiation of common labyrinth progenitor cells of the chorion to more restricted SynT precursors (Chapter 3). By contrast, neural stem cells require Mrj for self-renewal and thus maintenance of the stem cell population (Chapter 4). Despite this apparent difference in mechanism, the question is whether or not there may be a similar underlying cause. Unlike in trophoblast cells, the aggregation of intermediate filaments in neural precursor cells due to *Mrj* deficiency is not apparent and rules out this Mrj-substrate interaction as the foundation for stem cell regulation in both cases.

β-catenin, in addition to its role in cell adhesion, is involved in the canonical Wnt signalling pathway. Briefly, free β-catenin that is not associated with adherens junctions is normally targeted for proteasomal degradation via the GSK/Axin/APC protein complex (reviewed by Huang and He, 2008). When Wnt binds to its cell surface receptor Frizzled, β-catenin degradation is blocked, allowing it to enter the nucleus to regulate gene transcription. In $Mrj^{-/-}$ TS cells, we hypothesize that non-degraded keratin overloads the proteasome (Chapter 2). As a result, β-catenin may not be degraded leading to increased cytoplasmic protein not associated with the cell membrane (Chapter 3). Therefore, β-catenin is free to enter the nucleus to cause ectopic expression of genes downstream of the Wnt pathway. Others have shown that losing negative regulators of canonical Wnt pathway results in tumour formation (Katoh and Katoh, 2007), reminiscent of the *Mrj* phenotype in which the cells remain in a progenitor state and are highly migratory

(Chapter 3). In the context of neural stem cells, Wnt/β-catenin signalling also acts to promote self-renewal (Falk et al, 2008). Therefore, in contrast to trophoblast cells, we might expect to observe decreased Wnt/β-catenin signalling in *Mrj*$^{-/-}$ neurospheres.

ECM proteins are essential for the establishment of most stem cell niches by regulating stem cell properties such as self-renewal and differentiation (Scadden, 2006). Despite recognizing the general location of trophoblast progenitor cells in wildtype conditions, the characteristics of the chorionic trophoblast stem cell niche has not yet been described. We have shown that a reduction in Ln α5 expression in *Mrj*$^{-/-}$ chorions is associated with continued proliferation and inhibited differentiation suggesting that these progenitors require Ln α5 as part of their microenvironment to promote more restricted differentiation. Plating *Mrj*$^{-/-}$ TS cells on Ln α5 and assessing the expression profiles of genes required for SynT differentiation may shed some light on this issue. Interestingly, Ln α5 is expressed in the developing neural tube and, like *Mrj*$^{-/-}$ embryos, *Ln α5* deficiency causes exencephaly (Miner et al, 1998). Fewer BrdU-positive cells are also observed in *Ln α5*$^{-/-}$ neural tubes compared to wildtype (Miner et al, 1998). Cultured neurospheres are known to produce their own ECM molecules including laminins and fibronectin (Campos et al, 2004) such that each sphere essentially represents a stem cell niche (Campos, 2004). Our results showing that *Mrj* mutant neural stem cells have reduced self-renewal potential may be attributed to reduced Ln α5 expression. This hypothesis indicates that the absence of Mrj similarly reduces laminin expression in both neural and trophoblast stem cell contexts. However, Ln α5 in a neural stem cell niche would have a different function in comparison to a trophoblast stem cell niche. Further

analysis of Ln α5 expression and function in both neural tubes and neurospheres is essential.

BIBLIOGRAPHY

Adams, R.H., Porras, A., Alsonso, G., Jones, M., Vinetersten, K., Panelli, S. et al. (2000) Essential role of p38alpha MAP kinase in placental but not embryonic cardiovascular development. *Mol Cell* 6, 109-116.

Adamson, S.L., Lu, Y., Whiteley, K.J., Holmyard, D., Hemberger, M., Pfarrer, C. and Cross, J.C. (2002) Interactions between trophoblast cells and the maternal and fetal circulation in the mouse placenta. *Dev Biol* 250, 358-373.

Adelman, D.M., Gertsenstein, M., Nagy, A., Simon, M.C. and Maltepe, E. (2000) Placental cell fates are regulated in vivo by HIF-mediated hypoxia responses. *Genes Dev* 14, 3191-3203.

Aerts, L. and Van Assche, F.A. (2003) Intra-uterine transmission of disease. *Placenta* 24, 905-911.

Alpy, F., Jivkov, L., Klein, A., Arnold, C., Huss, Y., Kedinger, M., Simon-Assmann, P. and Lefebvre, O. (2005) Generation of a conditionally null allele of the laminin α1 gene. *Genesis* 34, 59-70.

Amarai, M.D. (2005) Processing of CFTR: Traversing the cellular maze – How much CFTR needs to go through to avoid cystic fibrosis? *Pediatr Pulmonol* 39, 479-491.

Ameen, N.A., Figueroa, Y. and Salas, P.J. (2001) Anomalous apical plasma membrane phenotype in CK8-deficient mice indicates a novel role for intermediate filaments in the polarization of simple epithelia. *J Cell Sci* 114, 563-575.

Anson-Cartwright, L., Dawson, K., Holmyard, D., Fisher, S.J., Lazzarini, R.A. and Cross, J.C. (2000) The glial cells missing-1 protein is essential for branching morphogenesis in the chorioallantoic placenta. *Nature Genet* 25, 311-314.

Arai, T., Kasper, J.S., Skaar, J.R., Ali, S.H., Takahashi, C. and DeCaprio, J.A. (2003) Targeted disruption of p185/Cul7 gene results in abnormal vascular morphogenesis. *Proc Natl Acad Sci USA* 100, 9855-9860.

Antonson, P., Schuster, G.U., Wang, L., Rozell, B., Holter, E., Flodby, P. et al. (2003) Inactivation of the nuclear receptor coactivator RAP250 in mice results in placental vascular dysfunction. *Mol Cell Biol* 23, 1260-1268.

Barak, Y., Nelson, M.C., Ong, E.S., Jones, Y.Z., Ruiz-Lozano, P., Chien, K.R. et al. (1999) PPAR gamma is required for placental, cardiac, and adipose tissue development. *Mol Cell Biol* 4, 585-595.

Bardag-Gorce F., Riley N., Nguyen V., Montgomery R.O., French B.A., Li J., van Leeuwen F.W. et al. (2003) The mechanism of cytokeratin aggresome formation: the role of mutant ubiquitin (UBB+1). *Exp Mol Patho.* 74, 160-167.

Bardag-Gorce F., Vu J., Nan L., Riley N., Li J. and French S.W. (2004) Proteasome inhibition induces cytokeratin accumulation in vivo. *Exp Mol Pathol* 76, 83-89.

Bader, B.L., Rayburn, H., Crowley, D. and Hynes, R.O. (1998) Extensive vasculogenesis, angiogenesis, and organogenesis precede lethality in mice lacking all alpha v integrins. *Cell* 95, 507-519.

Beck, F., Erler, T., Russell, A. and James, R. (1995) Expression of Cdx-2 in the mouse embryo and placenta: possible role in patterning of the extra-embryonic membranes. *Dev Dyn* 204, 219-227.

Begay, V., Smink, J. and Leutz, A. (2004) Essential requirement of CCAAT/enhancer binding proteins in embryogenesis. *Mol Cell Biol* 24, 9744-9751.

Bence N.F., Sampat R.M., and Kopito R.R. (2001) Impairment of the ubiquitin-proteasome system by protein aggregation. *Science* 292, 1552-1555.

Bertram, P.G., Zeng, C., Thorson, J., Shaw, A.S. and Zheng, X.F. (1998) The 14-3-3 proteins positively regulate rapamysin-sensitive signaling. *Curr Biol* 8, 1259-1267.

Bertrand, N., Castro, D.S. and Guillemot, F. (2002) Proneural geners and the specification of neural cell types. *Nat Rev Neurosci* 3, 517-530.

Bilder, D. (2004) Epithelial polarity and proliferation control: links from the *Drosophila* neoplastic tumor suppressors. *Genes Dev* 18, 1909-1925.

Blom, H.J., Shaw, G.M., den Heije,r M. and Finnell, R.H. (2006) Neural tube defects and folate: case far from closed. *Nature Rev Neurosci* 7, 724-731.

Boudreau N., Myers C., and Bissell M.J. (1995) From laminin to lamin: regulation of tissue-specific gene expression by the ECM. *Trends Cell Biol* 5, 1-4

Breier G., Albrecht U., Sterrer S., and Risau W. (1992) Expression of vascular endothelial growth factor during embryonic angiogenesis and endothelial cell differentiation. *Development* 114, 521-532.

Brouns, M.R., Matheson, S.F., Hu, K.Q., Delalle, I., Cainess, V.S., Silver, J. et al. (2000) The adhesion signalling molecule p190 RhoGAP is required for morphogenetic processes in neural development. *Development* 127, 4891-4903.

Bultman, S., Gebuhr, T., Yee, D., La Mantia, C., Nicholson, J., Gilliam, A. et al. (2000) A Brg1 null mutation in the mouse reveals functional differences among mammalian SWI/SNF complexes. *Mol Cell* 6, 1287-1285.

Butterfield, A.D., Drake, J., Pocernich, C. and Castegna, A. (2001) Evidence of oxidative damage in Alzheimer's disease brain: central role for amyloid β-peptide. *Trends Mol Med* 7, 548-554.

Byland, M., Andersson, E., Novitch, B.G., and Muhr, J. (2003) Vertebrate neurogenesis is counteracted by Sox1-3 activity. *Nat Neurosci* 6, 1162-1168.

Cai, S.L., Tee, A.R., Short, J.D., Bergeron, J.M., Kim, J., Shen, J. et al. (2006) Activity of TSC2 is inhibited by AKT-mediated phosphorylation and membrane partitioning. *J Cell Biol* 173, 279-289.

Campos, L.S. (2004) Neurospheres: insights into neural stem cell biology. *J Neurosci Res* 78, 761-769.

Campos, L.S., Leaone, D.P., Relvas, J.B., Brakebusch, C., Fassler, R., Suter, U. and ffrench-Constant, C. (2004) Beta1 integrins activate a MAPK signalling pathway in neural stem cells that contributes to their maintenance. *Development* 131, 3433-3444.

Carrell R.W. (2005) Cell toxicity and conformational disease. *Trends Cell Biol* 15, 574-580.

Castellucci, M., Kosanke, G., Verdenelli, F., Huppertz, B. and Kaufmann, P. (2000) Villous sprouting: fundamental mechanisms of human placental development. *Hum Reprod Update* 6, 485-494.

Castro, R., Rivera, I., Ravasco, P., Camilo, M.E., Jakobs, C., Blom, H.J., and de Almeida, I.T. (2004). 5,10-methylenetetrahydrofolate reductase (MTHFR) 677C→T and 1298A→C mutations are associated with DNA hypomethylation. *J Med Genet* 41, 454-458.

Cattaneo, E. and McKay, R. (1990) Proliferation and differentiation of neuronal stem cells regulated by nerve growth factor. *Nature* 347, 762-765.

Chan, K.T., Cortesio, C.L. and Huttenlocher, A. (2007) Integrins in cell migration. *Methods in Enzymology* 426, 47-67.

Chawengsaksophak, K., de Graaff, W., Rossant, J., Deschamps, J., and Beck, F. (2004) Cdx2 is essential for axial elongation in mouse development. *Proc Natl Acad Sci USA* 101, 7641-7645.

Chen, Z. Karaplis, A.C., Ackerman, S.L., Pogribny, I.P., Melnyk, S., Lussier-Cacan, S. et al. (2001) Mice deficient in methylenetetrahydogolate reductase exhibit hyperhomocysteinemia and decreased methylation capacity, with neuropathology and aortic lipid deposition. *Hum Mol Genet* 10, 433-443.

Chen, Z.F. and Behringer, R.R. (1995) *twist* is required in head mesenchyme for cranial neural tube morphogenesis. *Genes Dev* 9, 686-699.

Cheng, X., Belshan, M. and Ratner, L. (2008) Hsp40 facilitates nuclear import of the human immunodeficiency virus type 2 Vpx-mediated preintegration complex. *J Vir* 82, 1229-1237.

Chenn, A. and Walsh, C.A. (2002) Regulation of cerebral cortical size by control of cell cycle exit in neural precursors. *Science* 297, 365-369.

Christie, G.R., Williams, D.J., MacIsaac, F., Dickinson, R.J., Rosewell, I. and Keyse, S.M. (2005) The dual-specificity protein phosphotase DUSP9/MKP-4 is essential for placental function but is not required for normal placental development. *Mol Cell Biol* 25, 8323-8333.

Chuang, J.Z., Zhou, H., Zhu, M., Li, S.H., Li, X.J. and Sung, C.H. (2002) Characterization of a brain-enriched chaperone, MRJ, that inhibits Huntingtin aggregation and toxicity independently. *J Biol Chem* 277, 19831-19838.

Church, G.M., and Gilbert, W. (1984) Genomic Sequencing. *Proc Natl Acad Sci USA* 81, 1991-1995.

Ciruna, B., Jenny, A., Lee, D., Mlodzik, M. and Schier, A.F. (2006) Planar cell polarity signalling couples cell division and morphogenesis during neurulation. *Nature* 439, 220-224.

Constancia, M., Hemberger, M., Hughes, J., Dean, W., Ferguson-Smith, A., Fundele, R. et al. (2002) Placental-specific IGF-II is a major modulator of placental and fetal growth. *Nature* 417, 945-948.

Cooney, C.A., Dave, A.A. and Wolff, G.L. (2002) Maternal methyl supplements in mice affect epigenetic variation and DNA methylation of offspring. *J Nutr* 132, 2393S-2400S.

Copp, A.J. (2005) Neurulation in the cranial region – normal and abnormal. *J Ana.* 207, 623-635.

Copp, A.J., Greene, N.D.E. and Murdoch, J.N. (2003a) Dishevelled: Linking convergent extension with neural tube closure. *Trends Neurosci* 26, 453-455.

Copp, A.J., Greene, N.D.E. and Murdoch, J.N. (2003b) The genetic basis of mammalian neurulation. *Nature Rev Genet* 4, 784-793.

Coulombe, P.A., Hutton, M.E., Letai, A., Hebert, A., Paller, A.S. and Fuchs, E. (1991) Point mutations in human keratin 14 genesof epidermolysis bullosa simplex diseases. *J Cell Biol* 115, 1661-1674.

Coulombe, P.A. and Omary, M.B. (2002) 'Hard' and 'soft' principles defining the structure, function and regulation of keratin intermediate filaments. *Curr Opin Cell Biol* 14, 110-122.

Cremer, H., Lange, R., Christoph, A., Plomann, M., Vopper, G. Roes, J. et al. (1994) Inactivation of the N-CAM gene in mice results in size reduction of the olfactory bulb and defects in spatial learning. *Nature* 367, 455-459.

Cross, J.C., Flannery, M.L., Blanar, M.A., Steingrimsson, E., Jenkins, N.A., Copeland, N.G. et al. (1995) Hxt encodes a basic helix-loop-helix transcription factor that regulates trophoblast cell development. *Development* 121, 2513-2523.

Cross, J.C., Nakano, H., Natale, D.R., Simmons, D.G. and Watson, E.D. (2006) Branching morphogenesis during development of placental villi. *Differentiation* 74, 393-401.

Cross, J.C., Simmons, D.G. and Watson, E.D. (2003) Chorioallantoic morphogenesis and formation of the placental villous tree. *Ann NY Acad Sci* 995, 84-93.

Curtain, J.A., Quint, E., Tsipouri, V., Arkell, R.M., Cattanach, B., Copp, A.J. et al. (2003) Mutation of *Celsr1* disrupts planar polarity of inner ear hair cells and causes severe neural tube defects in the mouse. *Curr Biol* 13, 1129-1133.

Dai, Y.S., Xu, J. and Molkentin, J.D. (2005) The DnaJ-related factor Mrj interacts with nuclear factor of activated T cells c3 and mediates transcriptional repression through class II histone deacetylase recruitment. *Mol Cell Biol* 25, 9936-9948.

Dahlstrand, J., Lardelli, M. and Lendahl, U. (1995) Nestin mRNA expression correlates with the central nervous system progenitor cell state in many, but not all, regions of developing central nervous system. *Brain Res Dev Brain Res* 84, 109-129.

Darken, R.S., Scola, A.M., Rakeman, A.S., Das, G., Mlodzik, M. and Wilson, P.A. (2002) The planar cell polarity gene *strabismus* regulates convergent extension movements in *Xenopus*. *EMBO J* 21, 976-985.

de la Pompa, J.L., Wakeham, A., Correia, K.M., Samper, E. Brown, S., Aguilera, R.J. et al. (1997) Conservation of the Notch signaling pathway in mammalian neurogenesis. *Development* 128, 1139-1367.

Denk, H., Stumptner, C. and Zatloukal, K. (2000) Mallory bodies revisited. *J Hepatol.* 32, 689-702.

DeRossi, C., Bode, L., Eklund, E.A., Zhang, F., Davis, J.A., Westphal, V. et al. (2006) Ablation of mouse phosphomannose isomerase (Mpi) causes mannose 6-phosphate accumulation, toxicity and embryonic lethality. *J Biol Chem* 281, 5916-5927.

De Wals, P., Tairou, F., Van Allen, M.I., Uh, S.H., Lowry, R.B., Sibbald, B. et al. (2007) Reduction in neural-tube defects after folic acid fortification in Canada. *N Engl J Med* 357, 135-142.

DiFiglia, M., Sapp, E., Chase, K.O., Davies, S.W., Bates, G.P., Vonsattel, J.P. and Aronin N. (1997) Aggregation of huntingtin in neuronal intranuclear inclusions and dystrophic neurites in brain. *Science* 277, 1990-1993.

Doe, C.Q. (2008) Neural stem cells: balancing self-renewal with differentiation. *Development* 135, 1575-1587.

Donnison, M., Beaton, A., Davey, H.W., Broadhurst, R., L'Huillier, P. and Pfeffer, P.L. (2005) Loss of the extraembryonic ectoderm in Elf5 mutants leads to defects in embryonic patterning. *Development* 132, 2299-2308.

Downs, K.M. (2002) Early placental ontogeny in the mouse. *Placenta* 23, 116-131.

Down, K.M., Temkin, R., Gifford, S. and McHugh, J. (2001) Study of the murine allantois by allantoic explants. *Dev Biol* 233, 347-364.

Drake, A.J., Tang, J.I. and Nyirenda, M.J. (2007) Mechanisms underlying the role of glucocorticoids in the early life programming of adult disease. *Clin Sci (Lond)* 113, 219-232.

Duarte, A., Hirashima, M., Benedito, R., Trindade, A., Diniz, P., Bekman, E. et al. (2004) Dosage-sensitive requirement for mouse Dll4 in artery development. *Genes Dev* 18, 2474-2478.

Dunah, A.W., Jeong, J., Griffin, A., Kim, Y.M., Standaert, D.G., Jersch, S.M. et al. (2002) Sp1 and TAFII130 transcriptional activity disrupted in early Huntington's disease. *Science* 296, 2238-2243.

Elmore, C.L., Wu, X., Leclerc, D., Watson, E.D., Bottiglieri, T., Krupenko, N.I. et al. (2007) Metabolic derangement of methionine and folate metabolism in mice deficient in methionine synthase reductase. *Mol Genet Metab* 91, 85-97.

Enkhmanakh, B., Erdenechimeg, L., Chimge, N. et al. (2006) The TFII-I family of nuclear regulators is required for neural tube morphogenesis. *Birth Defects Res A Clin Mol Teratol* 76, 165.

Erber, A., Riemer, D., Bovenschulte, M. and Weber, K. (1998) Molecular phylogeny of metazoan intermediate filament proteins. *J Mol Evol* 47, 751-762.

Escalante-Alcalde, D., Hernandez, L., Le Stunff, H., Maeda, R., Lee, H.S., Jr. Gang, C. et al. (2003) The lipid phosphatase LPP3 regulates extra-embryonic vasculogenesis and axis patterning. *Development* 130, 4623-4637.

Esser, C., Alberti, S. and Hohfeld J. (2004) Cooperation of molecular chaperones with the ubiquitin/proteasome system. *Biochim Biophys Acta* 1695, 171-188.

Falk, S., Wurdak, H., Ittner, L.M., Ille, F., Sumara, G., Schmid, M.T. et al. (2008) Brain area-specific effect of TGF-beta signaling on Wnt-dependent neural stem cell expansion. *Cell Stem Cell* 2, 472-483.

Fan, B., Brennan, J., Grant, D., Peale, F., Rangell, L. and Kirchhofer, D. (2007) Hepatocyte growth factor activator inhibitor-1 (HAI-1) is essential for the integrity of the basement membranes in the developing placental labyrinth. *Dev Biol* 303, 220-230.

Fan, C.Y., Lee, S. and Cyr, D.M. (2003) Mechanisms for regulation of Hsp70 function by Hsp40. *Cell Stress. Chaperones.* 8, 309-316.

Fayazi, Z., Ghosh, S., Marion, S., Bao, X., Shero, M. and Kazemi-Esfarjani, P. (2006) A *Drosophila* ortholog of the human Mrj modulates polyglutamine toxicity and aggregation. *Neurobiol Dis* 24, 226-244.

Ferri, A.L. Cavallaro, M., Braida, D., Di Cristofano, A., Canta, A., Vezzani, A. et al. (2004) Sox2 deficiency causes neurodegeneration and impaired meurogenesis in adult mouse brain. *Development* 131, 3805-3819.

Fischer, A., Schumacher, N., Maier, M., Sendtner, M. and Gessler, M. (2004) The Notch target genes Hey1 and Hey2 are required for embryonic vascular development. *Genes Dev* 18, 901-911.

Friso, S., Choi, S.W., Girelli, D., Mason, J.B., Dolnikowski, G.G., Bagley, P.J. et al. (2002) A common mutation in the 5,10-methylenetetrahydrofolate reductase gene affects genomic DNA methylation through an interaction with folate status. *Proc Natl Acad Sci USA* 99, 5606-5611.

Fuchs, E. and Cleveland, D.W. (1998) A structural scaffolding of intermediate filaments in health and disease. *Science* 279, 514-519.

Fuchs, E. and Weber, K. (1994) Intermediate filaments: Structure, dynamics, function, and disease. *Annu Rev Biochem* 63, 345-382.

Fujiwara, T., Dehart, D.B., Sulik, K.K. and Hogan, B.L. (2002) Distinct requirements for extra-embryonic bone morphogenetic protein 4 in the formation of the node and primitive streak and coordination of left-right asymmetry in the mouse. *Development* 129, 4685-4696.

Gabriel, H.D., Jung, D., Butzler, C., Temme, A., Traub, O., Winterhager, E. and Willecke, K. (1998) Transplacental uptake of glucose is decreased in embryonic lethal connexin26-deficient mice. *J Cell Biol* 140, 1453-1461.

Galabova-Kovacs, G., Matzen, D., Piazzolla, D., Meissl, K., Plyushch, T., Chen, A.P. et al. (2006) Essential role of B-Raf in ERK activation during extraembryonic development. *Proc Natl Acad Sci USA* 103, 1325-1330.

Galceran, J., Hsu, S.C. and Grosschedl, R. (2001) Rescue of a Wnt mutation by an activated form of LEF-1: regulation of maintenance but not initiation of Brachyury expression. *Proc Natl Acad Sci USA* 98, 8668-8673.

Gallicano, G.I., Bauer, C. and Fuchs, E. (2001) Rescuing desmoplakin function in extra-embryonic ectoderm reveals the importance of this protein in embryonic heart, neuroepithelium, skin and vasculature. *Development* 128, 929-941.

Gallicano, G.I., Kouklis, P., Bauer, C., Yin, M., Vasioukhin, V., Degenstein, L. and Fuchs E. (1998) Desmoplakin is required early in development for assembly of desmosomes and cytoskeletal linkage. *J Cell Biol* 143, 2009-2022.

Garcion, E., Halilagic, A., Faissner, A. and Ffrench-Constant, C. (2004) Generation of an environmental nice for neural stem cell development by the extracellular matrix molecule tenascin C. *Development* 131, 3423-3432.

Ge, W., He, F., Kim, K.J., Blanchi, B., Coskun, V., Nguygen, Wu, X. et al. (2006) Coupling of cell migration with neurogenesis by proneural bHLH factors. *Proc Natl Acad Sci USA* 103, 1319-1324.

Ghandour, H., Chen, Z., Selhub, J. and Rozen, R. (2004) Mice deficient in methylene-tetrahydrofolate reductase exhibit tissue-specific distribution of folates. *J Nutr* 134, 2975-2978.

Gilbert, S., Loranger, A., Daigle, N. and Marceau, N. (2001) Simple epithelium keratin 8 and 18 provide resistance to Fas-mediated apoptosis. The protection occurs through a receptor-targeting modulation. *J Cell Biol* 154, 763-774.

Giroux, S., Trembley, M., Bernard, D., Cardin-Girand, J.F., Aubry, S., Larouche, L. et al. (1999) Embryonic death of Mek1-deficient mice reveals a role for this kinase in angiogenesis in the labrynthine region of the placenta. *Curr Biol* 9, 369-372.

Gnarra, J.R., Ward, J.M., Porter, F.D., Wagner, J.R., Devor, D.E., Grinberg, A. et al. (1997) Defective placental vasculogenesis causes embryonic lethality in VHL-deficient mice. *Proc Natl Acad Sci USA* 94, 9102-9107.

Goh, K.L., Yang, J.T. and Hynes, R.O. (1997) Mesodermal defects and cranial neural crest apoptosis in alpha5 integrin-null embryos. *Development* 124, 4309-4319.

Gong, Y., Mo, C. and Fraser, S.E. (2004) Planar cell polarity signalling controls cell division orientation during zebrafish gastrulation. *Nature* 430, 689-693.

Goodrich, L.V., Milenkovic, L., Higgins, K.M. and Scott, M.P. (1997) Altered neural cell fates and medulloblastoma in mouse patched mutants. *Science* 277, 1109-1113.

Graef, I.A., Chen, F., Chen, L., Kuo, A. and Crabtree, G. (2001) Signals transduced by Ca^{2+}/Calcineurin and NFATc3/c4 pattern the developing vasculature. *Cell* 105, 863-875.

Graham, V., Khudyakoc, J., Ellis, P. and Pevny, L. (2003) SOX2 functions to maintain neural progenitor identity. *Neuron* 39, 749-765.

Guillemot, F. (2007) Spatial and temporal specification of neural fates by transcription factor codes. *Development* 134, 3771-3780.

Guillemot, F., Caspary, T., Tilghman, S.M., Copeland, N.G., Gilbert, D.J., Jenkins, N.A. et al. (1994) Genomic imprinting of Mash2, a mouse gene required for trophoblast development. *Nature Genet* 9, 235-242.

Gurtner, G.C., Davis, V., Li, H., McCoy, M.J., Sharpe, A. and Cybulsky, M.I. (1995) Targeted disruption of the murine VCAM1 gene: essential role of VCAM-1 in chorioallantoic fusion and placentation. *Genes Dev* 9, 1-14.

Hadjantonakis, A.K., Gertsenstein, M., Ikawa, M., Okabe, M. and Nagy A. (1998) Generating green fluorescent mice by germline transmission of green fluorescent ES cells. *Mech Dev* 76, 79-90.

Haegel, H., Larue, L., Ohsugi, M., Fedorov, L., Herrenknecht, K. and Kelmer, R. (1995) Lack of β-catenin affects mouse development at gastrulation. *Development* 121, 3529-3537.

Hague, W.M. (2003) Homocysteine and pregnancy. *Best Pract Res Clin Obstet Gynaecol* 17, 459-469.

Hakem, R., Hakem, A., Duncan, G.S., Henderson, J.T., Woo, M., Soengas, M.S. et al. (1998) Differential requirement for caspase 9 in apoptotic pathways in vivo. *Cell* 94, 339-352.

Hamblet, N.S., Lijam, N., Ruiz-Lozano, P., Wang, J., Yang, Y., Luo, Z. et al. (2002) Dishevelled 2 is essential for cardiac outflow tract development, somite segmentation and neural tube closure. *Development* 129, 5827-5838.

Hanada, S., Harada, M., Kawaguchi, T., Kumemura, H., Taniguchi, E., Koga, H. et al. (2007) Keratin inclusions alter cytosolic protein localization in hepatocytes. *Hepatol Res* 37, 828-835.

Hancock, S.N., Agulnik, S.I., Silver, L.M. and Papaioannou, V.E. (1999) Mapping and expression analysis of the mouse ortholog of *Xenopus* Eomesodermin. *Mech Dev* 81, 205-208.

Hanai, R. and Mashima, K. (2003) Characterization of two isoforms of a human DnaJ homologue, HSJ2. *Mol Biol Rep* 30, 149-153.

Harbers, K., Muller, U., Grams, A., Li, E., Jaenisch, R. and Franz, T. (1996) Provirus integration into a gene encoding a ubiquitin-conjugating enzyme results in a placental defect and embryonic lethality. *Proc Natl Acad Sci USA* 93, 12412-12417.

Harris, M.J. and Juriloff, D.M. (2007) Mouse mutants with neural tube closure defects and their role in understanding human neural tube defects. *Birth Defects Res A Clin Mol Teratol* 79, 187-210.

Hart, D.J., Finglas, P.M., Wolfe, C.A., Mellon, F., Wright, A.J. and Southon, S. (2002). Determination of 5-methyltetrahydrofolate (13C-labeled and unlabeled) in human plasma and urine by combined liquid chromatography mass spectrometry. *Anal Biochem* 305, 206-213.

Hartl, F.U. and Hayer-Hartl, M. (2002) Molecular chaperones in the cytosol: from nascent chain to folded protein. *Science* 295, 1852-1858.

Hata, K., Okano, M., Lei, H. and Li, E. (2002) Dnmt3L cooperates with the Dnmt3 family of de novo DNA methyltransferases to establish maternal imprints in mice. *Development* 129, 1983-1993.

Hatakeyama, J., Bessho, Y., Katho, K., Ookawara, S., Fujioka, M., Guillemot, F. and Kageyama, R. (2004) Hes genes reulate size, shape and histogenesis of the nervous system by control of the timing of neural stem cell differentiation. *Development* 131, 5539-5550.

Hatano, N., Mori, Y., Oh-hora, M., Kosugi, A., Fujikawa, T., Nakai, N. et al. (2003) Essential role for ERK2 mitogen-activated protein kinase in placental development. *Genes Cells* 8, 847-856.

He, W., Ingraham, C., Rising, L., Goderie, S. and Temple, S. (2001) Multipotent stem cells from the moue basal forebrain contribute GABAergic neurons and oligodendrocytes to the cerebral cortex during embryogenesis. *J Neurosci* 21, 8854-8862.

Helfand, B.T., Chang, L. and Goldman, R.D. (2004) Intermediate filaments are dynamic and motile elements of cellular architecture. *J Cell Sci* 117, 133-141.

Hernandez-Verdun, D. (1974) Morphogenesis of the syncytium in the mouse placenta. Ultrastructural study. *Cell Tissue Res* 148, 381-396.

Hernandez-Verdun, D. and Legrand, C. (1975) In vitro study of chorionic and ectoplacental trophoblast differentiation in the mouse. *J Embryol Exp Morphol* 34, 633-644.

Hesse, M., Franz, T., Tamai, Y., Taketo, M.M. and Magin, T. (2000) Targeted deletion of keratins 18 and 19 leads to trophoblast fragility and early embryonic lethality. *EMBO J* 19, 5060-5070.

Hesse, M., Watson, E.D., Schwaluk, T. and Magin, T. (2005) Rescue of keratin 18/19 doubly deficient mice using aggregation with tetraploid embryos. *Eur J Cell Biol* 84, 355-361.

Hildebrand, J.D. and Soriano, P. (1999) Shroom, a PDZ domain-containing actin-binding protein, is required for neural tube morphogenesis in mice. *Cell* 99, 485-497.

Hildebrand, J.D. and Soriano, P. (2002) Overlapping and unique roles for C-terminal binding protein 1 (CtBP1) and CtBP2 during mouse development. *Mol Cell Biol* 22, 5296-5307.

Hirabayashi, Y. and Gotoh, Y. (2005) Stage-dependent fate determination of neural precursors cells in mouse forebrain. *Neurosci Res* 51, 331-336.

Hohfeld, J., Cyr, D.M. and Patterson C. (2001) From the cradle to the grave: molecular chaperones that may choose between folding and degradation. *EMBO Rep* 2, 885-890.

Holmberg, J., Clarke, D.L. and Frisen, J. (2000) Regulation of repulsion versus adhesion by different splice forms of an Eph receptor. *Nature* 408, 203-206.

Hong, K.H., Seki, T. and Oh, S.P. (2007) Activin receptor-like kinase 1 is essential for placental vascular development in mice. *Lab Invest* 87, 670-679.

Huang, H. and He, X. (2008) Wnt/β-catenin signalling: new (and old) players and new insights. *Curr Opin Cell Biol* 20, 119-125.

Huangfu, D., Liu, A., Rakeman, A.S., Murcia, N.S., Niswander, L. and Anderson, K.V. (2003) Hedgehog signalling in the mouse requires intraflagellar transport proteins. *Nature* 426, 83-87.

Hunter, P.J., Swanson, B.J., Haendel, M.A., Lyons, G.E. and Cross, J.C. (1999) Mrj encodes a DnaJ-related cochaperone that is essential for murine development. *Development* 126, 1247-1258.

Hurst, D.R., Mehta, A., Moore, B.P., Phadke, P.A., Meehan, W.J., Accavitti, M.A. et al. (2006) Breast Cancer metastasis suppressor 1 (BRMS1) is stabilized by the Hsp90 chaperone. *Biochem Biophys Res Commun* 348, 1429-1435.

Huser, M., Luckett, J., Chiloeches, A., Mercer, K., Iwobi, M., Giblett, S. et al. (2001) MEK kinase activity is not necessary for Raf-1 function. *Embo J* 20, 1940-1951.

Inoue, A., Li, T., Roby, S.K., Valentine, M.B., Inoue, M., Boyd, K. et al. (2007) Loss of ChlR1 helicase in mouse causes lethality due to the accumulation of aneuploid cells generated by cohesion defects and placental malformation. *Cell Cycle* 6, 1646-1654.

Ishikawa, H., Bischoff, R. and Holtzer, H. (1968) Mitosis and intermediate-sized filaments in developing skeletal muscle. *J Cell Biol* 38, 538-555.

Ishikawa, T., Tamai, Y., Zorn, A.M., Yoshida, H., Seldin, M.F., Nishikawa, S. and Taketo, M.M. (2001) Mouse Wnt receptor gene Fzd5 is essential for yolk sac and placental angiogenesis. *Development* 128, 25-33.

Ishibashi, M., Ang, S.L., Shiota, K., Nakanishi, S., Kageyama, R. and Guillemot, F. (1995) Targeted disruption of mammalian hairy and Enhancer of split homolog-1 (HES-

1) leads to up-regulation of neural helix-loop-helix factors, premature neurogenesis, and severe neural tube defects. *Genes Dev* 9, 3136-3148.

Itoh, M., Yoshida, Y., Nishida, K., Narimatsu, M., Hibi, M. and Hirano, T. (2000) Role of Gab1 in heart, placenta, and skin development and growth factor- and cytokine-induced extracellular signal-regulated kinase mitogen-activated protein kinase activation. *Mol Cell Biol* 20, 3695-3704.

Izawa, I., Nishizawa, M., Ohtakara, K., Ohtsuka, K., Inada, H. and Inagaki, M. (2000) Identification of Mrj, a DnaJ/Hsp40 family protein, as a keratin 8/18 filament regulatory protein. *J Biol Chem* 275, 34251-34527.

Jackson, M., Baird, J.W., Nichols, J., Wilkie, R., Ansell, J.D., Graham, G. and Forrester, L.M. (2003) Expression of a novel homeobox gene *Ehox* in trophoblast stem cells and pharyngeal pouch endoderm. *Dev Dyn* 228, 740-744.

Janneau, J.L., Maldonado-Estrada, J., Tachdjian, G., Miran, I., Motte, N., Saulnier, P. et al. (2002) Transcriptional expression of genes involved in cell invasion and migration by normal and tumoral trophoblast cells. *J Clin Endocrinol Metabol* 87, 5336-5339.

Jaquemar, D., Kupriyanov, S., Wankell, M., Avis, J., Benirschke, K., Baribault, H. and Oshima, R. (2003) Keratin 8 protection of placental barrier function. *J Cell Biol* 161, 749-756.

Jessel, T.M. (2000) Neuronal specification in the spinal cord: inductive signals and transcriptional codes. *Nat Rev Genet* 1, 20-29.

Kaati, G., Bygren, L.O., Pembrey, M. and Sjostrom, M. (2007) Transgenerational response to nutrition, early life circumstances and longevity. *Eur J Hum Genet* 15, 784-790.

Kalyani, A.J., Piper, D., Mujtaba, T., Lucero, M.T. and Rao, M.S. (1998) Spinal cord neuronal precursors generate multiple neuronal phenotypes in culture. *J Neurosci* 18, 7856-7868.

Karabinos, A., Schmidt, H., Harborth, J., Schnabel, R. and Weber, K. (2001) Essential roles for four cytoplasmic intermediate filament proteins in *Caenorhabditis elegans* development. *Proc Natl Acad Sci* 83, 7863-7868.

Katoh, M. and Katoh, M. (2007) Wnt signalling pathway and stem cell signalling network. *Clin Cancer Res* 13, 4042-4045.

Kibar, Z., Capra, V. and Gros, P. (2007) Toward understanding the genetic basis of neural tube defects. *Clin Genet* 71, 295-310.

Kibar, Z., Vogan, K.J., Groulx, N., Justice, M.J., Underhill, D.A. and Gros, P. (2001) Ltap, a mammalian homolog of Drosophila Strabismus/Van Gogh, is altered in the mouse neural tube mutant loop-tail. *Nature Genet* 28, 251-255.

Kilpatrick, T.J. and Barlett, P.F. (1993) Cloning and growth of multipotential neural precursors: requirements for proliferation and differentiation. *Neuron* 10, 255-265.

Kim, S. and Coulombe, P.A. (2007) Intermediate filament scaffolds fulfill mechanical, organizational, and signalling functions in the cytoplasm. *Genes Dev* 21, 1581-1597.

Kim, S., Wong, P. and Coulombe, P.A. (2006) A keratin cytoskeletal protein regulates protein synthesis and epithelial cell growth. *Nature* 441, 362-365.

Kingdom, J., Huppertz, B., Seaward, G. and Kauffman, P. (2000) Development of the placental villous tree and its consequences for fetal growth. *Eur J Obstet Gynecol Reprod Biol* 92, 35-43.

Klaffky, E.J., Gonzáles, I.M. and Sutherland A.E. (2006) Trophoblast cells exhibit differential responses to laminin isoforms. *Dev. Biol.* 292, 277-289.

Klaffky, E.J., Williams, R., Yao, C.C., Ziober, B., Kramer, R. and Sutherland, A.E. (2001) Trophoblast-specific expression and function of the integrin α7 subunit in the peri-implantation mouse embryo. *Dev. Biol.* 239, 161-175

Kourie, J.I. (2001) Mechanisms of amyloid β protein-induced modification in ion transport systems: implications for neurodegenerative diseases. *Cell Mol Neurobiol* 21, 173-213.

Kozak, K.R., Abbott, B. and Hankinson, O. (1997) ARNT-deficient mice and placental differentiation. *Dev Biol* 191, 297-305.

Knock, E., Deng, L., Wu, Q., Leclerc, D., Wang, X.L. and Rozen R. (2006) Low dietary folate initiates intestinal tumors in mice, with altered expression of G2-M checkpoint regulators polo-like kinase 1 and cell division cycle 25c. *Cancer Res* 66, 10349-10356.

Krebs, L.T., Shutter, J.R., Tangaki, K., Honjo, T., Stark, K.L. and Gridley, T. (2004) Haplosufficient lethality and formation of arteriovenous malformations in Notch pathway mutants. *Genes Dev* 18, 2469-2473.

Krebs, L.T., Xue, Y., Norton, C.R., Shutter, J.R., Maguire, M., Sundberg, J.P. et al. (2000) Notch signalling is essential for vascular morphogenesis in mice. *Genes Dev* 14, 1343-1352.

Kruger, O., Plum, A., Kim, J.S., Winterhager, E., Maxeiner, S., Hallas, G. et al. (2000) Defective vascular development in connexin 45-deficient mice. *Development* 127, 4179-4193.

Ku, N.O., Michie, S., Resurreccion, E.Z., Broome, R.L. and Omary, M.B. (2002) Keratin binding to 14-3-3 proteins modulates keratin filaments and hepatocytes mitotic progression. *Proc Natl Acad Sci* 99, 4373-4378.

Ku, N.O. and Omary, M.B. (2000) Keratins turn over by ubiquitination in a phosphorylation-modulated fashion. *J Cell Biol* 149, 547-552.

Kuang, S.Q., Liao, L., Zhang, H., Pereira, F.A., Yuan, Y., DeMayo, F.J., Ko, L. and Xu, J. (2002) Deletion of the cancer-amplified coactivator AIB3 results in defective placentation and embryonic lethality. *J Biol Chem* 277, 45356-45360.

Kuida, K., Haydar, T.F., Kuan, C.Y., Gu, Y., Taya, C., Karasuyama, H. et al. (1998) Reduced apoptosis and cytochrome c-mediated caspase activation in mice lacking caspase-9. *Cell* 94, 325-337.

Kwee, L., Baldwin, H.S., Shen, H.M., Stewart, C.L., Buck, C., Buck, C.A. and Labow, M.A. (1995) Defective development of the embryonic and extraembryonic circulatory systems in vascular cell adhesion molecule (VCAM-1) deficient mice. *Development* 121, 489-503.

Lardelli, M., Williams, R., Mitsiadis, T. and Lendahl, U. (1996) Expression of the Notch 3 intracellular domain in mouse central nervous system progenitor cells is lethal and leads to disturbed neural tube development. *Mech Dev* 59, 177-190.

Lechleider, R.J., Ryan, J.L., Garrett, L., Eng, C., Deng, C., Wynshaw-Boris, A. and Roberts, A.B. (2001) Targeted mutagenesis of Smad1 reveals an essential role in chorioallantoic fusion. *Dev Biol* 240, 157-167.

Leone, D.P., Relvas, J.B., Campos, L.S., Hemmi, S., Brakebusch, C., Fassler, R. et al. (2005) Regulation of neural progenitor proliferation and survival by beta1 integrin. *J Cell Sci* 118, 2589-2599.

Lescisin, K.R., Varmuza, S. and Rossant J. (1988) Isolation and characterization of a novel trophoblast specific cDNA in the mouse. *Genes Dev* 2, 1639-1646.

Li, E., Bestor, T.H. and Jaenisch, R. (1992) Targeted mutation of the DNA methyl-transferase gene results in embryonic lethality. *Cell* 69, 915-926.

Li, Y. and Behringer, R.R. (1998) Esx1 is an X-chromosome-imprinted regulator of placental development and fetal growth. *Nature Genet* 20, 309-311.

Li, Y., Lemaire, P. and Behringer, R.R. (1997) Esx1, a novel X chromosome-linked homeobox gene expressed in mouse extraembryonic tissues and male germ cells. *Dev Biol* 188, 85-95.

Li, Z.F., Wu, X., Jiang, Y., Lui, J., Wu, C., Inagaki, M., Izawa, I. et al. (2008) Non-pathogenic protein aggregates in skeletal muscle in MLF1 transgenic mice. *J Neuro Sci* 264, 77-86.

Liao, J., Lowthert, L.A., Ghori, N. and Omary, M.B. (1995) The 70-kDa heat shock proteins associate with glandular intermediate filaments in an ATP-dependent manner. *J Biol Chem* 270, 915-922.

Liao, J. and Omary, M.B. (1996) 14-3-3 proteins associate with phosphorylated simple epithelial keratins during cell cycle progression and act as a solubility cofactor *J Cell Biol* 133, 345-357.

Liao, J., Price, D. and Omary M.B. (1997) Association of glucose-regulated protein (grp78) with human keratin 8. *FEBS Lett* 417, 316-320.

Livak, K.J. and Schmittgen, T.D. (2001) Analysis of relative gene expression data using real-time quantitative PCR and the 2(-Delta Delta C(T)) Method. *Methods* 25, 402-408.

Lois, C. and Alvarez-Buylla, A. (1993) Proliferating subventricular zone cells in the adult mammalian forebrain can differentiate into neurons and glia. *Proc Natl Acad Sci USA* 90, 2074-2077.

Lotz, K., Pyrowolakis, G. and Jentsch, S. (2004) BRUCE, a giant E2/E3 ubiquitin ligase and inhibitor of apoptosis protein of the trans-Golgi network, is required for normal placenta development and mouse survival. *Mol Cell Biol* 24, 9339-9350.

Lu, H., Hesse, M., Peters, B. and Magin, T.M. (2005) Type II keratins precede type I keratins during early embryonic development. *Eur J Cell Biol* 84, 709-718.

Lu, X., Borchers, A.G., Jolicoeur, C., Rayburn, H., Baker, J.C. and Tessier-Lavigne, M. (2004) PTK7/CCK-4 is a novel regulator of planar cell polarity in vertebrates. *Nature* 430, 93-98.

Luo, J., Sladek, R., Bader, J.A., Matthyssen, A., Rossant, J. and Giguere, V. (1997) Placental abnormalities in mouse embryos lacking the orphan nuclear receptor ERR-beta. *Nature* 388, 778-782.

Ma, G.T., Soloveva, V., Tzeng, S.J., Lowe, L.A., Pfendler, K.C., Iannaccone, P.M. et al. (2001) Nodal regulates trophoblast differentiation and placental development. *Dev Biol* 236, 124-135.

Ma, S., Charron, J. and Erikson, R.L. (2003) Role of Plk2 (Snk) in mouse development and cell proliferation. *Mol Cell Biol* 23, 6936-6943.

Magera, M.J., Lacey, J.M., Casetta, B. and Rinaldo, P. (1999) Method for the determination of total homocysteine in plasma and urine by stable isotope dilution and electrospray tandem mass spectrometry. *Clin Chem* 45, 1517-1522.

Magin, T., Schroder, R., Leitgeb, S., Wanninger, F., Zatloukal, K., Grund, C. and Melton, D.W. (1998) Lessons from keratin 18 knockout mice: formation of novel keratin filaments, secondary loss of keratin 7 and accumulation of liver-specific keratin 8-positive aggregates. *J Cell Biol* 140, 1441-1451.

Mahlapuu, M., Ormstead, M., Enerback, S. and Carlsson, P. (2001) The forkhead transcription factor Foxf1 is required for differentiation of extra-embryonic and lateral plate mesoderm. *Development* 128, 155-166.

Maina, F., Casagranda, F., Audero, E., Simeone, A., Comoglio, P.M., Klein, R., and Ponzetto, C. (1996) Uncoupling of Grb2 from the Met receptor in vivo reveals complex roles in muscle development. *Cell* 87, 531-542.

Maltepe, E. and Simon, M.C. (1998) Oxygen, genes, and development: an analysis of the role of hypoxic gene regulation during murine vascular development. *J Mol Med* 76, 391-401.

Mana, M.P., Aeder, S. and Sutherland, A.E. (2001) Trophoblast giant-cell differentiation involves changes in cytoskeleton and cell motility. *Dev Biol* 230, 43-60.

Martin-Belmonte, F. and Mostov, K. (2008) Regulation of cell polarity during epithelial morphogenesis. *Curr Opin Cell Biol* 20, 227-234.

McClellan, A.J., Tam, S., Kaganovich, D. and Frydman, J. (2005) Protein quality control: chaperones culling corrupt conformations. *Nature Cell Biol* 7, 736-741.

Meacham, G.C., Browne, B.L., Zhang, W., Kellermayer, R., Bedwell, D.M. and Cyr, D.M. (1999) Mutations in the yeast Hsp40 chaperone protein Ydj1 cause defects in Axl1 biogenesis and pro-a-factor processing. *J Biol Chem* 274, 34396-34402.

Melcer, S., Gruenbaum, Y. and Krohne, G. (2007) Invertebrate lamins. *Exp Cell Res* 313, 2157-2166.

Miner, J.H., Cunningham, J. and Sanes, J.R. (1998) Roles for laminin in embryogenesis: exencephaly, syndactyly and placentopathy in mice lacking the laminin α5 chain. *J Cell Biol* 143, 1713-1723.

Mitra, A., Fillmore, R.A., Metge, B.J., Rajesh, M., Xi, Y., King, J. et al. (2008) Large isoform of MRJ (DNAJB6) reduces malignant activity of breast cancer. *Breast Cancer Res* 10, R22

Miyoshi, J. and Takai, Y. (2008) Structural and functional associations of apical junctions with cytoskeleton. *Biochimica et Biophysica Acta* 1778, 670-691.

Mizutani, K., Yoon, K., Dang, L., Tokuna, A. and Gaiano, N. (2007) Differential Notch signalling distinguishes neural stem cells from intermediate progenitors. *Nature* 449, 351-355.

Mo, F.E., Muntean, A.G., Chen, C.C., Stolz, D.B., Watkins, S.C. and Lau, L.F. (2002) CYR61 (CCN1) is essential for placental development and vascular integrity. *Mol Cell Biol* 22, 8709-8720.

Molosky, A.V., He, S., Bydon, M., Morrison, S.J. and Pardel, R. (2006) Bmi-1 promotes neural stem cell self-renewal and neural development but not mouse growth and survival by prepressing the p16Ink4a and p19Arf senescence pathways. *Genes Dev* 19, 1432-1437.

Molofsky, A.V., Pardal, R., Iwashita, T., Park, I.K., Clarke, M.F. and Morrison, S.J. (2003) Bmi-1 dependence distinguishes neural stem cell self-renewal from progenitor proliferation. *Nature* 425, 962-967.

Monkley, S.J., Delaney, S.J., Pennisi, D.J., Christiansen, J.H. and Wainwright, B.J. (1996) Targeted disruption of the Wnt2 gene results in placentation defects. *Development* 122, 3343-3353.

Morasso, M.I., Grinberg, A., Robinson, G., Sargent, T.D. and Mahon KA. (1999) Placental failure in mice lacking the homeobox gene Dlx3. *Proc Natl Acad Sci U S A* 96, 162-167.

Morgan, H.D., Santos, F., Green, K., Dean, W. and Reik W. (2005) Epigenetic reprogramming in mammals. *Hum Mol Genet* 14 Spec No 1, 47-58.

Morin-Kensicki, E.M., Boone, B.N., Howell, M., Stonebraker, J.R., Teed, J., Alb, J.G. et al. (2006) Defects in yolk sac vasculature, chorioallantoic fusion and embryonic axis elongation in mice with targeted disruption of Yap65. *Mol Cell Biol* 26, 77-87.

Morris-Kay, G.M and Tan, S.S. (1987) Mapping cranial neural crest cell migration pathways in mammalian embryos. *Trends Genet* 3, 257-261.

Morris-Kay, G.M. and Tuckett, F. (1985) The role of microfilaments in cranial neurulation in rat embryos: effects of short-term exposure to cytochalasin D. *J Embryol Exp Morph* 88, 333-348.

Morrison, S.J. and Kimble, J. (2006) Asymmetric and symmetric stem-cell divisions in development and cancer. *Nature* 441, 1068-1074.

Moser, M., Li, Y., Vaupel, K., Kretzschmar, D., Kluge, R., Glynn, P. and Buettner, R. (2004) Placental failure and impaired vasculogenesis result in embryonic lethality for neuropathy target esterase-deficient mice. *Mol Cell Biol* 24, 1667-1679.

Mudgett, J.S., Ding, J., Guh-Siesel, L., Chartrain, N.A., Yang, L., Gopal, S. and Shen, M.M. (2000) Essential role for p38alpha mitogen-activated protein kinase in placental angiogenesis. *Proc Natl Acad Sci USA* 97, 10454-10459.

Murcia, N.S., Richards, W.G., Yoder, B.K., Mucenski, M.L., Dunlap, J.R. and Woychik, R.P. (2000) The *Oak Ridge Polycystic Kidney* (*orpk*) disease gene is required for left-right axis determination. *Development* 127, 2347-2355.

Murdoch, J.N., Doudney, K., Paternotte, C., Copp, A.J. and Stanier, P. (2001a) Severe neural tube defects in the loop-tail mouse result from mutation of Lpp1, a novel gene involved in floor plate specification. *Hum Mol Genet* 10, 2593-2601.

Murdoch, J.N., Henderson, D.J., Doudney, K., Gaston-Massuet, C., Phillips, H.M., Paternotte, C. et al. (2003) Disruption of scribble (Scrb1) causes severe neural tube defects in the circletail mouse. *Hum Mol Genet* 12, 87-98.

Murdoch, J.N., Rachel, R.A., Shah, S., Beermann, F., Stanier, P., Mason, C.A. and Copp, A.J. (2001b) Circletail, a new mouse mutant with severe neural tube defects: chromosomal localization and interaction with the loop-tail mutation. *Genomics* 78, 55-63.

Nagy, A., Gertsenstein, M., Vintersten, K., and Behringer, R. (2003a) Summary of mouse development: Neurulation. In *Manipulating the Mouse Embryo: A Laboratory Manual*. Cold Spring Harbour, NY: Cold Spring Harbour Laboratory Press pp. 93-97.

Nagy, A., Gertsenstein, M., Vintersten, K., and Behringer, R. (2003b) Assembling aggregates between diploid and tetraploid embryos. In *Manipulating the Mouse Embryo: A Laboratory Manual*. Cold Spring Harbour, NY: Cold Spring Harbour Laboratory Press pp. 496-497.

Nakamura, Y., Hamanda, Y., Fujiwara, T., Enomoto, H., Hiroe, T., Tanaka, S. et al. (2006) Phospholipase C-delta1 and –delta3 are essential in the trophoblast for placental development. *Mol Cell Biol* 25, 10979-10788.

Natale, D.R., Starovic, M. and Cross, J.C. (2006) Phenotypic analysis of the mouse placenta. *Methods Mol Med* 121, 275-293.

Nilsson, S.K., Johnston, H.M., Whitty, G.A., Williams, B., Webb, R.J., Denhardt, D.T. et al. (2005) Osteopontin, a key component of the hematopoietic stem cell niche and regulator of primitive hematopoeitic stem cells. *Blood* 106, 1232-1239.

Nucifora, F.C., Jr., Sasaki, M., Peters, M.F., Huang, H., Cooper, J.K., Yamada, M. et al. (2001) Interference by huntingtin and atrophin-1 with cbp-mediated transcription leading to cellular toxicity. *Science* 291, 2423-2428.

Ohlsson, R., Falck, P., Hellstrom, M., Lindahl, P., Bostrom, H., Franklin, G., Ahrlund-Richter, L. et al. (1999) PDGFB regulates the development of the labyrinthine layer of the mouse fetal placenta. *Dev Biol* 212, 124-136.

Ohtsuka, K. and Hata, M. (2000) Mannamilan HSP40/DNAJ homologs: cloning of novel cDNAs and a proposal for their classification and nomenclature. *Cell Stress Chaperones* 5, 98-112.

Oka, C., Nakano, T., Wakeham, A., de la Pompa, J.L., Mori, C., Sakai, T., Okazaki, S. et al. (1995) Disruption of the mouse RBP-J kappa gene results in early embryonic death. *Development* 121, 3291-3301.

Okano, M., Bell, D.W., Haber, D.A. and Li, E. (1999) DNA methyltransferases Dnmt3a and Dnmt3b are essential for de novo methylation and mammalian development. *Cell* 99, 247-257.

Oriolo, A.S., Walk, F.A., Canessa, G. and Salas, P.J. (2006) GCP6 binds to intermediate filaments: A novel function of keratins in the organization of microtubules in epithelial cells. *Mol Biol Cell* 18, 781-794.

Owens, D.W. and Lane, E.B. (2003) The quest for the function of simple epithelial keratins. *Bioessays* 25, 748-758.

Pan, Z., Sikandar, S., Witherspoon, M., Dizon, D., Nguyen, T., Benirschke, K., Wiley, C. et al. (2008) Impaired placental trophoblast lineage differentiation in *Alkbh1*$^{-/-}$ mice. *Dev Dyn* 237, 316-327.

Papadaki, C., Alexiou, M., Cecena, G., Verykokakis, M., Bilitou, A., Cross, J.C. et al. (2007) Transcriptional repressor erf determines extraembryonic ectoderm differentiation. *J Biol Chem* 282, 30285-30294.

Pardi, G., Marconi, A.M. and Cetin, I. (2002) Placental-fetal interrelationship in IUGR fetuses – a review. *Placenta* 23, Suppl A, S136-S141.

Parekh, V., McEwen, A., Barbour, V., Takahashi, Y., Rehg, J.E., Jan, S.M. and Cunningham, J.M. (2004) Defective extraembryonic angiogenesis in mice lacking LBP-

1a, a member of the grainyhead family of transcription factors. *Mol Cell Biol* 24, 7113-7129.

Park, M. and Moon, R.T. (2001) The planar cell-polarity gene *stbm* regulates both neural and mesodermal convergent extension: parallel forces elongating the body axis. *Nature Cell Biol* 4, 20-25.

Parr B.A., Cornish V.A., Cybulsky M.I., and McMahon A.P. (2001) Wnt7b regulates placental development in mice. *Dev Biol* 237, 324-332.

Pei, L. (1999) Pituitary tumor-transforming gene protein associates with ribosomal protein S10 and a novel human homologue of DnaJ in testicular cells. *J Biol Chem* 274, 3151-3158.

Peifer, M. (1993) The product of the *Drosophila* segment polarity gene armadillo is part of a multi-protein complex resembling the vertebrate adherens junction. *J Cell Sci* 105, 993-1000.

Pembrey, M.E., Bygren, L.O., Kaati, G., Edvinsson, S., Northstone, K., Sjostrom, M. and Golding, J. (2006) Sex-specific, male-line transgenerational responses in humans. *Eur J Hum Genet* 14, 159-166.

Perng, M.D., Cairns, L., van der, I., Prescott, A., Hutcheson, A.M. and Quinlan R.A. (1999). Intermediate filament interactions can be altered by HSP27 and alphaB-crystallin. *J Cell Sci* 112, 2099-2112.

Petrs-Silva, H., Chiarini, L.B. and Linden, R. (2008) Nuclear proteasomal degradation and cytoplasmic retention underlie early nuclear exclusion of transcription factor Max upon axon damage. *Exp Neurol* (in press) doi:10.1016/j.expneurol.2008.06.001.

Pettersson, K., Svensson, K., Mattsson, R., Carlsson, B., Ohlsson, R. and Berkenstam, A. (1996) Expression of a novel member of estrogen response element-binding nuclear

receptors is restricted to the early stages of chorion formation during mouse embryogenesis. *Mech Dev* 54, 211-223.

Pfarrer, C., Macara, L., Leiser, R. and Kingdom, J. (1999) Adaptive angiogenesis in placentas of heavy smokers. Lancet 354, 303.

Philipp, M., Brede, M.E., Hadamek, K., Gessler, M., Lohse, M.J. and Hein, L. (2002) Placental alpha(2)-adrenoceptors control vascular development at the interface between mother and embryo. *Nature Genet* 31, 311-315.

Piedrahita, J.A., Oetama, B., Bennett, G.D., van Waes, J., Kamen, B.A., Richardson J. et al. (1999) Mice lacking the folic acid-binding protein Folbp1 are defective in early embryonic development. *Nature Genet* 23, 228-232.

Pignatelli, M. (1998) Integrins, cadherins and catenins: molecular cross-talk in cancer cells. *J Pathol* 186, 1-2.

Plum, A., Winterhager, E., Pesch, J., Lautermann, J., Hallas, G., Rosentreter, B. et al. (2001) Connexin31-deficiency in mice causes transient placental dysmorphogenesis but does not impair hearing and skin differentiation. *Dev Biol* 231: 334-347.

Pokutta, S. and Weis, W.I. (2002) The cytoplasmic face of cell contact sites. *Curr Opin Struct Bio.* 12, 255-262.

Porter, R.M. and Lane, E.B. (2003) Phenotypes, genotypes and their contribution to understanding keratin function. *Trends Genet* 19, 278-285.

Qian, X., Estaban, L., Vass, W.C., Upadhyaya, C., Papageorge A.G., Yienger K. et al. (2000) The Sos1 and Sos2 Ras-specific exchange factors: differences in placental expression and signalling properties. *EMBO J* 19, 642-654.

Qian, X., Shen, Q., Goderie, S.K., He, W., Capela, A., Davis, A.A. and Temple, S. (2000) Timing of CNS cell generation: a programmed sequence of neuron and glial cell production from isolated murine cortical stem cells. *Neuron* 28, 69-80.

Quinlan, M.P. and Hyatt, J.L. (1999) Establishment of the circumferential actin filament network is a prerequisite for localization of the cadherin-catenin complex in epithelial cells. *Cell Growth Differ* 10, 839-854.

Quinlan, R.A., Hatzfeld, M., Franke, W.W., Lustig, A., Schulthess, T. and Engel J. (1986) Characterization of dimer subunits of intermediate filament proteins. *J Mol Biol* 192, 337-349.

Raydice, G.L., Rayburn, H., Matsunami, H., Knudsen, K.A., Takeichi, M. and Hynes, R.O. (1997) Developmental defects in mouse embryos lacking N-cadherin. *Dev Biol* 181, 64-78.

Rakeman, A.S. and Anderson, K.V. (2006) Axis specification and morphogenesis in the mouse embryo require Nap1, a regulator of WAVE-mediated actin branching. *Development* 133, 3075-3085.

Rao, M. (2004) Stem and precursor cells in the nervous system. *J Neurotrauma* 21, 415-427.

Rashbass, P., Cooke, L.A., Herrmann, B.G. and Beddington, R.S. (1991) A cell autonomous function of Brachyury in T/T embryonic stem cell chimaeras. *Nature* 353, 348-351.

Reynolds, B.A., Tetzlaff, W. and Weiss, S. (1992) A multipotent EGF-responsive striatal embryonic progenitor cell produces neurons and astroctyes. *J Neurosci* 12, 4565-4574.

Reynolds, B.A. and Weiss, S. (1992) Generation of neurons and astrocytes from isolated cells of the adult mammalian central nervous system. *Science* 255, 1707-1710.

Reynolds, B.A. and Weiss, S. (1996) Clonal and population analysis demonstrate that an EGF-responsive mammalian embryonic CNS precursor is a stem cell. *Dev Biol* 175, 1-13.

Riethmacher, D., Brinkmann, V. and Birchmeier, C. (1995) A targeted mutation in the mouse E-cadherin gene results in defective preimplanation development. *Proc Natl Acad USA* 92, 855-859.

Rodriguez, T.A., Sparrow, D.B., Scott, A.N., Withington, S.L., Preis, J.I., Michalicek, J. et al. (2004) Cited1 is required in trophoblast for placental development and for embryo growth and survival. *Mol Cell Biol* 24, 228-244.

Ross, C.A. (2002) Polyglutamine pathogenesis: emergence of unifying mechanisms for Huntington's disease and related disorders. *Neuron* 35, 819-822.

Ross, C.A. and Poirier, M.A. (2005) What is the role of protein aggregation in neurodegeneration? *Nature Rev Mol Cell Biol* 6, 891-898.

Rossant, J. and Cross, J.C. (2001) Placental development: Lessons from mouse mutants. *Nature Rev Genet* 2, 538-548.

Rossant, J. and Spence, A. (1998) Cimeras and mosaics in mouse mutant analysis. *Trends Genet* 14, 358-63.

Sachs, M., Brohmann, H., Zechner, D., Muller, T., Hulksen, J., Walther, I. et al. (2000) Essential role of Gab1 for signalling by the c-Met receptor in vivo. *J Cell Biol* 150, 1375-1384.

Sah, V.P., Attardi, L.D., Mulligan, G.J., Williams, B.O., Bronson, R.T. and Jacks, T. (1995) A subset of p53-deficienct embryos exhibit exencephaly. *Nature Genet* 10, 175-180.

Salas, P.J., Rodriguez, M.L., Viciano, A.L., Vega-Salas, D.E. and Hauri, H.P. (1997) The apical submembrane cytoskeleton participates in the organization of the apical pole in epithelial cells. *J Cell Biol* 137, 359-375.

Saunders, D.N., Hird, S.L., Withington, S.L., Dunwoodie, S.L., Henderson, M.J., Biben, C. et al. (2004) Edd, the murine hyperplastic disc gene, is essential for yolk sac vascularization and chorioallantoic fusion. *Mol Cell Biol* 24, 7225-7234.

Saxton, T.M., Cheng, A.M., Ong, S.H., Lu, Y., Sakai, R., Cross, J.C. and Pawson, T. (2001) Gene dosage-dependent functions for phosphotyrosine-Grb2 signalling during mammalian tissue morphogenesis. *Curr Biol* 11, 662-670.

Scadden, D.T. (2006) The stem cell niche as an entity of action. *Nature* 441, 1075-1079.

Schmidt, C., Bladt, F., Goedecke, S., Brinkmann, V., Zschiesche, W., Sharpe, M. et al. (1995) Scatter factor/hepatocyte growth factor is essential for liver development. *Nature* 373, 699-702.

Schorpp-Kistner, M., Wang, Z.Q., Angel, P. and Wagner, E.F. (1999) JunB is essential for mammalian placentation. *EMBO J* 18, 934-948.

Schreiber, M, Wang ZQ, Jochum W, Fetka I, Elliott C, and Wagner EF. (2000) Placental vascularisation requires the AP-1 component fra1. *Development* 127, 4937-4948.

Schweizer, J., Bowden, P.E., Coulombe, P.A., Langbein, L., Lane, E.B., Magin, T.M. et al. (2006) New consensus nomenclature for mammalian keratins. *J Cell Biol* 174, 169-174.

Seki, N., Hattori, A., Hayashi, A., Kozuma, S., Miyajima, N. and Saito, T. (1999) Cloning, tissue expression, and chromosomal assignment of human MRJ gene for a member of the DNAJ protein family. *J Hum Genet* 44, 185-189.

Shalom-Barak, T., Nicholas, J.M., Wang, Y., Zhang, X., Ong, E.S., Young, T.H. et al. (2004) Peroxisome Proliferator-Activated Receptor {gamma} Controls Muc1 Transcription in Trophoblasts. *Mol Cell Biol* 24, 10661-10669.

Shane, B. and Stokstad, E.L. (1985) Vitamin B12-folate interrelationships. *Annu Rev Nutr* 5, 115-141.

Shawlot, W. and Behringer, R.R. (1995) Requirement for Lim1 in head-organizer function. *Nature* 374, 425-430.

Shawlot, W., Deng, J.M., Fohn, L.E. and Behringer, R.R. (1998) Restricted β-galactosidase expression of a hygromycine-*lacZ* gene targeted to the β-actin locus and embryonic lethality of β-actin mutant mice. *Transgenic Res* 7, 95-103.

Shi, W., van den Hurk, J.A., Alamo-Bethencourt, V., Mayer, W., Winkens, H.J., Ropers, H.H. et al. (2004) Choroideremia gene product affects trophoblast development and vascularization in mouse extra-embryonic tissues. *Dev Biol* 272, 53-65.

Shi, Y., Sun, G., Zhao, C. and Stewart, R. (2008) Neural stem cell self-renewal. *Crit Rev Oncol Hematol* 65, 43-53.

Shum, A.S.W. and Copp, A.J. (1996) Regional differences in morphogenesis of the neuroepithelium suggest multiple mechanisms of spinal neurulation in the mouse. *Anat Embryol* 194, 65-73.

Sibley, C.P., Birdsey, T.J., Brownbill, P., Clarson, L.H., Doughty, I., Grazier, J.D., Greenwood, S.L. et al. (1998) Mechanisms of maternofetal exchange across the human placenta. *Biochem Soc Trans* 26, 86-91.

Simmons, D.G. and Cross, J.C. (2005) Determinants of trophoblast lineage and cell subtype specification in the mouse placenta. *Dev Biol* 284, 12-24.

Simmons, D.G., Fortier, A.L. and Cross, J.C. (2007) Diverse subtypes and developmental origins of trophoblast giant cells in the mouse placenta. *Dev Biol* 304, 567-578.

Simmons, D.G., Natale, D.R., Begay, V., Hughes, M., Leutz, A. and Cross, J.C. (2008) Early patterning of the chorion leads to trilaminar trophoblast cell structure in the placental labyrinth. *Development* 135, 2083-2091.

Simons, M., Gloy, J., Ganner, A., Bullerkotte, A., Bashkurov, M., Kronig, C., Schermer, B. et al. (2005) Inversin, the gene product mutated in nephronophthisis type II, functions as a molecular switch between Wnt signaling pathways. *Nature Genet* 37, 537-543.

Singh, U., Sun, T., Looman, C., Heuchel, R., Elliott, R., Freichel, M. et al. (2007) Expression and function of the gene encoding the voltage-dependent calcium channel beta3-subunit in the mouse placenta. *Placenta* 28, 412-20.

Sinclair, K.D., Allegrucci, C., Singh, R., Gardner, D.S., Sebastian, S., Bispham, J. et al. (2007) DNA methylation, insulin resistance, and blood pressure in offspring determined by maternal periconceptual B vitamin and methionine status. *Proc Natl Acad Sci USA* 104, 19351-19356.

Skinner, M.K. (2008) What is an epigenetic transgenerational phenotype? F3 or F2. *Reprod Toxicol* 25, 2-6.

Smith D.E., Franco del Amo F., and Grindley T. (1992) Isolation of *Sna*, a mouse gene homologous to the Drosophila genes *snail* and *escargot*: its expression pattern suggests multiple roles during post-implantation development. *Development* 116, 1033-1039.

Smith, D.E., Kok, R.M., Teerlink, T., Jakobs, C. and Smulders, Y.M. (2006) Quantitative determination of erythrocyte folate vitamer distribution by liquid chromatography-tandem mass spectrometry. *Clin Chem Lab Med* 44, 450-459.

Smedley, M.J. and Stansstreet, M. (1986) Calcium and neurulation in mammalian embryos. II. Effects of cytoskeletal inhibitors an calcium antagonists on the neural folds of rat embryos. *J Embryol Exp Morph* 93, 167-178.

Sohn, S.J., Sarvis, B.K., Cado, D. and Winoto, A. (2002) ERK5 MAPK regulates embryonic angiogenesis and acts as a hypoxia-sensitive repressor of vascular endothelial growth factor expression. *J Biol Chem* 277, 43344-43351.

Solloway, M.J. and Robertson, E.J. (1999) Early embryonic lethality in Bmp5;Bmp7 double mutant mice suggests functional redundancy within the 60A subgroup. *Development* 125, 4607-4616.

Stauffer, D.R., Howard, T.L., Nyun, T. and Hollenberg, S.M. (2001) CHMP1 is a novel nuclear matrix protein affecting chromatin structure and cell-cycle progression. *J Cell Sci* 114, 2383-2393.

Stecca, B., Nait-Oumesmar, B., Kelley, K.A., Voss, A.K., Thomas, T. and Lazzarini, R.A. (2002) *Gcm1* expression defines three stages of chorioallantoic interaction during placental development. *Mech Dev* 115, 27-34.

Stefani, M. (2007) Generic cell dysfunction in neurodegenerative disorders: Role of surfaces in early protein misfolding, aggregation, and aggregate toxicity. *The Neuroscientist* 13, 519-531.

Steingrimsson, E., Tessarollo, L., Reid, S.W., Jenkins, N.A. and Copeland, N.G. (1998) The bHLH-Zip transcription factor Tfeb is essential for placental vascularization. *Development* 125, 4607-4616.

Stern, C.D. (2006) Neural induction: 10 years on since the ‘default model’. *Curr Opin Cell Biol* 18, 692-697.

Stumpo, D.J., Bock, C.B., Tuttle, J.S. and Blackshear, P.J. (1995) MARCKS deficiency in mice leads to abnormal brain development and perinatal death. *Proc Natl Acad Sci USA* 92, 944-948.

Stumpo, D.J., Byrd, N.A., Phillips, R.S., Ghosh, S., Maronpot, R.R., Castranio, T., Meyers, E.N. et al. (2004) Chorioallantoic fusion defects and embryonic lethality resulting from disruption of Zfp36L1, a gene encoding a CCCH tandem zinc finger protein of the Tristetraprolin family. *Mol Cell Biol* 24, 6445-6455.

Styers, M.L., Salazar, G., Love, R., Peden, A.A., Kowalczyk, A.P. and Faundez, V. (2004) The endo-lysosomal sorting machinery interacts with the intermediate filament cytoskeleton. *Mol Cell Biol* 15, 5369-5382.

Swanson, D.A., Liu, M.L., Baker, P.J., Garrett, L., Stitzel, M., Harris, M. et al. (2001) Taargeted disruption of the methionine synthase gene in mice. *Mol Cell Biol* 21, 1058-1065.

Szabo, R., Molinolo, A., List, K. and Bugge, T.H. (2007) Matripase inhibition by hapatocyte growth factor activator inhibitr-1 is essential for placental development. *Oncogene* 26, 1546-1556.

Tamai, Y., Ishikawa, T., Bosl, M.R., Mori, M., Nozaki, M., Baribault, H., Oshima, R.G. and Taketo, M.M. (2000) Cytokeratins 8 and 19 in the mouse placental development. *J Cell Biol* 151, 563-572.

Tamura, T. and Picciano, M.F. (2006) Folate and human reproduction. *Am J Clin Nutr* 83, 993-1016.

Tanaka, S., Kunath, T., Hadjantonakis, A.K., Nagy, A. and Rossant, J. (1998) Promotion of trophoblast stem cell proliferation by FGF4. *Science* 282, 2072-2075.

Tarkowski, A.K., Witkowska, A. and Opas J. (1977) Development of cytochalasin in B-induced tetraploid and diploid/tetraploid mosaic mouse embryos. *J Embryol Exp Morphol* 41, 47-64.

Tateossian, H., Powles, N., Dickinson, R., Ficker, M. and Maconochie, M. (2004) Determination of downstream targets of FGF signalling using gene trap and cDNA subtractive approaches. *Exp Cell Res* 292, 101-114.

Temple, S. (1998) Division and differentiation of isolated CNS blast cells in microculture. *Nature* 340, 471-3.

Temple, S. (2001) The development of neural stem cells. *Nature* 414, 112-117.

Tetzlaff, M.T., Bai, C., Finegold, M., Wilson, J., Harper, J.W., Mahon, K.A. and Elledge, S.J. (2004) Cyclin F disruption compromises placental development and affects normal cell cycle execution. *Mol. Cell Biol.* 24, 2487-2498.

Thorey, I.S., Meneses, J.J., Neznanov, N., Kulesh, D.A., Pedersen, R.A. and Oshima, R.G. (1993) Embryonic expression of human keratin 18 and K18-beta-galactosidase fusion genes in transgenic mice. *Dev Biol* 160, 519-534.

Threadgill, D.W., Dlugosz, A.A., Hansen, L.A., Tennenbaum, T., Lichti, U., Yee, D., LaMantia, C. et al. (1995) Targeted disruption of mouse EGF receptor: effect of genetic background on mouse phenotype. *Science* 269, 230-234.

Thumkeo, D., Keel, J., Ishizaki, T., Hirose, M., Nonomura, K., Oshima, H., Oshima, M. et al. (2003) Targeted disruption of the mouse rho-associated kinase 2 gene results in intrauterine growth retardation and fetal death. *Mol Cell Biol* 23, 5043-5055.

Tropepe, V., Hitoshi, S., Sirard, C., Mak, T.W., Rossant, J. and van der Kooy, D. (2001) Direct neural fate specification from embryonic stem cells: a primitive mammalian neural stem cell stage acquired through a default mechanism. *Neuron* 30, 65-78.

Upadhya, S.C. and Hegde, A.N. (2007) Role of ubiquitin proteasome system in Alzheimer's disease. *BMC Biochem* 8, S12.

Uy, G.D., Downs, K.M. and Gardner, R.L. (2002) Inhibition of trophoblast stem cell potential in chorionic ectoderm coincides with occlusion of the ectoplacental cavity in the mouse. *Development* 129, 3913-3924.

van der Linden, I.J., den Heijer, M., Afman, L.A., Gellekink, H., Vermeulen, S.H., Kluijtmans, L.A. and Blom, H.J. (2006) The methionine synthase reductase 66A>G polymorphism is a maternal risk factor for spina bifida. *J Mol Med* 84, 1047-54.

van Meeteren, L.A., Ruurs, P., Stortelers, C., Bouwman, P., van Rooijen, M.A., Pradere, J.P., Pettit, T.R. et al. (2006) Autotaxin, a secreted lysophospholipase D, is essential for blood vessel formation during development. *Mol Cell Biol* 26, 5015-5022.

van Nes, J., de Graaf, W., Lebrin, F., Gerhard, M., Beck, F. and Deschamps, J. (2006) The Cdx4 mutation affects axial development and reveals an essential role of Cdx genes in the ontogenesis of the placental labyrinth in mice. *Development* 133, 419-28.

Vasser, R., Coulombe, P.A., Degenstein, L., Albers, K. and Fuchs, E. (1991) Mutant keratin expression in transgenic mice causes marked abnormalities resembling a human genetic disease. *Cell* 64, 365-380.

Vega, R.B., Matsuda, K., Oh, J., Barbosa, A.C., Yang, X., Meadows, E., McAnally, J. et al. (2004) Histone deacetylase 4 controls chondrocyte hypertrophy during skeletogenesis. *Cell* 119, 555-566.

Vincent, S.D., Dunn, N.R., Sciammas, R., Shapior-Shalef, M., Davis, M.M., Calame, K. et al. (2005) The zinc finger transcriptional repressor Blimp/Prdm1 is dispensable for early axis formation but is required for specification of primordial germ cells in the mouse. *Development* 132, 1315-1325.

Voss AK, Thomas T, and Gruss P. (2000) Mice lacking HSP90beta fail to develop a placental labyrinth. *Development* 127, 1-11.

Wakimoto, K., Kobayashi, K., Kuro, O.M., Yao, A., Iwamoto, T., Yanaka, N. et al. (2000) Targeted disruption of Na^{+}/Ca^{2+} exchanger gene leads to cardiomyocyte apoptosis and defects in heartbeat. *J Biol Chem* 275, 36991-36998.

Wallingford, J.B. and Harland, R.M. (2001) *Xenopus* Dishevelled signalling regulates both neural and mesodermal convergent extension: parallel forces elongating the body axis. *Development* 128, 2581-2592.

Wallingford, J.B. and Harland, R.M. (2002) Neural tube closure requires Dishevelled-dependent convergent extension of the midline. *Development* 129, 5815-5825.

Wang, Y., Guo, N. and Nathans, J. (2006) The role of Frizzled3 and Frizzled6 in neural tube closure and in the planar polarity of inner-ear sensory hair cells. *J Neurosci* 26, 2147-2156.

Wang, Z., Moro, E., Kovacs, K., Yu, R. and Melmed, S. (2003) Pituitary tumor transforming gene-null male mice exhibit impaired pancreatic beta cell proliferation and diabetes. *Proc Natl Acad Sci USA* 100, 3428-3432.

Ware, C.B., Horowitz, M.C., Renshaw, B.R., Hunt, J.S., Liggit, D., Koblar, S.A. et al. (1995) Tarageted disruption of the low-affinity leukemia inhibitory factor receptor gene causes placenta, skeletal, neural and metabolic defects and results in perinatal death. *Development* 121, 1283-1299.

Watanabe, M., Osada, J., Aratani, Y., Kluckman, K., Reddick, R., Malinow, M.R. and Maeda, N. (1995) Mice deficient in cystathionine beta-synthase: animal models for mild severe homocyst(e)inemia. *Proc Natl Acad Sci USA* 92, 1585-1589.

Watson, E.D. (2007) 2005 Trophoblast Research Award lecture: Defects in the keratin cytoskeleton disrupt normal placental development and trophoblast function. *Placenta* 28, S111-115.

Watson, E.D. and Cross, J.C. (2005) Development of structures and transport functions in the mouse placenta. *Physiology (Bethesda)* 20, 180-193.

Watson, E.D., Geary-Joo, C., Hughes, M. and Cross, J.C. (2007) The Mrj co-chaperone mediates keratin turnover and prevents the formation of toxic inclusion bodies in trophoblast cells of the placenta. *Development* 134, 1809-1817.

Welser, J.V., Lange, N.D., Flintoff-Dye, N., Burkin, H.R. and Burkin, D.J. (2007) Placental defects in alpha7 integrin null mice. *Placenta* 28, 1219-1228.

Westhoff, B., Chapple, J.P., van der, S.J., Hohfeld, J. and Cheetham, M.E. (2005) HSJ1 is a neuronal shuttling factor for the sorting of chaperone clients to the proteasome. *Curr. Biol.* 15, 1058-1064.

Wendling, O., Chambon, P. and Mark, M. (1999) Retinoid X receptors are essential for early mouse development and placentogenesis. *Proc Natl Acad Sci USA* 96, 547-551.

Windhoffer, R., Kolsch, A., Woll, S. and Leube, R.E. (2006) Focal adhesions are hotspots for keratin filament precursor formation. *J Cell Biol* 173, 341-348.

Wilhelmson, K., Litjens, S.H., Kuiman, I., Tshimbalanga, N., Janssen, H., van den Bout, I. et al. (2005) Nesprin-3, a novel outer nuclear membrane protein, associates with the cytoskeletal linker protein plectin. *J Cell Biol* 171, 799-810.

Wilson, D.B. (1980) Cellular proliferation in the exencephalic brain of the mouse embryo. *Brain Res* 195, 139-148.

Wu, L., de Bruin, A., Saavedra, J.I., Starovic, M., Trimboli, A., Yang, Y. et al. (2003) Extra-embryonic function of RB is essential for embryonic development and viability. *Nature* 421, 942-947.

Xu, W.M., Baribault, H. and Adamson, E.D. (1998) Vinculin knockout results in heart and brain defects during embryonic development. *Development* 125, 327-337.

Xu, X., Weinstein, M., Li, C., Naski, M., Cohen, R.I., Ornitz, D.M., Leder, P. and Deng, C. (1998) Fibroblast growth factor receptor 2 (FGFR2)-mediated reciprocal regulation loop between FGF8 and FGF10 is essential for limb induction. *Development* 125, 753-765.

Yamada, K., Gravel, R.A., Toraya, T. and Matthews, R.G. (2006) Human methionine synthase reductase is a molecular chaperone for human methionine synthase. *Proc Natl Acad Sci USA* 103, 9476-9481.

Yan, L., Carr, J., Ashby, P.R., Murry-Tait, V., Thompson, C. and Arthur, J.S. (2003) Knockout of ERK5 causes multiple defects in placental and embryonic development. *BMC Dev Biol* 3, 11-13.

Yang, J., Boerm, M., McCarty, M., Bucana, C., Fidler, I.J., Zhuang, Y. and Su, B. Mekk3 is essential for early embryonic cardiovascular development. *Nature Genet* 24, 309-313.

Yang, J.T., Rayburn, H. and Hynes, R.O. (1995) Cell adhesion events mediated by alpha 4 integrins are essential in placental and cardiac development. *Development* 121, 549-560.

Yang, Z.Z., Tschopp, O., Hemmings-Mieszczak, M., Feng, J., Brodbeck, D., Perentes, E. and Hemmings, BA. (2003) Protein kinase B alpha/Akt1 regulates placental development and fetal growth. *J Biol Chem* 278, 32124-32131.

Ying, Y. and Zhao, G.Q. (2001) Cooperation of endoderm-derived BMP2 and extraembryonic ectoderm-derived BMP4 in primordial germ cell generation in the mouse. *Dev Biol* 232, 484-492.

Ylikorkala, A., Rossi, D.J., Korsisaari, N., Luukko, K., Alitalo, K., Henkemeyer, M. and Makela TP. (2001) Vascular abnormalities and deregulation of VEGF in Lkb1-deficient mice. *Science* 293, 1323-1326.

Yoon, K. and Gaiano, N. (2005) Notch signaling in the mammalian central nervous system: insights from mouse mutants. *Nature Neurosci* 8, 709-715.

Zhang, Y., Yang, Z., Cao, Y., Zhang, S., Li, H., Huang, Y. et al. (2008) The Hsp40 family chaperone protein DnaJB6 enhances Schlafen1 nuclear localization which is critical for promotion of cell cycle arrest in T cells. *Biochem J* 413, 239-250.

Zhao, Q., Behringer, R.R. and De Crombrugghe, B. (1996) Prenatal folic acid treatment suppresses acrania and meroanencephaly in mice mutant for the *Cart1* homebox gene. *Nature Genet* 13, 275-283.

Zheng, B., Tang, T., Tang, N., Kudlicka, K., Ohtsubo, K., Ma, P. et al. (2006) Essential role of RGS-PX1/sorting nexin 13 in mouse development and regulation of endocytosis dynamics. *Proc Natl Acad Sci USA* 103, 16776-81.

Zhong, W., Jiang, M.M., Schonemann, M.D., Meneses, J.J., Pedersen, R.A., Jan, L.Y. and Jan, Y.N. (2000) Mouse numb is an essential gene involved in cortical neurogenesis. *Proc Nat. Acad Sci USA* 97, 6844-6849.

Zhu, J., Motejlek, K., Wang, D., Zang, K., Schmidt, A. and Reichardt, L.F. (2002) Beta8 integrins are required for vascular morphogenesis in mouse embryos. *Development* 129, 2891-2903.

Zhu, Y., Qi, C., Jia, Y., Nye, J.S., Rao, M.S. and Reddy, J.K. (2000) Deletion of PBP/PPARBP, the gene for nuclear receptor coactivator peroxisome proliferator-

activated receptor-binding protein, results in embryonic lethality. *J Biol Chem* 275, 14779-14782.

Zhu, Y.J., Crawford, S.E., Stellmach, V., Dwivedi, R.S., Rao, M.S., Gonzalez, F.J., Qi, C. and Reddy, J.K. (2003) Coactivator PRIP, the peroxisome proliferator-activated receptor-interacting protein, is a modulator of placental, cardiac, hepatic, and embryonic development. *J Biol Chem* 278, 1986-1990.

Zimek, A. and Weber, K. (2005) Terestrial vertebrates have two keratin gene clusters; striking differences in teleost fish. *Eur J Cell Biol* 84, 623-635.

APPENDIX A

GRANDMATERNAL MUTATION IN FOLATE METABOLISM CAUSES CONGENITAL MALFORMATIONS

Experiments were designed by E. Watson, J. Cross and R. Gravel. The *Mtrr*^{gt} mice were created by BayGenomics (http://baygenomics.ucsf.edu/). The gene trap insertion was confirmed by X. Wu who also performed the qRT-PCR experiments. The mouse breeding and genotyping was carried out by W. Jia. Total homocysteine concentrations were measured by E. Fung and F. Snyder. The remaining experiments, as well as the writing of the majority of the chapter, represent the work of E. Watson.

A.1 Abstract

Folate is a vitamin required for normal embryonic growth and development including neural tube closure and heart formation. The enzyme methionine synthase reductase (MTRR) is necessary for utilization of methyl groups from the folate cycle. We show here that a hypomorphic mutation of the *Mtrr* gene results in congenital malformations that mimic folate deficiency including neural tube defects (NTDs), heart abnormalities and developmental delay. Importantly, the spectrum and frequency of these defects was not associated with the embryonic genotype but rather was dependent upon the grandmaternal genotype. This indicates that grandmaternal polymorphisms in the folate pathway pose a risk for congenital malformations and imply that the full impact of folate fortification may take more than one generation to overcome.

A.2 Introduction

Mild maternal folate deficiency during human pregnancy has been associated with serious congenital malformations including abnormal neural tube closure, irregular heart development and growth restriction (Tamara and Picciano, 2006). The implementation of folate fortification of cereal products and public education has reduced the frequency of neural tube defects (NTDs) by 46% (De Wals et al, 2007). However, failure to eliminate NTDs by maternal folate supplementation suggests another influence.

Folate acts as a carrier of methyl groups destined for downstream targets including homocysteine for methionine synthesis. Therefore, folate and methionine metabolism are intimately linked (Fig. A.1A). The main circulating folate, methyltetrahydrofolate (Smith et al, 2006), is generated by methylenetetrahydrofolate

reductase (MTHFR) (Ghandour et al, 2004; Hart et al, 2002). Its methyl group is exclusively transferred by methionine synthase (MS, encoded by the gene *Mtr*) to homocysteine to form methionine and tetrahydrofolate (Shane and Stokstad, 1985). In turn, methionine synthesis is critical for the generation of S-adenosylmethionine (AdoMet) which serves as the methyl donor for dozens of substrates including hormones, lipids, proteins and DNA (Blom et al, 2006).

A.3 Results

A.3.1 Mtrr^{gt} *is knock-down mutation resulting in adult homocysteinemia*

In mammals, methionine synthase reductase (MTRR, encoded by the *Mtrr* gene) is the enzyme responsible for the activation of MS through the reductive methylation of its vitamin B_{12} cofactor (Yamada et al, 2006). As a result, MTRR is required for normal progression of the folate and methionine cycles. To explore the relationship between disrupted folate metabolism and developmental abnormalities, we generated *Mtrr*-deficient mice using an embryonic stem (ES) cell line (XG334; from BayGenomics) containing a randomly inserted gene-trap (gt) into the *Mtrr* gene locus. A similar mouse strain using the same ES cell line was independently derived by Elmore et al (Elmore et al, 2007). Insertion of the gene-trap vector into intron 9 of the *Mtrr* locus was determined by Southern blotting and DNA sequencing (Elmore et al, 2007), and was verified in this study (data not shown). For genotyping purposes, we generated a three-primer polymerase chain reaction (PCR) using primers that flanked the gene-trap insertion site combined with primers specific to either the 5' or 3' ends of the gene-trap vector (Fig. A.1B). This allowed us to distinguish between *Mtrr*$^{+/+}$, *Mtrr*$^{+/gt}$ and *Mtrr*$^{gt/gt}$ mice.

FIGURE A.1 – *Mtrr*^{gt} is a knock-down mutation resulting in hyperhomocysteinemia. (A) Schematic diagram of the folate and methionine cycles. MTRR, methionine synthase reductase; MS, methionine synthase; DHF, dihydrofolate; THF, tetrahydrofolate; MTHFR, methylene tetrahydrofolate reductase; S-AdoMet, S-Adenosylmethionine; CBS, cystathionine β-synthase; BHMT, betaine-homocysteine methyltransferase. (B) Gene-trap was randomly inserted into intron 9 of the *Mtrr* gene locus to produce the *Mtrr*^{gt} allele (top). Gel image of PCR genotyping results using DNA from *Mtrr*$^{+/+}$ (+/+), *Mtrr*$^{+/gt}$ (+/gt) or *Mtrr*$^{gt/gt}$ (gt/gt) mice (bottom). To genotype, PCR primers flanking the gene-trap insertion site (blue and red arrows) detect the wildtype allele (127 bp). These primers in combination with either a primer annealing to the 5' end of the gene trap (green arrow; 204 bp) or the 3' end (small black; 550 bp) detect the gene-trapped allele. L, ladder. (C) Quantitative RT-PCR analysis of wildtype *Mtrr* mRNA expression levels in the brain, liver, kidney and heart of *Mtrr*$^{+/+}$, *Mtrr*$^{+/gt}$ and *Mtrr*$^{gt/gt}$ adult mice. The expression level from *Mtrr*$^{+/+}$ mice was normalized to 1. Data are presented as means ± s.d. from three independent experiments. *P<0.05, **P<0.01, ***P<0.005. (D) Range of plasma total homocysteine concentrations (μM) in *Mtrr*$^{+/+}$ (white bars) and *Mtrr*$^{gt/gt}$ adult mice (black bars).

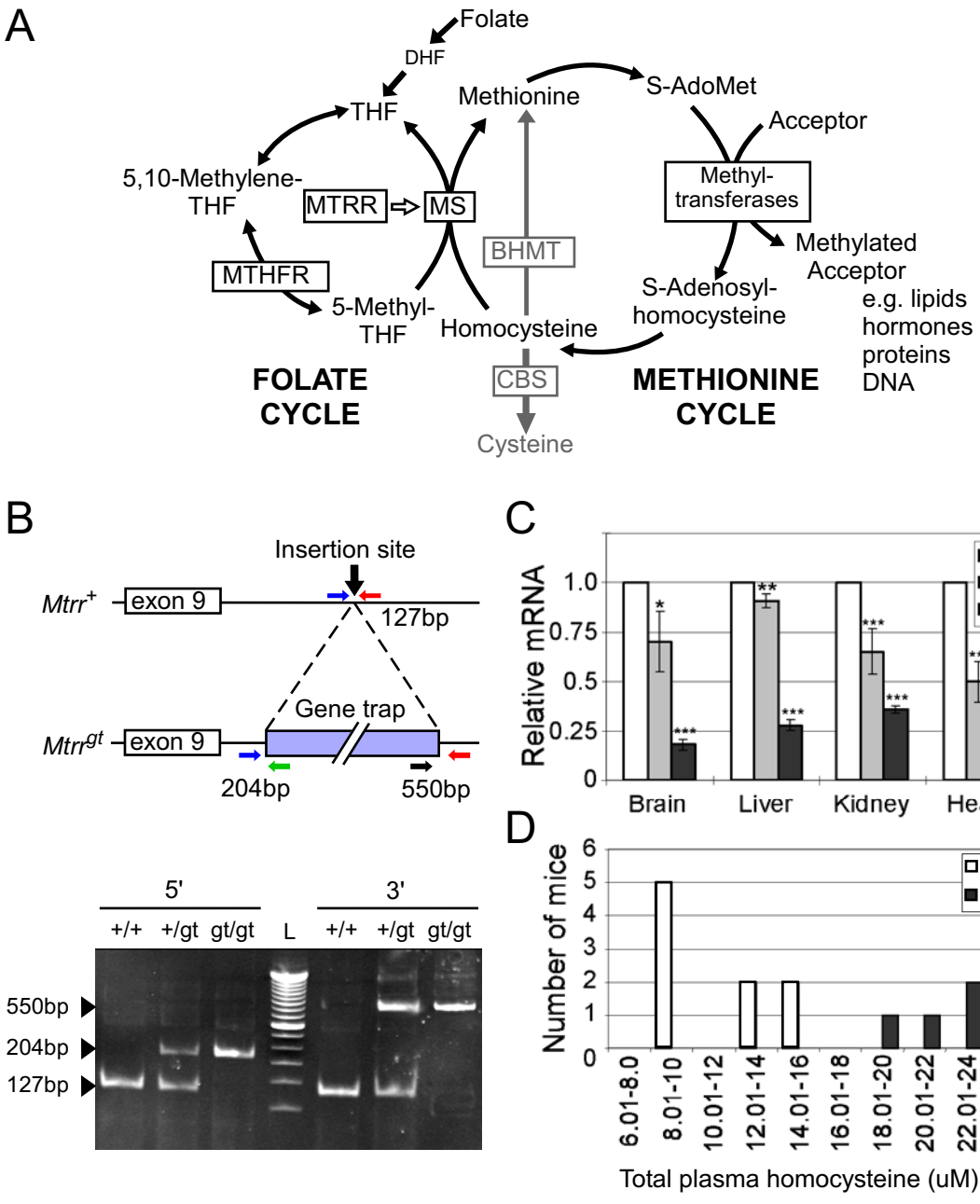
A
Folate
DHF
THF
Methionine
S-AdoMet
Acceptor
5,10-Methylene-
THF
MTRR
MS
Methyl-
transferases
BHMT
Methylated
Acceptor
e.g. lipids
hormones
proteins
DNA
MTHFR
5-Methyl-
THF
Homocysteine
S-Adenosyl-
homocysteine
FOLATE
CYCLE
CBS
METHIONINE
CYCLE
Cysteine
B
Insertion site
Mtrr+
exon 9
127bp
Gene trap
Mtrrgt
exon 9
204bp
550bp
5'
3'
+/+ +/gt gt/gt L +/+ +/gt gt/gt
550bp
204bp
127bp
C
Relative mRNA
1.0
0.75
0.5
0.25
0
+/+
+/gt
gt/gt
Brain
Liver
Kidney
Heart
D
Number of mice
6
5
4
3
2
1
0
+/+
gt/gt
6.01-8.0
8.01-10
10.01-12
12.01-14
14.01-16
16.01-18
18.01-20
20.01-22
22.01-24
24.01-26
Total plasma homocysteine (uM)

To test whether transcription of wildtype *Mtrr* mRNA was disrupted by the gene-trap insertion, we performed quantitative RT-PCR on RNA collected from various tissues of $Mtrr^{+/+}$, $Mtrr^{+/gt}$ and $Mtrr^{gt/gt}$ mice. Messenger RNA levels were normalized to expression levels in $Mtrr^{+/+}$ tissues. Despite the gene-trap insertion, we detected wildtype mRNA transcripts in all $Mtrr^{gt/gt}$ tissues tested, ranging from 6.7-36.0% of $Mtrr^{+/+}$ levels (Fig. A.1C). In accordance with these data, $Mtrr^{+/gt}$ tissues contained more wildtype mRNA than the expected 50% (50-91% of $Mtrr^{+/+}$; Fig. A.1C). This may be due to splicing around the gene-trap insertion in some splice products. As a result, $Mtrr^{gt}$ is a knock-down mutation. Increased levels of maternal plasma homocysteine are used as an indicator of folate deficiency (Hague, 2003; Piedrahita et al, 1999). Therefore, using tandem mass spectrometry, we measured plasma homocysteine concentrations in adult mice. We detected an average of 22.7 ± 2.3 μM total homocysteine in $Mtrr^{gt/gt}$ mice (mean ± s.d., n=6 mice) (Fig. A.1D), a value 2.1 fold greater ($P<0.001$) than in $Mtrr^{+/+}$ mice (10.8 ± 2.4 μM, n=9 mice). Note that these quantities show a higher baseline than those reported earlier (Elmore et al, 2007) but are due to different methods of analysis. Together, these data reveal that *Mtrr* mutant mice are a model for studying the impact of folate deficiency and hyperhomocysteinemia.

A.2.2 **Mtrr** *deficiency leads to developmental delay and severe congenital defects*

To determine whether $Mtrr^{gt/gt}$ mice had any defects, we analyzed the progeny of $Mtrr^{+/gt}$ intercrosses. A normal Mendelian ratio was observed at weaning age (36:56:23 in 20 litters), indicating that $Mtrr^{gt/gt}$ mice were viable. Gross analysis revealed no obvious phenotype in $Mtrr^{gt/gt}$ adult mice. However, we noticed that the litter sizes were

significantly smaller (5.75 pups/litter, n=20 litters) compared to control wildtype litters with the same genetic background (C57Bl/6; 8.25 pups/litter, n=8 litters). We therefore analyzed the embryos of *Mtrr*$^{+/gt}$ intercrosses during gestation. We observed at embryonic day (E) 10.5 that 90.6% of embryos (n=53 embryos) from control wildtype litters were normal in contrast to only 55.5% of the embryos from *Mtrr*$^{+/gt}$ parents (n=155 embryos) (Table A.1). Similar numbers of resorptions were present (9.4% and 11.6%, respectively) suggesting that there was no difference in embryonic lethality occurring prior to E10.5. Many of the remaining embryos from *Mtrr*$^{+/gt}$ intercrosses showed severe congenital malformations not present in control litters, ranging from developmental delay to neural tube and heart defects (Fig. A.2 and Fig. A.3). Genotyping results indicated that all embryonic genotypes were similarly affected (Table A.1). We found that 18.1% of embryos ($P<0.05$) were developmentally delayed by approximately 0.5-2.0 days (Fig. A.2A, B, C and Table A.1), although they otherwise appeared normal. This may be likened to intrauterine growth restriction (IUGR) in humans. In addition, 14.8% of embryos ($P<0.005$) exhibited congenital defects (Fig. A.2, Fig. A.3 and Table A.2). NTDs constituted the most frequent abnormality observed (9.0% of embryos) including exencephaly (Fig. A.3D, E) or small head and branchial arches (Fig. A.3C) which may be attributed to poor neural crest development. A significant percentage of embryos (5.7%) exhibited heart abnormalities (Fig. A.2 and Table A.2) including reversed cardiac looping (Fig. A.2H, I), unlooped hearts (Fig. A.2J), enlarged hearts (Fig. A.2K), and pericardial edema (Fig. A.2L). Other defects included incomplete embryonic turning (3.2%; Fig. A.2D), abnormal placental development (4.4% of embryos) whereby chorioallantoic attachment was off-centre (Fig. A.2F) or failed to occur (Fig. A.2H), and haemorrhaging

TABLE A.1 – Maternal and grandmaternal *Mtrr* deficiency causes congenital defects at E10.5

Matings & Genotypes of Progeny	Total # of litters	Total # of implant-ation sites	Average # of implant-ation sites/litter§	Delayed develop-ment (%)	Delayed with other defects (%)	Resor-ptions (%)
Wildtype ♀ x Wildtype ♂	7	53	7.6 ± 0.78	0.0	0.0	9.4
Mtrr$^{+/gt}$ ♀ x *Mtrr*$^{+/gt}$ ♂	17	155	9.12 ± 0.61			
Mtrr$^{+/+}$				5.8	4.5	0.6
Mtrr$^{+/gt}$				7.1	6.5	7.1
Mtrr$^{gt/gt}$				5.2	3.2	1.3
Unknown				0.0	0.6	2.6
Total				18.1*	14.8**	11.6
†*Mtrr*$^{+/+}$ ♀ x *Mtrr*$^{+/+}$ ♂	7	47	6.71 ± 1.01			
Mtrr$^{+/+}$				0.0	2.1	14.9
‡*Mtrr*$^{+/+}$ ♀ x *Mtrr*$^{+/+}$ ♂	7	56	8.14 ± 0.55			
Mtrr$^{+/+}$				30.4**	17.9***	17.9
Mtrr$^{+/gt}$ ♀ x *Mtrr*$^{+/+}$ ♂	7	54	7.71 ± 1.13			
Mtrr$^{+/+}$				14.8	7.4	5.6
Mtrr$^{+/gt}$				13.0	5.6	13.0
Unknown				0.0	0.0	1.9
Total				27.8*	13.0*	20.5
Mtrr$^{gt/gt}$ ♀ x *Mtrr*$^{+/+}$ ♂	7	53	7.57 ± 0.84			
Mtrr$^{+/gt}$				28.3*	18.9***	13.2

§Mean ± s.e.; †*Mtrr*$^{+/+}$ female with *Mtrr*$^{+/+}$ mother; ‡*Mtrr*$^{+/+}$ female with *Mtrr*$^{+/gt}$ mother. *P<0.05, **P<0.005, ***P<0.0001.

FIGURE A.2 – Developmental delay and congenital defects in embryos from *Mtrr*-deficient conditions at E10.5. (A) A normal appearing *Mtrr*$^{+/+}$ embryo compared to developmentally delayed *Mtrr*$^{+/+}$ embryos that resembled (B) E9.5 and (C) E8.5 staged embryos. (D) An *Mtrr*$^{+/gt}$ embryo with incomplete turning. (E) Normal placental development in which the allantois (umbilical cord; arrowhead) attached to the centre of the chorion from an *Mtrr*$^{+/gt}$ embryo. (F) An *Mtrr*$^{+/gt}$ placenta with off-centred chorioallantoic attachment (arrowhead). (H) An *Mtrr*$^{+/+}$ embryo without chorioallantoic attachment. Asterisk indicates the retracted allantois. (G) A normal heart with normal leftward looping in an *Mtrr*$^{+/gt}$ embryo. Various heart defects were observed including (H, I) reversed (rightward) looping (*Mtrr*$^{+/+}$ embryo; box in H depicts region of higher magnification shown in I), (J) absence of heart looping (dotted line depicts unlooped heart; *Mtrr*$^{+/gt}$ embryo), (K) an enlarged heart (arrowhead; *Mtrr*$^{+/+}$ embryo) and (L) pericardial edema (arrowhead; *Mtrr*$^{+/+}$ embryo). (M-O) Multiple conceptuses exhibited haemorrhages (arrow) within (M) the embryo, (N) the placenta and/or (O) the yolk sac (all examples are *Mtrr*$^{+/gt}$). Scale bars: A-F, H-O = 1mm; G = 0.5mm. Genotype (+/+, +/gt or gt/gt) in upper right hand corner of each panel represents the embryonic genotype.

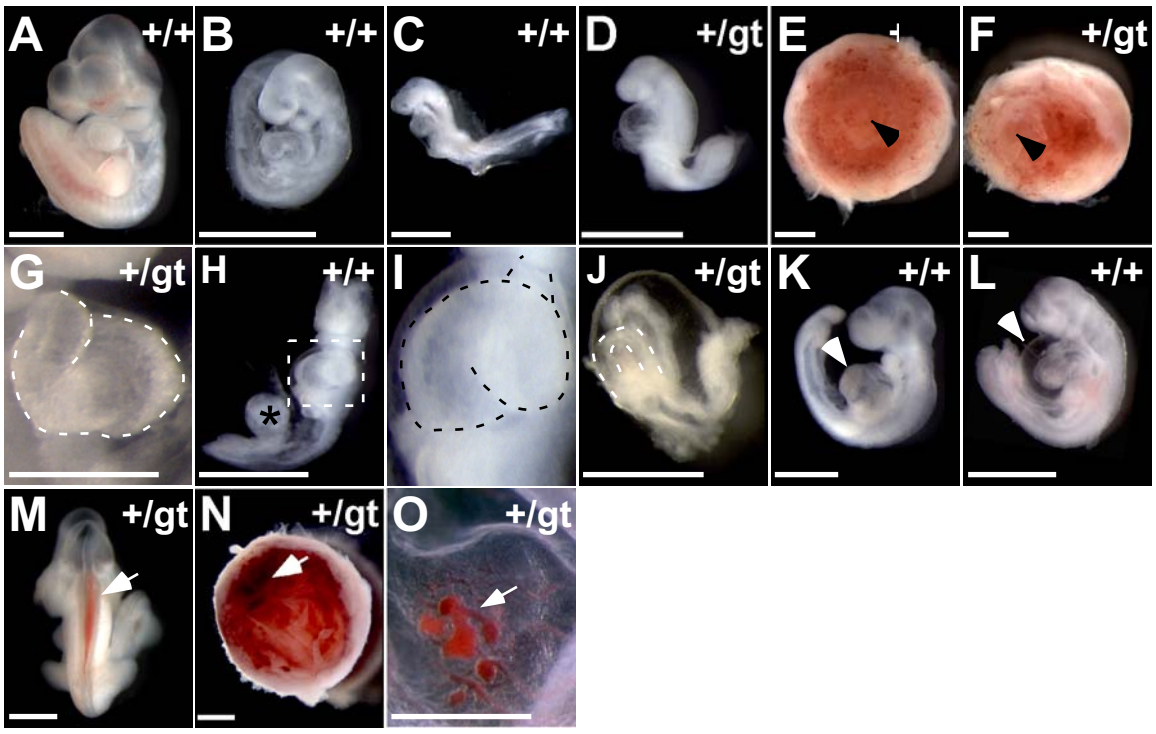
A +/+
B +/+
C +/+
D +/gt
E
F +/gt
G +/gt
H +/+
I
J +/gt
K +/+
L +/+
M +/gt
N +/gt
O +/gt

within the placenta (2.5%; Fig. A.2N), yolk sac (0.6%; Fig. A.2O) and/or embryo (1.2%; Fig. A.2M). Notably, 18.8% of these severely affected embryos exhibited more than one congenital malformation. Most of these abnormalities have been associated with human folate deficiency (Tamura and Picciano, 2006).

Given that all genotypes from *Mtrr*$^{+/gt}$ intercrosses were equally affected, we suspected the developmental abnormalities above were due to a maternal effect. To test this hypothesis, we crossed littermate *Mtrr*$^{+/+}$, *Mtrr*$^{+/gt}$ and *Mtrr*$^{gt/gt}$ female mice to *Mtrr*$^{+/+}$ males to eliminate the paternal mutant allele contribution and to focus on the effects of maternal *Mtrr* deficiency. *Mtrr*$^{+/+}$ intercrosses at E10.5 yielded 83.0% normal embryos (n=47 embryos), a result comparable to wildtype control crosses (90.6%; n=53 embryos) (Table A.1). However, when *Mtrr*$^{+/gt}$ or *Mtrr*$^{gt/gt}$ females were crossed to *Mtrr*$^{+/+}$ males, only 38.7% (n=54) and 39.6% (n=53) of embryos, respectively, were normal (Table A.1). The number of resorptions was not significantly higher compared to control crosses. However, *Mtrr*$^{+/gt}$ and *Mtrr*$^{gt/gt}$ females carried embryos with developmental delay (27.8% and 28.3%, respectively; $P<0.05$) and severe congenital malformations (13.0% [$P<0.05$] and 18.9% [$P<0.001$], respectively) such as exencephaly, heart defects, placental abnormalities and haemorrhaging as described above (Table A.1 and Table A.2). Interestingly, 3.7% of embryos from *Mtrr*$^{+/gt}$ females exhibited spina bifida-like protrusions off of the spinal cord (Fig. A.3H, I). Also, 15.2% and 8.0% of severely affected embryos from *Mtrr*$^{+/gt}$ or *Mtrr*$^{gt/gt}$ mothers, respectively, exhibited more than one congenital malformation. Together, these data suggest that reducing maternal *Mtrr* expression may lead to abnormal embryonic development.

FIGURE A.3 – Exencephaly and spina bifida in embryos from *Mtrr*-deficient conditions. Normal neural tube closure at E10.5 in (A) the cranial (Cr) and (B) the spinal cord (Sc) regions of an $Mtrr^{+/+}$ embryo. (C) An $Mtrr^{gt/gt}$ embryo at E10.5 with underdeveloped branchial arches and head (neurocristopathy). (D-E) Exencephaly in an $Mtrr^{+/gt}$ embryo at E10.5. Arrowhead indicates the region of open neural tube. Note that the spinal cord region is normal. (F) The head of a normal $Mtrr^{+/gt}$ embryo at E18.5. (G) A developmentally delayed $Mtrr^{+/gt}$ embryo at E18.5 with exencephaly (arrowhead). (H, I) A spina bifida-like protrusion from the spinal cord (arrowhead) of an $Mtrr^{+/+}$ embryo from a $Mtrr^{+/gt}$ female x $Mtrr^{+/+}$ male cross at E10.5. Scale bars = 1mm. Genotype (+/+, +/gt or gt/gt) in upper right hand corner of each panel represents the embryonic genotype.

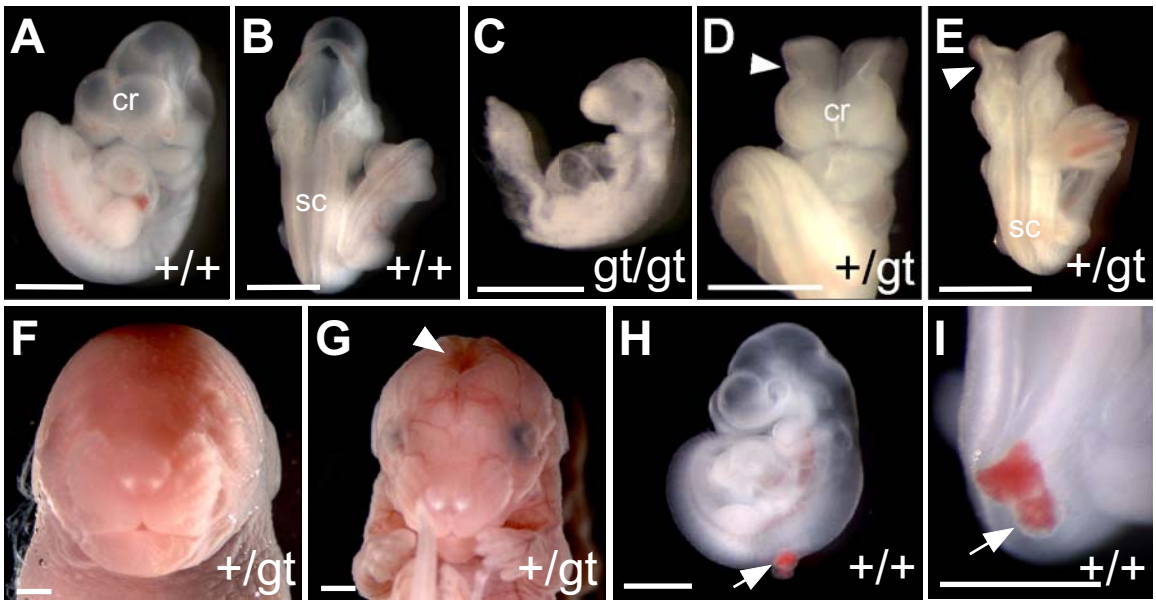
A
cr
+/+
B
sc
+/+
C
gt/gt
D
cr
+/gt
E
sc
+/gt
F
+/gt
G
+/gt
H
+/+
I
+/+

Folate deficiency in humans can result in congenital abnormalities or miscarriage (De Wals et al, 2007). Therefore, to determine whether the affected embryos observed at E10.5 would have survived to term, we assessed mouse fetuses that developed in *Mtrr*-deficient mothers near term. We repeated the above matings (*Mtrr*$^{+/gt}$ intercrosses and *Mtrr*$^{+/+}$, *Mtrr*$^{+/gt}$ and *Mtrr*$^{gt/gt}$ females crossed to *Mtrr*$^{+/+}$ males) and dissected fetuses at E18.5. Although the majority of embryos were normal in appearance, with normal weights and lengths, a significant number of resorptions ($P<0.05$) were present compared to control crosses (Table A.3). This suggested that most of the affected embryos at E10.5 died prior to birth. In addition, we observed one fetus at E18.5 from an *Mtrr*$^{+/gt}$ intercross that exhibited developmental delay and exencephaly (Fig. A.3G). Together, these data demonstrated that maternal mutations in *Mtrr* result in either embryonic lethality between E10.5 and E18.5 or serious congenital abnormalities at birth.

A.3.3 Mtrr *deficiency in the maternal grandmother causes congenital defects*

While dissecting embryos from *Mtrr*$^{+/+}$ female mice crossed to *Mtrr*$^{+/+}$ males, we noticed that some litters showed the range of developmental defects observed in litters from *Mtrr*$^{+/gt}$ and *Mtrr*$^{gt/gt}$ females. Pedigree analysis revealed that the abnormal litters were traced to *Mtrr*$^{+/gt}$ maternal grandmothers whereas the normal litters had *Mtrr*$^{+/+}$ maternal grandmothers. Upon further investigation, we found that 83.0% of embryos (n=47) from *Mtrr*$^{+/+}$ intercrosses with *Mtrr*$^{+/+}$ maternal grandmothers were normal at E10.5 (Table A.1 and Table A.2), results similar to control wildtype crosses. In contrast, only 33.8% of embryos (n=56) with *Mtrr*$^{+/gt}$ maternal grandmothers and wildtype parents were normal. We found that 30.4% of embryos displayed developmental delay and 17.9% exhibited

TABLE A.2 – Embryonic defects reveal a maternal and grandmaternal effect of *Mtrr* deficiency at E10.5[a]

Matings	Wildtype	$Mtrr^{+/+}$♀ x $Mtrr^{+/+}$♂		$Mtrr^{+/gt}$♀ x $Mtrr^{+/+}$♂		
Progeny Genotype	$Mtrr^{+/+}$	†$Mtrr^{+/+}$	‡$Mtrr^{+/+}$	$Mtrr^{+/+}$	$Mtrr^{+/gt}$	Unknown
Resorption	9.4	14.9	17.9	5.6	13.0	1.9
C.A. defect:						
No attachment	-	-	-	-	-	-
Off-center attachment	-	-	8.9	-	-	-
Haemorrhaging:						
TGC layer	-	-	-	-	1.9	-
Labyrinth	-	-	1.8	-	1.9	-
Yolk sac	-	-	1.8	-	-	-
Embryo	-	-	-	1.9	-	-
Embryo not turned	-	-	5.4	1.9	1.9	-
Heart abnormality:						
Not looped	-	-	-	-	-	-
Reversed looping	-	-	-	1.9	-	-
Enlarged heart	-	-	5.4	-	-	-
Pericardial edema	-	-	1.8	-	-	-
Neural defects:						
Small head	-	-	5.4	1.9	-	-
Exencephaly	-	2.1	7.1	1.9	1.9	-
Spina bifida	-	-	-	3.7	-	-
Total implantation sites	**53**	**47**	**56**	**23**	**30**	**1**

[a]Values expressed as percentages of total. Maternal grandmother genotypes: † = $Mtrr^{+/+}$; ‡ = $Mtrr^{+/gt}$. C.A. = chorioallantoic attachment.

TABLE A.2 Continued.

Matings	*Mtrr*$^{gt/gt}$♀ x *Mtrr*$^{+/+}$♂	*Mtrr*$^{+/gt}$♀ x *Mtrr*$^{+/gt}$♂			
Progeny Genotype	*Mtrr*$^{+/gt}$	*Mtrr*$^{+/+}$	*Mtrr*$^{+/gt}$	*Mtrr*$^{gt/gt}$	Unknown
Resorption	13.2	0.6	7.1	1.3	2.6
C.A. defect:					
No attachment	-	0.6	-	-	-
Off-center attachment	7.5	1.3	1.9	0.6	0.6
Haemorrhaging:					
TGC layer	-	0.6	1.9	-	-
Labyrinth	-	-	-	-	-
Yolk sac	-	0.6	-	-	-
Embryo	3.8	-	0.6	0.6	-
Embryo not turned	-	0.6	1.3	1.3	-
Heart abnormality:					
Not looped	-	-	0.6	-	-
Reversed looping	-	0.6	-	-	-
Enlarged heart	5.7	0.6	1.3	1.3	-
Pericardial edema	-	1.3	-	-	-
Neural defects:					
Small head	1.9	1.3	1.3	1.9	-
Exencephaly	7.5	1.9	1.3	1.3	-
Spina bifida	-	-	-	-	-
Total implantation sites	**53**	**36**	**77**	**37**	**5**

[a]Values expressed as percentages of total. C.A. = chorioallantoic attachment.

TABLE A.3 – Weights, lengths and neural tube status in embryos from *Mtrr*-deficient conditions at E18.5

Matings	**Wildtype ♀ x Wildtype ♂**	***Mtrr*$^{+/gt}$♀ x *Mtrr*$^{+/gt}$♂**			
Total # of Litters	6	7			
Total # of implantation sites	52	57			
Average implantation sites/litter	8.66 ± 0.49§	8.14 ± 0.40			
Progeny Genotype	***Mtrr*$^{+/+}$**	***Mtrr*$^{+/+}$**	***Mtrr*$^{+/gt}$**	***Mtrr*$^{gt/gt}$**	**Unknown**
Viable embryos (%)	92.3	12.5	53.6	8.9	-
Resorptions (%)	7.7	-	-	-	26.3*
Average Weight (g)	1.46 ± 0.025	1.48 ± 0.072	1.50 ± 0.036	1.42 ± 0.073	-
Average Length (cm)	2.08 ± 0.021	2.09 ± 0.077	2.17 ± 0.037	2.10 ± 0.138	-
Exencephalic embryos (%)	-	-	2.4	-	-

Matings	***Mtrr*$^{+/gt}$♀ x *Mtrr*$^{+/+}$♂**			***Mtrr*$^{gt/gt}$♀ x *Mtrr*$^{+/+}$♂**
Total # of Litters	6			8
Total # of implantations sites	51			57
Average implantation sites/litter	8.50 ± 0.89			7.13 ± 0.85
Progeny Genotype	***Mtrr*$^{+/+}$**	***Mtrr*$^{+/gt}$**	**Unknown**	***Mtrr*$^{+/gt}$**
Viable embryos (%)	27.4	54.9	-	82.5
Resorptions (%)	-	-	17.6*	17.5*
Average Weight (g)	1.31 ± 0.043	1.40 ± 0.020	-	1.48 ± 0.018
Average Length (cm)	2.00 ± 0.062	2.12 ± 0.033	-	2.12 ± 0.027
Exencephalic embryos (%)	-	-	-	-

§Mean ± s.e.; *P<0.05

congenital abnormalities (Table 1 and Table A.2). By contrast, developmental delay was not present in litters from *Mtrr*$^{+/+}$ intercrosses with *Mtrr*$^{+/+}$ maternal grandmothers and the appearance of congenital defects was extremely rare. We only detected one abnormal embryo (exencephaly) from an *Mtrr*$^{+/+}$ maternal grandmother at E10.5 (Table A.2). Importantly, the frequencies of abnormalities in litters from *Mtrr*$^{+/+}$ mothers and *Mtrr*$^{+/gt}$ grandmothers were not significantly different than litters from *Mtrr*$^{+/gt}$ or *Mtrr*$^{gt/gt}$ mothers (Table A.1). It is also critical to note that *Mtrr*$^{+/gt}$ and *Mtrr*$^{gt/gt}$ females with affected litters were derived from *Mtrr*$^{+/gt}$ mothers. This indicated that the embryonic defects may be the result of *Mtrr* deficiency within the maternal grandmother. We also analyzed 12 pedigrees in which the mother, father and maternal grandmother were all wildtype yet the paternal grandparents were *Mtrr*$^{+/gt}$. We found that all embryos were normal except for two cases of exencephaly in two litters fathered by the same male (data not shown). This may have been caused by an independent event since the other 10 litters fathered by 5 males had no abnormalities. These results indicate that *Mtrr* genotypes of the paternal grandparents likely do not influence developmental outcome.

A.4 Discussion

It is widely acknowledged that maternal nutritional folate status is important for fetal development. Although folate fortification has resulted in a reduction of NTD incidence in human populations, it has not eliminated their occurrence (from 1.58 to 0.86 per 1000 births in Canada) (De Wals et al, 2007). Few genetic studies have conclusively shown that maternal mutations in genes involved in folate metabolism affect development, regardless of the fetal genotype. The human *MTRR* 66A→G polymorphism in mothers

has recently been associated with fetal NTDs, independent of the child's genotype (van der Linden et al, 2006). However, our data here imply that neither the embryonic nor the maternal genotype is as important as the grandmaternal genotype.

The main focus of multigenerational effects has been on environmental factors (toxins and nutrition) that influence embryonic or postnatal development (Cooney et al, 2002; Drake et al, 2007; Kaati et al, 2007; Pembrey et al, 2006; Skinner, 2008). There is little data in the vertebrate literature that suggests multigenerational effects due to a genetic mutation. Here, the spectrum and frequency of congenital malformations was similar when comparing litters from *Mtrr*-deficient mothers to those from *Mtrr*-deficient maternal grandmothers. We detected only one exencephalic embryo at E10.5 with an $Mtrr^{+/gt}$ maternal *great*-grandmother but wildtype maternal grandmother and parents (out of six pedigrees analyzed; data not shown). The reduced frequency implies that the effect of *Mtrr* deficiency is not likely to persist for more than two generations.

The "grandmother effect" of *Mtrr* deficiency could be explained in two ways. First, since folate is required for a variety of metabolic processes (Tamura and Picciano, 2006), *Mtrr*-deficient females though viable and fertile may have defects that result in an abnormal uterine environment leading to altered fetal metabolic programming that impacts her daughters. For example, the intrauterine environment of diabetic mothers can influence fetal development such that her daughters will have a greater risk of gestational diabetes (Aerts and Van Assche, 2003). Alternatively, since folate is a source of methyl groups for downstream targets including DNA (Blom et al, 2006), the fetal abnormalities may be the result of an epigenetic effect. The human *MTHFR* 677C→T polymorphism has been shown to lead to a global reduction in DNA methylation (Castro et al, 2004;

Friso et al, 2002). Furthermore, DNA methyltransferase 3B (*Dnmt3b*) is required for normal DNA methylation and global DNA methylation is reduced in *Dnmt3b*-deficient mice resulting in embryonic developmental delay and NTDs (Okano et al, 1999), a phenotype reminiscent of *Mtrr* deficiency as shown here. Genomic imprinting of germ cells occurs while a fetus is in utero (Morgan et al, 2005; Skinner, 2008). Consequently, abnormal folate metabolism in the grandmother while she is pregnant could result in reduced transmission of folate intermediates to the fetus thereby affecting DNA methylation profiles in her daughter's oocytes. This suggests that the full impact of folate fortification may take more than one generation. It will be key to evaluate global DNA methylation in the generations subsequent to the ancestor carrying the $Mtrr^{gt}$ allele.

A.5 Materials and Methods

Generation of $Mtrr^{gt}$ mice and dissections. ES cells with *Mtrr* gene-trap allele (XG334) were purchased from BayGenomics (http://baygenomics.ucsf.edu/) and were injected into C57Bl/6 blastocysts using standard procedures at BayGenomics. After confirmation of germline transmission, the progeny were backcrossed to C57Bl/6. Control wildtype C57Bl/6 mice were obtained from The Jackson Laboratory (http://jaxmice.jax.org/index.html) and were maintained separately from the *Mtrr* lineage. Embryos were dissected in phosphate buffered saline (PBS) (noon of the day when the vaginal plug was detected was considered E0.5). Experiments were performed in accordance with the Canadian Council on Animal Care and the University of Calgary Committee on Animal Care (Protocol No. M06109).

Diet. After weaning, all mice were fed normal rodent chow (Pico-Vac® Lab Rodent Diet, Code No 5061, PMI Nutrition International) containing the recommended daily-intake of folate for mice (~3 mg/kg of diet) (Knock et al, 2006).

Genotyping. A three-primer PCR reaction was used to detect the presence or absence of the gene trap. Two primers (5' AGATGTCCCTGC ATTCACCCAGAGCA and 5' CTTCAGTGATGAGGTAATTTAGC) flanking the gene-trap insertion site to detect the wildtype band (127bp) and an additional primer annealing to either the 5' end (5' CTCAAACTCTCCTCCTTCCCTCCC) or 3' end (5' AAATGTTGAATACTCATAC TCTTCC) of the gene trap to detect the mutant band (204bp or 550bp, respectively). PCR parameters: 30 seconds at 95ºC, 1 minute at 58ºC and 30 seconds at 72ºC for 30 cycles. DNA samples were obtained from ear or yolk sac tissue.

Quantitative reverse transcription PCR. Brain, kidney, heart and liver tissue was excised from *Mtrr*$^{+/+}$, *Mtrr*$^{+/gt}$ and *Mtrr*$^{gt/gt}$ mice. Total RNA extraction was completed using TRIzol reagent, according to manufacturer's instructions (Invitrogen, Fredrick, USA). The extract was treated with DNAse I (Gibco). Reverse-transcription reactions were performed with the Omniscript RT kit (Qiagen) by using 5 µg of RNA from each tissue in a 50 µL reaction. Relative quantitative PCR was carried out using 200 ng of RNA and primers that anneal to *Mtrr* exon 9 (5' CCCGTCCTGCCAGCCTCCGCTCA) and *Mtrr* exon 11 (5'CCCGTGCACA CTCCCTTCCTC). Only a 182 bp amplicon of wildtype *Mtrr* cDNA was generated since the gene trap insertion between exon 9 and 10 prevented proper splicing to exon 10. PCR amplification was conducted using iQ Syber Green Supermix (BioRad) with 160 nM of each primer (total reaction volume of 25 µL). Real time PCR was conducted in triplicate on an iCycler iQ Multicolor RT-PCR

detection system (BioRad) using an annealing temperature of 60^{o}C. Control PCR reactions were conducted in parallel with primers designed to detect mouse glyceraldehyde-3'-phosphate-dehydrogenase (GAPDH) mRNA (5' TGCACCACCA ACTGCTTAGC and 5' GGCATG GACTGTGGTCATGAG) 87 bp amplicon).

Quantitative values were obtained by the cycle number (C_t), the point at which fluorescence significantly increased above background during exponential amplification. C_t is inversely proportional to the amount of a specific mRNA species in the tissue from which the cDNA was derived. The relative amount of wildtype *Mtrr* transcript in *Mtrr*$^{+/+}$, *Mtrr* $^{+/gt}$ and *Mtrr* $^{gt/gt}$ mice was normalized to *GAPDH* in each sample using the formula $2^{-\triangle\triangle Ct}$ to calculate fold-change values, where $\triangle\triangle C_t$ is the difference between the mean experimental and standard $\triangle C_t$ values (Livak and Schmittgen, 2001). *Mtrr*$^{+/+}$ cDNA levels were used as the standard. The $\triangle C_t$ value equals the difference between the C_t value for each sample and the GAPDH internal control. We used this formula to determine a fold-change value of 1 for *Mtrr*$^{+/+}$ mRNA expression, while values less than one indicated decreased mRNA expression.

Total homocysteine concentration quantification. Plasma was collected by orbital bleeding of *Mtrr*$^{+/+}$ and *Mtrr*$^{gt/gt}$ adult mice. Total homocysteine in plasma was measured by LC-MS/MS (Waters 2795 Alliance HT HPLC and Quattro Ultima) operated in electrospray positive mode. A deuterated internal standard, d8-homocystine, was added to the plasma, followed by reduction of disulfides with dithiothreitol (Magera et al, 1999). Calibrators were prepared by spiking normal plasma with a range of known homocysteine concentrations. Ten μL of 5 μM d8-homocystine were added to 10 μL of each calibrator and plasma, followed by 20 μL of 0.5 M dithiothreitol. Tubes were

vortexed and held at room temperature for 15 minutes. Proteins were precipitated by adding 100 µL of acetonitrile with 10% formic acid and centrifuged at 12,800 g for 5 minutes and the clear supernatants were transferred to 96-well plates. Four µL were loaded onto a Waters XTerra MS C18 (3.5um, 2.1x50mm) column fitted with a 2.1x10mm guard column and eluted isocratically for 2 minutes at 0.25 mL/min with acetonitrile: water: formic acid (80:20:0.1). Waters QuanLynx software is used to quantify MRM transitions of 136>90 and 140>94.

Equipment and Software. Primers for PCR were designed by Primer3 software (http://primer3.sourceforge.net/). A Leica MZ95 dissection microscope (Wetzlar) with a Photometrics Coolsnap cf camera (Roper Scientific) and Openlab 2.2.2 imaging software program (Improvision) were used to obtain embryo images. Minimal image processing was performed by Adobe Photoshop 7.0 and figures were constructed using Canvas X.